THE DYNAMICS OF FLOATING BODIES IN A REGULAR WAVE ENVIRONMENT

BY

K.J. WILLIAMS

B.Sc., M.I.H.T., M.I.A.H.R.

Thesis submitted to The City University

for the degree of Doctor of Philosophy

in the Department of Civil Engineering

October 1986

SYNOPSIS

Theoretical and numerical investigations have been carried out on the use of the Integral Equation Method of solution for the Potential Theory problem of the interaction between a floating body and a train of regular waves in a two-dimensional domain.

In particular, a numerical study has been carried out of the indirect method of solution of the integral equation resulting from a distribution of Green's Function sources over a boundary coincident with the immersed surface of the body. It is demonstrated that a significant increase in solution efficiency, with no loss of precision, can be effected by improvements in the general numerical techniques of solution together with the use of a polynomial type distribution of elements over the source boundary. It is also demonstrated that significant improvements in solution accuracy for rectangular aspects can be achieved by a slight 'rounding' of the submerged edges of the mathematical model.

An experimental investigation of the interaction between a train of regular waves and a substantially rectangular floating body includes measurements of the reflection and transmission characteristics, for both the fixed and floating mode of the body, together with measurements of the body motions.

The primary objective of the experimental study is the validation of theoretically predicted interaction parameters derived from the above methods. The experimental program was designed both to determine the extent of validity of Potential Theory within regimes

where diffraction effects predominate, and also to determine the conditions under which the use of Potential Theory alone becomes invalid due to the significant presence of non-linear effects.

As a consequence of the results of this investigation, recommendations are made both with regard to the possible achievement of further improvements in solution efficiency and, more importantly, with regard to a general improvement of solution accuracy by the inclusion of the above-mentioned non-linear effects in the theoretical formulations.

ACKNOWLEDGEMENTS

The work reported in this thesis was carried out in the Civil Engineering Department of The City University, London.

Dr. K. Arumugam's supervision of the work has been greatly appreciated and the assistance of staff and colleagues at The City University has been of considerable value. Particular thanks must be extended to Mr. P.L. Carr, Dr. K.S. Virdi and Dr. L.F. Boswell not only for their assistance in academic matters, but also for their constant and valued encouragement during the period of this research.

The author wishes to thank Dr. L.E. Coates (now of Birmingham University) for his assistance in the initial period of writing-up.

Mr. P.L. Carr was responsible for the development of the software pertaining to the Fast Fourier Transform algorithm, and Dr. D.M. Ellix (now of B.H.R.A) afforded valuable assistance in developing the methods of wave profile analysis contained in section 5.8.2.

The author is indebted to Dr. K.S. Virdi for his assistance in the development of the method of solution of Complex Matrix Equations contained in Appendix A4.2.

Messrs. S. Ely and J. Rose were responsible for the construction of the experimental model, and Mr. A. Saeed manufactured the bearing arrangements. The author wishes to extend particular thanks to Mr. N. Andrews, Laboratory Superintendent, who gave unstintingly of his

time and valued common-sense in the course of the experimental study.

The author acknowledges, with thanks, the exceptional facilities provided by Mr. D. Tongue, Computer Operations Supervisor, to enable the considerable amount of computational work to be completed on time.

For the constant encouragement and facilities afforded, during the writing-up period, by Prof. H.B. Sutherland and the staff of the Department of Civil Engineering, University of Glasgow, the author extends thanks.

The writer gratefully acknowleges the work of Mrs. J. Lawn who, by virtue of expertise and much effort, completed the typing of the manuscript in less than a month.

This work was made possible by the award of maintenance and support grants by the Science and Engineering Research Council.

CONTENTS

Page Number

Synopsis.

Acknowledgements.

Contents.

List of Figures.

List of Tables.

CHAPTER 1. INTRODUCTION

1.1 General Introduction. 1

1.2 Introduction to the Present Study. 5

CHAPTER 2. LITERATURE SURVEY

2.1 Introduction. 8

2.2 Historical Review. 9

2.3 The Integral Equation Method. 16

2.4 Experimental Validation of Theory. 33

CHAPTER 3. WAVE HYDRODYNAMICS AND FLOATING BODY DYNAMICS

3.1 Introduction. 58

3.2 Definitions and Sign Conventions. 60

3.3 The Velocity Potential. 61

3.4 The Body Motion. 65

3.5 The Equations of Motion. 68

3.6 The Hydrodynamic Coefficients. 71

3.7 Forces, Moments and Motions. 74

CHAPTER 4. NUMERICAL ANALYSIS

4.1 Introduction. 81

4.2 The Two-Dimensional Source Strength

Distribution Equation. 83

Page Number

4.3 The Source Strength Integral Equation Formulation. 85

4.4 Numerical Solution of the Fredholm Equations. 88

4.4.1 The Fixed Body Case. 88

4.4.2 The Floating Body Case. 93

4.5 Numerical Evaluation of the Discretised Source Distribution Function. 95

4.6 Numerical Evaluation of the Discretised Velocity Potential. 98

4.7 Numerical Evaluation of the Green's Function Expressions. 99

4.7.1 The Integral Formulation. 101

4.7.2 The Series Formulation. 107

4.7.3 Comparison between the Integral and Series Formulation. 109

4.7.4 Convergence criteria. 110

4.8 Computational Efficiency Considerations. 112

4.9 Limitations of the Green's Function Integral Equation Method. 115

4.9.1 Irregular Frequencies. 115

4.9.2 Ill-Conditioning of Matrix Equations. 118

4.10 Comparison with Published Data. 120

CHAPTER 5. THE EXPERIMENTAL INVESTIGATION

5.1 Introduction. 132

5.2 Objectives of the Experimental Study. 135

5.3 Experimental Parameters. 136

5.3.1 The Diffraction Parameter. 136

5.3.2 Non-Dimensional Parameters. 138

Page Number

5.3.3 Choice of Body Geometry and Dimensions. 139

5.4 Experimental Apparatus. 141

5.4.1 The Experimental Flume and Wave-Generation. 141

5.4.2 The Floating Body. 144

5.5 Measurement of Experimental Data. 153

5.5.1 Free-Surface Displacement. 153

5.5.2 Translatory Body Motions. 154

5.5.3 Rotational Body Motions. 154

5.6 Calibration of Measuring Equipment. 155

5.6.1 Static Calibration. 155

5.6.2 Dynamic Calibration. 158

5.7 Collection and Processing of Raw Data. 163

5.8 Analysis of Data. 166

5.8.1 Resolution of Periodic Data. 166

5.8.2 Free-Surface Displacement. 167

5.8.3 Body Motions. 177

CHAPTER 6. PRESENTATION OF RESULTS

6.1 Introduction. 182

6.2 Floating Body Details. 184

6.3 Numerical Results. 185

6.4 Fixed Body Wave-Effects. 187

6.5 Floating Body Wave-Effects. 188

6.6 Energy Conservation Characteristics. 188

6.7 Floating Body Motions. 189

6.8 Accuracy of Experimental Results. 190

6.8.1 Collection and Primary Analysis of Periodic Data. 191

Page Number

6.8.2 Free-Surface Displacement. 192

6.8.3 The Body Motions. 196

6.8.4 Non-Dimensional Parameters. 198

6.8.5 Systematic Errors. 199

6.8.6 Abnormal Experimental Errors. 201

CHAPTER 7. DISCUSSION OF RESULTS

7.1 Introduction. 294

7.2 The Numerical Results. 295

7.2.1 General Aspects. 295

7.2.2 Green's Function Evaluation. 298

7.2.3 Element Distribution. 300

7.3 The Experimental Results. 306

7.3.1 Fixed Body Reflection and Transmission. 306

7.3.2 Floating Body Reflection and Transmission. 309

7.3.3 Floating Body Motions. 311

7.4 Conclusions and Recommendations. 318

APPENDIX A1. THE TWO-DIMENSIONAL SOURCE DISTRIBUTION EQUATION. 325

APPENDIX A2. THE GREEN'S FUNCTION FORMULATIONS. 327

A2.1 The Normal Gradient. 327

A2.2 The Imaginary Part. 327

A2.3 The Integral Form of the Real Part. .. 328

A2.4 The Series Form of the Real Part. 330

APPENDIX A3. THE GREEN'S FUNCTION LIMIT AT ITS SOURCE. ... 335

Page Number

APPENDIX A4. NUMERICAL DETAILS. 338

A4.1 Solution of the Modified Dispersion Equation. 338

A4.2 Solution of a Complex Matrix Equation. 341

A4.3 Numerical Integration of a Sinusoidal Function using Simpson's Rule. 346

A4.4 Numerical Evaluation of the Incident Wave Potential. 348

A4.5 Numerical Evaluation of the Exciting Force Components. 349

A4.6 Numerical Evaluation of the Complex Amplitudes of Motion. 351

A4.7 Numerical Evaluation of the Reflection and Transmission Coefficients. 353

APPENDIX A5. BOUNDARY ELEMENT DISTRIBUTION. 355

A5.1 Rectangular Immersed Surface with Square Edges. 356

A5.2 Rectangular Immersed Surface with Radial Edges. 359

APPENDIX A6. EVALUATION OF THE REFLECTION AND TRANSMISSION CHARACTERISTICS OF A FLOATING BODY. 361

APPENDIX A7. THE COMPUTER PROGRAM. 370

A7.1 Introduction. 370

A7.2 Program Operation. 371

A7.3 Subroutines and Functions within the Program. 372

A7.4 Computer Operational Requirements. .. 375

APPENDIX A8. LIST OF REFERENCES. 382

APPENDIX A9. NOMENCLATURE. 393

LIST OF FIGURES

Figure		Page Number
3.1	Body Motion Definition.	60
3.2	Fluid Domain Definition.	61
4.1	Removal of Source-Point Singularity. ..	86
4.2 - 4.5	Diffraction Program Results for a substantially rectangular floating body - comparison with published data. ..	128-131
5.1	Floating Body Details.	145
5.2	Rotational Bearing Detail.	147
5.3	Biaxial Bearing Arrangement Detail. ...	149
5.4	Typical Wave-Probe Static Calibration. ...	157
5.5	Typical Displacement Transducer Static Calibration.	157
5.6	Typical Wave-Probe Dynamic Calibration. ..	160
5.7	Typical Displacement Transducer Dynamic Calibration.	161
5.8	Typical Accelerometer Calibration.	162
5.9	Flow-chart for Collection, Analysis and Presentation of Experimental Results. ...	165
5.10	Typical Wave Profile Analysis.	176
5.11	Measurement of Pitch Rotation.	178
6.1 - 6.6	Fixed Body Reflection and Transmission Characteristics - Numerical Results. ...	236-241
6.7 - 6.12	Floating Body Reflection and Transmission Characteristics - Numerical Results. ...	241a-246
6.13 - 6.18	Floating Body Motions - Numerical Results.	247-252
6.19 - 6.26	Fixed Body Reflection and Transmission Characteristics - Experimental Results. ...	253-260

Figure		Page Number
6.27 - 6.29	Fixed Body Reflection and Transmission Characteristics - Experimental Errors. ...	261-263
6.30 - 6.37	Floating Body Reflection and Transmission Characteristics - Experimental Results. ...	264-271
6.38 - 6.40	Floating Body Reflection and Transmission Characteristics - Experimental Errors. ...	272-274
6.41 - 6.42	Fixed and Floating Body Energy Conservation.	275
6.43 - 6.50	Floating Body Motions - Experimental Results.	276-283
6.51 - 6.53	Floating Body Motions - Experimental Errors.	284-286
6.54 - 6.56	Floating Body Reflection and Transmission Characteristics - Effects of Inertia Error.	287-289
6.57 - 6.59	Floating Body Motions - Effects of Inertia Error.	290-292
6.60	Effect of Resonance on Wave Profile Analysis.	293
A2.1 - A2.3	Green's Function Evaluations - Behaviour of the Modified and Unmodified P.V. integrals.	332-334
A3.1	The Green's Function Limit at its Source.	335
A4.2	Solution of Modified Dispersion Equation.	339
A5.1	Element Distribution - Square-Edged Body.	356
A5.2	Element Distribution - Radially-Edged Body.	359
A7.1	Flow-Chart for Program FLOATER.	375
A7.2	Green's Function Integral Evaluation Flow-Chart for Subroutine GINTEG.	376
A7.3	Green's Function Series Evaluation Flow-Chart for Subroutine GSER1.	377

Figure		Page Number
A7.4	Green's Function Evaluation	
	Flow-Chart for Subroutine GREENS.	378
A7.5	Computer Requirements.	381

LIST OF TABLES

Table		Page Number
4.7.1	Numerical Integration of the Modified Green's Functions.	102
4.7.2	Effect of Stepped Integration of the Green's Function Remainder Integral.	105
4.7.3	Comparison of Integral and Series Evaluation of the Green's Function.	108
4.10.1/2	Floating Body Details.(to be read in conjunction with Figs.4.2/3/4/5)	126-127
5.3.1	Diffraction Parameter Variations.	138
5.3.2	Proposed Body Immersed Surface Aspects.	141
5.8.1	Proposed Investigational Frequencies.	167
5.8.2	Reflected and Transmitted Wave Analysis. (To be read in conjunction with Fig.5.10)	175
6.1	Experimental Body Configurations.	203
6.2/3	Body Discretisation Details.	203
6.4 - 6.11	Floating Body Details.	204-211
6.12 - 6.19	Fixed Body Reflection and Transmission Characteristics - Experimental Results. ..	212-219
6.20 - 6.27	Floating Body Reflection and Transmission. Characteristics - Experimental Results.	220-227
6.28 - 6.35	Floating Body Motions - Experimental Results.	228-235
A4.1	Comparison of Methods of Solution of a Complex Matrix Equation.	345

CHAPTER 1 INTRODUCTION

1.1 General Introduction.

The ability to withstand ocean conditions of the utmost severity is a fundamental requirement of any offshore structure or marine vehicle. To this end, the design of such must be based on a comprehensive knowledge and understanding of the physics of wave motion and, in particular, the hydrodynamics of wave/structure interaction. Contributions to the development thereof have been made by applied mathematicians, naval architects and engineers from many disciplines and a considerable number of theoretical and experimental studies, covering an extensive range of topics, have been carried out in this regard.

The behaviour of gravity waves has been studied by the applied mathematician since the nineteenth century and a number of alternative wave theories are currently available. The first applications of classical wave theories to problems of engineering significance, however, were concerned with the problems of ship motion and the naval architect has subsequently provided major contributions towards the development of a better understanding of wave-structure interaction in both theoretical and physical terms. In recent years, the expansion of offshore activity by the oil and gas industry has generated increased research efforts in this field and the continuing exploitation of offshore energy resources, both in terms of fossil fuel and wave energy abstraction, guarantees that momentum will be maintained in this regard.

A number of mechanisms give rise to wave induced forces on fixed obstacles and the governing mechanisms are determined by the geometry and location of the obstacle, together with the size of the obstacle in relation to the incident wave field. If the characteristic dimension of the obstacle is small in comparison to the length of the incident wave, the wave-induced force consists of two components: the drag force component, resulting from the presence of an oscillating fluid wake, and the inertia force component which results from the displacement, by the obstacle, of an equivalent mass of fluid. As the obstacle characteristic dimension increases with respect to the incident wave length, sufficient to result in deformation of the ambient wave field, the waves undergo significant diffraction by the obstacle which is, as a consequence, subjected to a diffraction force. It is assumed, in such a regime, that the drag force becomes insignificant and may be neglected, permitting the formulation of a potential theory problem. Consideration of the appropriate boundary conditions enables a solution to be obtained for the diffracted wave potential and subsequent evaluation of the hydrodynamic pressure and force components. If the obstacle is floating, additional boundary value problems are required for each degree of motional freedom, the solutions of which permit the evaluation of potentials relating to the waves generated by each mode of body motion.

A number of alternative methods have been employed for the formation and solution of these boundary value problems but, with the exception of a few simple fixed obstacle geometries, no exact solutions are available and the required solutions must be obtained by numerical means. Both the Finite Element and Hybrid Element approaches have been successfully used in this regard but by far the

most popular methods appear to be Ursell's multipole method and the method of integral equations,both of which require the introduction of fluid singularities and subsequent solution of a system of linear algebraic equations.

The integral equation method has been used in a variety of ways, not necessarily restricted to the solution of hydrodynamic interaction problems, and is variously referred to as the Source Distribution Method, the Boundary Element Method (B.E.M) and the Boundary Integral Equation Method (B.I.E.M.). In recognition of its first accredited use to obtain solutions to hydrodynamic interaction problems of practical significance, the method is often referred to by naval architects as the Frank Close Fit Method. In recent years, a fully three-dimensional approach has been developed to obtain predictions of the parameters pertaining to the hydrodynamic interaction between waves and fixed or floating structures and a number of computer programs have been developed for commercial usage in this regard. Notwithstanding this development, however, it would appear that the principal method of analysis of marine vehicles is the use of two-dimensional modelling in conjunction with an appropriate strip theory.

A considerable number of experimental investigations have been carried out with regard to wave/structure interaction. In the case of fixed bodies which are small in relation to the incident wave length, the majority of these investigations have been devoted to the provision of data relevant to the use of semi-empirical formulae in determining the significant wave induced force components. To a certain extent, the same can be said of those investigations pertaining to fixed obstacles spanning a significant proportion of

the incident wave length. In the main, however, the primary purpose of such investigations was the validation of theoretical predictions derived from the solution of potential theory problems. The results of these investigations, together with those pertaining to floating obstacles of similar dimension, are particularly useful since they provide an indication of the extent of validity of the theoretical predictions subject to the assumptions of small amplitude wave theory and inviscid flow conditions.

In recent decades, great advances have been made both in the general understanding of wave/structure interaction and the development of theoretical models as a basis for reliable design. Until comparatively recent years, however, much of the work has been restricted to two particular areas. The bulk of engineering research has been concentrated on the behaviour of offshore drilling platforms, necessitating the analysis of fixed vertical structures located on the ocean floor and spanning all or part of the water depth, whilst research in the context of naval architecture has been largely directed towards the development of an acceptable ship motion theory, entailing the two- and three-dimensional analysis of single, elongated structures in the free-surface with or without forward speed effects. However, recent developments in the oil industry have necessitated the application of established theories to a new breed of problem with the advent of increasingly complex support systems for offshore drilling platforms, with varying degrees of basal fixity and structural rigidity, the multi-legged construction of which requires additional consideration of the effects of column proximity and consequent mutual interaction. Similar recent developments have taken place in the field of naval architecture with the increasing use of multi-hulled marine

vehicles, and the "alternative energy" field with regard to the abstraction of wave kinetic energy by means of single flexible or multiform hinged floating structures.

1.2 Introduction to the Present Study.

A study has been made of the interaction between a train of regular waves and a substantially rectangular surface-piercing obstacle which may be fixed or freely floating. This thesis includes a theoretical and numerical investigation of the integral equation method used to obtain theoretical predictions of the parameters pertaining to the hydrodynamic interaction in a two-dimensional domain, and an experimental investigation specifically designed to validate these theoretical predictions.

The application of the integral equation method to obtain solutions of potential theory problems may take a number of forms, each of which is based on a result due to Green's Theorem. The two formulations most frequently used in the context of hydrodynamic interaction problems both employ a singular solution of an associated potential theory problem. This singular solution is variously referred to as the Green's Function, the Wave Function or the Wave Source. The first method assumes that the unknown potential, at any point within the fluid domain, may be represented by a distribution of single and double sources over the immersed surface of the obstacle. Application of the immersed surface kinematic condition results in the formation of an integral equation which may be solved directly for the unknown potential on the immersed body surface, thereby resulting in this method being

referred to as the direct method. The second method assumes the unknown potential to be represented by a surface distribution of single sources only, with an initially unknown spacial variation of strength over the immersed surface of the obstacle. Application of the immersed surface kinematic condition gives rise to an integral equation for the source strength distribution function, the solution of which can be used to derive the unknown potential. As a consequence of the inclusion of an intermediate computational step, the evaluation of the entirely fictitious source strength distribution function, this method is referred to as the indirect method. A further variation of the indirect formulation exists, in which the unknown velocity potential is represented by a distribution of single sources over a fictitious boundary outside the fluid domain, but this method is not in common usage except in cases of obstacles with no abrupt changes in immersed surface geometry.

The theoretical predictions of the hydrodynamic interaction parameters have been obtained, in this thesis, by means of the indirect formulation employing a distribution of single sources over the immersed surface of the obstacle.

The numerical investigation has two distinct aspects, the first of which is an examination of the computational efficiency with which the solution is obtained. The second aspect of the investigation is concerned with the sensitivity of the solution to different levels of discretisation of the immersed surface of the obstacle. Both investigations were carried out with a view to optimising the overall numerical procedure in terms of computation time and solution accuracy. To this end, a computer program has been

written, full details of which can be found in the appendices to this thesis.

An experimental program has been designed and carried out with the primary purpose of validating the predictions of linear, small amplitude potential theory subject to the assumptions of inviscid flow. In particular, the experiments have been concerned with the hydrodynamic interaction between a train of small amplitude regular waves and a substantially rectangular obstacle in fixed or freely floating mode. Additionally, the experimentation was designed with a view to determining the conditions under which the occurrence of viscous flow separation at the edges of the obstacle renders potential theory problems invalid. Ideally, a complete validation of the theory would entail examination of all parameters pertaining to the hydrodynamic interaction. However, this was precluded by a lack of time and suitable experimental facilities. As a consequence, the investigation was limited to the experimental measurement of the body reflection and transmission characteristics, together with the amplitudes of body motion, and subsequent comparison with the appropriate theoretical predictions output by the computer program.

CHAPTER 2 LITERATURE SURVEY

2.1 Introduction

The literature devoted to the theoretical and experimental investigation of wave-structure interaction is extensive and covers a considerable range of topics. Such literature has been written from both the point of view of the Civil Engineer (interaction between waves and fixed structures) and from the point of view of the Naval Architect (ship motion theory). Consequently, the scope of this literature survey has been restricted to include only those texts which are directly relevant to the subject matter of this thesis together with those which include developments and results which are of particular significance to this study.

The initial part of this chapter deals with the historical development of floating body theory in general terms. Since the major contributions in this field have been instigated by a desire to initiate and subsequently develop increasingly sophisticated methods of prediction of the hydrodynamic parameters associated with the behaviour of ships at sea, the historical review is largely concerned with the development of ship motion theory from the eighteenth century to the present day.

The majority of the subject matter contained in this thesis is devoted to a study of the Source Strength/Integral Equation method of solution of the hydrodynamic parameters associated with the interaction between an obstacle and a train of regular waves. As a consequence, a detailed review is given of the use and development

of this solution technique. Since this method has been extensively used not only for the solution of floating body hydrodynamics but also for the solution of the response of fixed structures to waves, the content of this section of the review has been collated from previous studies of both aspects.

The confidence with which any theoretically developed technique can be used for the solution of practical problems is entirely dependent upon the establishment of the physical conditions under which the theory is valid. Numerous experimental studies have been carried out for the purpose of validating the various theoretical methods of solution of hydrodynamics problems of engineering significance and a review of the relevant studies, together with the conclusions reached therefrom, is contained in the final section of the chapter.

2.2 Historical Review.

The history of ship motion theory may be traced back to the eighteenth century[11], the studies of Euler and Bernoulli being the earliest known attempts to formulate and to solve the equations of ship motions in calm water and in waves.

It is generally accepted, however,that the real beginning came with the investigations of W.Froude[22] and R.E.Froude[21] who studied the rolling motion of a ship in beam seas. These studies were carried out under the assumption that the beam and draught of the ship was small in comparison to the incident wavelength and that, as a result, the presence of the ship does not alter the pressure field

of the incident wave system. This work was extended in 1896 and 1898 by Krylov[59-60] who derived a more general description for ship oscillations using the same fundamental assumptions. This particular theory, known as the Froude-Krylov Hypothesis, made use of equations of motion which resemble those in present use, with the exception of terms for the hydrodynamic reaction (added-mass and wave damping) and the wave diffraction effects.

The Froude-Krylov approach dominated ship motion analysis for almost half a century. During this period, notable contributions to the theory came from Lewis[66] and Lockwood-Taylor[67] who initiated the inclusion of the added mass-inertia terms subject to the neglect of free-surface effects. Additionally, numerical procedures were developed to include the orbital motion effect of waves, known generally as the Smith effect. With all these modifications and corrections, the equations of ship motions assumed the form of a set of linear coupled, second order, ordinary differential equations with constant coefficients.

While Naval Architects concentrated their efforts on methods of predicting the behaviour of ships based on mainly intuitive reasoning, the mathematicians and physicists attempted to tackle the problem using a more rigorous and analytic approach. It is accepted that the first in this field was the Soviet mathematician Steklow[89] who formulated the ship motion problem as a boundary value problem of mathematical physics. In the following years, many investigations were undertaken on various aspects of the hydrodynamics of ship motion theory. These constituted the foundations of the computational methods in use today. Amongst others, significant contributions came from the works of Kochin[56]

and Havelock[36-37].

A unique effort, bringing together both the naval architectural and the mathematical approaches, was made by Haskind[31] in his study of the coupled heaving and pitching motions of a ship. Haskind was also the first to indicate the dependence of added-mass and wave damping upon the frequency of oscillation[34] and went on, some years later, to develop a set of practical empirical relationships for the initial estimation of the parameters of ship motion[32].

In the following years, the studies of John[48-49] and Peters and Stoker[81] formed the essence of today's understanding of ship motion theory. John carried out a rigorous mathematical formulation of the equations of motion and indicated a method of solving the linearised problem by the application of Green's Theorem to a specified mathematical wave function. On the other hand, Peters and Stoker derived a thin-ship theory by the introduction of small parameter expansion techniques. Although this approach was not successful from the point of view of practicality, the method opened up new and fertile grounds.

Notwithstanding these developments, however,the main breakthrough in ship motion theory came with the publication of the classic paper by Korvin-Kroukovsky and Jacobs[58] which presented an easily usable method for the practical computation of ship motion parameters, with forward speed effect, based upon engineering use of aerodynamic slender body theory. This method was called the "Strip Theory".

Strip Theory is still the principal method in use for predicting the behaviour of ships as a result of wave action, although there exist

a number of versions. These versions differ in their basic approach to the problem formulation and their method of solution. The approach of Korvin-Kroukovsky and Jacobs was based on engineering judgement and the various terms in the equations of motion derived from a somewhat arbitrary definition of the relative motion of the ship and the adjacent water particles. Even though the agreement between subsequent experiments and the Korvin-Kroukovsky and Jacobs strip theory was usually satisfactory, a major objection to the theory was that the forward speed terms in the equations of motion did not satisfy the symmetry relationship, proved by Timman and Newman[94], between the coupling terms of heave/pitch and pitch/heave. Subsequent strip theories, however, remedied this defect by satisfying the Timman and Newman symmetry relations.

In subsequent years, improvements of the problem formulation have been proposed, both from the intuitive and theoretical viewpoints. Such examples of the former and latter approaches are, respectively, the studies of Gerritsma and Beukelman[26] and Ogilvie and Tuck[76]. An important feature of these improvements was the elimination of the concept of relative motion. Instead, the total motion was derived from the linear superposition of the radiation and diffraction problem. This approach, forming the basis of current theory, postulated that the forces acting on a body oscillating under the influence of an incident wave could be regarded as the sum of those forces and moments acting on the body oscillating in still water and those acting on the restrained, or fixed, body. This approach was also adopted by Haskind[33], Hanaoka[30] and Newman[74], and is of particular importance from the experimental point of view.

The numerical computation of the hydrodynamic reactive forces (added-mass and damping), based on two-dimensional modelling, have been carried out by three different types of approach. The first and simplest was the use of conformal mapping techniques with no free-surface effects. Apart from the classical extended Joukowski transformation technique of Lewis[66], which was enhanced by Landweber and Macagno[63-64], Wendel[105] and Hwang[44] used the Schwarz-Christoffel transformation to obtain the added-mass.

The second approach, attributable to Ursell[95], is the use of a series of multipoles. Its use, in the context of Naval Hydrodynamics, was developed by Grim[28], Tasai[92-93], Porter[82] and De Jong[17]. This method, applicable only to two-dimensional domains, expresses the velocity potential in terms of a source potential at the origin and a linear combination of symmetric multipole potentials, all of which satisfy the Laplace equation and the free-surface boundary condition. A combination of these satisfies the remaining boundary conditions i.e. the radiation, bottom boundary and immersed surface kinematic conditions. The problem was originally considered by Ursell for the case of heave motions of a circular cylinder in water of infinite depth, resulting in the velocity potential being symmetric about a vertical axis through the origin. The extension of this method, to symmetric but less regular boundaries, is generally attributed to the concurrent but independent studies of Tasai[92] and Porter[82], although Grim[28] had previously considered the problem for Lewis-Form sections. In each of these approaches, Ursell's results are applied by transforming the geometry of interest onto a rectangular cylinder by means of a polynomial transformation defined by the Laurent Series. The method was extended by De Jong[17] to the

skew-symmetric problems of sway and roll by constructing the velocity potential from a dipole at the origin and a linear superposition of skew-symmetric multipole potentials satisfying the required boundary conditions. Further extensions to this technique have been made by Count[13], who generalised both the transformation algorithm and the form of the multipoles[14] to facilitate the appliance of the method to cross-sections which are non-symmetric with respect to the vertical axis, and Ursell[98] and Sayer and Ursell[87] in the case of finite depths.

The third approach is the use of source distributions over the immersed surface of the floating body. This can also be attributed to Ursell[96], although the practical use of this source distribution method was initiated by Frank[20], resulting in the fact that it is often referred to as the "Frank Close-Fit" method. (A full review of the development of this and other source distribution methods is given in section 2.3 of this chapter).

To overcome some conceptual and practical shortcomings of the strip theory, various attempts have been made to include the effects of three-dimensionality. Computations, however, indicated that improved accuracy did not necessarily result from the application of such corrections. In fact, predictions actually worsened on inclusion of the appropriate corrections. The only approach which appeared promising was that proposed by Grim[29]. Essentially a quasi three-dimensional approach, this method did not receive wide practical acceptance because of the more complicated computations required.

Attempts to calculate the fully three-dimensional hydrodynamic

properties of oscillating bodies in or below the free surface of a fluid are not new and, in fact, calculations have been made for simple geometric shapes by Havelock[38]. In addition, Kochin[57] had derived the Green's Function for three-dimensional singularities. The possibility of using a fully three-dimensional method as a practical method of calculation became possible after the famous paper by Hess and Smith[41] who proposed a computer-oriented surface distribution of sources for the numerical evaluation of potential flow around arbitrarily shaped bodies in the context of aircraft design. The development of such methods has, however, been slow due to the excessively large computer core and time requirements required for meaningful applications of the method. Available numerical results have been presented by Garrison and Chow[25], Faltinsen and Michelsen[19], who suggested an alternative formulation of the Green's Function expression, Hogben and Standing[43] and Garrison[23] who used a combination of Monacella's singularity removal method[71] and another standard form for the evaluation of the singular-integral term of the Green's Function based on the integration, term by term, of a series expansion of the expression. (Detailed reviews of these and other papers can be found in section 2.3 of this chapter).

Alternative approaches have also been made to use the Finite Element Method, derived from a variational formulation introduced by Bai and Yeung[4] for the two-dimensional case, for a three-dimensional evaluation of wave forces. In this regard, Yue, Chen and Mei[109] have performed calculations for bodies of simple geometry and have compared their results with known solutions. However, such an approach has been limited to stationary structures.

2.3 The Integral Equation Method.

The integral equation method constitutes the basis for a considerable number of computer programmes used for the numerical solution of the wave diffraction and radiation problem in hydrodynamics.

The original formulations of these problems in the form of integral equations may be attributed to John[49] and Ursell[96] permitting the way to be paved for subsequently computed numerical solutions.

Since the integral equation formulation, postulated by John, introduces the use of a Green's Function, it may be regarded as a combination of two potential theory methods. In this classic paper, any function which satisfies the governing differential equations, together with the specified conditions at the bottom and free-surface boundaries to the domain, is referred to as a "Wave Function". John's study is primarily concerned with the determination of such a function which defines the motion of the fluid from consideration of the kinematic condition on the body's immersed surface together with the far field condition. The required function is subdivided into two separate and distinct components, the first of which is termed the "primary" wave component and represents the wave motion in the absence of an obstacle. The second component defines a wave which results from the presence of the obstacle and which behaves like an outgoing progressive wave at large distances from the obstacle.

The Wave (or Green's) Function chosen behaves in such a fashion and is used with the primary wave function in the application of Green's

Theorem. More information can be provided about the components of the function by inspection of the series form of the Green's Function introduced by John who demonstrates that the second main component of the function may be represented as the sum of a "secondary" wave component and a "local" wave component. The secondary component corresponds to the first term in the series expression and satisfies the Sommerfield radiation condition whilst the local component vanishes at an infinite distance from the point of generation and is represented by the remaining terms in the series.

Having analysed the behaviour of the wave function at infinity, an integral equation formulation is arrived at by locating the singular point on the body surface and applying the kinematic body boundary condition. John showed that the subsequent solution, if it exists, is unique when the diffracting body is fixed, pierces the free-surface and has geometric properties such that no part of its immersed surface lies outside a cylinder drawn vertically downwards from the intersection of the body and the free-surface. If the body floats, however, John could only prove uniqueness at high frequencies of prescribed sinusoidal oscillation.

This particular study was carried out for three-dimensional motion resulting from the interaction of a sinusoidal wave with a bounded obstacle. It is pointed out, however, that exactly analogous uniqueness theorems can be proved for two-dimensional motions. A similar wave function decomposition is possible also, with the second wave component consisting of two further components: one which progresses in the reverse direction to the primary (incident) wave, this being the reflected component, and one which combines

with the primary wave to give the transmitted component.

With regard to the existence of a solution for the integral equation formulation pertaining to surface-piercing bodies, two complications arise. The first concerns the locus of intersection of the immersed surface of the body and the free surface at which the integral equation kernel becomes singular, rendering normal Fredholm theory invalid. This problem can only be overcome by ensuring that the body surface meets the free-surface at right-angles. The second problem arises from the fundamental assumption, involved in the application of the method to problems of Potential Theory, that the unknown potential at any point within the domain may be represented as due to a distribution of sources over the boundary of the domain. At certain incident wave frequences, termed 'irregular frequencies' by John, the integral equation has eigenfunctions, resulting in a singular solution. Each eigensolution in fact represents a non-trivial source distribution over the body surface which leaves the flow-field undisturbed. John showed that the lowest irregular frequency is $\sqrt{gD}$ (where D is the body draught) and is therefore high, and of little consequence, for shallow draughted bodies. Frank[20] showed that, even for substantially draughted bodies,the lowest irregular frequency is too high to be of any practical significance.

For many physically significant problems of potential theory, exact solutions of integral equation formulations are not available, resulting in the necessity for numerical solution techniques. Such techniques, for example those introduced by Jaswon[46] and Symm[90], are particularly valuable tools and form the basis of the Boundary Element Method. Jaswon includes a theoretical study of the

Fredholm integral equation of the first kind, performed with a view to its numerical exploitation and emphasising the value of Green's Theorem, whilst Symm details the techniques of numerical discretisation required for the solution of integral equations, some of which would not be amenable to any other treatment. The considerable flexibility of the method is demonstrated by the presentation of solutions to problems with complex domain geometries involving the use of Fredholm equations of the first and second kind together with coupled integral equations.

The previously mentioned study by John[49] is particularly thorough and the decomposition of the wave motion, the integral equation formulation and the derivation of a series form for the Green's Function, collectively form the basis of many subsequent studies of wave diffraction and radiation. However, no solutions are presented in this study.

To the best of this author's knowledge, it would appear that the first solutions evaluated for this class of problem were those obtained by Ursell[96] for a partially submerged circular cylinder. The initial integral equation formulation takes the same form as that presented by John, namely the Green's theorem, but the formulation is reduced to a representation of the required potential as a distribution of sources only, solution being subsequently obtained by an iterative procedure. It would appear that this study was motivated by the failure, for large values of the diffraction parameter, of the multipole method previously introduced by the author[95].

The earliest solutions obtained by using a discretisation procedure,

involving the subdivision of the immersed body surface into a number of elements enabling the Fredholm integral equation to be expressed in terms of a finite number of linear equations which can be solved by straightforward methods, appear to be attributable to Kim[55]. This study consisted of the numerical computation of the hydrodynamic coefficients, pertaining to the translational modes of motion, for two- and three-dimensional models. The results presented show good agreement with previously published results[82,93,95] derived largely from application of Ursell's multipole method. An interesting feature of this paper is the solution of the integral equation for a function which has no physical significance (the source strength distribution function) followed by back substitution to obtain the solution for the discretised unknown potential. The adoption of this approach, together with its subsequent popularity, is surprising since the formulation differs from that presented by John in which Green's Theorem is involved. The Green's Theorem formulation, in which the unknown potential is represented as the sum of a distribution of wave sources and double sources, yields the required solution directly without necessitating the prior solution for the source strength distribution function. As a consequence, the two methods are generally referred to as 'indirect' or 'direct' respectively. Despite the apparent drawbacks of the indirect method in comparison with the direct method of integral equaton solution, the majority of published works utilize this particular method of solution and the author is unaware of any comparative studies indicating a possible reason for this preference.

Published works making use of the indirect method of integral equation solution include Frank[20] (two-dimensional floating

bodies); Faltinsen and Michelsen[19] (three-dimensional floating bodies); Garrison and Chow[25] (three-dimensional submerged fixed bodies) and Hogben and Standing[43] (three-dimensional vertical cylinders, submerged and surface-piercing). Those making use of the direct solution method include Naftzger and Chakrabarti[72] (two-dimensional fixed horizontal cylinders) and Adee and Martin[2] (two-dimensional floating bodies).

The paper published by Frank[20] is worthy of particular mention as it appears to be the first practical application of the Source Distribution/Integral Equation method, resulting in the fact that this particular method has subsequently been referred to by Naval Architects as the 'Frank Close-Fit' method. The study consisted of the numerical computation of the hydrodynamic coefficients for a number of substantially rectangular ship sections for a practical range of values of the diffraction parameter. For computation purposes, an infinite water depth was assumed, necessitating the use of a Green's Function appropriately modified for deep water conditions. To the best of this authors knowledge, this particular study was the first to take account of the effects of varying degrees of subdivision of the immersed surface of the body with regard to the previously mentioned discretisation procedure. The criterion of subdivision employed by Frank was that the cylindrical cross sections should be closely approximated by a polygonal succession of straight line elements. The assumption was made that the source strength on each element was constant and acted at the centroid of each element. No details were given, however, of element size limits to render this assumption valid. Similarly, no account appeared to be taken of the permissable variation in lengths of adjacent elements such that the overall accuracy of solution

remained substantially unaffected.

A feature of particular interest in this study is the graphical presentation of results pertaining to incident wave frequences in the immediate vicinity of the irregular frequencies first indicated by John[49]. In addition to providing a clear illustration of the erratic behaviour of results in this vicinity, the graphical presentation suggests that the frequency related extent of the erratic behaviour is reduced by finer subdivision of the immersed surface into boundary elements. It can be seen that, even for a comparatively coarse degree of subdivision, the extent of this erratic behaviour is sufficiently localised to permit the use of graphical or numerical interpolation techniques to obtain corrected solutions within the affected region.

The papers by Hogben and Standing[43] and Hogben, Osborne and Standing[42], reporting essentially the same study, present a theoretical and experimental comparison of the vertical and horizontal forces associated with the interaction between a train of regular waves and submerged or surface-piercing vertical cylinders of various cross-sectional aspects. In similar fashion to a study previously carried out by Garrison and Chow[25] on the hydrodynamic response characteristics of bottom-seated fully submerged storage tanks, theoretical predictions were obtained from the indirect solution of a discretised integral equation resulting from a distribution of three-dimensional, finite-depth Green's Functions. This method is generally regarded as a fully three-dimensional approach in comparison with the pseudo three-dimensional approach of applying a strip-theory to the results obtained from a two-dimensional sectional analysis. It was reported by the

authors[43] that the original Green's Function expressions, derived by Wehausen and Laitone[104], exhibited erratic behavioral patterns under deep-water conditions, due to numerical shortcomings. As a consequence, an interesting modification was made to the original expressions resulting in a reported improvement in deep-water behaviour. (A similar modification is made to the corresponding two-dimensional expression used in this study. Full details can be found in Appendix A2.3 of this thesis). It must be concluded that the modification, together with the overall approach, was satisfactory since the numerical results presented agree exactly with those computed from the closed-form series technique introduced by MacCamy and Fuchs[68] for the case of vertical surface-piercing circular cylinders.

Agreement between numerical predictions and experimental measurement was generally good with the exception of those pertaining to a submerged cylinder, the top of which was in close proximity to the free-surface. The authors attribute this discrepancy to a violation of linear boundary conditions incurred by the breaking of waves over the top of the cylinder.

It is generally accepted that satisfactory numerical solutions for sharp-cornered bodies may only be obtained if a degree of "rounding" is applied to the corners of the mathematical model prior to discretisation, subject to the geometric and inertial properties of the model remaining substantially unchanged by the procedure. This is partly attributable to the fact that John's existence proof (mentioned earlier in this section) did not extend to bodies with sharp corners but was restricted to bodies with smooth 'Lyapunov' type immersed surface aspects. It is mainly attributable, however,

to the fact that an inability to define the outward normal vector at a corner results in a discontinuous source strength distribution function, at this point, with its associated numerical inaccuracies. Hess and Smith[41] treat this matter in some detail in the proposal of a source distribution method developed by them to compute the potential flow around bodies of arbitrary shape in the context of aircraft design. This approach was extended by Hogben *et al.* to the context of the hydrodynamic problem. As a consequence, several recommendations were propounded by them in respect of the subdivision of an immersed three-dimensional surface into discrete boundary elements. (These are dealt with in detail in Appendix A5 of this thesis).

It must be said however that, notwithstanding any numerical improvements achieved by this rounding technique, the validity of theoretical predictions for sharp-cornered bodies, in a physical sense, is somewhat questionable as a consequence of non-linear viscous flow separation induced by the sharp corners under certain conditions.

A fundamental assumption made, to permit the straightforward discretised numerical solution of the Fredholm integral equation, is that the source strength may be regarded as constant over the extent of any given boundary element, resulting in the use of an equivalent point source acting at the element centroid. This was investigated in some detail by Hess and Smith who concluded that the assumption was valid for field and source point separations greater than four element diameters but for smaller separations, the source should be represented as a combination of sources and quadripoles. Subsequent authors have, in fact, relaxed this requirement having

found it sufficient to assume a point source throughout, except when considering the influence of an element at its own centroid. Lacey[61] investigated the effect of assuming a higher order (linear and quadratic) source strength distribution on individual elements of a submerged horizontal cylinder using two-dimensional modelling. Inspection of the results presented indicates than any improvement to be gained from the use of higher order source strength distributions is insignificant for any practical purposes. The author is, however, unaware of any similar investigations pertaining to floating bodies and is therefore unable to comment on the use of higher order distributions in this context.

Hess and Smith proposed that, in order to avoid the inherent singular behaviour of the Green's Function expression when the field point approaches the source point along the immersed surface boundary, the influence of a source element at its own centroid could be approximated by assuming the source to be uniformly distributed over the element rather than concentrated at the element centroid. Hogben *et al.*[43] considered this matter in some detail and formulated a limiting value of the Green's Function expressions when field and source point coincide on a three-dimensional boundary. (Such a formulation has been adapted for the two-dimensional case and can be found in Appendix A3 of this thesis.)

As outlined above, two of the major numerical problems associated with the use of a source distribution boundary coincident with the obstacle boundary are the occurrence of irregular frequencies together with the logarithmic singularities contained within the Green's Function expressions. The problem of irregular frequencies

occurs only in the case of surface-piercing bodies but the problem of logarithmic singularities is inherent to all obstacles whether surface-piercing or not. Both of these problems, however, can be overcome by the use of an auxiliary or fictitious boundary which is distinct from the boundary of the domain.

The first use of a separate source distribution boundary would appear to be Oliveira[77]. The author of this study classifies the method as an integral equation method but presents the theory as a matrix equation derived from the linear superposition of independent elementary solutions. Initial testing of this method with various locations of the source distribution boundary indicated a degree of failure in cases of substantial separation of source and domain boundary. The author's application of the method to several problems, together with his comparisons with solutions obtained by other methods, demonstrated that improved accuracy could be achieved by the use of an auxiliary source distribution boundary which was located sufficiently remote from the domain boundary to remove the effects of the logarithmic singularities.

The use of auxiliary source distribution boundaries, in the context of the numerical solution of hydrodynamic problems, has been studied in some depth by Coates[12] and Lacey[61]. Coates investigated the effect on three-dimensional problems by a numerical and experimental study of the forces acting on vertical surface-piercing cylinders, whilst Lacey carried out a largely numerical study on the interaction between regular waves and a submerged, fixed horizontal circular cylinder, the former study using three-dimensional modelling and the latter using two-dimensional modelling. Both authors found that a considerable improvement in results could be

achieved by using a boundary separation of sufficient magnitude to remove the effect of the singular kernel of the integral equation but not sufficiently great to incur ill-conditioning effects in the resultant matrix equation. Lacey found that the most accurate results could be obtained by using an internal source distribution boundary separated from the cylinder boundary by a distance equal to 30% of the cylinder radius. The results presented by Lacey demonstrate quite conclusively that, in the case of a fully submerged fixed horizontal cylinder, the regular kernel method (separated boundaries) was significantly more efficient than the singular kernel method (coincident boundaries) in that, under a given set of conditions, progressively finer subdivision of the boundaries resulted in a more rapid convergence to the correct result using the regular kernel method with, according to the author, no significant indication of matrix ill-conditioning.

It has previously been stated that the ability to achieve a reasonably straightforward discretised solution to the integral equation depends on the assumption that the source strength remains constant over the extent of any given boundary element. It is similarly assumed that the element distribution is such that the value of the Green's Function remains reasonably constant over any given boundary element. The analysis of any body having areas of high curvature necessitates a sufficiently high concentration of elements in those areas to permit accurate modelling of the body geometry. This results in a similarity of magnitude of the Green's Function on adjacent elements. This, in turn, leads to a distinct lack of diagonal dominance in the matrices used in the discretised solution technique, giving rise to ill-conditioning and consequent loss of numerical stability. It is the opinion of this author that

the use of an internal auxiliary boundary in the analysis of such bodies will exacerbate the situation and that any increase of computational efficiency to be gained from such use will be significantly outweighed by inaccuracies arising from matrix ill-conditioning. As a consequence, it is felt that the use of auxiliary boundaries in such cases is not advisable.

Three comparatively recent studies by Hearn and Donati[39], Eatock Taylor[18] and Hearn, Donati and Mahendran[40] indicate that, notwithstanding the fact that a considerable number of studies have been carried out using the Green's Function/Integral Equation method of analysis, there are still subsidiary topics which demand a more detailed consideration if the method is to be applied efficiently and reliably. In particular, it has been shown that the application of the method to the design of offshore structures is not necessarily straightforward and requires an appreciation of the effects of different discretisation schemes.

In this regard the paper by Hearn and Donati, together with the subsequent paper of Hearn, Donati and Mahendran, both merit further review since they concern the application of the Boundary Element Integral Equation method to solve the hydrodynamic problem for various bodies in motion.

It is stated that the first of these papers was prepared with the intention of making sea-keeping theories more comprehensive to the practicing Naval Architect and, taken with the second paper which presents the results of analyses peformed in preparation for an experimental study of wave energy devices, demonstrates that the application of the three-dimensional integral equation formulation,

and the two-dimensional formulation in conjunction with Strip Theory, is not a straightforward process.

The first paper, reporting the application of the method to a warship and a merchant vessel, is particularly concerned with the problems of numerical stability. It is noted that different results may be obtained by different discretisations due either to possible improvements in the geometrical representation of the body or to the improved numerical stability of the system of algebraic equations. It is also noted that particular discretisations may prove to be more acceptable to some motions than to others. The problem of irregular frequencies is also identified by the onset of numerical instability, but this cannot be avoided by improvement of the discretisation, since it is an inherent feature of the analysis of surface-piercing bodies using this method.

The second paper includes a hydrodynamic analysis of two floating structures: a rigid body form of the Lancaster Flexible Bag and an articulated Cockerell Raft system. Results for the rigid structure, which has a simple geometry, confirm several simple facts pertaining to the relationship between discretisation and numerical instability. The analysis of the articulated system, however, resulted in considerable numerical instability due to discretisation problems in the vicinity of the hinge. Owing to the fact that the complete analysis of the articulated structure requires that all possible configurations of the raft system are considered, the three-dimensional programme was extended to permit simultaneous solution of twenty radiation and ten diffraction problems. An interactive computational analysis was devised to enable failures to be identified and to permit subsequent introduction of modifications

to the discretisation. In this manner, it was established that satisfactory predictions could only be achieved by a detailed discretisation, thus demonstrating that proper application of the method is by no means straightforward and requires not only an appreciation of the effects of discretisation schemes but also a greater understanding of the sources of numerical instability.

The problems of wave hydrodynamics have also been solved using the application of Green's identity formula to a distribution of simple and double sources over the entire boundary of the fluid domain.

The first application of this method, initiated by Jaswon[46] and Symm[90], to free-surface problems where the free-surface extends to infinity, was reported by Bai and Yeung[4]. The method entails the use of an integral equation with the unknown function being the potential along the entire fluid boundary. An alternative scheme, to deal with the case of an infinitely deep fluid, was also presented. The authors considered the case of oscillating cylinders in the free surface of a finite and infinite depth fluid for which they computed the hydrodynamic coefficients. The results presented agree excellently with results obtained by the more conventional methods[51,65,97]. It was noted that, in the case of a finite depth fluid, the computation time involved was approximately the same as that required for the conventional Green's Function method but that, for a fluid of infinite depth, the computation time was around five times as long.

The use of a source distribution over the whole boundary of the fluid domain permits consideration of fluid domains with any bottom configuration, a feature which is not amenable to analysis using the

Green's Function formulation. Despite this significant advantage, however, together with the fact that this method overcomes the 'irregular frequency' problem, this approach has not been widely used in subsequent studies. Exceptions to this are the study of wave interaction with large submerged structures by Bird and Shepherd[9] and the study of the interaction of waves with elastically moored floating breakwaters by Yamamoto, Yoshida and Ijima[107].

It is pertinent to review the paper by Yamamoto *et al.* since it reports a study which is similar in many ways to that which is reported in this thesis. The study entailed the theoretical and experimental investigation of the body motions and transmission characteristics associated with the interaction between a train of regular waves and an elastically moored floating breakwater. Two-dimensional mathematical modelling was used.

Despite the previously cited advantage that the source and doublet distribution method may be used in the analysis of arbitrarily shaped domains, since a source distribution is considered over the entire boundary of the fluid domain, there is one major disadvantage associated with its use. In order to solve the far-field radiation condition, imaginary vertical domain boundaries must be considered at large distances from the obstacle/fluid interface. Since the entire fluid boundary is considered, this procedure results in a prohibitively large number of source points on the sub-divided free-surface. This problem was overcome by the assumption that the scattered wave, normally represented by an infinite series of scattered wave terms, decays exponentially with increasing distance from the obstacle and thus becomes insignificant at a comparatively

small distance from the obstacle/wave interface i.e. the point of generation of the scattered wave. At distances greater than this, it was assumed that the wave profile consisted of transmitted and reflected components only, the potential of which was analagous to the standard expression derived from linear theory. A series of numerical tests enabled the authors to conclude that, provided the imaginary vertical domain boundaries were located at distances in excess of one incident wavelength from the obstacle/wave interface, the error associated with the solution could be limited to the order of 1-3%. Using two-dimensional modelling with a linear element length of the order of 1/20 of the incident wave length, a series of numerical evaluations were carried out and compared with previously published data for the case of a fixed cylinder[16], a fixed rectangular cylinder[10] and a moored rectangular cylinder[45]. The authors report excellent agreement in all cases, although no graphical or numerical comparison is presented.

In a brief review of the analysis of hydrodynamic loading on offshore structures by boundary element methods, Eatock-Taylor[18] details how the integral equation method may be used in conjunction with the Finite Element method. This method is variously called the "Boundary Element Coupled Method" and the "Hybrid Element Method".

The Finite Element Method, on account of its consideration of the whole fluid domain, is particularly well suited to compact, closed domains with complicated geometries. However, there are certain difficulties, both numerical and computational, associated with the use of this method in the analysis of exterior problems in which part of the domain extends to infinity. The Green's Function

Integral Equation method, however, is ideally suited to such problems since the boundary conditions at infinity are automatically satisfied. It is therfore suggested that the Hybrid Element method combines the advantages of both the aforementioned methods. Another cited advantage is that careful choice of the dimensions of the interior domain, in which the Finite Element Method is used, eliminates the problem of the previously mentioned irregular frequencies.

2.4 Experimental Validation of Theory.

The linear potential theory formulation of wave scattering and radiation problems is well established and solutions may be obtained by a variety of methods, both numerical and analytic, enabling predictions to be made with regard to the wave reaction and body response characteristic associated with the interaction of an incident wave system with an obstacle inserted therein.

If the various theoretical models are to be of subsequent practical use, the validity of the theory must be established by comparison with experimental measurements for a comprehensive and exhaustive range of problems. The various features which distinguish the different problems are, for example, whether the object is fixed or in motion, whether it is entirely submerged or surface-piercing and whether the modelling is two- or three-dimensional.

At this stage, two important points must be emphasised with regard to comparison between theory and experiment for validatory purposes. The first point concerns the range of parameters and conditions over

which theoretical predictions have been compared with experimental measurements. Validation of theory under one particular set of conditions does not necessarily guarantee validity under other related but essentially different conditions. This is particularly true if the presence of non-linear effects is suspected. The second and equally important point is that, if a set of experiments is designed and undertaken with a view to validation of a particular theoretical model, the experimental conditions must be such that no substantial violations are incurred with respect to the boundary value problem as posed. (As an example of this, Sarpkaya and Isaacson[85] recommend that, if linear wave theory is to be validated by experiment, incident wave heights should be chosen such that higher order components of velocity potential are at least one order of magnitude smaller than the fundamental velocity potential component). Such experiments[15] may be distinguished from others[61,99] in which the physical conditions are purposely chosen to violate those upon which simplified linear theory is based. In the absence of any general and complete higher order theory for wave/obstacle interaction, such studies are of value in determining the limits of validity of linear theory.

Before considering in detail the available experimental studies which most closely resemble the study reported in this thesis, a number of additional studies may be mentioned which are concerned with the validation, by experiment, of potential theory as pertaining to wave/obstacle interaction.

Several experimental studies have been carried out to determine whether linear diffraction theory provides satisfactory predictions for the horizontal force on a surface-piercing vertical circular

cylinder. To the best of this authors knowledge, the most recent publications in which these studies have been reviewed are Sarpkaya and Isaacson[86], Coates[12] and Lacey[61].

In the case of the vertical circular cylinder, it is generally accepted[43,86] that diffraction effects become significant when the cylinder diameter is greater than one fifth of the incident wavelength. Examination of the force results of Hogben and Standing[43] and Mogridge and Jamieson[70], reproduced by Sarpkaya and Isaacson for comparative purposes, indicate that the experimental results obtained for the interaction between a train of regular waves and a vertical cylinder agree excellently with theoretical predictions in regions where pure inertial forces dominate. However, in regions where diffraction effects become significant, a noticeable departure from theory occurs. Both sets of experimental results demonstrate, with a degree of consistency, that this departure occurs at a value of the cylinder diameter/wavelength ratio of approximately 0.24. This departure is of great significance if the use of linear theory is proposed for problems in which diffraction effects dominate. However, it must be noted that in the majority of studies carried out in the diffraction regime, the actual force measurements observed are significantly less than those predicted by linear theory. Hogben *et al.* consider this to be reassuring from the point of view of the designer.

Coates observed that measurements of pressure distribution demonstrate less satisfactory agreement with theoretical predictions than do force measurements. Hogben *et al.* suggest that this may be attributable to the presence of certain non-linear second harmonic pressure fluctuations which do not decay in the usual way with

depth. They also draw attention to the incurrence of spurious temperature effects when measuring pressure fluctuations.

One further feature, identified by Sarpkaya and Isaacson in their review, is that the bulk of the data has been obtained for waves of small steepness where the effects of wave non-linearity are not expected to be significant. They suggest that the available evidence therefore provides sufficient justification for the confident use of linear theory to provide solutions to problems of this nature. No indication is given, however, of the suitability of linear modelling for defining the interaction of the obstacle and the steeper waves which would be encountered under realistic ocean conditions. Garrison[24] suggests an upper limit of unity for the ratio of wave height to cylinder diameter, beyond which the effects of non-linear viscous forces dominate.

A study of particular importance, with regard to the validity of linear theory, was that carried out by Salvasen[83] concerning the generation of waves by a fixed two-dimensional obstacle in steady flow conditions. The results obtained show that linear theory gives a poor representation of wave/obstacle interaction, for a small depth of obstacle submergence, due to non-linear effects. These findings serve to illustrate the necessity for further investigation of interaction problems pertaining to obstacles in or just below the free-surface.

A study of similar relevance was carried out by Dean and Ursell[15] who investigated the forces and wave effects resulting from the interaction between a semi-immersed horizontal cylinder and a train of regular waves, using two-dimensional modelling. This study can be

considered in two parts, the first of which consists of a comparison between the experimentally measured vertical and horizontal force components with those predicted by theory, and the second of which consists of a comparison between the theoretically predicted diffracted wave form and that experimentally measured. The parameters chosen to indicate the form of the diffracted wave were the far-field reflection and transmission characteristics of the body. In both aforementioned parts, the theoretical predictions were obtained by the application of the multipole method, first introduced by Ursell[95] and detailed in section 2.3 of this chapter, and the study was carried out using waves of small steepness to comply with the conditions imposed by linear theory.

The experimental measurement of the force components demonstrated good agreement with theoretical predictions, the average error being approximately 6%, but the measurement of the diffracted wave profile showed less satisfactory agreement, the average error being about 12%. The fact that this error was largely applicable to the reflection coefficients, the transmission coefficients showing acceptable agreement between theory and experiment, led the authors to conclude that a loss of energy was associated with the wave reflection process. Two suggested reasons were given for this lack of agreement, the first of which was the reported presence of observable second harmonics in the wave train. The authors concluded that this was a feasible source of error since the subsequent use of a surface baffle at the nodal points of the combined wave profile led to a significant improvement in agreement. The second suggested reason for the measured reflection coefficents being significantly less than those predicted by theory was the possibility of vorticity in the wave reflection process although no

evidence, in the form of a report of noticeable vortex shedding, was presented to support this suggestion.

An equally feasible reason for the discrepancy, in the opinion of this author, arises from the examination of the wave profile analysis technique employed in the study. Wave amplitude measurements were recorded at regular intervals along the experimental flume and analysis of the resultant envelope permitted resolution of the overall profile into positive (incident and transmitted) and negative (reflected) components with respect to the direction of travel. A fundamental assumption made in this regard is that the amplitude envelope exhibits a sinusoidal variation with respect to length along the experimental flume. As a consequence,the maxiumum value of the sinusoid can be regarded as the sum of the positive and negative components while the minimum value of the sinusoid represents the numerical difference between the two component amplitudes. The two resulting equations permit resolution of the two unknown components. It must be pointed out, however, that this assumption is only valid if the negative component is small in comparison to the positive component. Such a condition invariably pertains to the downstream wave profile since the use of an efficient energy absorbing beach ensures that the beach reflected component is small in comparison to the component transmited by the body. This, however, is not always the case with the upstream profile since the body reflected wave is very often of a comparable order of magnitude to the incident wave, thus rendering the assumption invalid. In this case, accurate component resolution can only be achieved by analysis of the sinusoidal variation of the amplitude squares with respect to the position along the flume, the maximum and minimum values being the sum and difference respectively

of the squares of the amplitudes of the positive and negative wave components. A brief mathematical exercise shows that, in the case of comparable magnitude components, the amplitude variation is a root sine curve with a smooth crest and sharp trough. It is the experience of this author that an *a priori* assumption of sinusoidal amplitude variation leads to an overestimation of the minimum value of the envelope resulting in a significant underestimation of the negative (reflected) component. This sugestion for a possible source of error is reinforced by the fact that the most significant departure from theory occurred under conditions of high body reflectance.

The study by Dean and Ursell was repeated comparatively recently by Martin and Dixon[69] but was extended to give an indication of the variation of experimental values with wave steepness. The force measurements obtained in this study exhibited satisfactory agreement with theoretical predictions in the case of waves of small steepness but significant departure from theory occurred with waves of increasing steepness. As with the previous study, the measured reflection coefficients were significantly different from those predicted by theory in the case of small steepness waves. Interestingly though, the magnitude of the discrepancy did not exhibit any systematic variation with waves of increasing steepness as would reasonably be expected.

An extensive study was carried out by Lacey[61] to investigate the limits of validity of linear theory with regard to a horizontal circular cylinder located at various depths below the surface of a train of regular waves. To this end, the parameters measured experimentally were the pressure distribution on the obstacle

boundary and the induced wave characteristics. In order to investigate the significance of non-linear effects, the behaviour of the parameters was studied for waves of increasing steepness such that linear boundary conditions were purposely violated. The theoretical predictions were obtained from the use of the indirect method of solution of the source strength distribution formulation employing two-dimensional Green's Functions.

The experimental results pertaining to the body reflection and transmission characteristics are of particular interest since they exhibit deviations from theory which are at total variance with those obtained from the two previously cited studies. In these studies the major deviation from theory occurred with the reflected wave component, the transmitted component agreeing satisfactorily with theoretical prediction. In the study by Lacey, however, the measured reflected wave components agree well with theory but the measured amplitude of the transmitted wave was significantly less than that predicted by theory. Lacey concluded that this was due to a significant loss of energy in the process of wave/obstacle interaction, possibly attributable to viscous separation, which was largely dissipated in the transmitted wave. This loss of energy, obtained from consideration of the relative amplitudes of the reflected and transmitted waves, was found to be approximately 7% for incident waves of small amplitude, but increased to the order of 20% for waves of maximum steepness H/L = 0.08.

The experimental measurements of the pressure distribution on the obstacle boundary were generally in good agreement with theoretical predictions, the maximum deviation being approximately 5%, with the exception of those pertaining to locations near the free-surface.

The author concluded that this could be attributable to localised high particle velocities in the shallow water region immediately above the obstacle, leading to abnormally high pressures in this region. In general, the discrepancy between theory and experiment increased significantly with increasing wave steepness and also with increasing values of the diffraction parameter thereby demonstrating the need for further investigation, not only in regions where diffraction effects are dominant, but also under conditions where non-linear effects become significant.

Having detailed and discussed those experimental studies pertaining to the interaction between waves and fixed obstacles, consideration must now be given to studies which involve an experimental investigation of the interaction between waves and obstacles with one or more motional degrees of freedom. Such studies may be classified according to two sub-groups: those in which a forced motion is applied to the body and those in which the body is freely floating or, at most, partially restrained in one or more of the motional modes.

The experimental study carried out by Ursell, Dean and Yu[99] is reported to be the first confirmation of the validity of linear wave theory for forced motions of a body in otherwise still water. The theoretical formulation of the wave motion due to a piston-type wavemaker, introduced by Havelock[35], expresses the velocity potential in the form of a localised wave, which vanishes at a distance of the few wavelengths from the wavemaker, and a constant amplitude harmonic wave travelling away from the wavemaker. The experimental procedure, designed to simulate a longitudinally infinite fluid domain by means of complete energy absorbtion by

beaches at either end of the experimental wave flume, was used in two separate sets of experiments. The first set of experiments entailed the generation and measurement of waves of small steepness to comply with linear theory boundary conditions. The results from this set of experiments show good agreement with theory in that the measured heights of the generated waves differed from theoretical predictions by 3-4% at most. The second set of experiments, however, were specifically designed to violate linear conditions by generating waves of a steepness in excess of that which would be acceptable to small amplitude wave theory, the intention being to establish the importance of wave steepness in this regard. The measured heights of the generated waves exhibited a significant and, more importantly, systematic deviation from theory, the experimental values being around 10% smaller than theoretical predictions. The authors conclude that this confirms the validity of small amplitude wave theory.

The study carried out by Yu and Ursell[108], regarded by the authors as a sequel to the previously cited study and of greater practical significance, compares theoretical and experimental amplitudes of surface waves generated by the forced heaving oscillation of a circular cylinder in water of constant finite depth. Theoretical predictions were obtained from an extension of Ursell's multipole method to the case of waves in water of finite depth. The experimental technique of wave profile analysis was identical to that employed by Dean and Ursell and was considered by the authors to completely eliminate the effect of reflections from the vertical end beaches. It was suggested that this technique, despite being more elaborate than that used by Ursell *et al.*[99], was more effective and would result in the accurate evaluation of the

generated wave amplitude that would have been observed in a wave flume of infinite length. The results presented show good agreement between theory and experiment, the experimental measurements being generally lower than theoretical predictions by about 3%. A noticeable feature of the results, however, was the increase in magnitude of the discrepancy with increasing values of the diffraction parameter suggesting perhaps, as with previous studies, certain doubts as to the applicability of linear theory to diffraction regimes. Notwithstanding these discrepancies, however, the results of the investigations under differing depth conditions gave a good indication of the importance of finite depth effects with regard to generated wave heights.

To the best of this authors knowledge, the first comprehensive study of the effects of forced translatory and rotational oscillations of a body in water of finite depth was that carried out by Vugts[101]. This study consisted of a comparison between theory and experiment of hydrodynamic coefficients, exciting forces and generated wave amplitudes pertaining to cylinders of various cross-section using two-dimensional modelling. The various cross-sections used were Lewis-Form, triangular, circular and rectangular and the theoretical predictions were obtained by the multipole method, introduced by Ursell for the specific case of heaving circular cylinders and extended by De Jong[17] for the non-symmetric sway and roll modes of motion. The theoretical predictions of the hydrodynamic coefficients were computed for a semi-circular immersed profile and subsequently transformed to those pertaining to other aspects by the use of conformal mapping techniques. A similar procedure was adopted to compute the generated wave amplitudes. The formulation of Newman[73], relating the exciting forces acting on an axisymmetric

body to damping coefficients and the far-field potential by consideration of the Haskind Relations, was applied to compute the theoretical predictions of the exciting force components.

The experimental technique employed was to provide a forced sinusoidal oscillation to the cylinder in each of the three modes of motion pertaining to two-dimensional modelling. Consideration of the measured in-phase and quadrature components of the applied force, in conjunction with the measured amplitude of motion, enabled the evaluation of the hydrodynamic coefficients from the equations of motion. Insertion of these parameters into Newman's formulation, together with the measured amplitude of the generated waves, permitted evaluation of the exciting force components. (A more detailed review of this study, including a comparison of the theoretical and experimental results with those obtained from the Source Strength/Integral Equation formulation, can be found in section 4.10 of this thesis).

A feature of the presented results which merits particular mention is the considerable discrepancy between theory and experiment of the damping and coupled damping parameters associated with the roll mode of motion. Examination of the graphical results presented in this regard shows that the magnitude of the discrepancy increases systematically with increasing frequency and amplitude of motion. It is of particular interest to observe that the discrepancy is most pronounced in the case of immersed profiles with sharp corners, such as the triangular and rectangular aspects. The author suggested that this discrepancy could possibly be attributable to the effects of viscosity both with regard to skin friction and vortex shedding resulting from flow separation at the sharp corners. An empirical

expression was proposed, defining the consequent correction to the roll damping parameters as being a function of the frequency and amplitude of motion. Owing to the constant amplitude of the forced motion in each set of experiments, this implies that the required correction factor is a function of the velocity of motion of the body and that the empirical coefficients used in the expression are functions of the viscosity of the fluid and the body geometry.

A subsequent study of the motions of a freely floating body carried out by Vugts[102], the results of which are presented by Wehausen[103] in a review of the paper, shows that the effects of viscous roll damping only become significant at the natural frequency of roll motion of the body, when a relatively small correction to the potential damping term in the equations of motion results in a comparatively large reduction in resonant roll amplitude. A similar review of this study, carried out by Salvasen, Tuck and Faltinsen[84], reports the use by Vugts of a quasi-linear correction to the roll damping terms in the equations of motion. Such a correction factor, derived from expressions postulated by Kato[50] for skin friction and by Tanaka[91] for eddy-making resistance, is a function of the maximum roll velocity of the body extremities, the frequency of motion, the fluid viscosity and the body geometry.

The results presented in the above reviews demonstrate that acceptable agreement, between theory and actuality, can only be achieved in the vicinity of the system resonant frequency if the effects of viscosity are accounted for in the theoretical computation procedure.

A similarly comprehensive study was carried out some years later by Keuning and Beukelman[52] who experimentally measured the hydrodynamic coefficients of a rectangular pontoon, of immersed surface aspect ratio (Length/Draught) of 4.2, in shallow water using forced oscillation techniques. The reason for this study, according to the authors, was the absence of experimental results pertaining to such small draught sections from forced oscillation tests in shallow water.

The experimental procedure entailed the application of a forced oscillatory motion, in all six directional modes associated with three-dimensional modelling, to the body and subsequent evaluation of the hydrodynamic coefficients using the same technique as previously discussed with reference to Vugts' study. Of particular interest was the fact that similar sets of experiments were carried out at various flume depths to investigate the effect of still water depth on added-mass and damping. In addition, the amplitude of forced motion was varied to provide a check on the limits of validity of linear theory with regard to wave steepness.

The theoretical predictions of the hydrodynamic coefficients were obtained by several methods according to the particular flume depth used. For deeper water (flume depth/body draught = 4.55) the authors used the multipole method (c.f. Vugts[101]) and the Frank Close-Fit method. In both cases, infinite depth conditions were assumed since the authors considered that bottom effects would be negligible and could, consequently, be ignored. This assumption is, perhaps, a little surprising in view of the results presented by Kim[53] which clearly demonstrated the effect of finite depth on added-mass, particularly at low frequency. For shallow water

(flume depth/body draught = 1.2;1.75) the method used was that introduced by Kiel[51]. This method is basically an extension of Ursell's multipole method, extended by De Jong[17] for the case of finite depth and further extended by Kiel for the specific case of rectangular bodies in shallow depth water. In all cases, sectional parameters were computed using two-dimensional modelling, followed by the application of Strip Theory to evaluate the equivalent three-dimensional parameters, thus making the study of particular relevance to the investigation detailed herein. The results presented clearly illustrate the influence of water depth on the hydrodynamic parameters, particularly in the case of heave motion. A similar comment can be made with regard to the dependence of translatory hydrodynamic parameters on the amplitude of forced oscillation. This is particularly evident in the case of heave damping. The authors conclude that, since this latter dependence increases with increasing frequency, viscosity effects are the most likely cause. This conclusion is further supported by their report of observable vortex shedding from the sharp corners at high frequencies of oscillation. Unfortunately, no reliable experimental results are presented for roll motion owing to a reported combination of equipment malfunction and an apparent inability to ensure that the axis of rotation of the body in this mode passed through the body centroid in compliance with the linearised equations of motion.

Comparison between theory and experiment was generally good in the case of deep water. However, a substantial deviation from theory was exhibited with regard to the added-mass at low frequency, possibly attributable to the neglect of finite depth effects as discussed previously. The suggested influence of viscous effects is

demonstrated by a degree of deviation from theory of the heave damping coefficient at high frequency, the experimentally measured damping being substantially greater than that predicted by theory. In shallow water conditions, however, agreement was significantly poorer than in deep water conditions, particularly in the case of low frequency damping. Unfortunately, no explanation is offered for this discrepancy, perhaps emphasising the need for further examination of the shallow depth problem.

In a subsequent discussion of this study, two important points were mentioned, both pertaining to the influence of viscous damping effects. In reply to a suggestion[100] that lack of structural rigidity in the experimental apparatus might be a cause of the reported deviation of high frequency damping from theory, the authors re-stated their conviction that viscous damping effects were responsible, particularly in view of the observed vortex shedding from unradiussed edges. The authors reported that subsequent re-calculation of the heave damping results on the basis of constant velocity (decreasing amplitude of motion with increasing frequency of oscillation) yielded a more-or-less constant difference between the theoretically predicted potential damping and the experimentally measured damping, thus confirming the effect of viscous damping. In the course of this discussion, it was pointed out by Patel[80] that the results of a study[79], carried out by him to investigate the effect of vortex shedding by bodies in oscillatory flow, indicated that a slight rounding of submerged edges was sufficient to significantly reduce the effect of vortex shedding such that experimental damping agreed satisfactorily with the values predicted by potential theory. The authors concurred with this finding but suggested that a determination of the submerged edge radius

influence at model scale was of questionable value due to scale effects.

For comparative purposes, it is worthwhile to mention at this point the experimental study carried out by Faltinsen and Michelsen[19] in which a forced oscillation technique was used to experimentally measure the exciting forces and hydrodynamic coefficients pertaining to a floating rectangular box. The appropriate theoretical predictions were obtained by two methods, both of which utilised an indirect solution of the Green's Function/Source Distribution formulation for the case of infinite depth.

The first method entailed the computation of sectional parameters, using the two-dimensional Frank Close-Fit method, in combination with the strip theory introduced by Salvesen *et al.*[84] as an extension of the theory first postulated by Korvin-Kroukovsky and Jacobs[58]. The strips were oriented in a lengthwise direction in a similar fashion to the procedure of Kim and Chou[54] who, it is reported by the authors, obtained satisfactory results for the prediction of motions of a barge with length/beam ratio equal to 1.5.

The second method entailed the use of a three-dimensional Green's Function Source Distribution technique, similar in formulation to that used by Hogben *et al.*[42,43] for the study of wave forces acting on a vertical cylinder. An interesting feature of the formulation used in this study was the authors' modification of the standard form of the three-dimensional Green's Function expression as defined by Wehausen and Laitone[104]. The particular value integrand in the integral form of the Green's Function expression

was converted from an infinite to a finite integral by making use of an alternative representation of the Bessel Functions, contained therein, in conjunction with the use of the exponential integral as defined by Abramovitz and Stegun[1]. However, in view of the fact that the integral form of the Green's Function is used only in cases of small source point/field point separations (see section 4.7.3 of this thesis), it must be suggested that this modification is of limited validity in the context of accuracy of results and computational effort.

A surprising aspect of both methods of solution was the disregard of the Haskind Relations in the process of computing the exciting force, thus necessitating additional computational effort to compute the scattered wave potential, a parameter of no relevance to the investigation. No explanation is given for this procedure.

A series of numerical tests was carried out to investigate the sensitivity of the three-dimensional source distribution formulation to progressively finer sub-division of the immersed body surface into boundary elements. With the exception of the parameters pertaining to the rotational modes of motion, the results presented exhibit very little sensitivity to the source distribution density. However, no meaningful numerical conclusion can be drawn from this behaviour since no details are given, other than the overall number of elements, of the nature of element distribution in the vicinity of sharp corners etc. A considerable discrepancy is evident, however, between the theoretical predictions obtained from the three-dimensional source distribution method and those derived from the application of Strip Theory to the two-dimensional section parameters. Since the experimental results, in general, agree well

with those using the former method, the authors conclude that satisfactory analysis is not possible from the use of a two-dimensional approach in conjunction with Strip Theory. This is a particularly interesting conclusion in view of that reached by the authors of the previously cited paper, and only serves to emphasise the need for further investigation in this regard.

There finally remains to be considered experiments with freely floating bodies. Compared to the number of experimental studies carried out using the technique of forced oscillation, there have been comparatively few studies on the behaviour of freely floating bodies. Apart from the comprehensive investigation carried out by Vugts[102], reviews of which have been made by many authors, two comparatively recent studies which merit particular attention, in that they closely resemble the experimental investigation reported in this thesis, are those carried out by Yamamoto, Yoshida and Ijima[107] and Yamamoto[106]. Despite the fact that these two studies are classified as pertaining to "freely floating bodies", it must be said that this classification is slightly erroneous since the investigations were carried out on the motions and wave effects associated with elastically moored floating breakwaters under the influence of water waves.

The first of these studies entailed a comparison between theory and experiment of the transmission characteristics and body motions of a circular and a rectangular floating breakwater in a train of regular waves. Two-dimensional modelling was used to enable theoretical prediction of these parameters by the source and doublet distribution technique described in the previous section of this chapter. Strip Theory was not used in this case since the

transverse width of the breakwater closely matched the experimental flume width to accurately simulate the two-dimensional flow condition. The effect of the elastic mooring forces is accounted for by the inclusion of the spring constants in the equations of motion in a similar way to that detailed in Appendix A4.6 of this thesis. However, owing to the fact that the moorings were oblique, thus exerting restraining forces in a horizontal and vertical direction, accurate measurements were required for the initial tension in the spring moorings at equilibrium. This differs from the formulation contained herein in which only symmetrical horizontal restraint is imposed, thus avoiding the necessity of initial spring tension measurement.

The results presented, for the heave and surge motion of the body together with measured transmission coefficients, demonstrate excellent agreement between theory and experiment in the case of the partially immersed circular breakwater. However, some deviation is exhibited in the case of the rectangular section. This is particularly pronounced with regard to the heave motion and transmission coefficient in the region of the system's natural frequency. The authors attribute this, quite reasonably, to the damping out of the heaving motion of the breakwater by viscous flow separation at the sharp submerged edges. This conclusion is reinforced by the fact that no such deviation is evident in the case of the circular section breakwater.

A noticeable feature of the experimental procedure detailed in this paper is the fact that measurements were taken during the first two or three cycles of wave motion. According to the authors, this procedure was adopted because the breakwater system was observed to

settle down to a steady harmonic motion almost immediately. It is the experience of this author, from tests carried out in the course of the present study, that such quick settling down is most definitely not the case, particularly in instances of high body reflection. Depending on the degree of reflection from the floating body and the degree of reflectance of the wave generator, it was found that steady state conditions were not reached until the reflected wave front had sufficient time to travel at least three times along the length of the flume between the obstacle and the generator - considerably longer than two or three cycles of the incident wave. It must, therefore, be suggested that the experimental results be viewed with a certain degree of caution.

A second possible source of error was the apparent lack of any experimental procedure to eliminate the effect of tank reflection. In the absence of any information to the contrary it must be assumed that, since only transmission characteristics were considered, the effects of beach reflection in the transmission zone were so small as to be considered insignificant. Depending on the energy absorbtive properties of the beach, this might possibly have proved to be an over-optimistic assumption.

The second study by Yamamoto[106] was regarded by the author as an extension of the previously cited study. It was felt that, whilst the first study provided excellent experimental verification of the theoretical formulation pertaining to small scale models interacting with regular waves, further investigation was required into the interaction of large scale models with random waves. As with the previous study, a two-dimensional source and doublet distribution technique was employed to generate the theoretical predictions. Two

models of different cross-section were used for the tests, the first of which was rectangular and the second of which was described by the authors as having a "three-circle profile". This was essentially a substantially rectangular cross-section with radial ends, the diameters of which were one third of the overall length of the model. In both cases, the oblique spring mooring force was adjusted to ensure coincidence between the body centroid and still water level at equilibrium.

It was intended by the authors to investigate the theory, first postulated by St.Denis and Pierson[88], that the profile of a random wave can be considered as the linear sum of a finite number of fundamental waves, the relative energy proportions of which can be quantified by the appropriate spectral density function. The measurement technique employed to determine the spectral density functions of both the random incident wave and the corresponding body response was identical to that used in the investigation reported herein. The output signal from each measurement device was analysed using the Fast Fourier Transform technique, fully described in chapter 5 of this thesis, enabling the overall signal to be expressed as a combination of discrete frequency components. Comparison of the spectral density function of the incident wave with those pertaining to the body motions, mooring forces and transmitted wave enabled the frequency response functions of those parameters to be evaluated. (For a more detailed description of this theory, together with the experimental techniques required, the reader is directed to the report of a study carried out by Osment[78] concurrently to that reported herein). In order to achieve a complete validation of this theory, it was necessary to carry out a series of measurements of body response to regular waves

at a comprehensive range of discrete frequences and compare the results with the spectral response function of the body under the action of a random wave.

A feature of the analysis technique used in this investigation which is of particular relevance to the present study is the resolution of the incident and reflected wave spectra from the confused wave system created by multiple reflections between the wave generator and the floating breakwater model. To this end, the technique of Goda and Suzuki[27] was employed, entailing the analysis of simultaneous output signals from two wave probes separated by a known distance. (For a full description of this method, the reader is referred to section 5.8.2 of this thesis). It must be pointed out at this stage that, despite the rejection of this particular method of component resolution for the analysis of regular waves in the study reported herein, the technique of Goda and Suzuki remains the only suitable method of wave component resolution in the case of random waves.

In general, the frequency response functions obtained from analysis of the random wave tests agree excellently with those obtained from the regular wave tests with the possible exception of low frequencies, corresponding to a body length/wave length ratio of less than 0.2, where significant discrepancies were evident. No explanation for this deviation is given by the authors. Nevertheless, the generally good agreement of results demonstrates the validity of the linear superposition theory in the analysis of random wave regimes. Comparison of experimental measurements with theoretical predictions was generally good with the exception of the frequency domains in the vicinity of the resonant frequencies of the

various systems and also in frequency domains where diffraction effects clearly predominate. The deviations exhibited in the latter frequency domain concur with similar deviations encountered in other studies, suggesting the need for further investigations into the validity of linear theory for the solution of hydrodynamic problems in diffraction regimes. However, it must be suggested that the practical relevance of such studies, pertaining to regimes in which the floating body length is of a similar order of magnitude to the incident wavelength, is somewhat questionable.

A feature of the deviation between theory and experiment, in the vicinity of the modal reasonant frequencies, was the fact that the deviatory trend was more pronounced in the case of the rectangular, sharp-cornered profile than with the radially edged profile. The author concluded that this could be attributed to a significant loss of energy incurred in the process of vortex shedding as a result of viscous flow separation at the sharp corners. As a consequence of sets of tests performed at different wave energy levels, the results of which were suitably non-dimensionalised, the author concluded that the effect of viscous damping was reasonably linear and was therefore predictable, with an acceptable degree of precision, from linear theory.

A series of similar tests was also performed on large scale models to investigate the effects of scale. The results presented demonstrate good agreement between small and large scale response characteristics for values of the diffraction parameter less than 0.3, thereby suggesting the absence of significant non-linear effects in this regime. At larger values of the diffraction parameter, however, a significant discrepancy becomes evident

between the two sets of results. Since the experimental measurements for the large scale test agree with the theoretical predictions using a mathematical model based on the geometry of the large scale physical model, the authors conclude that linear theory is valid even in regimes where diffraction effects dominate. This conclusion is based on the authors statement that the abovementioned discrepancy can be attributed to slight differences in mooring conditions between the two sets of tests. However, no information is presented to support this statement which leads to a certain degree of doubt being placed on the validity of the author's conclusion.

CHAPTER 3. WAVE HYDRODYNAMICS AND FLOATING BODY DYNAMICS

3.1 Introduction

This chapter deals with the motion of the two-dimensional mechanical system consisting of a fluid and a partly immersed body. The fluid is assumed to be incompressible, inviscid and to have an irrotational motion. The surface of the fluid is assumed to extend longitudinally to infinity in both directions.

On account of the assumed irrotationality of motion, the state of the fluid may be completely described by a Velocity Potential $\Phi(x,y;t)$ which satisfies the Laplace Equation.

The boundary of the fluid consists of a fixed horizontal and impermeable bottom, the free-surface and the immersed surface of the body. On each of these surfaces, the condition pertains that the normal particle velocity is continuous across the surface, thus permitting expression of the particle velocity in terms of the derivatives of Φ. The kinematic free-surface boundary condition states that the fluid particle velocity, normal to the free-surface, is equal to the velocity of the free-surface itself in that direction, whilst the dynamic free-surface boundary condition states that the pressure at the free-surface is constant and equal to atmospheric pressure. Surface tension effects are neglected.

The kinematic boundary condition on the immersed surface of the body states that the normal velocity of the body, expressed in terms of its angular and translatory velocities, is equal to the normal

particle velocity of the fluid at the point of contact.

The fixed, horizontal and impermeable nature of the bottom gives rise to the condition that the normal (i.e. vertical) component of particle velocity thereon shall be zero.

It may be stated that the body moves under the influence of gravity and of the fluid pressure on the immersed surface. Under these conditions, no flow of energy takes place through the bottom or free surface. Energy is gained or lost by the system only through waves arriving or departing at the fluid boundary.

The additional assumption is made that the waves are of small amplitude and that the resulting motions are also of small amplitude. Under these conditions, errors resulting from the neglect of second or higher order terms may be regarded as insignificant, allowing the mathematical problem to be much simplified by linearisation.

When the body length is significant with regard to the incident wavelength, the incident waves undergo significant scattering or diffraction. The situation may, therefore, be conveniently considered in terms of a combination of two fundamental and related problems.

(i) The scattering (or diffraction) problem of an incident wave train interacting with a fixed body.

(ii) The wave generation problem of a body forced to oscillate in otherwise still water.

Resulting from the above mathematical linearisation, these two motions may be superposed with the wave forces of the scattering problem providing the forcing function in the wave generation problem. The solution of the boundary value problem permits the calculation of the exciting force on the body, the body's hydrodynamic coefficients together with the diffracted and generated wave fields. Insertion of these parameters in the relevant equations of motion enables a solution for the motion response of the body to be found.

3.2 Definitions and Sign Convention

The components of motion of the floating body are defined in three dimensions as shown in Fig.3.1.

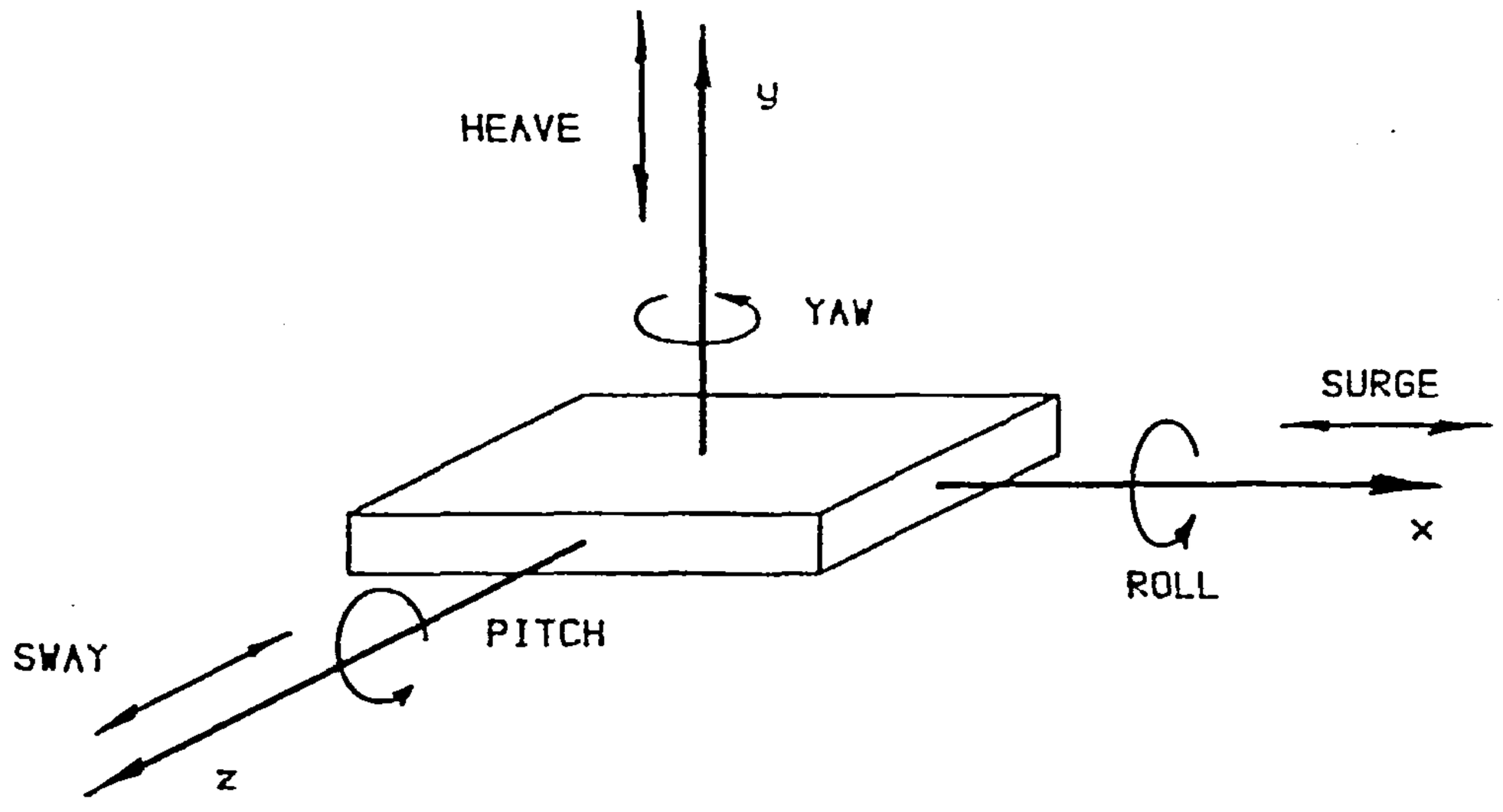

Fig.3.1 BODY MOTION DEFINITION

The translations: surge, heave and sway are taken as positive if they take place in the direction of the respective positive axis.

The rotations: roll, yaw and pitch are taken as positive if they take place in a clockwise direction around the relevant axis when viewed from the axis origin in the direction of the positive axis.

In two dimensions, only surge, heave and pitch need to be considered and they will hereinafter be designated as directions 1, 2 and 3 respectively.

The fluid domain is defined as shown in Fig.3.2

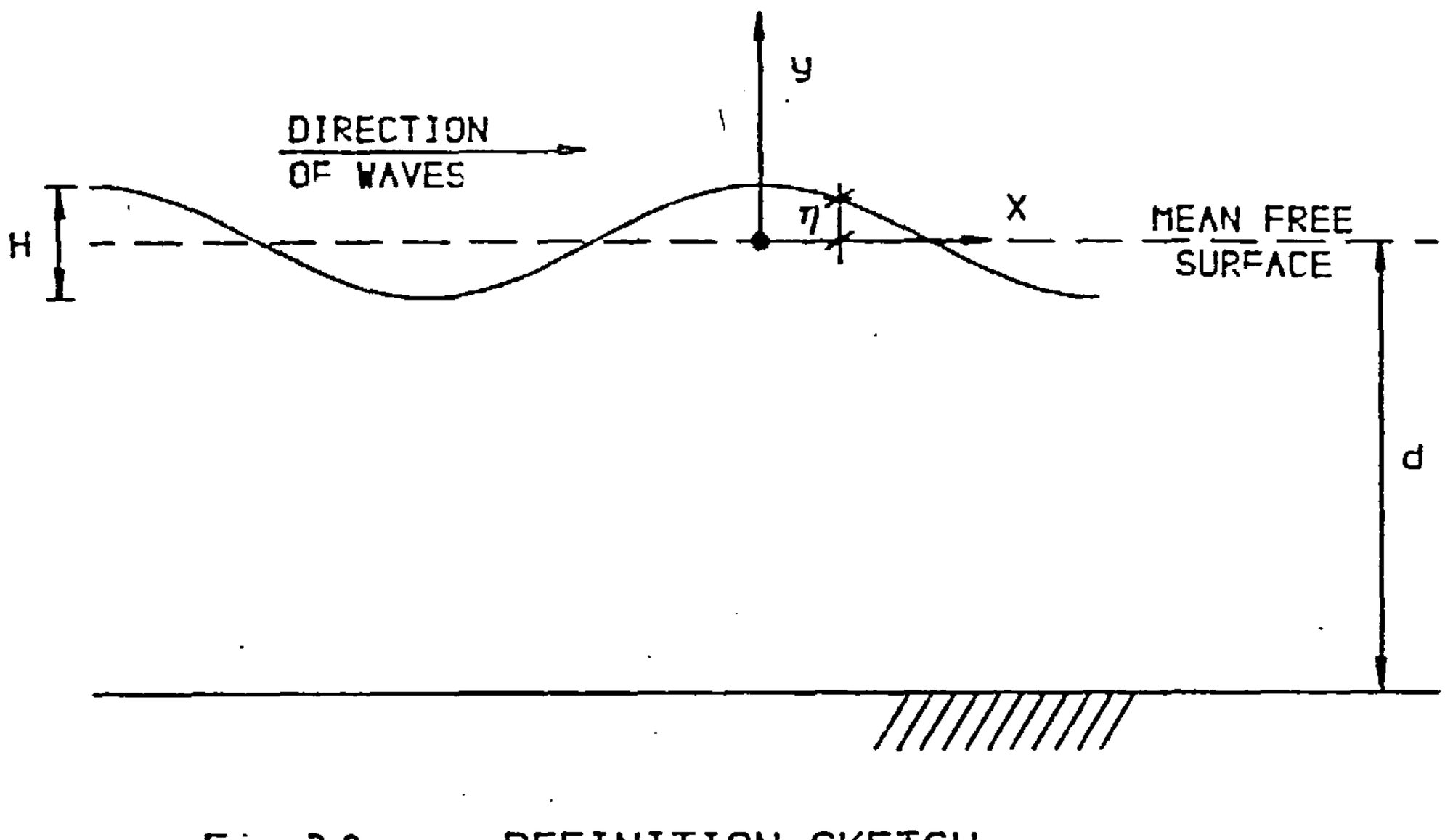

Fig. 3.2 DEFINITION SKETCH

3.3 The Velocity Potential

Consider an object, with surface denoted by $F(x,y) = 0$, immersed or partly immersed in an incompressible and inviscid fluid. The fluid (see Fig.3.2) is bounded by a horizontal bottom at $y = -d$ and a mean free surface which lies on the plane $y = 0$.

Resulting from the asssumed irrotationality of motion, the flow field in the presence of an incident wave train may be completely described by a Velocity Potential, defined in complex form thus:

$$\Phi(x,y;t) = \mathrm{Re}\{\phi(x,y)e^{-i\sigma t}\} \qquad (3.3.1)$$

where: Re{ } denotes the real part.

the time parameter t is understood to be real throughout.

The linearity of the problem permits the expression of the potential as the sum of three separate components:

$$\Phi = \Phi_W + \Phi_S + \Phi_F \qquad (3.3.2)$$

where: Φ_W is the known potential of the incident waves.

Φ_S is the unknown potential of the scattered waves.

Φ_F is the unknown potential of the waves generated by body motion.

The following conditions are satisfied by each of the three components together with their sum as given by equation (3.3.2):

a) The Laplace Equation:

$$\nabla^2\Psi(x,y;t) = 0 \qquad (3.3.3)$$

b) The bottom boundary condition:

$$\frac{\partial\Psi(x,y;t)}{\partial y} = 0 \qquad \text{at } y = -d \qquad (3.3.4)$$

c) The free-surface boundary condition resulting from the combination of the dynamic and kinematic free surface boundary conditions appropriately linearised in accordance with small amplitude wave theory:

$$\frac{\partial^2\Psi(x,y;t)}{\partial t^2} + g\frac{\partial\Psi(x,y;t)}{\partial y} = 0 \qquad \text{at } y = 0 \tag{3.3.5}$$

where: $\Psi = \Phi_W$, Φ_S, Φ_F and Φ respectively.

Detailed derivations of equation (3.3.5) are contained in many texts on small amplitude wave theory, e.g. Sarpkaya and Isaacson[85].

The potentials pertaining to the scattered and generated waves must, in addition, satisfy the far-field radiation condition guaranteeing that the waves are outgoing and have proper amplitude behaviour at infinity:

$$\lim_{|x|\to\infty} |x|^{\frac{1}{2}}\left\{\frac{\partial\Phi_S}{\partial|x|} - ik\Phi_S(x,y)\right\} = 0 \tag{3.3.6a}$$

$$\lim_{|x|\to\infty} |x|^{\frac{1}{2}}\left\{\frac{\partial\Phi_F}{\partial|x|} - ik\Phi_F(x,y)\right\} = 0 \tag{3.3.6b}$$

where: Φ_S and Φ_F are defined in similar fashion to equation (3.3.1).

Although the radiation condition has been introduced as an expression of a physical condition, it is also mathematically necessary if the solution of the problem posed is to be unique. Uniqueness proofs have been given by John[48] and Wehausen[103].

The kinematic boundary condition on the immersed surface of the body

states that the velocity of the body must equal the particle velocity of the fluid at the point of contact:

$$\frac{\partial \Phi_W}{\partial n} + \frac{\partial \Phi_S}{\partial n} + \frac{\partial \Phi_F}{\partial n} = V_n \qquad (3.3.7a)$$

where: V_n is defined by:

$$V_n = \mathrm{Re}\{v_n(x,y)e^{-i\sigma t}\} \qquad \text{on } \Gamma(x,y) = 0 \qquad (3.3.7b)$$

where: $v_n(x,y)$ denotes the complex function which represents the spacial normal component of velocity on the immersed surface.

Strictly speaking, this condition should be applied at the instantaneous position of the immersed surface. However, for purposes of mathematical simplification, the condition is applied at the equilibrium or rest position since, as a consequence of the small motions, any errors introduced thereby are small.

Following the superposition postulations made in Section 3.1, equation (3.3.7a) may be broken down into the following equations:

$$\frac{\partial \Phi_W}{\partial n} + \frac{\partial \Phi_S}{\partial n} = 0 \qquad \text{on } \Gamma(x,y) = 0 \qquad (3.3.8a)$$

$$\frac{\partial \Phi_F}{\partial n} = V_n \qquad \text{on } \Gamma(x,y) = 0 \qquad (3.3.8b)$$

3.4 The Body Motion

As a consequence of the assumption that the body oscillates harmonically with small amplitude motion, the three modes of oscillation may be written:

$$\alpha_j = a_j e^{-i\sigma t} \qquad \text{for } j = 1,2,3 \tag{3.4.1}$$

where: α_j is a translation for $j = 1,2$

α_j is a rotation for $j = 3$.

a_j is the corresponding amplitude of motion in the j^{th} direction and is assumed to be small

The normal velocity $V_n(x,y;t)$ is made up of three components associated with each mode of motion and each proportional to the corresponding velocity of motion[86]:

$$V_n = \sum_{j=1}^{3} \frac{\partial \alpha_j}{\partial t} . n_j \tag{3.4.2}$$

where: n_j represents the outward normal component scalar of velocity in the j^{th} mode of motion.

In formulating the equations of motion (see Section 3.5), the assumption is made that rotation of the body takes place about its centroid. With this in mind, the velocity components of the body may be expressed:

$$V_x = \frac{\partial \alpha_1}{\partial t} - (y-y_G) \frac{\partial \alpha_3}{\partial t} \tag{3.4.3a}$$

$$V_y = \frac{\partial \alpha_2}{\partial t} + x \frac{\partial \alpha_3}{\partial t} \qquad (3.4.3b)$$

where: the coordinates of the body centroid are $(0, y_G)$ in terms of the fluid axis system (Fig.3.2) at the rest position.

By definition:

$$V_n = V_x.n_x + V_y.n_y \qquad (3.4.4)$$

where: n_x, n_y are the direction cosines of the outward normal from the body at (x,y).

Combining equations (3.4.3) and (3.4.5) gives:

$$V_n = \frac{\partial \alpha_1}{\partial t}.n_x + \frac{\partial \alpha_2}{\partial t}.n_y + \frac{\partial \alpha_3}{\partial t}\left\{xn_y - (y - y_G)n_x\right\} \qquad (3.4.5)$$

Comparison between equations (3.4.2) and (3.4.5) shows that:

$$n_1 = n_x \qquad (3.4.6a)$$

$$n_2 = n_y \qquad (3.4.6b)$$

$$n_3 = xn_y - (y - y_G)n_x \qquad (3.4.6c)$$

Substitution of equation (3.4.1) into equation (3.4.2) gives:

$$V_n = \sum_{j=1}^{3} -i\sigma a_j n_j e^{-i\sigma t} \qquad (3.4.7)$$

Defining V_n according to equation (3.3.7b) and substituting in

equation (3.4.7) gives:

$$v_n = \sum_{j=1}^{3} -i\sigma a_j n_j \qquad (3.4.8)$$

It is convenient[86] to decompose the generated wave potential Φ_F into three components associated with each degree of freedom and each proportional to the displacement α_j.

Thus:

$$\Phi_F = \sum_{j=1}^{3} \alpha_j \phi_j^{(f)} \qquad (3.4.9)$$

Substituting from equation (3.4.1) gives:

$$\Phi_F = \sum_{j=1}^{3} a_j \phi_j^{(f)} e^{-i\sigma t} \qquad (3.4.10)$$

But:

$$V_n = \frac{\partial \Phi_F}{\partial n} = \sum_{j=1}^{3} a_j \frac{\partial \phi_j^{(f)}}{\partial n} e^{-i\sigma t} \qquad (3.4.11)$$

Comparison between equations (3.3.7b) and (3.4.11) yields:

$$v_n = \sum_{j=1}^{3} a_j \frac{\partial \phi_j^{(f)}}{\partial n} \qquad (3.4.12)$$

But, the normal velocity associated with the j^{th} directional motion is:

$$v_{n_j} = \frac{\partial \Phi_j^{(f)}}{\partial n} \qquad (3.4.13)$$

Substitution in equation (3.4.12) gives:

$$v_n = \sum_{j=1}^{3} a_j v_{n_j} \qquad (3.4.14)$$

Comparison betwen equations (3.4.8) and (3.4.14) shows that:

$$v_{n_j} = -i\sigma n_j \qquad (3.4.15)$$

3.5 The Equations of Motion

Following the sign convention as shown in Figs 3.1 and 3.2, the generalised equations of motion in two-dimensions may be stated thus:

$$m_1 \frac{\partial^2 \alpha_1}{\partial t^2} = \sum F_1 \qquad (3.5.1a)$$

$$m_2 \frac{\partial^2 \alpha_2}{\partial t^2} = \sum F_2 \qquad (3.5.1b)$$

$$I_3 \frac{\partial^2 \alpha_3}{\partial t^2} = \sum M_3 \qquad (3.5.1c)$$

where m denotes mass.

I denotes mass rotational inertia.

F denotes the sum of the extraneous forces acting on the body.

M denotes the sum of the extraneous moments acting on the body.

If $\underline{n}$ represents the unit normal vector at the body surface, the force and moment with respect to the body centroid are given by:

$$F = \int p\underline{n}\, d\Gamma \qquad (3.5.2a)$$

$$M = \int p(r - r_G) \times \underline{n}\, d\Gamma \qquad (3.5.2b)$$

where: the pressure p is determined from the linearised Bernoulli Equation:

$$p + \rho \frac{\partial \Phi}{\partial t} + \rho g y = 0 \qquad (3.5.3)$$

Insertion into equations (3.5.1) results in the specific equations of motion which may, using the notation of Wehausen[103], be expressed thus:

$$m_1 \frac{\partial^2 \alpha_1}{\partial t^2} = -\rho \int_\Gamma \frac{\partial \Phi}{\partial t} n_1\, d\Gamma \qquad (3.5.4a)$$

$$m_2 \frac{\partial^2 \alpha_2}{\partial t^2} = -\rho \int_\Gamma \frac{\partial \Phi}{\partial t} n_2\, d\Gamma - \rho g W \alpha_2 - \rho g W x_C \alpha_3 \qquad (3.5.4b)$$

$$I_3 \frac{\partial^2 \alpha_3}{\partial t^2} = -\rho \int_\Gamma \frac{\partial \Phi}{\partial t} n_3\, d\Gamma - \rho g W x_C \alpha_2 - \rho g (\forall H + W x_C^2) \alpha_3 \qquad (3.5.4c)$$

where: m = Body mass.

W = Waterplane area at equilibrium.

V = Displaced volume at equilibrium.

x_C = x-coordinate of the axis of rotation of the body in the pitching mode relative to the centroidal x-coordinate of the waterplane area.

H = Metacentric Height for pitch rotation

I_3 = Mass moment of inertia of the body for rotation in the pitching mode.

dΓ = The length of an element of the immersed two-dimensional "surface".

The integrals are taken in the fluid axis system rather than the body centroidal axis system. This simplification, and also the simplicity of the equations, is a consequence of the assumed small motions. Otherwise, the complete equations for the dynamics of a rigid body are required together with both coordinate systems.

For a body which is axi-symmetric about the x = 0 axis, the equations may be further simplified by noting that $x_C = 0$.

In order to exploit later the convenience of index notation, the equations may be re-written thus:

$$m_{ij} \frac{\partial^2 \alpha_j}{\partial t^2} = -c_{ij}\alpha_j - \rho \int_\Gamma \frac{\partial \Phi}{\partial t} n_i \, d\Gamma \qquad i = 1,2,3 \qquad (3.5.5)$$

$$j = 1,2,3$$

3.6 The Hydrodynamic Coefficients

Consider the integral term $\rho\int_{\Gamma}\frac{\partial\Phi}{\partial t}\,n_i\,d\Gamma$ in equation (3.5.5):

Substitution from equation (3.3.2) gives:

$$\rho\int_{\Gamma}\frac{\partial\Phi}{\partial t}\,n_i\,d\Gamma = \rho\int_{\Gamma}\frac{\partial}{\partial t}(\Phi_W + \Phi_S)n_i\,d\Gamma + \rho\int_{\Gamma}\frac{\partial\Phi_F}{\partial t}\,n_i\,d\Gamma \qquad (3.6.1)$$

Differentiation of equation (3.4.10) gives:

$$\frac{\partial\Phi_F}{\partial t} = \sum_{j=1}^{3} -i\sigma a_j\phi_j(f)e^{-i\sigma t} \qquad (3.6.2)$$

Expressing the complex potential ϕ_j in terms of its real and imaginary components gives:

$$\phi_j(f) = \phi_j'(f) + i\phi_j''(f)$$

Substitution in equation (3.6.2) and thence into the last term of equation (3.6.1) gives:

$$\rho\int_{\Gamma}\frac{\partial\Phi}{\partial t}\,n_i\,d\Gamma = \sum_{j=1}^{3}\Big\{-i\sigma\rho a_j e^{-i\sigma t}\int_{\Gamma}\phi_j'(f)n_i\,d\Gamma + \sigma\rho a_j e^{-i\sigma t}\int_{\Gamma}\phi_j''(f)n_i\,d\Gamma\Big\} \qquad (3.6.3)$$

In accordance with Wehausen[103], the left hand side of equation

(3.6.3) may be expressed in the form:

$$\rho\int_{\Gamma}\frac{\partial\Phi_F}{\partial t}\,n_i\,d\Gamma = \sum_{j=1}^{3}\left\{\mu_{ij}\,\frac{\partial^2\alpha_j}{\partial t^2} + \lambda_{ij}\,\frac{\partial\alpha_j}{\partial t}\right\} \qquad i=1,2,3 \qquad (3.6.4)$$

But from equation (3.4.1):

$$\frac{\partial\alpha_j}{\partial t} = -i\sigma a_j e^{-i\sigma t} \qquad (3.6.5a)$$

$$\frac{\partial^2\alpha_j}{\partial t^2} = \sigma^2 a_j e^{-i\sigma t} \qquad (3.6.5b)$$

Thus:

$$\rho\int_{\Gamma}\frac{\partial\Phi_F}{\partial t}\,n_i\,d\Gamma = \sum_{j=1}^{3}\left\{\mu_{ij}(\sigma^2 a_j e^{-i\sigma t}) + \lambda_{ij}(-i\sigma a_j e^{-i\sigma t})\right\} \qquad (3.6.6)$$

Comparison of the real and imaginary parts of equations (3.6.6) and (3.6.3) shows that:

$$\mu_{ij} = \frac{\rho}{\sigma}\int_{\Gamma}\mathrm{Imag}\left\{\phi_j^{(f)}\right\}n_i\,d\Gamma \qquad (3.6.7a)$$

$$\lambda_{ij} = -\rho\int_{\Gamma}\mathrm{Re}\left\{\phi_j^{(f)}\right\}n_i\,d\Gamma \qquad (3.6.7b)$$

where: μ_{ij}, λ_{ij}, are termed the "added-mass" and "damping" coefficients in the i^{th} direction due to motion in the j^{th} direction.

From equations (3.4.13) and (3.4.15), it may be inferred that:

$$\frac{\partial \Phi_i^{(f)}}{\partial n} = -i\sigma n_i \qquad (3.6.8)$$

Rearrangement gives:

$$n_i = \frac{i}{\sigma} \frac{\partial \Phi_i^{(f)}}{\partial n} \qquad (3.6.9)$$

leading to the alternative expressions:

$$\mu_{ij} = \frac{i\rho}{\sigma^2} \int_\Gamma \mathrm{Imag}\left\{\phi_j^{(f)}\right\} \frac{\partial \Phi_i^{(f)}}{\partial n} d\Gamma \qquad (3.6.10a)$$

$$\lambda_{ij} = -\frac{i\rho}{\sigma} \int_\Gamma \mathrm{Re}\left\{\phi_j^{(f)}\right\} \frac{\partial \Phi_i^{(f)}}{\partial n} d\Gamma \qquad (3.6.10b)$$

In accordance with equation (3.6.8), $\frac{\partial \Phi_i^{(f)}}{\partial n}$ is always imaginary over Γ. Therefore μ_{ij} and λ_{ij} are always real.

By applying Green's Theorem to $\phi_j^{(f)}$ and $\phi_i^{(f)}$, and remembering that they both satisfy the Laplace Equation within the fluid domain, it may be shown that:

$$\mu_{ij} = \mu_{ji}$$

$$\lambda_{ij} = \lambda_{ji}$$

It must be noted at this point that the expressions for the added-mass and damping coefficients contained herein derive from the decomposition of the forced potential into three components, each of which is proportional to the respective amplitude of motion. Some

texts, e.g. Wehausen[103], decompose the potential in proportion to the velocities of motion. This leads to different expressions for the added-mass and damping coefficients. However, bearing in mind the different numerical values of the potential arising from such a decomposition, the resulting numerical values of the hydrodynamic coefficients are the same.

3.7 Forces, Moments and Motions.

The hydrodynamic forces given by the last term in equation (3.5.5) can be expressed in terms of components $F^{(f)}$, due to the generated potential, and components $F^{(e)}$ due to the incident and scattered potentials. The latter is called the "Exciting Force" and is identical to the wave induced force in the fixed body case. The component of the exciting force associated with the incident wave potential is the Froude-Krylov force.

The equations of motion (3.5.5) may therefore be re-arranged:

$$\sum_{j=1}^{3}\left\{m_{ij}\,\frac{\partial^2\alpha_j}{\partial t^2} + c_{ij}\alpha_j\right\} = F_i^{(e)} + F_i^{(f)} \qquad i = 1,2,3 \qquad (3.7.1)$$

Substitution from equations (3.6.1) and (3.6.4) gives the i equations:

$$\sum_{j=1}^{3}\left\{(m_{ij} + \mu_{ij})\,\frac{\partial^2\alpha_j}{\partial t^2} + \lambda_{ij}\,\frac{\partial\alpha_j}{\partial t} + c_{ij}\alpha_j\right\} = F_i^{(e)} \qquad i=1,2,3 \quad (3.7.2)$$

Consideration of equation (3.6.1) shows that the exciting force components may be obtained from:

$$F_i^{(e)} = \rho \int_\Gamma \frac{\partial}{\partial t} (\Phi_W + \Phi_S) n_i \, d\Gamma \qquad (3.7.3)$$

This, of course, necessitates prior evaluation of the scattered potential.

As first pointed out by Haskind[33], and later emphasised by Newman[73], it is not, however, necessary to solve for the scattered potential Φ_S once the solution has been obtained for the generated potential Φ_F.

The derivation of the so-called "Haskind Relations" is presented by Wehausen[103] but, for purposes of completeness, is contained hereunder.

Consider the fluid region bounded by a two-dimensional "surface" Γ composed of:

(i)	Vertical boundaries at $x = \pm\infty$	(Γ_∞)
(ii)	An impermeable bottom boundary at $y = -d$	(Γ_B)
(iii)	The free-surface.	(Γ_F)
(iv)	The immersed surface of the body.	(Γ_0)

Within this region ϕ_s and $\phi_j^{(f)}$ are harmonic.

By use of Green's Theorem, it may be stated:

$$\int_{\Gamma}\left\{\Phi_S \frac{\partial \Phi_j^{(f)}}{\partial n} - \Phi_j(f) \frac{\partial \Phi_S}{\partial n}\right\} d\Gamma = 0 \qquad (3.7.4)$$

The radiation condition in two-dimensions states:

$$\lim_{|x|\to\infty} |x|^{\frac{1}{2}} \left\{\frac{\partial \Phi}{\partial |x|} - ik\Phi\right\} = 0$$

Since both Φ_S and $\Phi_j^{(f)}$ comply with the radiation condition:

$$\frac{\partial \Phi_S}{\partial |x|} = ik\Phi_S; \quad \frac{\partial \Phi_j^{(f)}}{\partial |x|} = ik\Phi_j(f); \qquad \text{at } \Gamma_\infty$$

Therefore, at Γ_∞, the integrand in equation (3.7.4) becomes:

$$\Phi_S\left\{ik\Phi_j^{(f)}\right\} - \Phi_j^{(f)}\left\{ik\Phi_S\right\}$$

which is clearly zero.

To comply with the bottom boundary condition:

$$\frac{\partial \Phi_S}{\partial y} = \frac{\partial \Phi_j^{(f)}}{\partial y} = 0 \qquad \text{at } y = -d$$

Thus, the integrand in equation (3.7.4) vanishes on Γ_B.

The free surface boundary condition states:

$$\frac{\partial^2 \Phi}{\partial t^2} + g \frac{\partial \Phi}{\partial y} = 0$$

But, as previously defined: $\Phi = \phi e^{-i\sigma t}$

Thus:

$$\frac{\partial^2 \Phi}{\partial t^2} = -\sigma^2 \phi e^{-i\sigma t}$$

The free-surface boundary condition may therefore be re-written:

$$\frac{\partial \phi}{\partial y} = \frac{\sigma^2 \phi}{g}$$

Since ϕ_S and $\phi_j^{(f)}$ both comply with the free surface boundary condition:

$$\frac{\partial \phi_S}{\partial y} = \frac{\sigma^2 \phi_S}{g}; \quad \frac{\partial \phi_j^{(f)}}{\partial y} = \frac{\sigma^2 \phi_j^{(f)}}{g} \qquad \text{on } \Gamma_F$$

It can therefore be seen that the integrand in equation (3.7.4) vanishes on Γ_F.

Thus, equation (3.7.4) may be re-expressed:

$$\int_\Gamma \left\{ \phi_S \frac{\partial \phi_j^{(f)}}{\partial n} - \phi_j^{(f)} \frac{\partial \phi_S}{\partial n} \right\} d\Gamma = 0 \qquad \text{on } \Gamma_0. \qquad (3.7.5)$$

From equation (3.7.3):

$$F_i^{(e)} = \rho \int_\Gamma \frac{\partial \Phi_W}{\partial t} n_i \, d\Gamma + \rho \int_\Gamma \frac{\partial \Phi_S}{\partial t} n_i \, d\Gamma \qquad (3.7.6)$$

But: $\Phi_W = \phi_W e^{-i\sigma t}$ and $\Phi_S = \phi_S e^{-i\sigma t}$ by definition.

Differentiation of these expressions followed by substitution in equation (3.7.6) yields:

$$F_i^{(e)} = \rho\int_{\Gamma} -i\sigma n_i \phi_W e^{-i\sigma t}\, d\Gamma + \rho\int_{\Gamma} -i\sigma n_i \phi_S e^{-i\sigma t}\, d\Gamma$$

Substitution from equation (3.6.8) gives:

$$F_i^{(e)} = \rho e^{-i\sigma t}\left\{\int_{\Gamma} \phi_W \frac{\partial \phi_i^{(f)}}{\partial n}\, d\Gamma + \int_{\Gamma} \phi_S \frac{\partial \phi_i^{(f)}}{\partial n}\, d\Gamma\right\} \qquad (3.7.7)$$

But from equation (3.7.5):

$$\int_{\Gamma} \phi_S \frac{\partial \phi_j^{(f)}}{\partial n}\, d\Gamma = \int_{\Gamma} \phi_j^{(f)} \frac{\partial \phi_S}{\partial n}\, d\Gamma$$

and from equation (3.3.8a) it can be inferred that:

$$\frac{\partial \phi_S}{\partial n} = -\frac{\partial \phi_W}{\partial n}$$

This permits re-expression of equation (3.7.7) thus:

$$F_i^{(e)} = \left\{F_o^{(e)}\right\}_i e^{-i\sigma t} \qquad (3.7.8)$$

where:

$$\left\{F_o^{(e)}\right\}_i = \rho\left\{\int_{\Gamma}\left[\phi_W \frac{\partial \phi_i^{(f)}}{\partial n} - \phi_i^{(f)} \frac{\partial \phi_W}{\partial n}\right] d\Gamma\right\}$$

This demonstrates that the evaluation of the exciting force components does not necessitate the prior evaluation of the scattered potential.

Consideration of equation (3.7.2) together with the fact that:

$$\alpha_j = a_j e^{-i\sigma t}; \quad \frac{\partial \alpha_j}{\partial t} = -i\sigma a_j e^{-i\sigma t}; \quad \frac{\partial^2 \alpha_j}{\partial t^2} = -\sigma^2 a_j e^{-i\sigma t};$$

permits expression of equation (3.7.8) thus:

$$\sum_{j=1}^{3} \left\{ \left[-\sigma^2 (m_{ij} + \mu_{ij}) - i\sigma\lambda_{ij} + c_{ij} \right] a_j \right\} = \left\{ F_o^{(e)} \right\}_i \qquad (3.7.9)$$

It has been demonstrated that:

(1) Evaluation of the hydrodynamic coefficients is possible from equations (3.6.7) or (3.6.10)

(2) Evaluation of the exciting force components is possible from equation (3.7.8)

(3) Evaluation of the body motion components is possible from equation (3.7.9) subject to prior evaluation of the parameters in (1) and (2) above.

Since all the equations used in the above evaluations contain terms petaining to the generated velocity potential, it becomes apparent that an initial requirement is the evaluation of these components. The absence of any terms referring to the scattered potential emphasises the usefulness of the Haskind Relations (3.7.8).

It must be stated, however, that in using the Wave-Source method described in following sections, the matrix equations formed to determine the scattered and generated potentials differ only in their right hand sides and can thus be combined. The additional

work required to evaluate the scattered potential is, therefore, minimal.

CHAPTER 4 NUMERICAL ANALYSIS

4.1 Introduction.

In this chapter, it will be demonstrated that the velocity potential describing a fluid in motion may be represented by a continuous distribution of sources over an essentially fictitious boundary. If the source distribution boundary is chosen to coincide with the fluid boundary, a number of integral equation formulations may be written, each of which is a Fredholm Integral Equation of the second kind containing singular kernels which may be simple sources or Green's Functions.

One method of solution requires that the velocity potential be expressed as the sum of potentials resulting from a continuous distribution of sources and double sources. The integral formulation is solved directly for the unknown velocity potential. The method is thus termed 'direct'.

Alternatively, the velocity potential may be represented by a continuous distribution of sources or double sources. The method of solution for the potential may be termed 'indirect' owing to the prior requirement that the integral equation formulations are solved for the unknown source distribution function.

If the source distribution boundary is located outside the fluid domain, the resulting Fredholm equations are of the second kind and contain regular kernel functions which may be simple sources or Green's Functions. It must be noted that, in this case, the direct

method of solution is inappropriate.

This chapter describes the numerical solution, using the 'indirect' method, of the singular kernel integral equation formulation of the linear diffraction boundary value problem for an obstacle in a two-dimensional domain.

The exact solution of the integral equation requires that the specified boundary conditions are satisfied at all points on the fluid boundary. However, an acceptable relaxation may be applied that only requires the satisfaction of boundary conditions at a discrete number of locations on the fluid boundary. The unknown velocity potential may thus be assumed to result from the presence of a discrete number of sources located on the fictitious source boundary, thus reducing the problem to that of solving a system of linear algebraic equations.

If a simple source is chosen as the kernel of the integral equation, the coefficients of the algebraic equations may be easily evaluated but the system of equations required to produce an acceptable solution may prove to be of considerable magnitude. Introduction of the appropriate Green's Function ensures that certain boundary conditions are automatically satisfied, thus further reducing the problem. Details of the numerical discretisation techniques required to evaluate the coefficients of the linear equations are given in this chapter, together with the numerical evaluation of the Green's Function appropriate to a two-dimensional domain with an impermeable bottom boundary at constant finite depth.

The efficacy of a numerical method is judged not only by the

accuracy of the solutions obtained but by the efficiency with which the computations are performed. In view of this, a substantial amount of effort was devoted to achieving maximum efficiency of evaluating the formulations without loss of accuracy. Details of the steps taken to ensure this state of affairs are included in this chapter, together with indications of the numerical limitations of the source strength integral formulation.

An unfortunate feature of the wave diffraction problem in a two-dimensional domain is that no exact solutions exist and initial program testing may only be achieved by comparison of results with published data. To this end, a theoretical analysis was performed on a two-dimensional freely floating body with a substantially rectangular immersed surface. The results are presented in graphical form at the end of this chapter.

4.2 The Two-Dimensional Source Strength Distribution Equation.

It may be shown (see Appendix A1) that the velocity potenial at some point ($\underline{x}$) in the fluid domain due to the presence of a simple source of strength 'm' located at ($\underline{\xi}$) may be represented by:

$$\phi(\underline{x}) = - \frac{m \log r(\underline{x},\underline{\xi})}{2\pi} \qquad (4.2.1)$$

where: $\underline{x}$ = (x,y) and represents a point in the fluid domain known hereinafter as the 'field point'.

$\underline{\xi}$ = (a,b) and represents the source location known hereinafter as the 'source point'.

$r^2 = (x-a)^2 + (y-b)^2$ and represents the separation between source and field points.

It can be shown that equation (4.2.1) is a singular solution of the Laplace Equation.

For the purpose of formulating and solving a linear surface-wave problem entailing the use of a pulsating source, a singular solution of the Laplace Equation, i.e. a Green's Function $G(\underline{x},\underline{\xi};t)$, is required which satisfies the free surface, bottom and radiation conditions described in section 3.3. Such a function has been constructed by Wehausen and Laitone[104] and is defined in Appendix A2.

The field point potential may thus be represented by

$$\Phi(\underline{x},t) = mG(\underline{x},\underline{\xi};t) \qquad (4.2.2)$$

where: Φ is the field point potential due to the presence of a pulsating Green's Function source of strength 'm' located at $(\underline{\xi})$.

Equation (4.2.2) may be extended to define the field point potential due to the presence of a distribution of pulsating sources of unknown strength located on a source boundary Γ:

$$\Phi(\underline{x};t) = \int_{\Gamma} f(\underline{\xi})G(\underline{x},\underline{\xi};t) \qquad (4.2.3)$$

where: $f(\underline{\xi})$ represents the unknown source strength distribution function.

Since Φ and G are harmonic functions and may be expressed as:

$$\Phi(\underline{x};t) = \phi(\underline{x})e^{-i\sigma t}$$

$$G(\underline{x},\underline{\xi};t) = g(\underline{x},\underline{\xi})e^{-i\sigma t}$$

equation (4.2.3) may be written in terms of spacial functions:

$$\phi(\underline{x}) = \int_{\Gamma} f(\underline{\xi})g(\underline{x},\underline{\xi})\, d\Gamma \qquad (4.2.4)$$

4.3 The Source Strength Integral Equation Formulation.

The kinematic boundary condition on the immersed surface of the body may be expressed as:

$$\frac{\partial\Phi(x,y)}{\partial n} = v_n \quad \text{on the immersed surface} \qquad (4.3.1)$$

where: v_n denotes the complex function which represents the magnitude of the normal spacial component of velocity given by:

$$V_n = Re\{v_n(x,y)e^{-i\sigma t}\} \qquad (4.3.2)$$

Applying this boundary condition to equation (4.2.4) gives:

$$v_n(\underline{x}) = \int_{\Gamma} f(\underline{\xi})\, \frac{\partial g(\underline{x},\underline{\xi})}{\partial n}\, d\Gamma \qquad (4.3.3)$$

This is a Fredholm Equation of the first kind and is used when the source distribution boundary does not coincide with the immersed

surface.

When the source distribution boundary coincides with the immersed surface it becomes apparent, from inspection of the Green's Function expressions in Appendix A2, that $\partial g/\partial n$ has a $1/r$ type singularity as ($\underline{x}$) approaches ($\underline{\xi}$) from the fluid domain. The effect of this singularity is removed by surrounding the source point with a semi-circular boundary as shown in Figure 4.1.

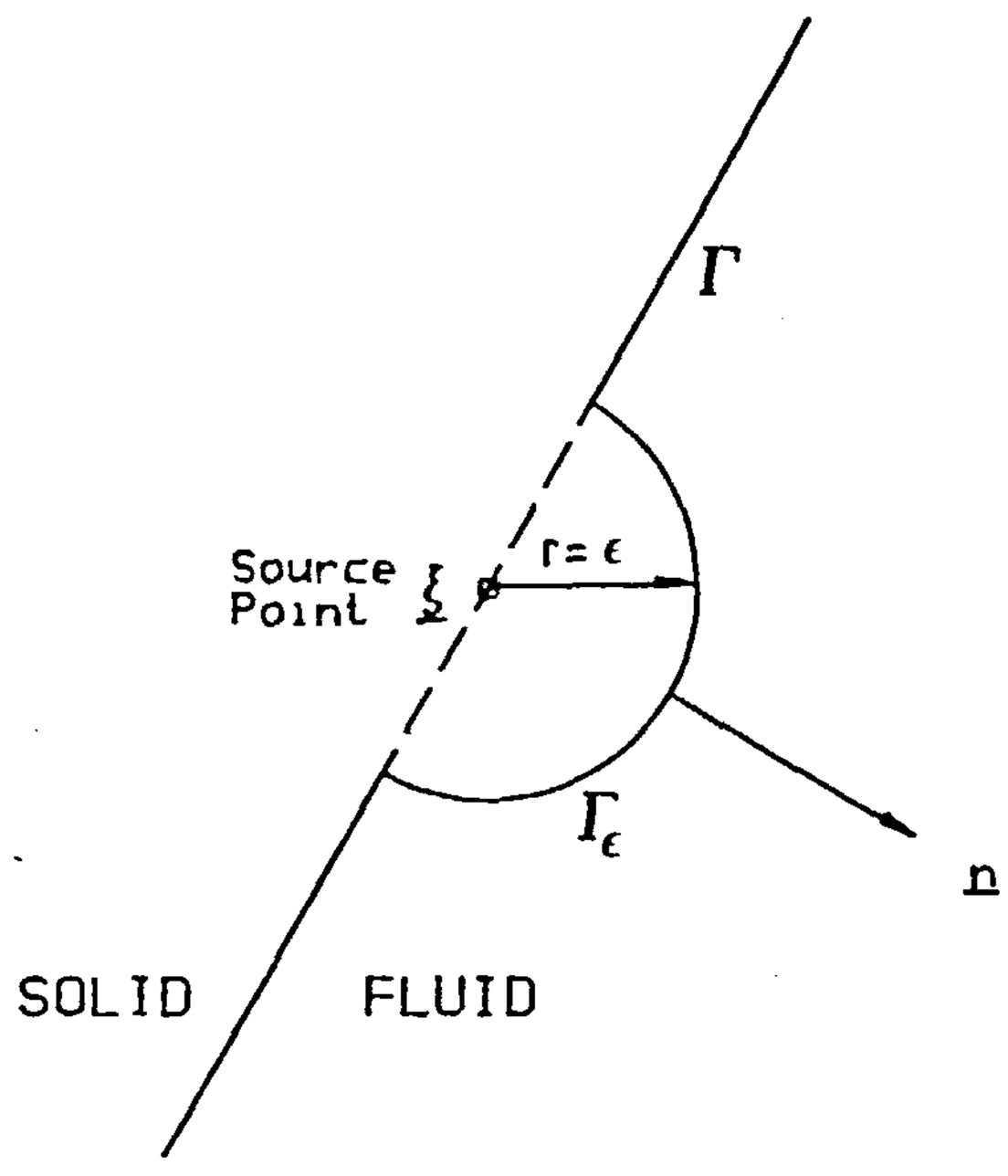

Fig.4.1 REMOVAL OF SOURCE POINT SINGULARITY

Equation (4.3.3) may be re-expressed as:

$$v_n(\underline{x}) = \int_{\Gamma} f(\underline{\xi}) \frac{\partial g(\underline{x},\underline{\xi})}{\partial n} \, d\Gamma + \lim_{\epsilon \to 0} \int_{\Gamma_\epsilon} f(\underline{\xi}) \frac{\partial g(\underline{x},\underline{\xi})}{\partial n} \, d\Gamma \qquad (4.3.4)$$

But on Γ_ϵ: $\quad \underline{x} = \underline{\xi} + \underline{r}\,\Big|_{r=\epsilon}$

$$g(\underline{x},\underline{\xi}) = \log r\Big|_{r=\epsilon} + O(\epsilon)$$

$$\frac{\partial g}{\partial n} = \frac{\partial g}{\partial r}$$

$$\partial\Gamma = r\Big|_{r=\epsilon}\, d\theta$$

$$f(\underline{\xi}) = f(\underline{x}) + O(\epsilon)$$

Thus the limiting value of the last term in equation (4.3.4) becomes:

$$\lim_{\epsilon\to 0} \int_0^{\pi} f(\underline{\xi}).\frac{1}{r}\Big|_{r=\epsilon}.r\Big|_{r=\epsilon}\, d\theta$$

$$= \lim_{\epsilon\to 0} \int_0^{\pi} [f(\underline{x}) + O(\epsilon)].\frac{1}{\epsilon}.\epsilon\, d\theta$$

$$= \lim_{\epsilon\to 0} \int_0^{\pi} [f(\underline{x}) + O(\epsilon)]\, d\theta$$

But: $\lim_{\epsilon\to 0} \int_0^{\pi} O(\epsilon)\, d\theta = 0$

Thus: $\lim_{\epsilon\to 0} \int_{\Gamma_\epsilon} f(\underline{\xi})\, \frac{\partial g(\underline{x},\underline{\xi})}{\partial n}\, d\Gamma = \pi f(\underline{x})$ (4.3.5)

Substitution in equation (4.3.4) leads to

$$v_n(\underline{x}) = \int_\Gamma f(\underline{\xi})\, \frac{\partial g(\underline{x},\underline{\xi})}{\partial n}\, d\Gamma + \pi f(\underline{x}) \qquad (4.3.6)$$

This is a Fredholm Integral Equation of the second kind and is used when the source distribution boundary coincides with the immersed surface of the body.

Both equations may be solved numerically for the unknown source strength distribution function $f(\underline{\xi})$, which may then be substituted in the source strength distribution equation (4.2.4) to evaluate the velocity potential at any point in the fluid domain.

4.4 Numerical Solution of the Fredholm Integral Equations.

Equation (4.3.6) states that:

$$v_n(\underline{x}) = \int_{\Gamma} f(\underline{\xi}) \frac{\partial g(\underline{x},\underline{\xi})}{\partial n} d\Gamma + \Theta \qquad (4.4.1)$$

where: $\Theta = 0$ if the source distribution boundary does not coincide with the immersed surface of the body (regular kernel method).

$\Theta = \pi f(\underline{x})$ if the source distribution boundary coincides with the immersed surface of the body (singular kernel method)

4.4.1 The Fixed Body Case.

On account of the assumed linearity of the problem, the total potential may be expressed as the sum of the incident wave potential

and the scattered wave potential:

$$\Phi = \Phi_W + \Phi_S \qquad (4.4.2)$$

Thus:

$$\frac{\partial \Phi}{\partial n} = \frac{\partial \Phi_W}{\partial n} + \frac{\partial \Phi_S}{\partial n} = v_n \quad \text{(by definition)} \qquad (4.4.3)$$

In the fixed body case, the normal velocity components at all points on the body surface are zero.

Thus:

$$\frac{\partial \Phi_S}{\partial n} = - \frac{\partial \Phi_W}{\partial n} \qquad \text{on the immersed surface}$$

If the source distribution boundary is chosen to coincide with the immersed surface of the body, equation (4.4.1) may be re-expressed:

$$- \frac{\partial \Phi_W(\underline{x})}{\partial n} = \int_{\Gamma} f(\underline{\xi}) \frac{\partial g(\underline{x},\underline{\xi})}{\partial n} \, d\Gamma + \pi f(\underline{x}) \qquad (4.4.4)$$

This integral equation may be solved numerically, beginning with the subdivision of the source distribution boundary into N elements of length $\Delta\Gamma_j (j = 1,2,\ldots,N)$ and identifying as node points the centroid of each element.

The continuous formulation of the problem indicates that equation (4.4.4) be satisfied at all points ($\underline{x}$) on the source distribution boundary $\Gamma(\underline{x}) = 0$. In order to obtain a discretised numerical solution, it is necessary to relax this requirement and apply the

condition at only N control points. The location of these points may, in principle, be chosen arbitrarily but for convenience the N node points at the element centroids are used.

Equation (4.4.4) is therefore replaced by the N equations:

$$\pi f(\underline{x}_i) + \int_{\Gamma} f(\underline{\xi}) \frac{\partial g(\underline{x}_i, \underline{\xi})}{\partial n} \, d\Gamma = - \frac{\partial \Phi_W(\underline{x}_i)}{\partial n} \qquad i = 1,2,\ldots,N \qquad (4.4.5)$$

Furthermore, the integral in equation (4.4.5) may be written as the sum of the integrals over the N elements of length $\Delta\Gamma_j$. As a valid approximation, the source strength distribution function $f(\underline{\xi})$ may be taken as constant over each element.

Lacey[61] investigated the validity of this approximation and concluded that there was no significant improvement in numerical results obtained from the use of higher order (linear and quadratic) distributions of source strength over individual elements.

Equation (4.4.5) may thus be expressed:

$$\pi f_i + \sum_{j=1}^{N} \alpha_{ij} f_j = \left\{ - \frac{\partial \Phi_W}{\partial n} \right\}_i \qquad i = 1,2,\ldots,N \qquad (4.4.6)$$

where: $$\alpha_{ij} = \int_{\Delta\Gamma_j} \frac{\partial g(\underline{x}_i, \underline{\xi})}{\partial n} \, d\Gamma$$

In physical terms, α_{ij} denotes the velocity induced at the i^{th} node point, in the direction normal to the surface at that point, by a source of unit strength distributed uniformly over the j^{th} element.

The definition of α_{ij} as given by equation (4.4.6) indicates that $\partial g/\partial n$ is to be integrated over the j^{th} element.

For discussion purposes, $\partial g/\partial n$ will be re-expressed in the form;

$$\frac{\partial g(\underline{x},\underline{\xi})}{\partial n} = \frac{\partial}{\partial n}\left[\log R(\underline{x},\underline{\xi})\right] + \frac{\partial g^{*}(\underline{x},\underline{\xi})}{\partial n}$$

Thus;

$$\alpha_{ij} = \int_{\Delta\Gamma_j} \frac{\partial}{\partial n}\left[\log R(\underline{x},\underline{\xi})\right] d\Gamma + \int_{\Delta\Gamma_j} \frac{\partial g^{*}(\underline{x},\underline{\xi})}{\partial n}\, d\Gamma \qquad (4.4.7)$$

The integrand in the second term of the above equation is regular throughout the fluid domain and oscillates with a wave length having an order of magnitude comparable to that of the incident wave. In practice, the incident wavelength is generally large in comparison to the dimensions of the immersed surface and it may therefore be assumed that $\partial g^{*}/\partial n$ varies slowly over the immersed surface and is very nearly constant over the element length.

The integrand in the first term of the equation is not, however, gradually varying as the point i approaches the point j. It is, in fact, singular as $R \rightarrow 0$. Thus, when field and source point coincide, the integrations must be evaluated properly as the above approximation is rendered invalid.

In general, however, $\partial g/\partial n$ may be taken as constant over the element and equal to its value at the element centroid.

Thus:

$$\alpha_{ij} = \Delta\Gamma_j \frac{\partial g(\underline{x}_i, \underline{\xi}_j)}{\partial n} \qquad (4.4.8)$$

Equation (4.4.6) may therefore be expressed in matrix notation:

$$\underset{(N,N)}{[A]} \quad \underset{(N,1)}{\{f\}} = \underset{(N,1)}{\{B\}} \qquad (4.4.9)$$

where: $A_{ij} = \delta_{ij} + \Delta\Gamma_j \frac{\partial g(\underline{x}_i, \underline{\xi}_j)}{\partial n}$

$$B_i = \left\{ - \frac{\partial \Phi W}{\partial n} \right\}_i$$

$$\delta_{ij} = 0 \quad \text{for } i \neq j$$

$$\delta_{ii} = \pi$$

Note that: subscript i refers to the field point (x_i, y_i);

subscript j refers to the source point (a_j, b_j);

The parameter $\partial g/\partial n$ may be evaluated from:

$$\frac{\partial g(\underline{x}_i, \underline{\xi}_j)}{\partial n} = \frac{\partial g(\underline{x}_i, \underline{\xi}_j)}{\partial x}_{(n_x)_i} + \frac{\partial g(\underline{x}_i, \underline{\xi}_j)}{\partial y}_{(n_y)_i} \qquad \text{for } i \neq j$$

where: n_x, n_y are the components of the unit normal vector defining the field point element orientation.

For purpose of clarity, the expressions for g, $\partial g/\partial x$ and $\partial g/\partial y$ are contained in appendix A2.

The parameter $\frac{\partial \Phi W(\underline{x}_i)}{\partial n}$ may be evaluated in similar fashion.

When i = j, it may be shown (see Appendix A3) that:

$$\frac{\partial g(\underline{x}_i, \underline{\xi}_j)}{\partial n} = \frac{\pi}{\Delta \Gamma_j}$$

However, this contribution is taken care of in equation (4.4.9) by virtue of the fact that $\delta_{ii} = \pi$ and need not, therefore, be included in the diagonal terms of the [A] matrix.

Since [A] and {B} are known, equation (4.4.9) may be solved for the unknown source strength distribution vector {f}.

4.4.2 The Floating Body Case.

The total potential may be regarded as the sum of the incident, scattered and generated potentials. The solution of the integral equation for the scattered source distribution has been detailed in section 4.4.1; it only remains, therefore, to consider the equation in terms of the generated source distributions.

Resulting from the Haskind Relations discussed in Chapter 3, the solution for the generated source distributions may be obtained without the prior solution for the scattered source distributions. However, if the scattered source distributions are required, as in this investigation, the computations may be combined in the following fashion:

If, as stated in Chapter 3, the directions of motion are defined:

Surge - Mode 1

Heave - Mode 2

Pitch - Mode 3

and, in addition: Scattering - Mode 4

the integral equation formulations may be expressed using index notation for convenience:

$$\pi f_k(\underline{x}) + \int_\Gamma f_k(\underline{\xi}) \frac{\partial g(\underline{x},\underline{\xi})}{\partial n} d\Gamma = (v_n)_k \qquad k = 1,2,3,4 \qquad (4.4.10)$$

Following the same discretisation procedure as adopted in Section (4.4.1), each of the k equations in (4.4.10) may be replaced by the N equations:

$$\pi f_k(\underline{x}_i) + \int_\Gamma f_k(\underline{\xi}) \frac{\partial g(\underline{\xi},\underline{x}_i)}{\partial n} d\Gamma = (v_n)_{ik} \qquad \begin{matrix} i = 1,N \\ k = 1,4 \end{matrix} \qquad (4.4.11)$$

where, from (3.4.15) and (4.4.3):

$$(v_n)_{ik} = -i\sigma(n_k)_i \qquad k = 1,2,3$$

$$(v_n)_{ik} = -\frac{\partial \Phi_W(\underline{x}_i)}{\partial n} \qquad k = 4$$

By making the same assumptions and approximations as in Section 4.2.1, equation (4.4.11) may be expressed as:

$$\pi f_{ik} + \sum_{j=1}^{N} \alpha_{ij} f_{jk} = (v_n)_{ik} \qquad \begin{matrix} i = 1,N \\ k = 1,4 \end{matrix} \qquad (4.4.12)$$

where: $\alpha_{ij} = \Delta\Gamma_j \frac{\partial g(\underline{x}_i, \underline{\xi}_j)}{\partial n}$

In matrix notation, equation (4.4.12) becomes

$$\underset{(N,N)}{[A]} \quad \underset{(N,k)}{[f]} = \underset{(N,k)}{[B]} \qquad (4.4.13)$$

where: $A_{ij} = \delta_{ij} + \Delta\Gamma_j \frac{\partial g(\underline{x}_i, \underline{\xi}_j)}{\partial n}$

$B_{ik} = (v_n)_{ik}$

$\delta_{ij} = 0 \quad \text{for } i \neq j$

$\delta_{ii} = \pi$

The same assumption may be made regarding the value of $\partial g/\partial n$ where field and source point coincide.

Equation (4.4.13) may be solved for the unknown source strength distribution matrix [f].

4.5 Numerical Evaluation of the Discretised Source Distribution Function.

In Section 4.2, the matrix equation to be solved for the discretised Source Distribution Function was expressed in general terms. It may now be expressed in specific terms relating to a two-dimensional floating body in a regular, finite depth regime.

In this section, the matrix elements referred to in equation (4.4.13) will be re-subscripted to avoid confusion with the complex quantity $i = \sqrt{-1}$ and the regular wave parameter $k = 2\pi/L$.

If the immersed surface of the body is subdivided into N boundary elements, equation (4.4.13) may be re-written:

$$\underset{(N,N)}{[A]} \quad \underset{(N,4)}{[f]} = \underset{(N,4)}{[B]} \tag{4.5.1}$$

Consider, firstly, the elements of the [A] matrix:

$$A_{jk} = \delta_{jk} + \Delta\Gamma_k \frac{\partial g(\underline{x}_j, \underline{\xi}_k)}{\partial n} \tag{4.5.2}$$

where: $\delta_{jk} = 0 \quad$ for $j \neq k$

$\delta_{jj} = \pi$

From equation (A2.3) of Appendix A2:

$$\frac{\partial g}{\partial n} = \frac{\partial g_1}{\partial n} + i \frac{\partial g_2}{\partial n}$$

Thus:

$$A_{jk} = \delta_{jk} + \Delta\Gamma_k \left\{ \frac{\partial g_1(\underline{x}_j, \underline{\xi}_k)}{\partial n} + i \frac{\partial g_2(\underline{x}_j, \underline{\xi}_k)}{\partial n} \right\} \tag{4.5.3}$$

Separation of real and imaginary parts, together with the limiting value of the normal gradient of the Green's Function at its source, leads to the following expression:

$$A_{jk} = C_{jk} + iD_{jk} \tag{4.5.4}$$

where: $C_{jk} = \Delta\Gamma_k \frac{\partial g_1(\underline{x}_j, \underline{\xi}_k)}{\partial n} \quad$ for $j \neq k$

$C_{jk} = \pi \quad$ for $j = k$

$$D_{jk} = \Delta\Gamma_k \frac{\partial g_2(\underline{x}_j, \underline{\xi}_k)}{\partial n} \qquad \text{for all } j,k$$

Consider now the elements of the [B] matrix:

$$B_{jm} = (v_n)_{jm} \tag{4.5.5}$$

where: $(v_n)_{jm} = -i\sigma(n_m)_j \qquad \text{for } m = 1,2,3$

$$(v_n)_{jm} = -\frac{\partial \Phi_W(\underline{x}_j)}{\partial n} \qquad \text{for } m = 4$$

The complex expressions for the incident wave potential are:

$$\Phi_W(\underline{x}_j) = -\frac{igH}{2\sigma} \frac{\text{Cosh } k(d+y_j)}{\text{Cosh } kd} e^{ikx_j} \tag{4.5.6a}$$

$$\frac{\partial \Phi_W(\underline{x}_j)}{\partial n} = \frac{\partial \Phi_W(\underline{x}_j)}{\partial x}(n_x)_j + \frac{\partial \Phi_W(\underline{x}_j)}{\partial y}(n_y)_j \tag{4.5.6b}$$

where: n_x and n_y are the direction cosines as previously defined.

As before, separation of real and imaginary parts, together with straightforward differentiation, leads to the following expression:

$$B_{jm} = G_{jm} + iH_{jm} \tag{4.5.7}$$

where $G_{jm} = 0 \qquad \text{for } m = 1,2,3$

$$G_{j4} = -\frac{gHk}{2\sigma \text{ Cosh } kd}\Big\{(n_x)_j \text{ Cosh } k(d+y_j) \text{ Cos } kx_j + (n_y)_j \text{ Sinh } k(d+y_j) \text{ Sin } kx_j\Big\}$$

$$H_{jm} = -i\sigma(n_m)_j \qquad \text{for } m = 1,2,3$$

$$H_{j4} = -\frac{gHk}{2\sigma \text{ Cosh } kd}\Big\{(n_x)_j \text{ Cosh } k(d+y_j) \text{ Sin } kx_j - (n_y)_j \text{ Sinh } k(d+y_j) \text{ Cos } kx_j\Big\}$$

By using the matrix solution method detailed in Appendix A4.2, the matrix equation (4.5.1) may be solved for the Source Distribution Function expressed in matrix notation:

$$[f] = \underset{(2N,4)}{\begin{bmatrix} E \\ F \end{bmatrix}} \qquad (4.5.8)$$

where: $f_{jm} = E_{jm} + iF_{jm}$

4.6 Numerical Evaluation of the Discretised Velocity Potential.

The equation from which the velocity potential may be evaluated is:

$$\Phi_m(\underline{x}) = \int_\Gamma f_m(\underline{\xi})g(\underline{x},\underline{\xi})\, d\Gamma \qquad (4.6.1)$$

where: m refers to the four modes referred to in Section 4.3.

Using similar reasoning as in Section 4.2. it may be stated that, since the value of the Green's Function varies slowly over the length of the body, its value may be taken as constant over each element and equal to its value at the element centroid. This permits equation (4.6.1) to be expressed in discretised form thus:

$$\Phi_m(\underline{x}_j) = \sum_{k=1}^{N} g(\underline{x}_j,\underline{\xi}_k)f_m(\underline{\xi}_k)\Delta\Gamma_k \qquad (4.6.2)$$

The parameters ϕ, f and g are complex quantities and may be defined:

$$\phi = \phi' + i\phi''$$

$$f = f' + if''$$

$$g = g' + ig''$$

Substitution in equation (4.6.2) together with separation into real and imaginary parts gives:

$$\phi'_m(\underline{x}_j) = \sum_{k=1}^{N} \left\{ g'_{jk} f'_{km} - g''_{jk} f''_{km} \right\} \Delta\Gamma_k \qquad (4.6.3a)$$

$$\phi''_m(\underline{x}_j) = \sum_{k=1}^{N} \left\{ g'_{jk} f''_{km} + g''_{jk} f'_{km} \right\} \Delta\Gamma_k \qquad (4.6.3b)$$

where: g'_{jk} and g''_{jk} may be evaluated from the expressions contained in Appendix A2.

f'_{km} and f''_{km} have been evaluated from equation (4.5.8);

It must be noted that, as with its normal gradient, the value of the Green's Function does not change gradually when the source point approaches the field point. In this case, the real part of the Green's Function must be evaluated from the expression derived in Appendix A3.

4.7 Numerical Evaluation of the Green's Function Expression.

The evaluation of the expressions defining the Green's Function and its normal gradient at the specified nodal points on the object

boundary resulting from the presence of a discrete number of point sources located on the source distribution boundary constitutes the basis of the formulation employed in the numerical solution of the hydrodynamics problem.

It can therefore be seen that the accuracy of the overall solution is significantly dependent upon the precision with which the individual functions are evaluated.

The degree of precision, however, is subject to diminishing returns in that, beyond a certain point, a relatively small improvement in precision is achieved at the expense of a disproportionately large amount of computation time. Since the subdivision of the immersed profile of the object into N boundary elements necessitates the evaluation of $3N^2$ Green's Functions (no distinction is made between the Green's Function and its gradients since the time required for evaluation is, in each case, of a comparable order of magnitude), it becomes obvious that the efficiency, both with regard to precision and time, with which each function is evaluated has considerable bearing on the overall solution efficiency.

The relationship between overall efficiency and the efficiency of individual function evalutions becomes even more signficiant in view of the fact that the bulk of CPU time required for the overall solution is consumed in evaluating the functions for inclusion in the matrices described in preceding sections. (In practice, the proportion of overall CPU time required for function evaluation is in the order of 95%).

Since the evaluation of the imaginary part of the function is solely

a matter of direct substitution in the appropriate expression, it presents no numerical problems. This section is concerned with the numerical techniques required for the evaluation of the real part of the function.

4.7.1 The Integral Formulation.

Inpsection of the expressions detailed in Appendix A2.3 shows that the Particular Value integral can be subdivided into two distinct parts:

(i) The Singular Portion $0 \leqslant \mu \leqslant \mu_1$

(ii) The Remainder Portion $\mu_1 \leqslant \mu \leqslant \mu_{max}$

Each part will be dealt with separately herein.

a) <u>The Singular Portion $0 \leqslant \mu \leqslant \mu_1$</u>

A preliminary series of tests demonstrated that there was no obvious advantage to be gained from taking the value of μ_1 to be anything other than 2k.

A series of tests, using parameters within the range of this investigation, was performed in order to decide the most efficient method of numerically integrating the modified functions in the range $0 \leqslant \mu \leqslant 2k$.

Two alternative methods of integration were investigated:

DEPTH (m) 1.200
FREQUENCY (Hz) 0.684
FIELD POINT COORDINATES (m) (0.1000, -0.0375)
SOURCE POINT COORDINATES (m) (0.0000, -0.0375)

METHOD 1

0 -> 0.999K SIMPSONS RULE
0.999K -> 1.001K TRAPEZOIDAL RULE
1.001K -> 2K SIMPSONS RULE

METHOD 2

0 -> 2K THREE EIGHTHS RULE

FUNCTION : GPVM

METHOD	NO.OF ORDINATES	INTEGRAL VALUE
1	42	-0.74984536
2	82	-0.74984591

FUNCTION : DGXPVM

METHOD	NO.OF ORDINATES	INTEGRAL VALUE
1	22	-0.80800964
2	82	-0.80801011

FUNCTION : DGYPVM

METHOD	NO.OF ORDINATES	INTEGRAL VALUE
1	26	1.8778552
2	82	1.8778605

Table 4.7.1 Numerical Integration of the Modified Green's Functions.

Method 1.

$0 \leqslant \mu \leqslant 0.999k$: Simpson's Rule.

$0.999k \leqslant \mu \leqslant 1.001k$: Trapezoidal Rule using a single interval.

$1.001k \leqslant \mu \leqslant 2k$: Simpson's Rule.

Method 2. (Monacella[71])

$0 \leqslant \mu \leqslant 2k$: Three-Eighths Rule avoiding the indeterminate central ordinate.

Both methods employed the same convergence criteria.

The results demonstrate conclusively that Method 1 is significantly more efficient than Method 2 with no loss of precision.

A typical test result is shown in Table 4.7.1.

The function notation in the table refers to the computer program functions used for evaluation:

GPVM : The modified Green's Function

DGXPVM : The x-gradient of GPVM

DGYPVM : The y-gradient of GPVM

b) <u>The remainder portion $2k \leqslant \mu \leqslant \mu_{max}$</u>

Consideration of equation (A2.7) of Appendix A2.3 shows that, at

large values of μ, the integrand approaches the form:

$$g_1(\text{integrand}) \rightarrow \frac{\frac{1}{2}\left\{\frac{\mu+\nu}{\mu}\right\}e^{\mu(b+y)}\text{Cos } \mu(x-a)}{\mu-\nu} \qquad (4.7.1a)$$

Straightforward differentiation leads to the corresponding expressions for the x and y gradients:

$$\frac{\partial g_1}{\partial x}(\text{integrand}) \rightarrow \frac{-\frac{1}{2}(\mu+\nu)e^{\mu(b+y)}\text{Sin } \mu(x-a)}{\mu-\nu} \qquad (4.7.1b)$$

$$\frac{\partial g_1}{\partial y}(\text{integrand}) \rightarrow \frac{\frac{1}{2}(\mu+\nu)e^{\mu(b+y)}\text{Cos } \mu(x-a)}{\mu-\nu} \qquad (4.7.1c)$$

It can thus be seen that, in all three cases, the integrand decays with $e^{\mu(b+y)}$ since the quantity (b+y) is invariably negative.

In the case of floating bodies, (b+y) is usually small resulting in slow decay of the integrands.

It can be seen from the above expressions that when (b+y) is zero, no integrand decay takes place in the case of the x and y gradients and the integrands converge to purely sinusoidal terms. However, since function evaluations are only required at the centroids of submerged boundary elements, the case is unlikely to arise and is of academic interest only.

In all three cases, however, when (b+y) is small the integrands commence a sinusoidal oscillation prior to significant decay taking place. This behaviour, clearly illustrated in Figures A2.1 to A2.3, presents problems in determining the point of acceptable convergence.

DEPTH (M) 1.200
FREQUENCY (Hz) 0.488
FIELD POINT COORDINATES (M) (0.0500, -0.0250)
SOURCE POINT COORDINATES (M) (0.0000, -0.0250)

FUNCTION : GPV

NO.OF STEPS	STEPPING FACTOR	NO.OF INTERVALS	INTEGRAL VALUE
6	1.55663	72	1.137445
7	1.46127	72	1.137445
8	1.39360	72	1.137446
9	1.34315	72	1.137445

INTEGRATION WITHOUT STEPPING

NO.OF INTERVALS : 256
INTEGRAL VALUE : 1.137445

FUNCTION : DGXPV

NO.OF STEPS	STEPPING FACTOR	NO.OF INTERVALS	INTEGRAL VALUE
8	1.51973	44	-5.910771
9	1.45068	48	-5.910772
10	1.39770	52	-5.910773
11	1.35580	56	-5.910773

INTEGRATION WITHOUT STEPPING

NO.OF INTERVALS : 128
INTEGRAL VALUE : -5.910818

FUNCTION : DGYPV

NO.OF STEPS	STEPPING FACTOR	NO.OF INTERVALS	INTEGRAL VALUE
6	1.55663	48	6.749044
7	1.46127	44	6.749044
8	1.39360	40	6.749053
9	1.34315	44	6.749046

INTEGRATION WITHOUT STEPPING

NO.OF INTERVALS : 128
INTEGRAL VALUE : 6.749067

Table 4.7.2 Effect of Stepped Integration of the Green's Function Remainder Integral.

The following method of numerical evaluation has therefore been adopted:

Taking the integrand expression for the x-gradient as an example, it can be seen that the integrand becomes zero at the following points:

$$\mu(x-a) = 0,\ \pi/2,\ \pi,\ 3\pi/2 \text{ etc.}$$

Similarly to the method suggested by Hogben and Standing[43], the function is integrated in step fashion using Simpson's Rule until the first zero point after $\mu = 2k$ has been reached.

Starting from $\mu = 2k$, the current value of μ is multiplied by a factor to determine the succeeding step length. Providing that the factor exceeds unity, this ensures that the step length becomes progressively larger as the integrand decays thus reducing, by a significant amount, the number of ordinates to be considered in the numerical integration. The integrand is then integrated over each step length using Simpson's Rule.

A series of tests, carried out using a suitable range of parameters, demonstrated that the optimum step factor was 1.44. Use of this step factor resulted in a 50-60% reduction in the number of computations required.

A typical result is shown in Table 4.7.2.

Having reached the first zero point after $\mu = 2k$, the function is integrated cycle by cycle, the step length being $2\pi/(x-a)$, until the

contribution to the overall integral by any individual cycle is negligible. The assumption is made that the remaining integral in the range $\mu_{max} < \mu < \infty$ is zero.

Three possible methods of cyclic integration were tested:

Method 1: Straightforward numerical integration over the whole cycle length.

Method 2 : Integrating 4 times over quarter-cycle steps and summing the results.

Method 3 : Subdividing the cycle length into the ratios suggested by Appendix A4.3 and summing the individual values.

The test results demonstrated conclusively that adoption of Method 3 would achieve a 30% reduction in the number of ordinate evaluations.

A flow-chart describing the computer subroutine used to evaluate the Green's Function integral formulation can be found in Appendix A7.

4.7.2 The Series Formulation.

From Appendix A2.4 it can be seen that the evaulation of the series formulation of the Green's Function is a straightforward summation operation.

It can be seen, however, that the summation terms for the function and its x and y gradients are similar in form. If each function was computed in a separate routine, a great many computations would be needlessly repeated incurring considerable expenditure of CPU time.

DEPTH	1.200 (m)
FREQUENCY	0.684 (Hz)
FIELD POINT Y-COORDINATE	-0.0250 (m)
SOURCE POINT Y-COORDINATE	-0.0250 (m)
WAVE NUMBER	1.920661 (1/m)

HORIZONTAL SEPARATION LIMIT (G1)	0.0047 (m)
HORIZONTAL SEPARATION LIMIT (DG1/DX)	0.0120 (m)
HORIZONTAL SEPARATION LIMIT (DG1/DY)	0.0115 (m)

HORIZONTAL SEPARATION	G1 (INTEGRAL)	NO.OF ORDINATES	G1 (SERIES)	NO.OF TERMS
0.006	-0.857795D 00	370	-0.857594D 00	313
0.005	-0.887233D 00	338	-0.886697D 00	313
0.004	-0.923093D 00	370	-0.922304D 00	361
0.003	-0.969148D 00	338	-0.968150D 00	457
0.002	-0.103387D 01	338	-0.103214D 01	601

HORIZONTAL SEPARATION	DG1/DX (INTEGRAL)	NO.OF ORDINATES	DG1/DX (SERIES)	NO.OF TERMS
0.014	0.123812D 02	358	0.123806D 02	264
0.013	0.131916D 02	338	0.131902D 02	265
0.012	0.141461D 02	342	0.141430D 02	265
0.011	0.152844D 02	246	0.152827D 02	313
0.010	0.166624D 02	254	0.166580D 02	313

HORIZONTAL SEPARATION	DG1/DY (INTEGRAL)	NO.OF ORDINATES	DG1/DY (SERIES)	NO.OF TERMS
0.013	-0.394727D 01	418	-0.394728D 01	361
0.012	-0.397859D 01	408	-0.397857D 01	385
0.011	-0.400791D 01	426	-0.400790D 01	433
0.010	-0.403511D 01	458	-0.403513D 01	457
0.009	-0.406008D 01	490	-0.406010D 01	505

Table 4.7.3 Comparison of Integral and Series Evaluation of the Green's Function

To avoid this, each function may be computed in the same routine, the summation term being modified accordingly.

A flow-chart describing the relevant computer subroutine can be found in Appendix A7.

4.7.3. Comparison between the Integral and Series formulation.

Many authors (e.g. Garrison[24]) state that the series formulation provides a more efficient function evaluation when the horizontal separation between source and field point is large.

Conversely, when the horizontal separation |x-a| is small, it becomes more efficient to use the integral formulation.

The results of a series of tests show that the optimum change over point is a function not only of horizontal source/field point separation but also of the combined field and source point depths below the mean free-surface of the fluid.

A typical test result is shown in Table 4.7.3.

The following empirical formulae have been derived in order to determine the optimum "change-over" point:

It is more efficient to use the Integral Formulation when:

$$|x-a| \leqslant \left|\frac{\text{Log}|b+y| + 5.021}{432.2}\right| \qquad \text{in the case of } g_1 \qquad (4.7.2a)$$

$$|x-a| \leqslant \left|\frac{\text{Log}|b+y| + 5.627}{218.8}\right| \qquad \text{in the case of } \frac{\partial g_1}{\partial x} \qquad (4.7.2b)$$

$$|x-a| \leqslant \left|\frac{\text{Log}|b+y| + 8.468}{474.2}\right| \qquad \text{in the case of } \frac{\partial g_1}{\partial y} \qquad (4.7.2c)$$

It must be said in hindsight, however, that very little benefit with regard to efficiency is gained from the accurate determination of the change point. Such benefit that might be gained is more than outweighed by the additional CPU time spent in computing the change-over value.

4.7.4 Convergence Criteria.

In order to obtain overall function evaluations which are precise to within a specified tolerance, a convergence residual criterion is computed from:

$$\text{RESCON} = 1 - \frac{\text{ACC}}{100}$$

where: RESCON denotes the convergence criterion

ACC denotes the required function precision in (%).

In the use of any iterative method, convergence testing is carried out after each iteration for the purpose of not only ensuring that the end result is sufficiently precise but also for the purpose of avoiding unnecessary computation. Generally, a comparison is made between two successive iterative values and if the difference between them, as a proportion of the overall value, is less than some specified value convergence is deemed to have been achieved. An

additional requirement is usually made that the absolute value of the most recently computed iteration should exceed a given value.

The use of Simpson's Rule for numerical integration of a function entailed making an initial estimate for the integral value using a minimum number of intervals (generally 2). The number of intervals was successively doubled with convergence tests, as described above, performed after each successive doubling of the number of intervals.

Similar convergence tests were performed after each successive step length in the stepped integration procedure, and after each cycle in the cyclic integration procedure, for the evaluation of the integral formulation of the real part of the Green's Function.

In all cases, a series of tests demonstrated that sufficiently precise evaluations could be achieved if the individual convergence criteria did not exceed 1/10 of the overall convergence criterion.

Convergence using the Series Formulation was found to be exceedingly gradual and the method of convergence testing required modification. It was found that sufficiently precise evaluations could only be achieved if convergence testing was carried out on three successive iterations. If the three successive iterations satisfied the convergence criterion, then convergence was deemed to have taken place.

A series of tests showed that an adequate convergence criterion was 1/100 that of the overall criterion.

4.8 Computational Efficiency Considerations.

In the process of matrix formation for the solution of the integral equations, described in Section 4.2, certain time-saving techniques can be employed as a result of the nature of the matrices and as a result of possible symmetry of the object profile about its vertical centroidal axis.

It must be noted, however, that the time-saving techniques resulting from axial symmetry, and described in this section, apply only to the particular type of element distribution employed in this investigation (see Appendix A5).

Consideration of the expressions in Appendix A2, defining the Green's Function and its gradients, allows the following observations to be made:

a) When field and source points are transposed, both the real and imaginary evaluations of the Green's Function remain unchanged.

b) When field and source points are transposed, both the real and imaginary evaluations of the Green's Function x-gradient remain unchanged in magnitude but undergo a sign change.

Regardless of body symmetry and element distribution, this results in a 30% reduction in the number of Green's Function evaluations required for matrix formation.

For an object profile which is symmetric, both with respect to geometry and element distribution, about the vertical axis through

the centroid, the following additional time-saving techniques, using the nomenclature of equations (4.5.4) and (4.5.7), may be applied:

c) In both the [C] and [D] matrices, the $(n-i+1)^{th}$ row is the reverse mirror image of the i^{th} row.

Thus:

$$C_{ij} = C_{n-i+1,n-j+1} \qquad i = 1,n; \quad j = 1,n;$$

$$D_{ij} = D_{n-i+1,n-j+1} \qquad i = 1,n; \quad j = 1,n;$$

d) In the [G] matrix:

$$G_{ij} = -G_{n-i+1,j} \qquad i = 1,n; \quad j = 4;$$

e) In the [H] matrix:

$$H_{ij} = -H_{n-i+1,j} \qquad i = 1,n; \quad j = 1,3;$$

$$H_{ij} = H_{n-i+1,j} \qquad i = 1,n; \quad j = 4;$$

Application of these properties results in a 50% reduction in computation time.

f) The matrix of Green's Functions required for the solution of equations (4.6.3) is symmetric about both diagonals. This enables a 75% reduction in CPU time for formation of the matrix.

In Appendix A4.2, which describes methods of solution of complex matrix equations, it can be seen that Methods 2 and 3 derive from the method outlined by Hogben and Standing[43]. Their method was

used in the solution of a three-dimensional source distribution matrix and required the inversion of the matrix pertaining to the imaginary parts of the normal gradient of the Green's Function. As will be seen, this is not possible in the solution for a two-dimensional source distribution matrix for certain immersed surface configurations.

From equation (4.5.4):

$$D_{ij} = \left\{\frac{\partial g_2(\underline{x}_i,\underline{\xi}_j)}{\partial x}(n_x)_i + \frac{\partial g_2(\underline{x}_i,\underline{\xi}_j)}{\partial y}(n_y)_i\right\}\Delta\Gamma_j \qquad (4.8.1)$$

If the i^{th} and m^{th} element are both on vertical surfaces:

$$(n_y)_i = (n_y)_m = 0$$

$$(n_x)_i = \pm(n_x)_m = \pm 1$$

Substitution of these values in equation (4.8.1), together with the expression for $\partial g_2/\partial x$ from equation (A2.4), yields the following:

$$\frac{D_{ij}}{D_{mj}} = \pm\frac{\text{Cosh } k(d+y_i)\text{Sin } k(x_i-a_j)}{\text{Cosh } k(d+y_m)\text{Sin } k(x_m-a_j)} \qquad (4.8.2)$$

It can be seen that if Sin $k(x_i-a_j)$ = Sin $k(x_m-a_j)$, the i^{th} and m^{th} row of the [D] matrix will have a common factor since the expression is independent of the column number j. The determinant of [D] will thus be zero preventing the use of solution techniques having the [D] matrix as the coefficient matrix.

The most likely case of the above situation arising is when the i^{th} and m^{th} element are on the same vertical surface, i.e when $x_i = x_m$.

It becomes obvious, therefore, that the determinant of [D] will become zero when the immersed surface of the object is substantially rectangular.

4.9 Limitations of the Green's Function-Integral Equation Method.

4.9.1 Irregular Frequencies.

John[49] proved the existence and uniqueness of the solutions to the two- and three-dimensional potential problems pertaining to oscillations of a rigid body in a free-surface. The solutions were subject to the provisions that no point of the immersed surface of the body would be outside a cylinder drawn vertically downward from the intersection of the body with the free-surface and that the free-surface would be intersected orthogonally by the body in its equilibrium position. This last provision derives from the fact that the kernel of the Fredholm equation is singular on the curve of intersection of the body and the free-surface rendering Fredholm theory invalid. This problem can be overcome by the orthogonality requirement.

John also showed that for a set of discrete 'irregular' frequencies, the integral equation method failed to give a solution. He demonstrated that the irregular frequencies occurred when the integral equation had eigenfunctions. At an irregular frequency, the matrix to be inverted in the process of obtaining a solution becomes singular as the number of boundary elements increases without limit i.e. as $N \rightarrow \infty$. In practice, with a finite number of boundary

elements, the determinant of this matrix becomes very small, not only at the irregular frequency but also within an interval about this frequency. The extent of this interval can be reduced by increasing the number of boundary elements.

Each eigensolution, in fact, represents a non-trivial source distribution over the body surface which leaves the external flow field undisturbed. The irregular frequencies are a feature of describing the body in terms of a distribution of sources and are not inherent in the original hydrodynamics problem. They can be eliminated by locating the sources inside the body boundary (the regular kernel method) or by solving the problem in another way.

Frank[20] graphically illustrates the behaviour of computed hydrodynamic coefficients in the region of an irregular frequency. It can be seen therein that, provided the solutions pertaining to the narrow band surrounding the irregular frequency are not considered in isolation, correct values may be obtained by graphical or numerical interpolation.

Frank (amongst others) evaluated the irregular frequencies for a rectangular two-dimensional floating body. For the purpose of completeness, however, details of the evaluation method are included herein:

Consider a rectangular two-dimensional floating body of length B and draught D:

Let $\Psi(x,y)$ be such that:

1. $$\frac{\partial^2\Psi}{\partial x^2} + \frac{\partial^2\Psi}{\partial y^2} = 0$$

in the region bounded by the immersed surface of the body and the extension of the free-surface within the body.

2. $\Psi = 0$

on the surface of the body below the free surface.

$$\text{i.e.} \quad \Psi = 0 \left\{ \begin{array}{lll} @\ x = 0; & 0 \leqslant y \leqslant D \\ @\ x = B; & 0 \leqslant y \leqslant D \\ @\ y = B; & 0 \leqslant x \leqslant B \end{array} \right\}$$

3. $$\frac{\partial\Psi}{\partial y} - \nu_n\Psi = 0$$

on the extension of the free-surface within the body, where ν_n is the deep-water wave number corresponding to the irregular radial frequencies σ_n, $n = 1,2,...$

Integration of Laplace's equation (condition 1) using the method of separation of variables and applying boundary condition 2 yields the eigenfunctions:

$$\Psi_n = A_n \, \mathrm{Sin}\left\{\frac{n\pi x}{B}\right\}\mathrm{Sinh}\left\{\frac{n\pi D}{B}\right\} \qquad n = 1,2,.... \qquad (4.9.1)$$

where: A_n are Fourier Coefficients to be determined from an appropriate boundary condition.

Applying the free surface boundary condition (3) on y = D for $0 \leqslant x \leqslant B$ gives the irregular wave numbers:

$$\nu_n = \left\{\frac{n\pi}{B}\right\}\mathrm{Coth}\left\{\frac{n\pi D}{B}\right\} \qquad n = 1,2,.... \qquad (4.9.2)$$

But: $\nu_n = \frac{2\pi}{L_n}$

Substitution in equation (4.9.2) yields:

$$\left\{\frac{B}{L}\right\}_n = \frac{n}{2}\,\mathrm{Coth}\left\{\frac{n\pi D}{B}\right\} \qquad (4.9.3)$$

where: $(B/L)_n$ is the body length/wavelength ratio corresponding to the n^{th} irregular wave frequency.

By substituting realistic values of B/D in equation (4.9.3), it can be seen that the irregular frequencies are too high to be of practical interest.

4.9.2 Ill-Conditioning of Matrix Equations.

The matrix equation:

$$[A]\,[X] = [B]$$

is said to be ill-conditioned if a small change in the matrix [B]

results in a disproportionately large change in the solution matrix [X].

Without going into the labororious procedure of computing the so-called 'ill-conditioning numbers', it can be stated that ill-conditioning of matrix equations is generally associated with a lack of dominance of the elements on the leading diagonal of the coefficient matrix [A]. The leading diagonal may be regarded as dominant if:

$$|A_{ii}| > \sum_{j \neq i} |A_{ij}| \qquad \begin{matrix} i = 1,2,\ldots,n \\ j = 1,2,\ldots,n \end{matrix}$$

The formulations used in the evaluation of the matrix elements discussed in section 4.2 dictate that lack of diagonal dominance will always be a feature of the coefficient matrices. It is this feature which suggests the lack of suitability of iterative solution techniques, such as the Gauss-Seidel method, since diagonal dominance is a necessary condition to ensure rapid convergence.

In this particular investigation it was found that, providing the degree of ill-conditioning was not especially severe, acceptably precise solutions could be obtained from the use of the Gauss-Jordan Elimination method employing Pivotal Element techniques to minimise round-off errors.

In view of the relaxation adopted to permit a discretised solution of the integral equations (4.4.4) and (4.4.10), it may be theorised that increasingly fine subdivision of the source and object boundaries will result in more precise solutions. To a certain extent this is the case in practice. However, there comes a point at

which any advantage to be gained from finer subdivision is outweighed by the effects of matrix ill-conditioning.

It has previously been stated that the possibility of an acceptably accurate discretised solution depends substantially on the fact that the Green's Function varies insignificantly over the length of a boundary element. As a consequence, finer subdivision of the boundaries results in elements around the leading diagonal of the coefficient matrix converging to the same order of magnitude, resulting in total lack of diagonal dominance which, in turn, leads to severe ill-conditioning of the equations.

In the case of body profiles containing areas of high curvature, it is recommended (see Appendix A5) that high element concentrations are required to model these areas adequately. It is also recommended that, in order to preserve accuracy, element lengths should change gradually between areas of high and low curvature. It becomes apparent, therefore, that ill-conditioned matrices will be a distinct feature of solutions for these body configurations, thus imposing severe limitations on the use of this method.

4.10 Comparison with Published Data.

Several texts (e.g. Salvesen, Tuck and Faltinsen[84]; Frank[20]) contain theoretical computations of the hydrodynamic coefficients, exciting forces and generated wave amplitudes pertaining to substantially rectangular sections. They do not, however, present experimental results for comparative and validatory purposes.

A systematic theoretical and experimental investigation was carried out by Vugts[101] on a variety of two-dimensional immersed surface profiles, including rectangular sections with differing aspect ratios, and many theoretical texts published since that date (e.g. Wehausen[103]; Adee and Martin[2]) utilise these results for comparison with their own theoretical results.

In order to provide a comparison with published data, a theoretical analysis was performed on a freely-floating rectangular section, with an immersed surface aspect ratio of 4, using the method and formulation described herein. Several authors (e.g. Sarpkaya and Isaacson[86]) cite the numerical advantages of smoothing-off sharp corners on the mathematical model to provide a continuous immersed surface. For comparative purposes, therefore, a similar analysis was performed on a substantially rectangular section, of similar immersed surface aspect ratio, having radial submerged edges.

To conform with the experimental data published by Vugts, a body length of 0.4m was used together with a flume depth of 2.0m.

In the case of the radially-edged body, the minimum element length was dictated by the number of constant length elements used to describe the radial edge. To comply with the recommendations contained in Appendix A5, pertaining to the subdivision of the immersed surface, four constant length elements were used on each radial edge. In the case of the squared-edged body, a similar minimum element length was chosen to validate a comparison of results with those obtained from the radially-edged body. In both cases, an element length ratio (see Appendix A5) of 0.99 was employed to minimise the variation in element length over the

immersed surface.

In the absence of any data being available with respect to the mass and inertia of the floating body used in Vugts' experimental analysis, suitable parameters were chosen to provide the required immersed surface aspect ratio. The body was assumed to be of uniform density and the inertia was computed accordingly. The radius of the edges of the substantially rectangular section was chosen to minimise any difference in mass or inertia parameters arising from the change in edge geometry.

The geometric, inertial and element distribution data pertaining to the two bodies is contained in tables 4.10.1 and 4.10.2 and the results are presented, in conjunction with Vugts' theoretical experimental results, in Figs. 4.2 to 4.5.

In the analysis performed by Vugts, conformal transformation techniques were employed to derive the theoretical added-mass and damping coefficients. The method of superposition of potential functions, postulated by Ursell[95] and developed by De Jong[17], was employed to derive the coefficients for a floating circular cylinder and these results were conformally transformed to those pertaining to a rectangular section by means of a standard five-parameter polynomial transformation.

The exciting forces acting on the body were obtained from the relationship, derived by Newman[73], between the exciting force and the damping coefficient for an axi-symmetric body.

The generated wave amplitudes were obtained by applying the

far-field boundary conditions to the generated potentials computed in the process of solving for the hydrodynamic coefficients.

Despite Vugts' use of deep-water approximations in his theoretical formulations, the actual depths specified are insufficient to achieve deep-water conditions at the lower end of the frequency range. A brief calculation, using the water depth and body length specified, shows that deep-water conditions were achieved for values of the diffraction parameter $\sigma(L/2g)^{\frac{1}{2}} > 0.7$. Thus comparison between Vugts' theoretical results and those derived from the source-distribution formulation is only valid for $\sigma(L/2g)^{\frac{1}{2}} > 0.7$. It can be seen from fig. 4.2 that agreement in this range is good.

The low frequency trend of Vugts' experimental added-mass coefficients in heave show good agreement with the theoretical added-mass coefficients derived from the source-distribution formulation. In the lower frequency range, Vugts' results for surge added-mass coefficients differ substantially from the source distribution results. Reference to Kim[53] shows that this deviation is entirely attributable to the neglect of finite depth effects mentioned above.

Whilst maintaining the same trends, the damping coefficients presented in Fig.4.3 differ in value from both the experimental and theoretical results presented by Vugts. Since values of damping coefficients in surge and heave do not display the same sensitivity to depth as the added-mass coefficients, it is unlikely that the difference results from neglect of finite depth. However, the constant difference exhibited in the case of the heave coefficients suggests the possibility of a systematic error in Vugts' computation

procedure. Since the exciting force coefficients are computed directly from the damping coefficients, a similar deviatory trend is to be expected and this is illustrated in Fig. 4.4. Agreement of results is good in the case of waves generated as a result of surge motion but not in the case of waves generated by heave. No obvious explanation can be given for this.

The experimental technique employed by Vugts was to apply a forced motion, of known amplitude, to the body. The external force was measured and inserted, together with the motion amplitude, into the equations of motions to give the hydrodynamic coefficients. The experimental results, however, must be treated with a certain degree of caution since zero values were assumed for the coupling coefficients of pitch into surge and the equations of motion modified accordingly. Inspection of additional results presented by Vugts demonstrated that this clearly was not the case.

For source-distribution results pertaining to surge and heave, there is very little difference between the results obtained from the square- and radially-edged bodies. The pitch results, however, exhibit a marked sensitivity to changes in edge geometry. In the absence of any obvious physical reason for this, it must be concluded that an inability to define the normal direction at a sharp corner gives rise to a discontinuity of the source strength distribution function at that point, resulting in numerial inaccuracies. In the preceding chapter, it was shown that the added-mass and damping coefficient matrices are symmetrical. The use of radial edges resulted in a marked improvement of agreement between reflected elements of the above matrices, thus providing further evidence to conclude that the improvement in results must be

attributed to numerical rather than physical reasons.

The non-dimensional parameters used in Figs.4.2 to 4.5 are detailed below:

Added-Mass Coefficients:

$$\bar{\mu}_{11} = \frac{\mu_{11}}{M} \qquad \bar{\mu}_{22} = \frac{\mu_{22}}{M} \qquad \bar{\mu}_{33} = \frac{\mu_{33}}{ML^2}$$

Damping Coefficients:

$$\bar{\lambda}_{11} = \frac{\lambda_{11}}{M}\left\{\frac{L}{2g}\right\}^{1/2} \qquad \bar{\lambda}_{22} = \frac{\lambda_{22}}{M}\left\{\frac{L}{2g}\right\}^{1/2} \qquad \bar{\lambda}_{33} = \frac{\lambda_{33}}{ML^2}\left\{\frac{L}{2g}\right\}^{1/2}$$

Exciting Force Components:

$$\bar{F}_1(e) = \frac{F_1(e)}{Mgk(H/2)} \qquad \bar{F}_2(e) = \frac{F_2(e)}{\rho gH(L/2)} \qquad \bar{F}_3(e) = \frac{F_3(e)}{\rho g(L^2/12)k(H/2)}$$

Generated Wave Ratios:

$$\bar{n}_1 = \frac{(H/2)}{n_1} \qquad \bar{n}_2 = \frac{(H/2)}{n_2}$$

where: M = Body mass per unit width.

L = Body length in direction of wave travel.

n = Generated wave amplitude.

All other symbols are as defined in Appendix A9.

COMPUTATION DATA

Greens Function Accuracy	99.990	(%)

GEOMETRICAL DATA (SQUARE EDGES)

Body Length	0.4000	(m)
Body Depth	0.2000	(m)
Draught	0.1000	(m)
Centroidal Y-Coordinate	0.00000	(m)
Metacentric Height	0.08333	(m)

INERTIAL DATA PER M.WIDTH (HOMOGENEOUS)

Density	500.000	(Kg/m^3)
Mass	40.000	(Kg)
Mass Moment of Pitching Inertia	0.667	($Kg.m^2$)

SPRING RESTRAINT DATA N/M (PER M.WIDTH)

Surge	FREE
Heave	FREE
Pitch	FREE

ELEMENT DISTRIBUTION DATA

Nominal Element Length Ratio	0.99	
No.of Side Elements	10	
No.of Base Elements	37	
Total No.of Elements	57	
Min.Element Length	0.010000	(m)
Max.Side Element Length	0.010000	(m)
Max.Base Element Length	0.011712	(m)
Side Element Length Ratio	1.000000	
Base Element Length Ratio	0.991261	

TABLE 4.10.1 Floating Body Details

COMPUTATION DATA

Greens Function Accuracy	99.990	(%)

GEOMETRICAL DATA (RADIAL EDGES)

Body Length	0.4000	(m)
Body Depth	0.1993	(m)
Edge Radius	0.0250	(m)
Length/Draught Ratio	4.0000	
Draught	0.1000	(m)
Centroidal Y-Coordinate	0.00032	(m)
Metacentric Height	0.08455	(m)

INERTIAL DATA PER M.WIDTH (HOMOGENEOUS)

Density	500.000	(Kg/m^3)
Mass	39.732	(Kg)
Mass Moment of Pitching Inertia	0.655	($Kg.m^2$)

SPRING RESTRAINT DATA N/M (PER M.WIDTH)

Surge	FREE
Heave	FREE
Pitch	FREE

ELEMENT DISTRIBUTION DATA

Nominal Element Length Ratio	0.99	
No.of Side Elements	7	
No.of Base Elements	33	
No.of Radial Elements	4	
Total No.of Elements	55	
Min.Element Length	0.009817	(m)
Max.Side Element Length	0.011422	(m)
Max.Base Element Length	0.011387	(m)
Side Element Length Ratio	0.978611	
Base Element Length Ratio	0.991314	

TABLE 4.10.2 Floating Body Details

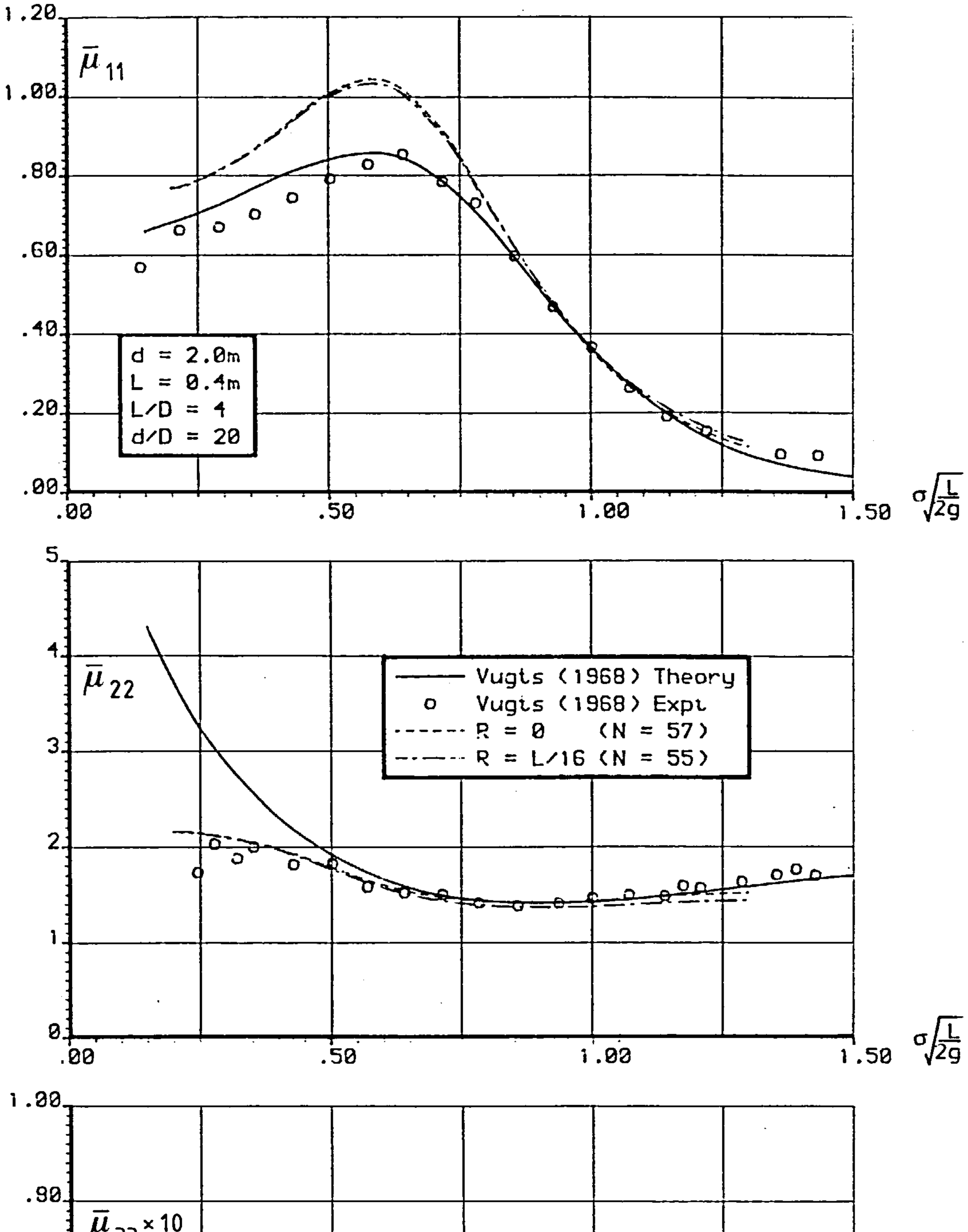

Fig.4.2 ADDED-MASS COEFFICIENTS

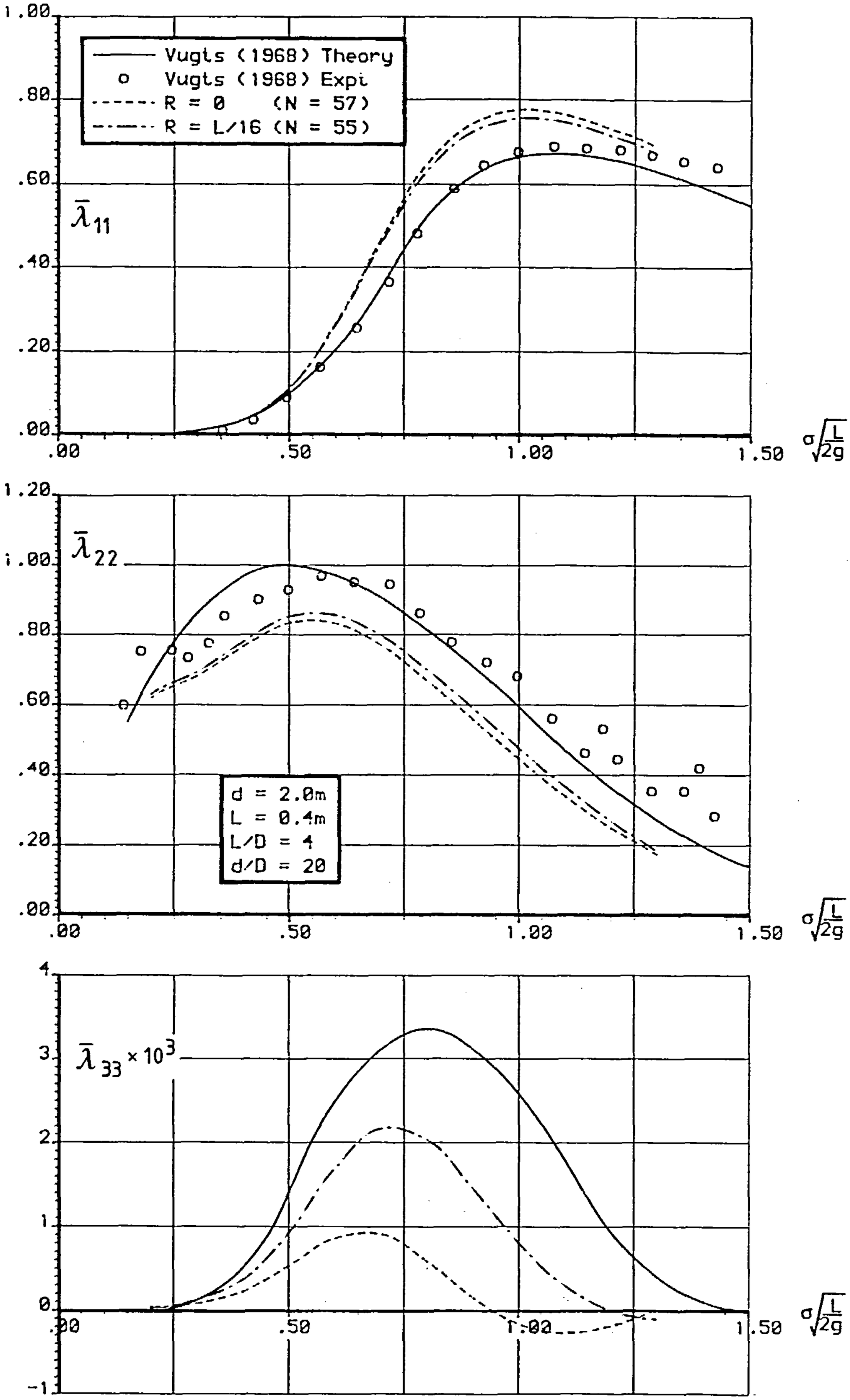

Fig.4.3 DAMPING COEFFICIENTS

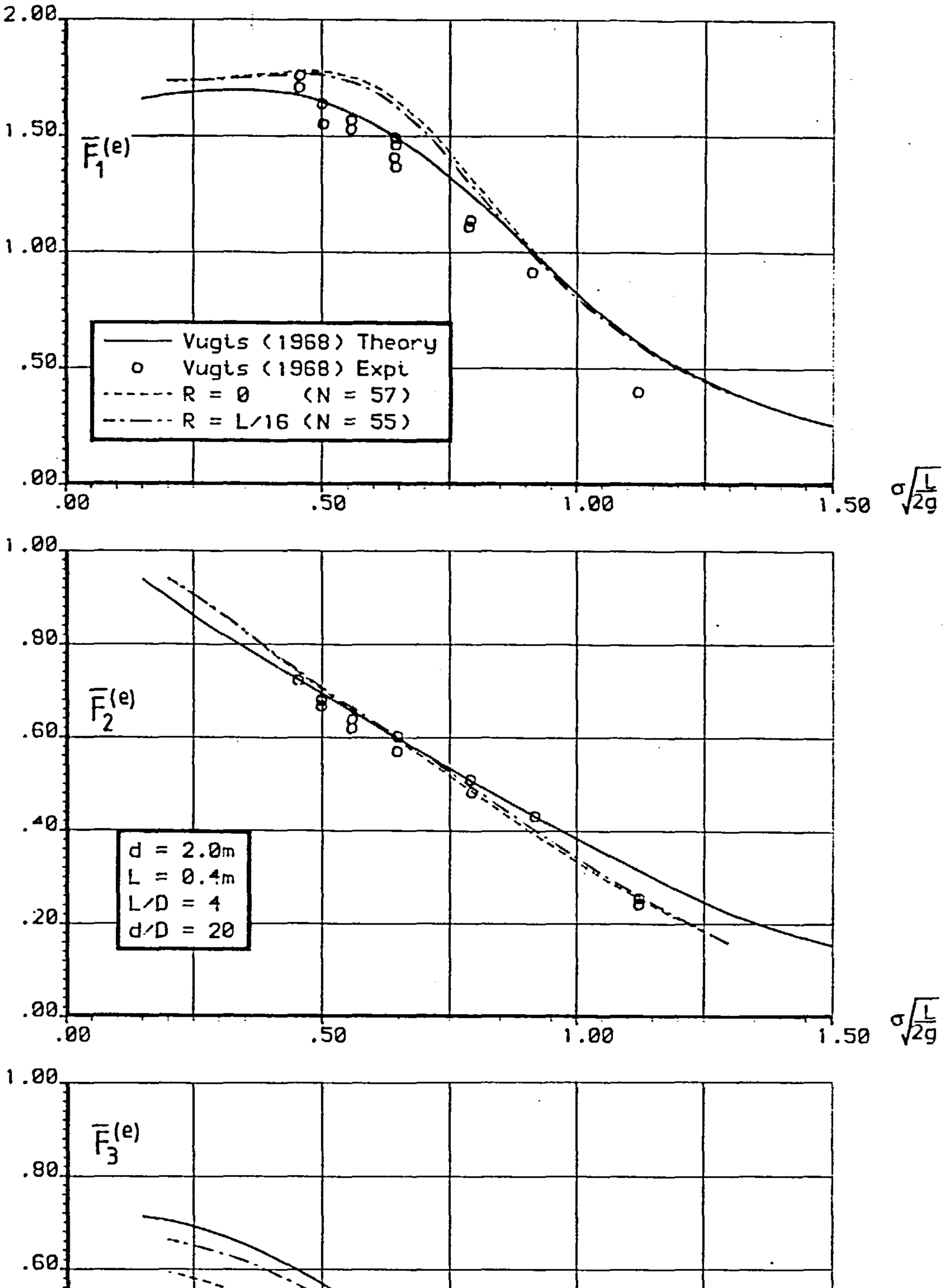

Fig.4.4 EXCITING FORCES AND MOMENTS

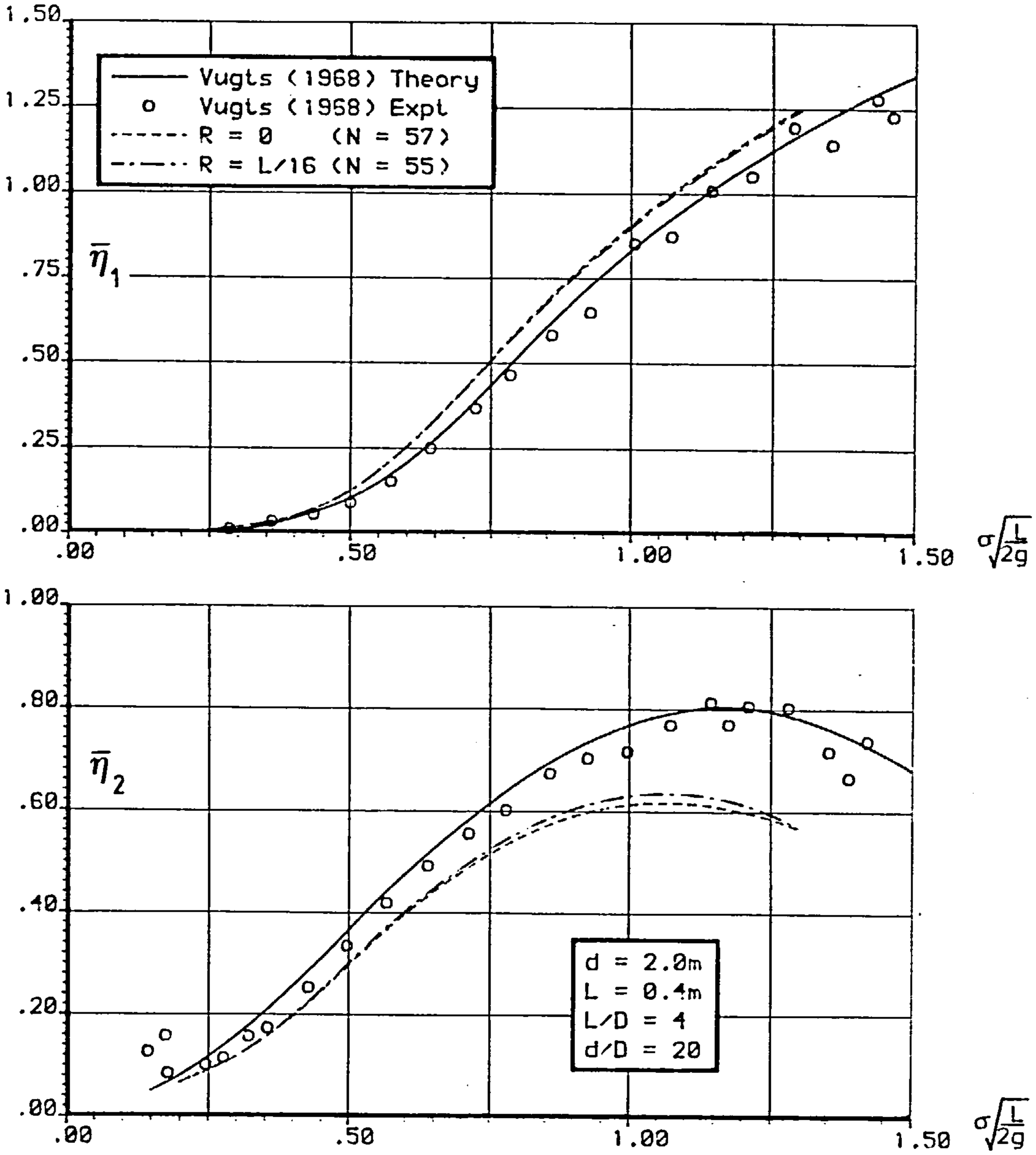

Fig.4.5 GENERATED WAVE AMPLITUDE

CHAPTER 5. THE EXPERIMENTAL INVESTIGATION

5.1 Introduction.

An experimental study has been carried out to investigate the interaction between a substantially rectangular body and a train of regular waves, with particular regard to the validation of parameters output by a computer program compiled using the methods previously detailed in Chapters 3 and 4.

Since the primary purpose of this experimental study was the validation of theory, it was felt that it should take the form of previous studies carried out with a similar purpose[101]. However, the limit of available experimental facilities, together with the more obvious time limitation, imposed certain constraints on the scope of the study, precluding the investigation of certain aspects of the system. This chapter discusses the selection of parameters to be validated by experimentation, together with the range of incident wave conditions over which the behaviour of the chosen parameters was to be investigated.

As a consequence of the fact that the hydrodynamic behaviour of a floating body is related not only to the incident wave characteristic but also to the body dimensions, it was felt that the variation in wave/body interaction should be investigated with regard to a non-dimensional diffraction parameter defining the relationship between the incident wave and the characteristic dimension of the body. In view of the fact that the range of incident waves was constrained by existing flume and wave-generation

facilities, both of which are discussed in this chapter, the body characteristic dimension had to be such that a suitable range of diffraction parameter could be achieved.

An inspection of the results obtained from previous studies has shown that floating body behaviour departs substantially from theoretical predictions in the region of the system's resonant frequency, particularly in the rotational modes of motion. It is suggested[84] that this departure is a consequence of the increase in viscous damping effects engendered by large rotational body motions. It is further suggested[52] that the effect of this damping may be somewhat alleviated by the rounding of submerged edges of the body. The limitation of experimental facilities precluded a comprehensive quantitative investigation of this phenomenon. However, it was felt that the adoption of rounded body edges, of various radii, would provide an indication of the validity of this suggestion. The decision to employ rounded body edges was also the result of practical and numerical considerations, both of which are discussed in this chapter.

The major problem associated with experimental studies of this type is the allowance of free and unrestricted motion of the body, a basic condition necessary to ensure a valid comparison between theory and actuality. For this reason, a considerable degree of attention had to be paid to the design of suitable bearing arrangements. An additional factor which had to be taken into account in this regard was the abstraction of the various motion components, the accurate measurement of which could be facilitated by the configuration of the bearings.

A feature of flume waves, generated in the fashion described in this chapter, is the significant presence of higher order components resulting in a departure from the assumed linearity of the system. The most obvious consequence of this is the presence of drift forces. It was thus necessary to design the translatory bearing arrangement to accommodate a facility for horizontal restraint of a type that could be quantified and included in the theoretical formulations. Full details of the construction of the body, together with details of the design and manufacture of the bearing arrangements, are given in this chapter.

The quality of data obtained from any experimental investigation is a direct function of the standard of equipment used in its collection. A major source of error, in this regard, is the accuracy with which such equipment is calibrated. For this reason, considerable attention was devoted to the calibration of measurement equipment, both statically and dynamically, with the intention of minimising the systematic error content of the eventual results. Another source of possible error is the method by which data is abstracted. Having selected the parameters to be measured, it was necessary to ensure the optimum method of measurement thereof, both with regard to acceptable experimental accuracy and expenditure of time. Full details of the methods of collection and analysis of data are given and, where alternative methods exist, each alternative is discussed and reasons given for its eventual acceptance or rejection.

5.2 Objectives of the Experimental Study.

The primary objective of the experimental study was the validation of the parameters output by a computer program compiled using the theoretical and numerical methods contained in Chapters 3 and 4. It was intended to determine whether, and under what conditions, the physical behaviour and induced wave-effects departed from the predictions resulting from linear diffraction analysis.

The parameters generated by the computer programme are as follows:

(i) Added-mass and damping characteristics of the body.

(ii) Exciting forces and phase angles, relative to the incident wave train, in the three directional modes.

(iii) Motion characteristics of the body in the three directions.

(iv) Reflection and transmission characteristics of the body in the fixed mode.

(v) Generated wave characteristics resulting from the motions of the floating body.

(vi) Overall reflection and transmission characteristics of the floating body as determined from the combined effects of (iv) and (v).

An experimental study pertaining to the added-mass and damping characteristics of the body, together with measurement of the exciting force components, would necessitate a technique similar to that employed by Vugts[101], in which a sinusoidally oscillating forced motion is applied to the body. Consideration of the in-phase and quadrature components of the applied force, in conjunction with the equations of motion, enables computation of the hydrodynamic

coefficients. Since the forced body motion is applied separately in the three directional modes, it is also possible to measure the generated wave amplitudes and phases. Owing to a lack of experimental facilities for this particular study, the provision of a forced motion was out of the question, therefore precluding any investigation of the abovementioned parameters.

It was adjudged that, since phase considerations are relatively unimportant in a practical context, sufficient validation could be obtained from an investigation limited to the following parameters:

(i) Amplitudes of body motion in the three directions.

(ii) Fixed-body Reflection and Transmission Coefficients.

(iii) Overall Reflection and Transmission Coefficients.

The lack of any suitable theory pertaining to higher order waves necessitated restriction of the investigation to motions and wave effects resulting from fundamental frequency incident waves.

5.3 Experimental Parameters.

5.3.1 The Diffraction Parameter.

In the manner of previous experimental studies in this field, it was intended to investigate the body motions and wave effects with respect to a dimensionless diffraction parameter which was variable over a suitable range.

Previous studies[84,101] have employed the dimensionless parameter:

$$DP = \sigma(B/2g)^{\frac{1}{2}} \qquad (5.3.1)$$

where: B = Body length in the direction of wave travel;

σ = Wave radial frequency;

It must be pointed out, however, that investigations in which this particular parameter has been used have been limited to deep-water conditions. Since the parameter takes no account of finite depth conditions, its use was considered unsuitable for studies involving intermediate or shallow depth conditions.

According to the linear dispersion equation :

$$\sigma^2 = gk \qquad \text{for deep-water conditions.} \qquad (5.3.2)$$

Substitution in equation (5.3.1) yields:

$$DP = (\pi B/L)^{\frac{1}{2}} \qquad (5.3.3)$$

where: L = Incident wave length

Since deep-water conditions were not feasible in this investigation, it was decided that a suitable diffraction parameter would be the ratio of body length to incident wave length B/L.

The difference between the two diffraction parameters with respect to depth conditions is illustrated below. It can be seen that the difference, and hence the validity of use, is significant for

intermediate depth conditions.

Depth (m)	Frequency (Hz)	Incident Wavelength (m)	Body Length (m)	$\sigma(B/2g)^{\frac{1}{2}}$	B/L
1.2	0.488	5.691	0.96	0.678	0.169
10.0	0.488	6.556	0.96	0.678	0.146

Table 5.3.1 Diffraction Parameter Variations.

In order to comply to a certain degree with realism, a maximum value of 0.5 was chosen for the diffraction parameter. A preliminary series of numerical evaluations showed that this would be sufficiently large to encompass the natural frequencies of the body in the heave and pitch modes. This was particularly important since the results of previous investigations had shown that the major departure from theoretical predictions would be likely to occur in this region.

5.3.2 Non-Dimensional Parameters.

Since the body motions and associated wave-effects were to be investigated with respect to a dimensionless diffraction parameter, it was necessary that they also be suitably non-dimensionalised. In accordance with previous investigations,the following dimensionless parameters were chosen:

$$R = \frac{n_R}{n_I}; \qquad T = \frac{n_T}{n_I}; \qquad \bar{a}_1 = \frac{a_1}{n_I}; \qquad \bar{a}_2 = \frac{a_2}{n_I}; \qquad \bar{a}_3 = \frac{Ba_3}{n_I};$$

where: η_I, η_R, η_T represent the incident, reflected and transmitted wave amplitudes respectively.

a_1, a_2 represent the translatory body motion amplitudes in surge and heave respectively.

a_3 represents the angular body motion amplitude in pitch.

R, T denote the Reflection and Transmission Coefficients.

5.3.3 Choice of Body Geometry and Dimensions.

For purposes of ease, speed and accuracy of construction, together with the more obvious economic reaons, a substantially rectangular profile was chosen for the floating body.

The Frank Close-Fit Method (see Chapter 4), on which this particular numerical method of analysis is based, was developed primarily for the purpose of predicting the behaviour of complex ship-shapes for which no explicit closed-form solutions exist. In this light, it would have been desirable to investigate the dynamic behaviour of a body possessing a ship-like profile. However, the lack of fabrication facilities and expertise precluded the construction of such a body.

Since the behaviour of the body was to be investigated with respect to the ratio of body length to incident wave length, the length of the body in the direction of travel of the incident wave was dependent on the range of incident wavelengths to be used in the investigation. A previous experimental study, carried out by the

author, of the generation and behaviour of regular waves in the laboratory flume showed that the maximum frequency at which well-behaved and stable regular waves could be generated was around 0.9Hz. Above this frequency, the waves lacked essential two-dimensional consistency owing to a marked degree of transverse oscillation. The proposed method of resolution of the free-surface profile into incident and reflected wave components (see section 5.8.2) required wave amplitude measurements to be taken at discrete locations over a range of approximately one incident wavelength. The available facilities were such that acceptably accurate resolution could be achieved for a maximum incident wavelength of 5m. For the proposed flume depth, this corresponded to a frequency of 0.45Hz. The frequency range of the incident waves was thus limited to between 0.45Hz and 0.9Hz. A few calculations, using the linear dispersion equation, showed that a body length of approximately 1.0m would enable investigations to be carried out over a diffraction parameter range of $0.1 \leqslant B/L \leqslant 0.5$. For practical purposes, the actual length chosen was 0.96m.

It was intended to investigate the validity of the theoretically formulated parameters for various length/draught ratios of the floating body. To this end, the aspect ratios chosen were 2, 4 and 8. Within each value of aspect ratio, it was intended to investigate the effect of different submerged transverse edge radii. The maximum edge radius was limited by the deviation from a 'substantially rectangular' aspect ratio. It was felt that substantial rectangularity was maintained providing the ratio of edge-radius to draught was not greater than 4. The minimum edge radius was limited by the computer storage space required to provide an adequate solution using an immersed surface subdivision which complied with

the recommendations stated in Chapter 4 and Appendix A5.

In view of these limitations, the following sets of investigations were proposed:

	L/D = 2			L/D = 4			L/D = 8		
D/R	4	8	16	4	8	16	4	8	16
L/R	8	16	32	16	32	64	32	64	128

Table 5.3.2 Proposed Body Immersed Surface Aspects

The values of draught/radius were chosen principally for the sake of economy and minimisation of the construction time. It can be seen from the above table that, with the exception of the largest and smallest radius, multiple use could be obtained from each radial edge, thus minimising the number of different radial edges requiring construction.

5.4 Experimental Apparatus.

5.4.1 The Experimental Flume and Wave Generation.

The experiments were carried out in a sunken flume of total length 65m, nominal width 1.8m and total depth from floor level of 2m. A beach consisting of ridged concrete planks was constructed at the downstream end of the flume to provide a means of energy dissipation. The beach was set at a slope of approximately 6^{o} from the horizontal and rose from the base of the flume to a height of 1.3m where it became horizontal and continued to the vertical

downstream end of the flume. In order to avoid the possibility of 100% wave reflections from the vertical end wall, the effective beach height dictated that the depth of water in the flume should not exceed 1.25m.

A preliminary series of experiments showed the dissipative properties of the beach to be acceptable for experimental purposes. Within the range of wave frequencies investigated at that time, the average beach reflection factor was found to be approximately 2%, while not exceeding 4% in any particular instance. Owing to the excellent energy dissipation provided by the beach, it was not found necessary in this investigation to take into account secondary body motions engendered by waves reflected from the beach.

A train of regular waves was generated by vertical oscillations of a triangular cross-sectioned wedge having a vertical angle of attack of approximately 30^{o}. A servo-unit reacted to an oscillating D.C. voltage signal input, in this case, from a standard sinusoidal signal generator. The servo-unit operated a hydraulic pump which motivated the wedge.

A disadvantage of many signal generators is that the frequency is set by a ten-division dial, the scale of which operates on a decade system: 0.1 → 1.0 → 10.0 → 100.0 etc. The resultant coarse resolution enables frequencies to be set with only limited accuracy. In the normal course of events, this would not pose a significant problem. However, the proposed method of frequency analysis (see section 5.8.1) necessitated the setting of frequency to a greater degree of precision. The particular type of signal generator used in this investigation possessed certain features which permitted small

alterations in frequency to be achieved by the input of a constant D.C. voltage. Used in conjunction with a ten-turn potentiometer and a digital timer/counter, this feature enabled frequencies to be set with considerable accuracy.

An unfortunate feature of wedge-generated waves is the presence of additional second and higher order free waves with dispersive properties which are independent of the fundamental wave. In the absence (to the best of the author's knowledge) of any simple theory for this type of wave generation, it can be reasonably concluded that the higher order free waves result from fluid/wedge interaction. The wedge oscillations provide a pulsating velocity component to the fluid, which does not vary exponentially with depth in the manner predicted by Stokesian theory. The difference in velocity distributions gives rise to a surfeit of energy which is dissipated in the form of higher order free waves. Previous studies carried out by the author have shown that the amplitude of the second-order free wave is of a similar order of magnitude to that of the Stokesian second-order component and, in many cases, greater. It can be seen, therefore, that the presence of free waves cannot be ignored in any study involving second and higher order components. However, this investigation entailed measurement of fundamental components only and, since the method of analysis (see section 5.8.1) enabled resolution of an oscillating signal into discrete sinusoidal frequency bands, the higher order wave and motion components could be neglected.

5.4.2 The Floating Body.

The body was constructed as shown in Figure 5.1. For reasons of water-resistance, robustness and economy together with ease and speed of construction, the material chosen for the body itself was 20mm marine-bonded plywood. The water-resistant properties of the material were further enhanced by several coats of proprietary yacht varnish finished with a single coat of bituminous paint.

To minimise the possibility of the occurrence of transverse forces and motions, and to preserve the essential two-dimensionality of the system, it was necessary for the transverse width of the body to conform as closely as possible with the width of the flume. A series of measurements showed that this could be achieved, whilst leaving sufficient space to ensure unimpaired motion, by specifying a transverse body width of 1795mm.

At the maximum required depth of flotation of the body, the draught was 480mm. It was envisaged that the maximum incident wave height would be in the region of 50mm. A series of numerical evaluations of the predicted body motion amplitudes and phase angles, resulting from the action of incident waves of known height, was carried out for the proposed range of experimental frequencies. The results of this preliminary investigation showed that, for an incident wave height of 50mm, the maximum freeboard necessary to preclude the possibility of over topping was about 100mm. Allowing a certain margin of error for non-linear wave behaviour in the immediate vicinity of the body, it was adjudged that a freeboard of 120mm would be appropriate, resulting in an overall body depth of 600mm.

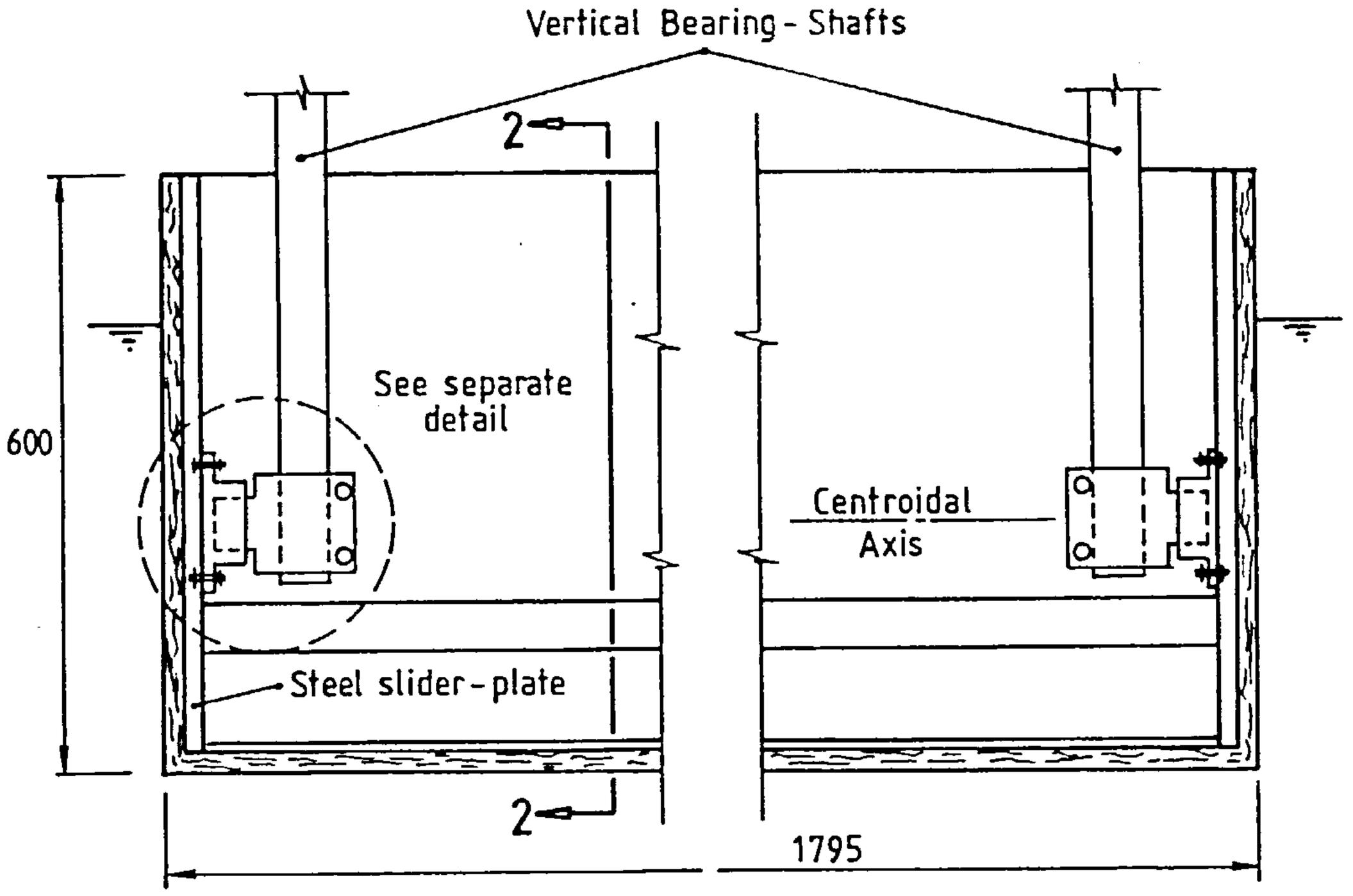

SECTION 1-1 FACE ELEVATION

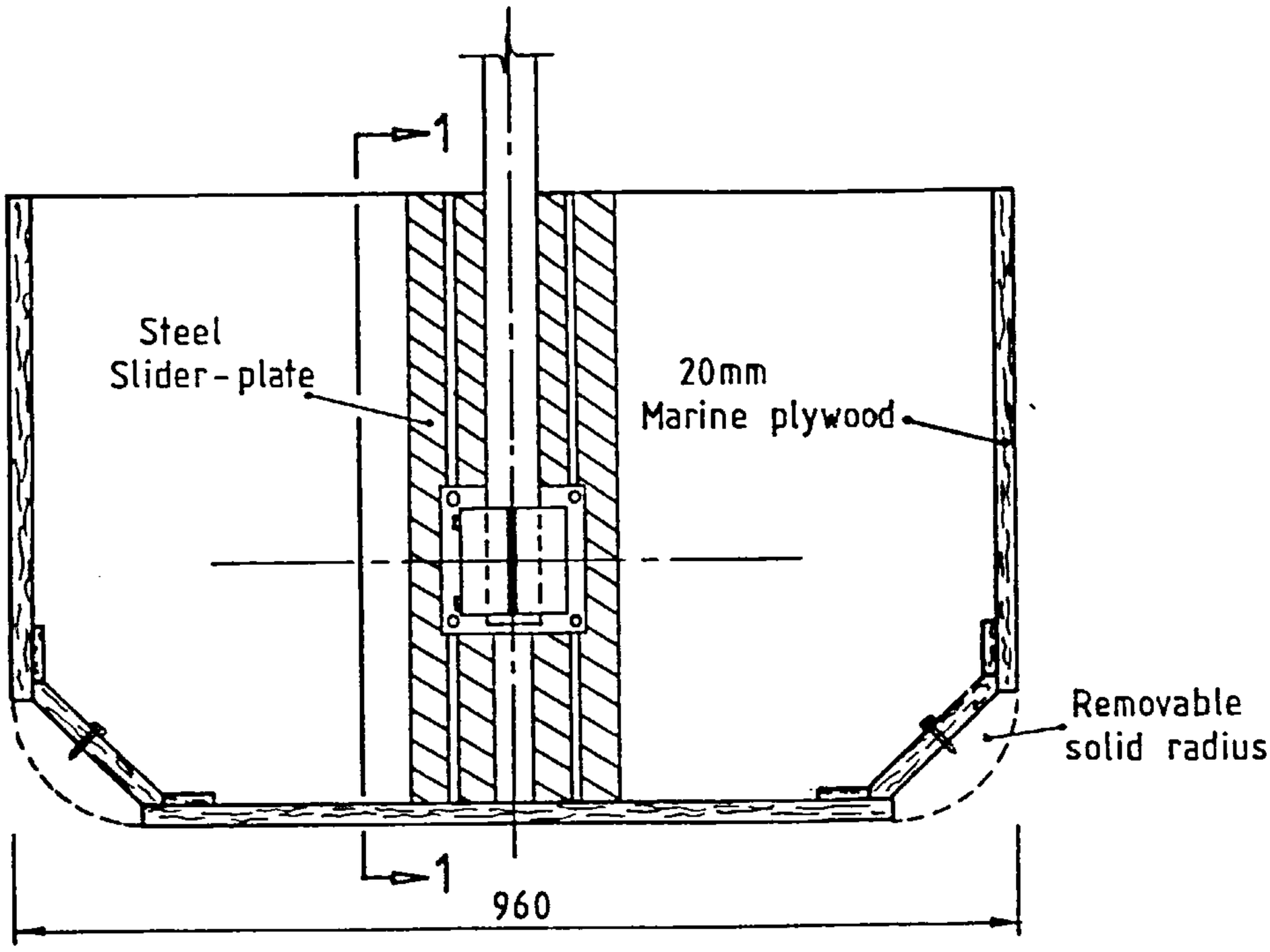

SECTION 2-2 END ELEVATION

Fig.5.1 FLOATING BODY - GENERAL ARRANGEMENT

The removable radial edges consisted of several layers of 20mm plywood glued together and planed to the appropriate dimensions, rendering them effectively solid. Countersunk-head screws, inserted through holes pre-drilled at 300mm c/c along the corner bracing member and screwed directly into the solid radial edge, provided the required degree of fixity and tightness of fit to the main frame of the body. Watertightness was preserved by the insertion of a compressible grommet into the countersink prior to screwing tight.

Since the experimental measurements of the three directional components of the overall body motion were required, the bearings had to be designed accordingly.

In formulating the equations of motion of the body, a fundamental assumption is made that body rotation takes place about an axis coincident with the body's centroidal axis. To comply with this assumption, it was decided to physically constrain pitch rotation to take place about this axis. Owing to the likelihood of the body centroid varying for different conditions of ballasting, it was necessary for the vertical location of the rotational bearings to be easily adjustable. To facilitate ease of adjustment, steel slider-plates were fixed to the side-walls of the body, onto which the rotational bearings were mounted (see Fig.5.2). Following adjustment to the required vertical location, the bearings could then be locked into position.

In order to alleviate the effect of fractional misalignment of the axial shaft, commercially produced rotation bearings are generally capable of a certain degree of rotation in a direction orthogonal to the primary axis of rotation. The bearings used in this

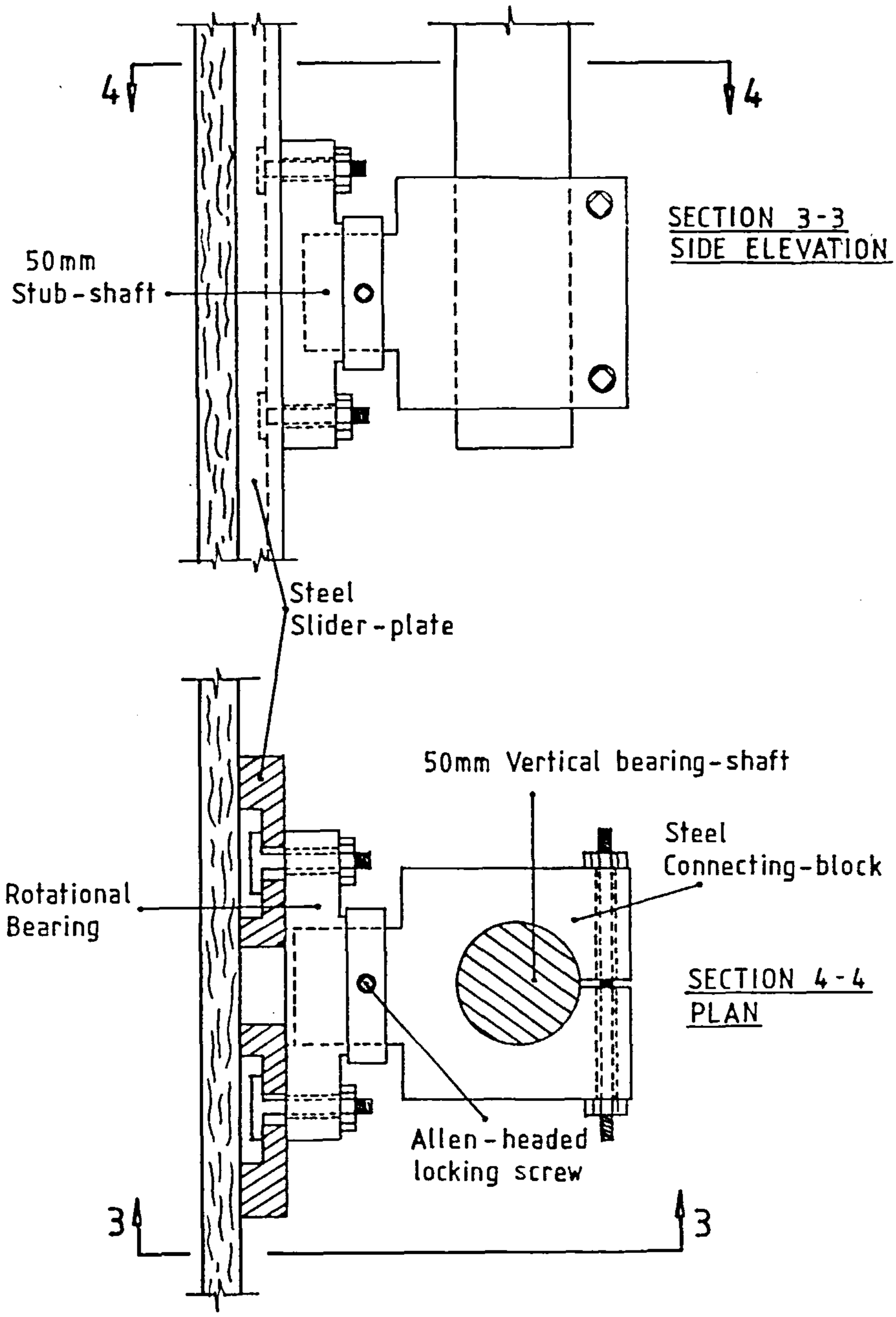

Fig.5.2 ROTATIONAL BEARING DETAIL

investigation unfortunately possessed this capability, thus presenting some initial problems in maintaining perpendicularity between the vertical bearing shafts and the axis of rotation of the body. Constant perpendicularity was eventually achieved by the use of a machined steel shim inserted in the body of the bearing and designed to restrict orthogonal rotation when the bearing base-plate was locked against the steel slider-plate.

To provide horizontal and vertical translatory motions, together with separate measurement thereof, a bi-axial bearing was designed as shown in Figure 5.3. Since relative vertical motion of the floating body and the vertical bearing shaft was prevented by the steel connecting block, the bearing shaft moved vertically with the body but relative to the steel bearing plate which was vertically restrained by the fixture of the horizontal bearing shaft to the supporting structure. The bearing plate, however, was free to move in a horizontal direction. Owing to possible frictional resistance in the bearings, the possibility of damage to the bearings resulting from moment transfer could not be overlooked. A bearing separation of approximately 500mm was adjudged sufficient to minimise this possibility. The use of a bearing plate, which was free to move in a horizontal direction, resulted in additional translatory inertia. This, however, was easily accounted for by the inclusion of an additional mass term in the equation of motion pertaining to the horizontal direction.

The presence of Stokesian and free second-order components in any flume-generated wave gives rise to the probability of horizontal drift of a floating obstacle in the direction of travel of the waves. To ensure true sinusoidal horizontal motion taking place

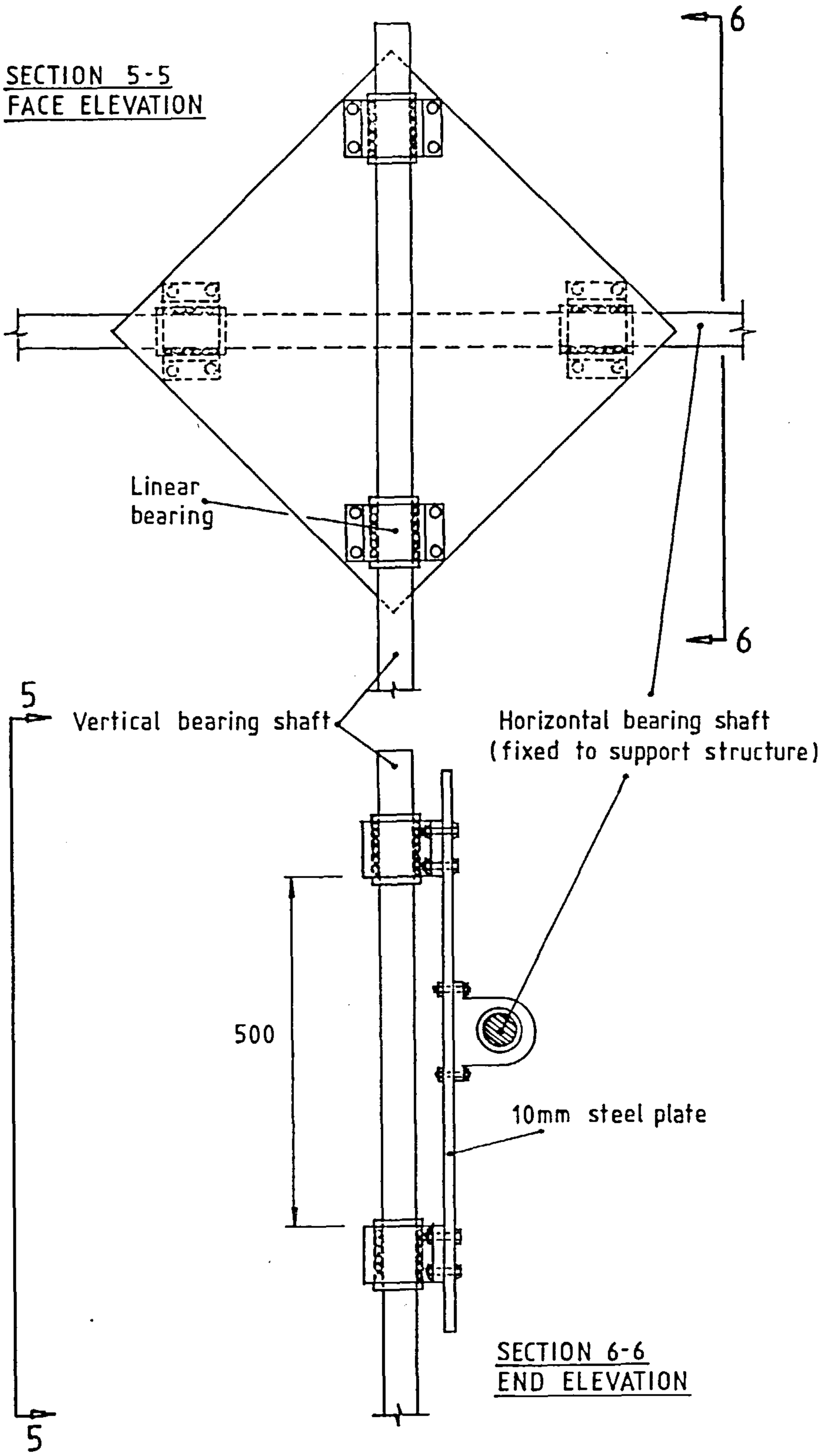

Fig.5.3 BIAXIAL BEARING DETAIL

about a constant mean position, it was necessary for the horizontal motion of the body to be partially restrained by springs. This was achieved by restraining each horizontal bearing plate by means of springs attached to immovable collars fixed to the horizontal bearing shafts. The fact that the restraint was imposed on the bearing plate, and not the body itself, ensured that the horizontal restraint force effectively acted through the body centroid. In this way, mathematical complications in the equations of motion, arising from restraint force eccentricity, could be avoided. As a result of the bearing design, the freedom of motion in the heave and pitch directions was independent of the freedom of motion in the surge direction. Thus, any horizontal restraint imposed acted solely in that direction.

To provide a constant restraint stiffness, the ratio of restraint force to displacement, it was a requirement that each spring remained in tension throughout the complete cycle of motion of the body. Compliance with this requirement was achieved by the attachment of springs to both the upstream and downstream edges of the bearing plate. With both sets of springs attached, the body naturally found its own equilibrium position. Any minor adjustment of this equilibrium position, to ensure orthogonality of the transverse axis of the body with respect to the direction of travel of the incident wave train, was carried out by movement of the collars clamped to the horizontal bearing shafts.

A few numerical evaluations were carried out, for a variety of body draught and incident wave conditions, to ensure that the induced horizontal resonant frequency of the mechanism, resulting from the presence of spring restraints in that direction, did not intrude

within the proposed experimental frequency range. For the sake of convenience and consistency of results, it was decided to use a constant spring strength for each flotation depth setting. A series of preliminary physical tests was performed to determine the particular spring strength required for each draught setting, the criterion being that horizontal drift be <u>just</u> prevented throughout the proposed frequency range of the investigation. Account was taken of the restraint imposed by the springs by the insertion, in the equations of motion, of a constant of proportionality relating horizontal force to displacement, that constant being the spring stiffness.

In order to achieve the depths of flotation specified for the investigation, a considerable quantity of ballast was needed. For ease of inertial and centroidal computation, together with ease of handling, pre-cast concrete blocks were chosen as the ballast medium. However, to enable the dimensions of the ballast blocks to be determined, the weight of the body had to be ascertained together with that of the bearing arrangements. This necessitated the completion of construction of the body and testing for watertightness prior to casting of the blocks.

In order that all joints and points of possible ingress of water could be subjected to the maximum hydrostatic pressure likely to be encountered under experimental conditions, it was intended to immerse the body in water to the maximum possible draught. The fact that the ballast blocks had not yet been cast, together with the absence of any suitable alternative, resulted in the exercise being less straightforward than first impressions would indicate.

Consideration was given to the idea of filling the body with water and noting any leaks that appeared, the philosophy being that a point of leakage would indicate a point of possible water ingress. This idea, however, was discounted owing to the fact that, under these conditions of loading, the joints would be subjected to negative stress. The test would not, therefore, give a reliable indication of watertightness. The only effective way of achieving the necessary depth of immersion was to restrain the body on the bottom of the empty flume and then fill the flume up to the required depth. To this end, two transverse scaffold poles were fixed to the side railing of the flume. Affixed to these poles were four vertical poles resting on blocks in the base of the body. It was intended that vertical displacement of the body would, in this way, be prevented on filling the flume. Having achieved the required immersion, it was intended to leave the body in this position for 24 hours. However, insufficient consideration was given to the magnitude of the axially-acting reactive forces, engendered by the upthrust, at each point of contact between the base of the body and the vertical scaffold member. In the course of the test, this point loading resulted in significant opening of the joints, subsequently necessitating substantial repair operations. The problem was ameliorated by resting the vertical scaffold members on a plane framework of timber, situated in the base of the body, which effectively distributed the point loads over the area of the base.

In order to avoid the laborious and inconvenient exercise of weighing the body with each of the five pairs of radial edges attached, the body was weighed once with the largest pair of radial edges attached and, from that weight and the body geometry, the average density of the body material was computed. This enabled

straightforward computation of the mass, centroidal and inertial parameters of the body with the remaining radial edges attached.

The computed ballast weights were approximately 660kg, 250kg, and 46kg for B/D = 2,4,8 respectively. It was appreciated that, owing to possible imperfections in the symmetry of mass distribution of the ballast, a uniform draught could not automatically be assumed. For this reason, some form of adjustment of ballast position had to be possible. The 46kg ballast was thus composed of four blocks of approximately 11½kg each. In the event of asymmetric draught occurring, these blocks could be re-positioned accordingly. The remaining ballast consisted of two blocks, the plan dimensions of which were such that, allowing for clearance in the area of the rotation bearing, a uniform distribution of ballast could be achieved over the transverse length of the body. These two blocks could then be used singly or in combination, in conjunction with the four movable blocks, to achieve the necessary flotation depths of the body.

5.5 Measurement of Experimental Data.

5.5.1 Free-Surface Displacement.

The oscillation of the free-surface was measured at fixed locations by means of vertically orientated parallel wire wave probes, of the resistance type, in conjunction with a dedicated amplifier based on a design developed at the Hydraulics Research Station (now Hydraulic Research Ltd.). Although this method of measurement is intrusive, the diameter of each arm of the probe is small in relation to the

wavelength of the surface oscillation. Consequently any disturbance of the surface, resulting from the presence of the probe, is minimal and can be regarded as insignificant. As the free-surface oscillates over the length of the probe, an oscillating voltage is output, amplified and recorded thus providing a measure of the free-surface oscillation.

5.5.2 Translatory Body Motions.

The translatory motions of the body were measured directly using induction-type displacement transducers affixed to one of the bearing plates (See Section 5.4). A constant D.C. excitation voltage is input to the transducer and displacement of an axially moving plunger, situated within the body of the transducer, causes this voltage to be modified in such a way that the output voltage is directly related to the plunger displacement. In order that surge and heave displacements could be measured directly, the transducer plungers were displaced by plates attached to the relevant bearing shafts.

5.5.3 Rotational Body Motions.

In the absence, to the best of the author's knowledge, of transducers capable of direct measurement of angular displacement, the rotational motion of the body had to be derived from measurements of rotational acceleration (See Section 5.8.3). This acceleration was obtained by means of two piezo-ceramic acceleration transducers fixed to opposite faces of the body. When a transducer

of this type is subjected to an acceleration, the resultant inertial force causes a piezo-ceramic module inside the transducer to deform and generate a charge proportional to the degree of deformation. A purpose built amplifier/converter receives the charge, which is then amplified and converted to a measurable voltage output proportional to the acceleration.

5.6 Calibration of Measuring Equipment.

5.6.1 Static Calibration.

The measurement of free-surface or body displacements, using the methods outlined in Sections 5.5.1 and 5.5.2, necessitated the prior determination of the relationship between displacement and the resulting voltage output. In the case of the wave probes, the procedure involved displacing the probe in still water through a sequence of known distances and recording the voltage output for each displacement. Static calibration of the displacement transducers necessitated the displacement of the transducer plunger through a similar sequence of known distances and recording the individual output voltages. A mathematical function could then be derived, relating the output voltage to the displacement.

Previous experimental studies involving the use of these particular wave-probes have assumed the relationship between displacement and output voltage to be linear. At the time the studies were carried out, this was a correct assumption and static calibration simply required the measurement of output voltage resulting from two displacements, the minimum necessary to obtain a linear

relationship. However, a comprehensive series of tests demonstrated that the passage of time has, to a certain degree, affected the linear voltage response of the probe/amplifier combination. As a result, it was felt that the displacement/voltage relationship could best be represented by a polynomial expression derived from a 'Least-Squares' regression exercise performed on the data set.

Owing to the possibility of significant variation of the voltage sensitivity of wave probes with temperature and time, it is advisable, in the interests of accuracy, to statically calibrate wave probes as regularly as possible, i.e. before every set of tests in which the probes are used. To this end, a dedicated interactive computer program was developed by the author to facilitate rapid polynomial static calibration of wave-probes in conjunction with the High Speed Scanner (see Section 5.7). This resulted in static calibration becoming a somewhat less arduous task and, therefore, less susceptible to avoidance.

Owing to the fact that the voltage response of the probe/amplifier combination could be adjusted by a potentiometer, inserted within the amplifier circuitry to make full use of the available scanner range, it was felt advisable to relate the probe displacement directly to the scanner output without performing the intermediate operation of computing the scanner voltage sensitivity.

The displacement transducers, available for use in the investigation, had been commercially calibrated but linearity had only been guaranteed over a rated stroke of 50mm. The displacements likely to be encountered in the course of the investigation were in excess of this rating and it was consequently felt advisable to

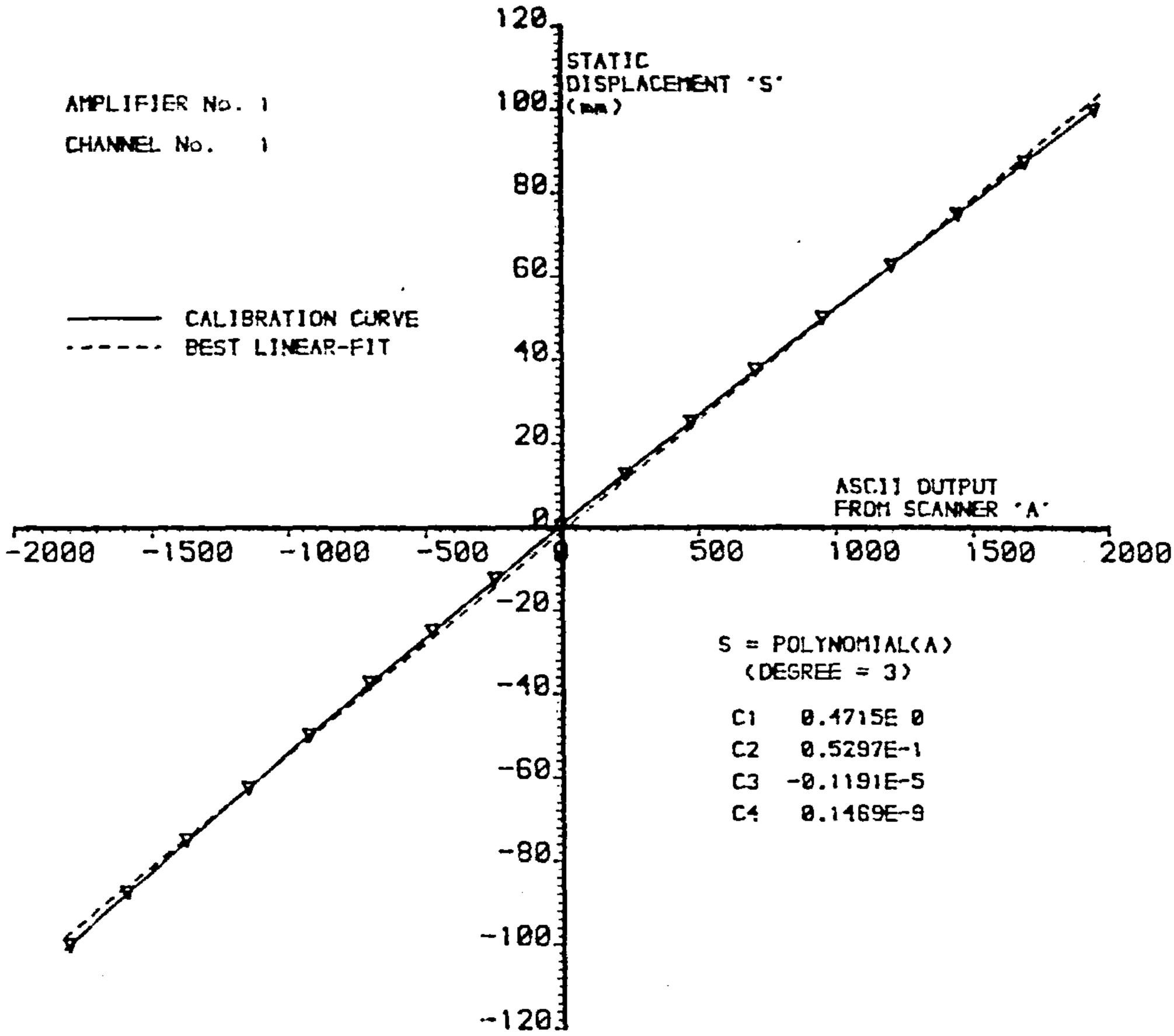

Fig.5.4 TYPICAL WAVE-PROBE STATIC CALIBRATION

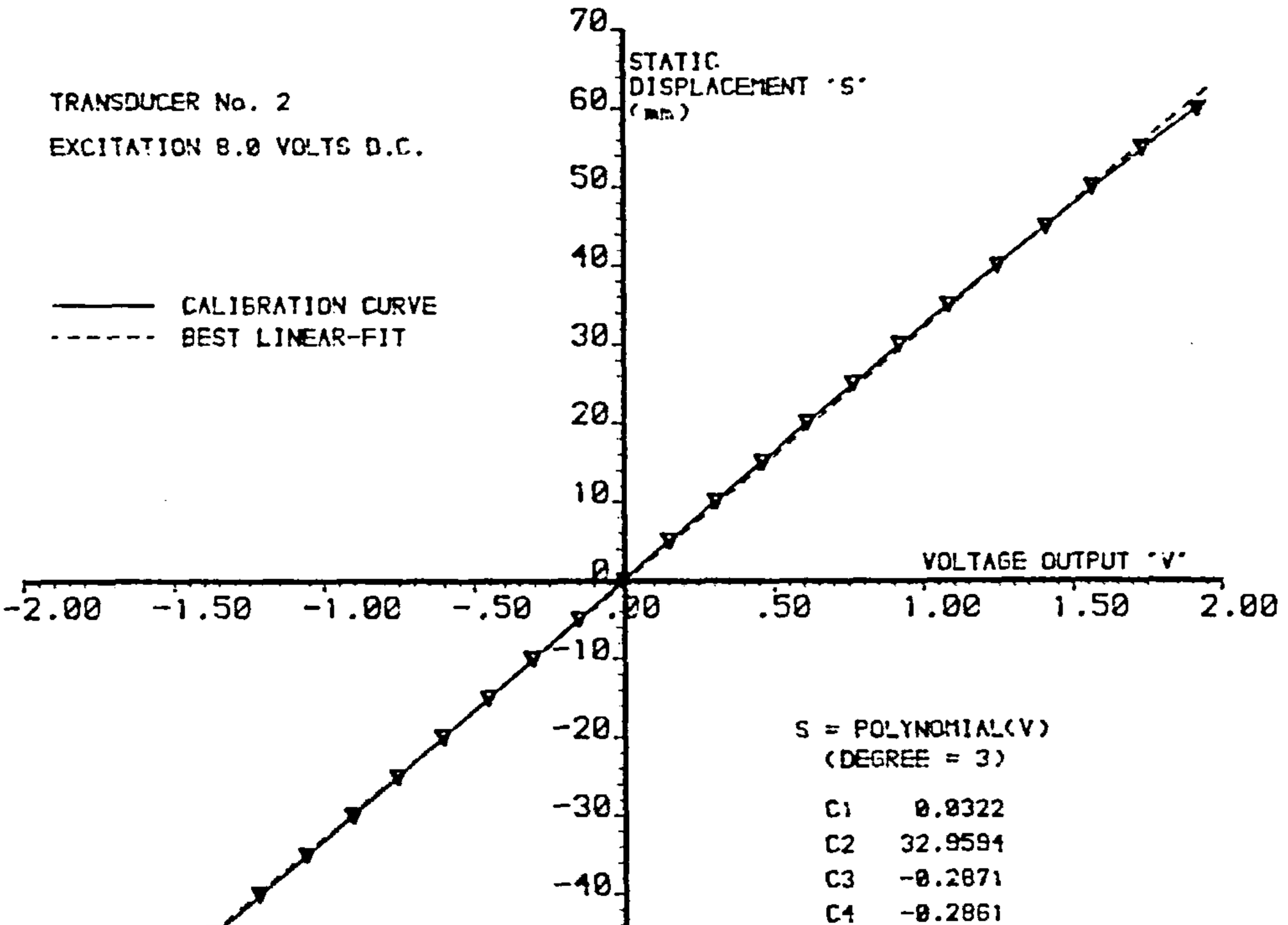

Fig.5.5 TYPICAL DISPLACEMENT TRANSDUCER STATIC CALIBRATION

perform a similar calibration exercise over the maximum attainable stroke range. However, in view of the fact that the voltage output sensitivity of the transducers did not vary with ambient temperature changes, the calibration exercise needed performing only once.

Typical static calibration results, shown in Figures 5.4 and 5.5, demonstrate a slight deviation from linearity in both cases. Subsequent tests on the voltage sensitivity of the High Speed Scanner showed a precise linear relationship between voltage input and digital output, leading to the conclusion that the deviation from linearity, observed in the static calibration, was a feature of the measurement device and not the High Speed Scanner.

5.6.2 Dynamic Calibration.

A feature of the measurement system described in section 5.5.1, which has only recently been appreciated, is the existence of a dynamic calibration factor applicable to both the amplitude and phase of an oscillating input signal. A series of tests, carried out by the author prior to this investigation, showed that the true amplitude and phase angle of sinusoidal oscillations of the free-surface deviated to a varying degree from those derived from static calibration procedures described in Section 5.6.1.

The preliminary test results showed the deviation in phase angle to be an inherent feature of the amplifier rather than the interaction between probe and free-surface, as it represented a constant time lag which was independent of the frequency and amplitude of the oscillating input signal.

The pattern of results pertaining to amplitude measurement, however, showed that there was a linear relationship between true and measured amplitude which varied with the frequency of oscillation of the free surface. Since the proposed scope of the experimental investigation did not include measurement of relative phase angles, the incurred phase shift between true and measured oscillation could be ignored. However, in the interests of quantifying all significant systematic errors, a series of calibration exercises was required to determine the dynamic amplification factor pertaining to amplitude measurement. Since there was insufficient time to carry out the considerable number of tests required to determine an acceptably precise mathematical relationship between input signal frequency and dynamic amplification factor, in order to obtain a generalised calibration expression, it was only possible to determine individual calibration factors applicable to the particular frequencies proposed in the investigation, these frequencies being pre-determined by the intended method of analysis (See Section 5.8.1).

At a known constant frequency, the wave-probe was vertically oscillated in still water, to simulate a regularly oscillating free-surface, by attaching it to the vertical connecting shaft of the wave-generator, with the wedge disconnected. By means of potentiometers within the generator circuitry, it was possible to vary the amplitude of motion of the probe over a suitable range thus enabling mathematical correlation between a set of discrete measured amplitudes and the corresponding amplitudes derived from static calibration data. In all cases, this correlation was found to be linear as shown in Figure 5.6. (For reasons of clarity, it must be noted that 'scanned stroke' refers to the stroke computed from

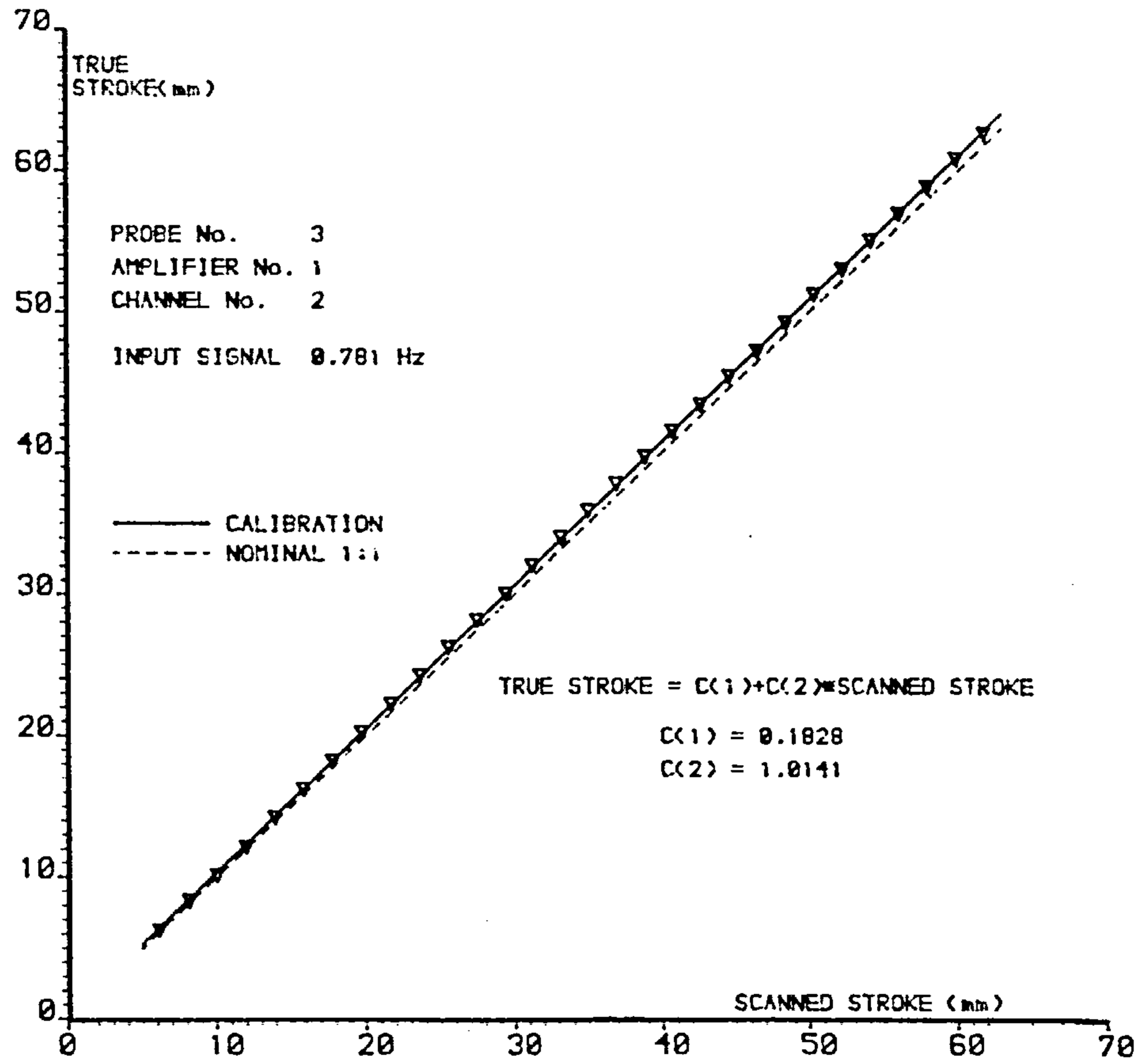

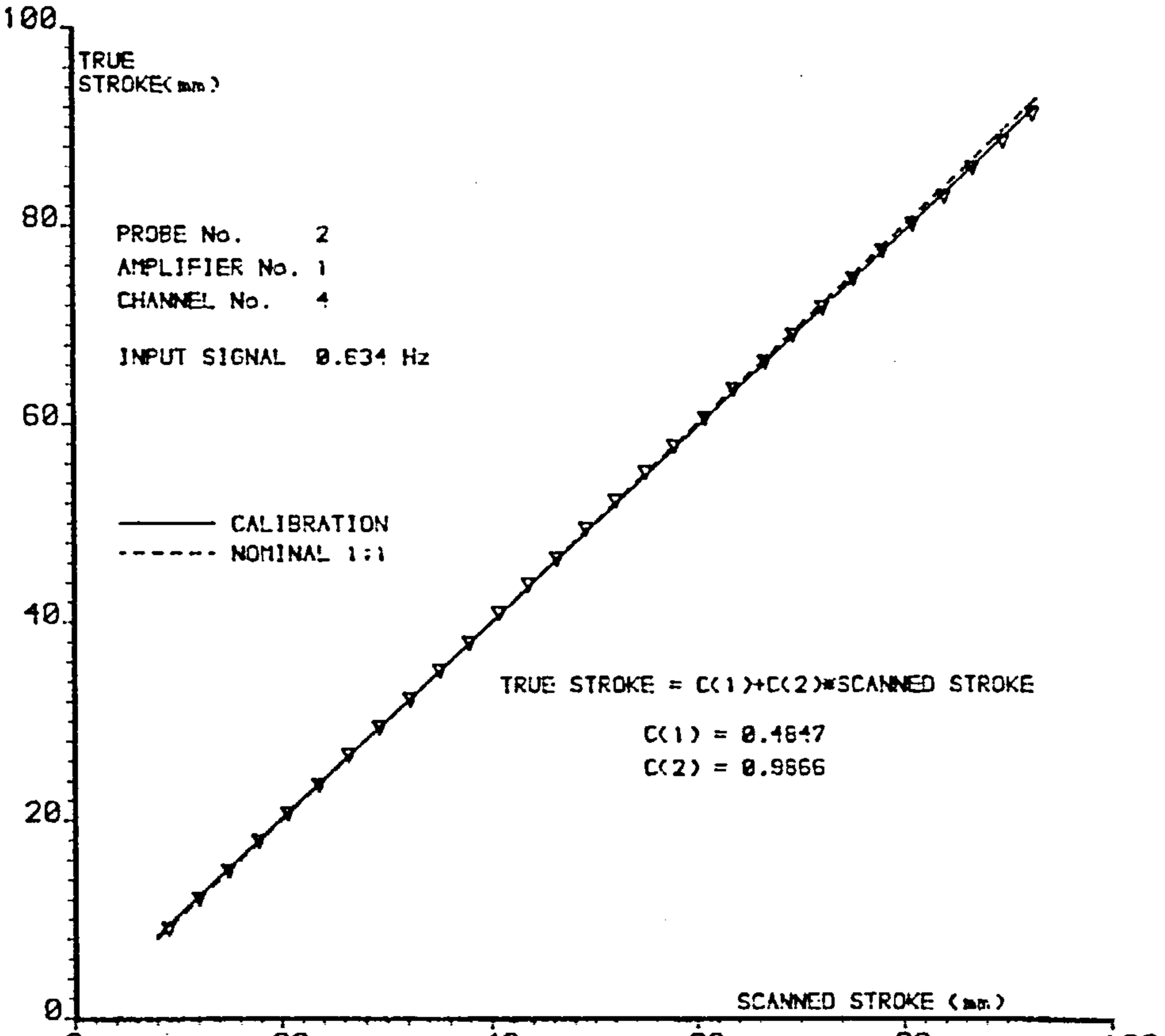

Fig.5.6 TYPICAL WAVE-PROBE DYNAMIC CALIBRATION

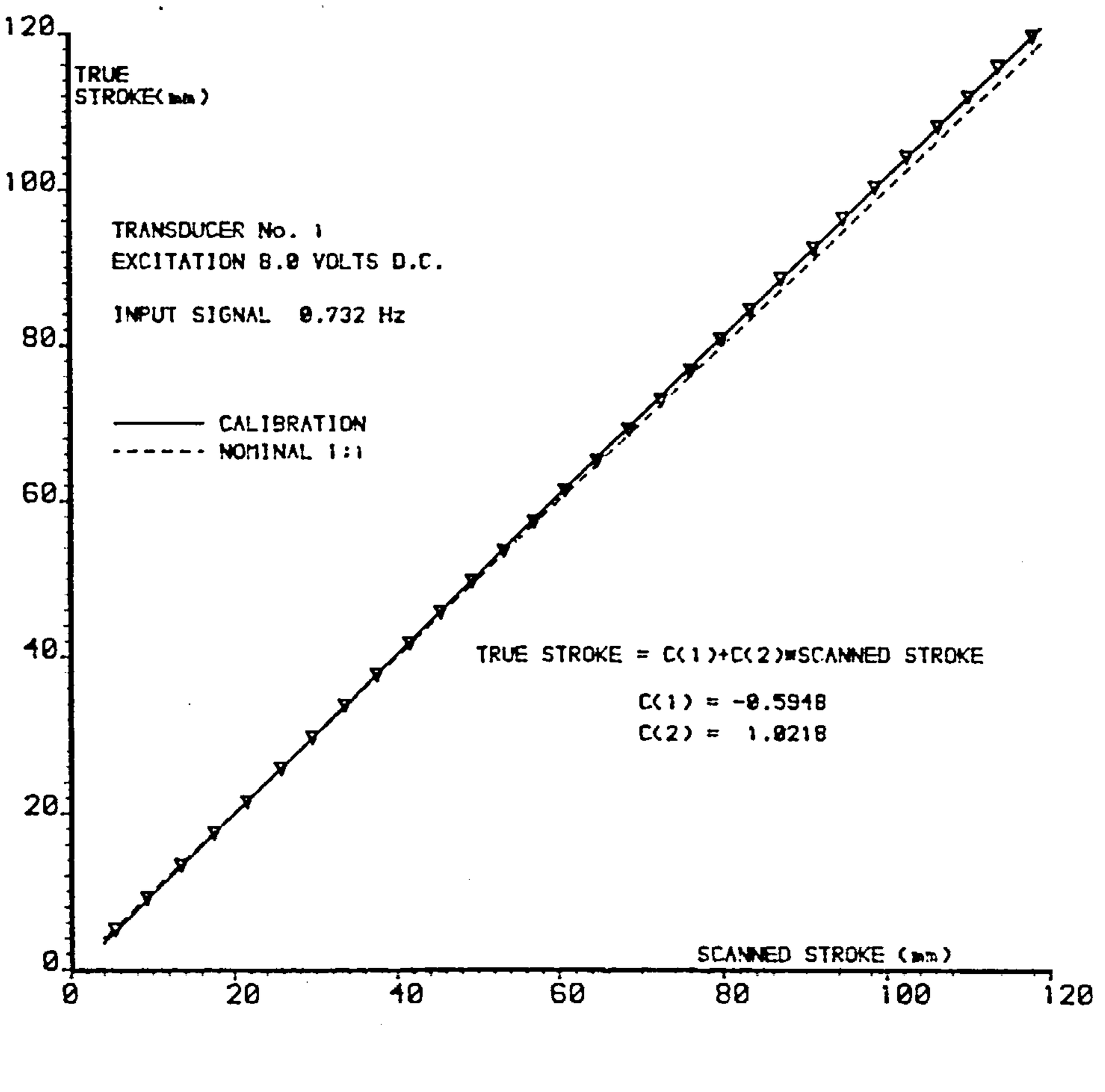

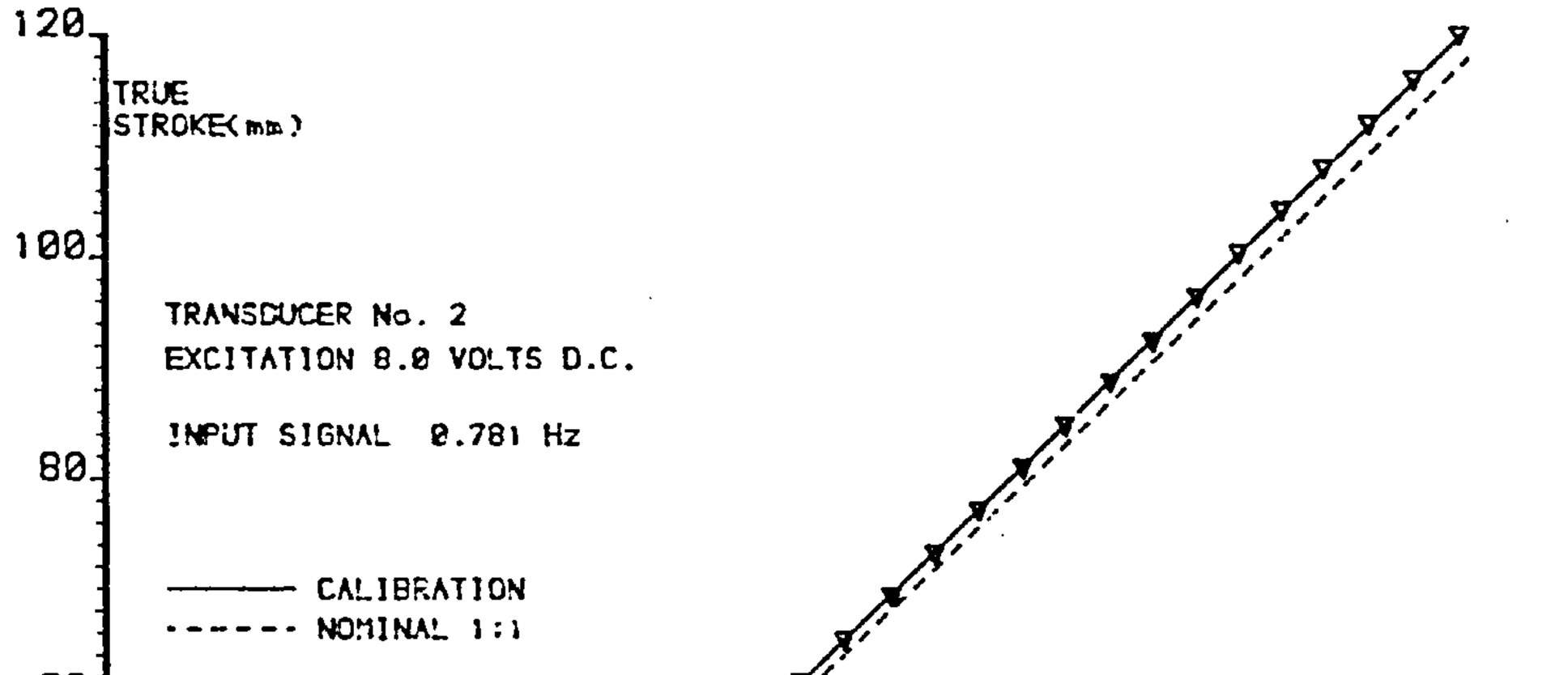

Fig.5.7 TYPICAL DISPLACEMENT TRANSDUCER DYNAMIC CALIBRATION

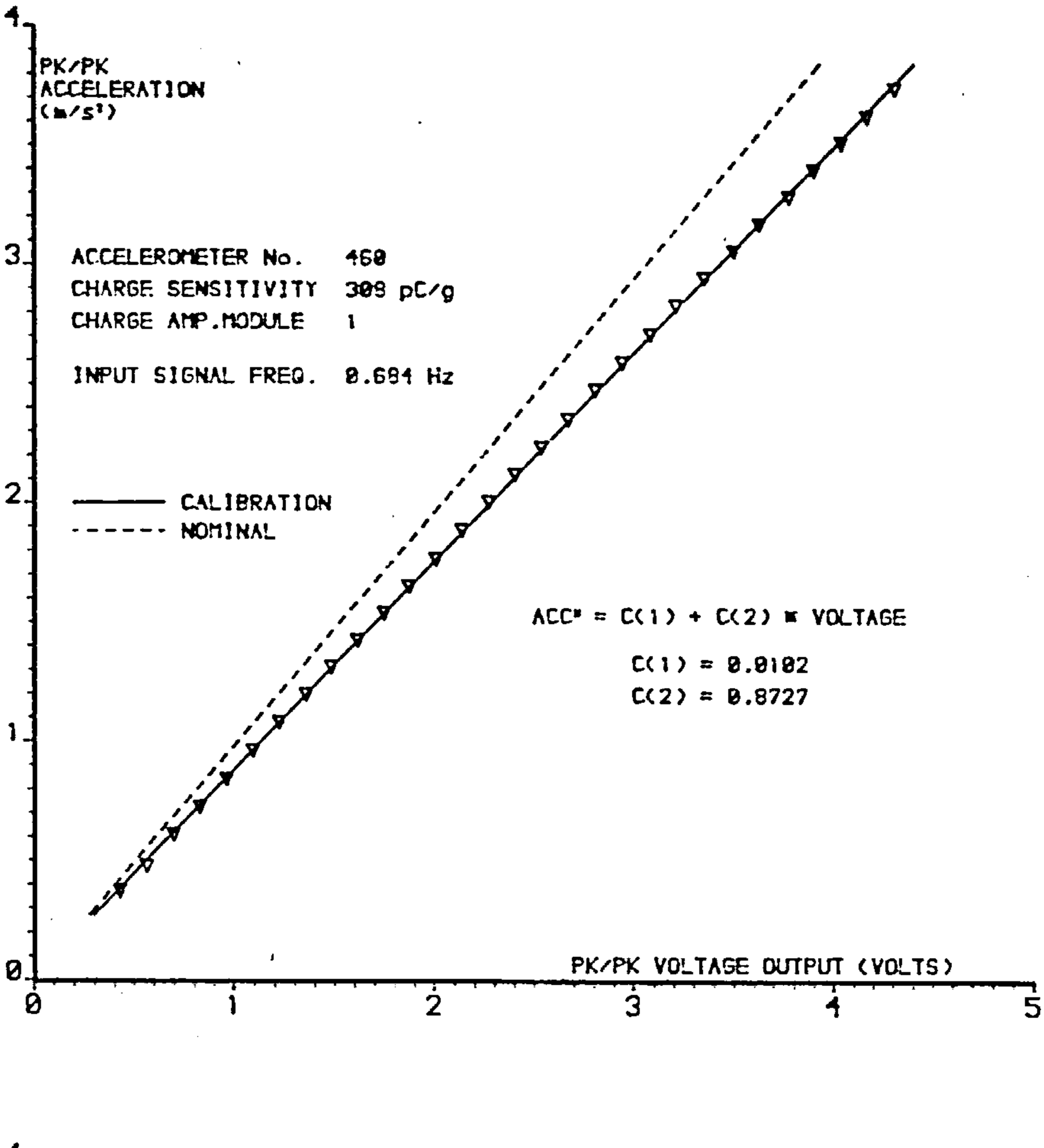

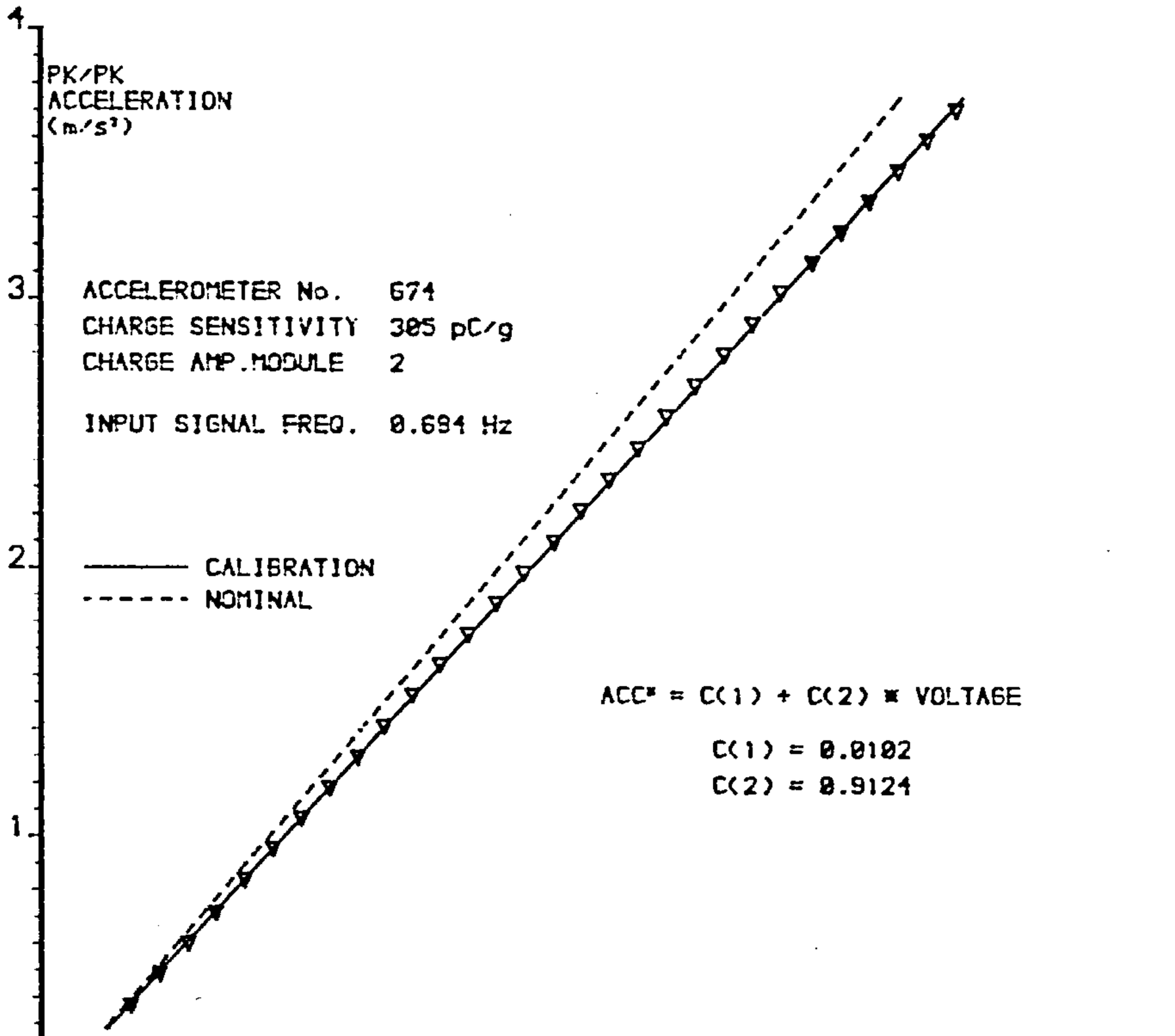

Fig.5.8 TYPICAL ACCELEROMETER CALIBRATION

measured values of the peak to peak wave-probe output voltage).

Since the dynamic response characteristics of the displacement transducers were not known, it was considered advisable to perform a similar series of tests thereon. Typical test results, shown in Figure 5.7, demonstrate the dynamic amplification to be significant when considered in terms of an acceptable overall magnitude of experimental error.

The accelerometers, to be used for the measurement of rotational body motion, had been factory-calibrated by the manufacturers prior to dispatch. It was stated, however, that the lowest frequency at which the calibration could be guaranteed was 2Hz. In view of the fact that the proposed range of investigational frequencies was substantially lower than this recommended minimum, calibration tests were carried out at each proposed frequency to correlate known accelerations, derived from measurements of motional amplitude, with those obtained from the manufacturers calibration data. Typical results, shown in Figure 5.8, demonstrate a considerable deviation between true and measured acceleration.

5.7 Collection and Processing of Raw Data.

The fluctuating voltage signals from the wave probes, together with those from the displacement and acceleration transducers, could be fed in continuous form into a High Speed Scanner module operated in conjunction with a DIGITAL PDP-11 micro-computer. Commercially supplied software enabled the sequential scanning of up to thirty two input channels at discrete user-determined intervals. Following

the performance of an analogue/digital conversion, the collected data could be written to disk files. Since the data thus obtained is in binary machine code, further software is required to convert it to octal or decimal form for further analysis. Certain modifications were carried out on the software to permit scanning in 'burst' fashion. In this way, successive passes over the specified number of sequential channels could be separated by a user-determined time interval, specified as a multiple of the mains period of 0.02 seconds, up to a maximum of ten seconds. In this way, it is possible to obtain a discretised scan of a fluctuating voltage signal input to a particular channel, subject to a minimum time interval of 0.02 seconds between successive scans. The sensitivity of each module of sixteen channels could be adjusted in 3dB intervals to record peak voltage inputs ranging from 20mV to 5V.

Further analysis, according to the methods described in section 5.8, could be carried out either using the micro-computer or the main-frame HONEYWELL 60/66 computer, depending on resource requirements. In order to facilitate transfer of text or data files between the micro and main-frame computers, an interface program was developed. In the absence of graphics facilities for the PDP-11 system, this interface feature proved most useful for graphical presentation of transferred data, using the HONEYWELL facilities.

A flow chart describing the overall procedure is shown in Fig.5.9.

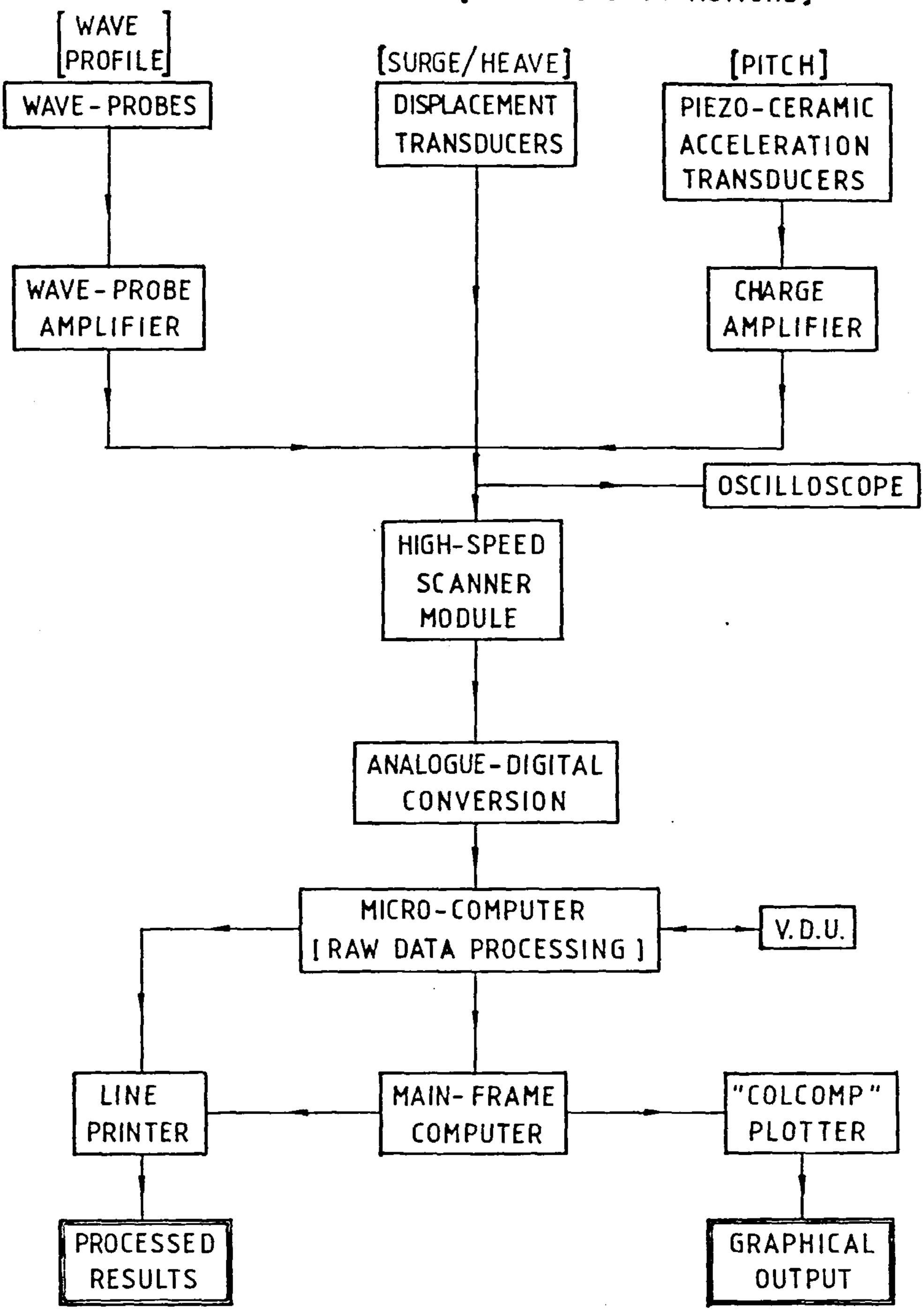

Fig.5.9 FLOW-CHART FOR COLLECTION, ANALYSIS AND PRESENTATION OF EXPERIMENTAL RESULTS

5.8 Analysis of Data.

5.8.1 Resolution of Periodic Data.

Since all data output from the measuring instruments was of a periodic nature, the analysis was carried out using the Fast Fourier Transform algorithm:

If N discrete observations of a fluctuating signal are made at time intervals of δt then, providing the value of N is an integer power of 2, resolution of the signal into the following components is possible:

$$S = a_o + a_1 \text{Cos } 2\pi f_1 t + b_1 \text{Sin } 2\pi f_1 t + a_2 \text{Cos } 2\pi f_2 t + b_2 \text{Sin } 2\pi f_2 t + \ldots\ldots \quad (5.8.1)$$

where: S represents the fluctuating input signal.

$f_n = n/N\delta t$.

For a signal which is essentially sinusoidal, it can be seen that precise evaluation of the fundamental and higher order frequency components is possible only if the total observation period is a multiple of the fundamental period of the signal. As a result of this constraint, the following frequencies were chosen for the investigation, permitting 512 observations to be made at time intervals subject to the scanning conditions described in Section 5.7:

Frequency (Hz)	Time Interval (secs)	No.of cycles observed
0.4883	0.02	5
0.5371	0.04	11
0.5859	0.02	6
0.6348	0.04	13
0.6836	0.02	7
0.7324	0.04	15
0.7813	0.02	8
0.8301	0.04	17
0.8789	0.02	9

Table 5.8.1 Proposed Investigational Frequencies.

It was adjudged that this would be a sufficient number of frequencies, over the required frequency range, to give a satisfactory spread of results for comparison with theoretical predictions.

5.8.2 Free-Surface Displacement.

As a consequence of the reflective and transmissive properties of the body, together with the slight reflective properties of the beach, the upstream and downstream free-surface profiles are composed of components travelling in both the positive and negative directions. In the case of the upstream profile, these components are the incident and body-reflected waves respectively. In the case of the downstream profile, the components are the body-transmitted and beach-reflected waves respectively. For a complete analysis of

the reflective and transmissive characteristic of the body, together with evaluation of the non-dimensional components of body motion (see Section 5.3.2), resolution of the free-surface profile into positive and negative components is required.

For comparative purposes, details are given of two methods of resolution together with comments on their usage:

Consider a flume wave consisting of the following fundamental frequency components:

(i) The incident component, having a positive direction of travel:

$$n_I = a_I \, Cos(kx-\sigma t) \qquad (5.8.2a)$$

(ii) The reflected component, having a negative direction of travel:

$$n_R = a_R \, Cos(kx+\sigma t+\epsilon_R) \qquad (5.8.2b)$$

where: ϵ_R is the phase angle of the reflected component relative to the incident wave.

Assuming linear superposition the combined wave profile, at any location x along the flume length, may be defined by the expression:

$$\{n_I+n_R\} = a_I \, Cos(kx-\sigma t) + a_R \, Cos(kx+\sigma t+\epsilon_R) \qquad (5.8.3)$$

Re-arrangement of this expression, into a form comparable with that of equation (5.8.1), yields:

$$\{n_I+n_R\} = A \text{ Cos } \sigma t + B \text{ Sin } \sigma t \qquad (5.8.4)$$

where: $A = a_I \text{ Cos } kx + a_R \text{ Cos}(kx+\epsilon_R)$

$B = a_I \text{ Sin } kx - a_R \text{ Sin}(kx+\epsilon_R)$

The components A and B may be evaluated, using the Fast Fourier Transform algorithm detailed in Section 5.8.1, from a time-based observation of the free-surface profile at the specified location.

Method 1 (see Goda and Suzuki[27]).

Consider the simultaneous observation of the free surface profile at 2 separate locations x_1 and $(x_1+\Delta x)$:

$$\left\{n_I+n_R\right\}_{X=X_1} = A_1 \text{ Cos } \sigma t + B_1 \text{ Sin } \sigma t \qquad (5.8.5a)$$

$$\left\{n_I+n_R\right\}_{X=X_1+\Delta X} = A_2 \text{ Cos } \sigma t + B_2 \text{ Sin } \sigma t \qquad (5.8.5b)$$

where: A_1, B_1, A_2, B_2 are in the form indicated by equation (5.8.4).

An algebraic exercise, performed on equations (5.8.5a) and (5.8.5b) yields the following parameters:

$$a_I = \frac{1}{2|\text{Sin } k\Delta x|} (F_I)^{1/2} \qquad (5.8.6a)$$

$$a_R = \frac{1}{2|\text{Sin } k\Delta x|} (F_R)^{1/2} \qquad (5.8.6b)$$

where: a_I = Incident wave amplitude.

a_R = Reflected wave amplitude.

$$F_I = (A_2 - A_1 \text{Cos } k\Delta x - B_1 \text{Sin } k\Delta x)^2 + (B_2 + A_1 \text{Sin } k\Delta x - B_1 \text{Cos } k\Delta x)^2$$

$$F_R = (A_2 - A_1 \text{Cos } k\Delta x + B_1 \text{Sin } k\Delta x)^2 + (B_2 - A_1 \text{Sin } k\Delta x - B_1 \text{Cos } k\Delta x)^2$$

An advantage to be gained from use of this method derives from the fact that component resolution can be effected directly using data obtained from simultaneous observation of the surface profile at two discrete locations. This minimises the data collection time for each particular set of conditions and, in investigations which entail the abstraction of data pertaining to a considerable number of different conditions, can result in a substantial reduction in the time required to complete the investigation.

Inspection of equations (5.8.6a) and (5.8.6b) shows that the accuracy of the resolved parameters is directly related to the precision with which the probe separation, Δx, is measured. In the course of this investigation, it would have been entirely feasible to position the wave probe trollies with the required degree of precision but, owing to the relatively imprecise manufacture of the trolleys and attendant railing, it would have been impossible to guarantee a correspondingly precise separation of the probes at the free-surface. As a consequence of the depth of the free-surface below the top of the flume, direct access to the free-surface was difficult, thus posing certain problems in carrying out an accurate physical check on wave probe separation. Had this method of resolution been adopted, however, these difficulties could possibly have been surmounted to ensure an acceptably accurate wave probe separation resulting in the incurrence of minimum analytic error.

The overriding disadvantage associated with the use of this method, and the reason behind its eventual rejection, was the lack of information to be gleaned from inspection of the individual results. The presence of behavioural abnormalities in the wave train, such as those induced by resonance, could only be detected from an inspection of the pattern of readings obtained from several probe locations. Whilst such a procedure would enable a realistic assessment to be made of the confidence with which individual results could be viewed, it would of course nullify any possible time-saving advantage to be gained from use of the method.

Method 2

Consideration of equation (5.8.4) shows that the measured wave amplitude, at any point x_i along the flume, may be defined by the expression:

$$\{A_o\}_i = \left\{a_I^2 + a_R^2 + 2a_I a_R \, Cos(2kx_i+\epsilon_R)\right\}^{\frac{1}{2}} \qquad (5.8.7)$$

It can be seen from this expression that the square of the measured wave amplitude varies sinusoidally with longitudinal flume position.

If a number of amplitude measurements are abstracted at various known positions along the flume, using the coordinate system defined in section 3.2, a correlation exercise may be performed, using the method of Least-Squares, to derive the following relationship between the data sets:

$$\{A_o\}^2 = c_1 + c_2 \, Cos(2kx+\delta) \qquad (5.8.8)$$

Comparison between equations (5.8.7) and (5.8.8) shows that:

$$c_1 = a_I^2 + a_R^2 \qquad (5.8.9a)$$

$$c_2 = 2a_I a_R \qquad (5.8.9b)$$

$$\delta = \epsilon_R \qquad (5.8.9c)$$

Substitution of equation (5.8.9b) in (5.8.9a) yields the following quartic equation:

$$4a_I^4 - 4c_1 a_I^2 + c_2^2 = 0 \qquad (5.8.10)$$

Reduction of this expression to quadratic form gives the following solution for a_I^2, indicating the existence of 2 roots:

$$a_I^2 = \frac{c_1}{2} \pm (c_1^2 - c_2^2)^{\frac{1}{2}} \qquad (5.8.11)$$

Substitution from equations (5.8.9a) and (5.8.9b), together with consideration of the fact that the value of a_R/a_I must not exceed unity, leads to the unambiguous expression:

$$a_I^2 = \frac{c_1}{2} + (c_1^2 - c_2^2)^{\frac{1}{2}} \qquad (5.8.12)$$

which can be solved for a_I and, by back substitution, a_R.

The principal reason for adoption of this method of resolution, in preference to the previously detailed alternative, lay in the fact that it offered the facility of detection of any abnormalities in wave behaviour. In order to take full advantage of this facility and, at the same time, obtain acceptably accurate results, it was

necessary to apply a certain amount of forethought to the process of data collection.

As a consequence of the predicted sinusoidal variation of the square of measured amplitude with flume position, the longitudinal range of sampling locations had to be sufficient to permit analysis of at least one complete variational cycle i.e one beat wavelength equal in magnitude to half the incident wave length. In order to detect the presence of behavioural abnormalities, indicated by deviation from the predicted sinusoidal variation, the range of sampling locations had to be such that graphical representation of the sinusoid included at least two troughs or crests. Compliance with this requirement dictated a minimum sample length of 1½ beat wave lengths.

It is a feature of statistically based regression techniques, such as those used in this method of analysis, that the parameters obtained therefrom are essentially estimates and are, consequently, subject to a certain margin of error. This error margin is a function not only of the scatter of input data about the regression curve but also of the number of data points considered in the analysis. An increase in sample size with a view to minimising the error would, however, lead to an increased expenditure of data collection time, a direct consequence of which would be an increase in overall project duration. In order that a compromise could be reached, enabling the acceptably accurate estimation of regression parameters from analysis of a minimal number of observations, it was necessary to determine the sampling density at which the error magnitude associated with each parameter became relatively insensitive to a change in sample size. The results of a series of

numerical tests, carried out on data obtained from a previous wave-profile investigation, showed that an acceptable degree of accuracy could be achieved from a sampling density of 20 observations per beat wavelength.

As a consequence of occasional minor imperfections in the wave generation, together with the normal random errors associated with any method of measurement, it was decided to take several measurements of wave amplitude at each sampling location in order to minimise the effect of random errors on the overall computation of the regression parameters. Inspection of the results obtained from a preliminary series of tests demonstrated that the stability of the wave train and the measuring equipment was such that no significant advantage could be derived from the abstraction of more than two measurements at any particular location.

A fundamental assumption, concerning the use of asymptotic values of potential functions to evaluate the far-field reflection and transmission characteristics of the body (See Appendix A6), is that the wave train may be defined by these characteristics at large distances from the body, i.e. at distances sufficient to ensure total decay of non-linear localised effects. A series of numerical evaluations, entailing comparison of the surface profile obtained from consideration of potential functions and that obtained from consideration of the far-field Reflection and Transmission Coefficients, showed that 99.99% of decay of localised effects took place within one incident wave length of the wave/body interface. In the absence of any numerical results pertaining to the surface profile immediately adjacent to either the wave generator or the beach, it is not unreasonable to assume that a similar distance is

BODY NUMBER 2 (Floating Mode)

Length	0.960	(m)
Nominal Draught	0.480	(m)
Submerged Edge Radius	0.060	(m)
Still Water Depth	1.199	(m)
Incident Wave Frequency	0.781	(Hz)
Theoretical Wave Number	2.469	(m^{-1})
Theoretical Beat Wavelength	1.272	(m)

THE UPSTREAM WAVE

Wave Number	2.482	(m^{-1})
Beat Wavelength	1.266	(m)
Incident Wave Amplitude	8.323	(mm)
Reflected Wave Amplitude	1.636	(mm)
Reflection Coefficient	0.197	

THE DOWNSTREAM WAVE

Wave Number	2.452	(m^{-1})
Beat Wavelength	1.281	(m)
Transmitted Wave Amplitude	6.373	(mm)
Beach Reflected Wave Amplitude	0.623	(mm)
Beach Reflection Coefficient	0.098	

BODY REFLECTION AND TRANSMISSION

Reflection Coefficient	R	0.1965
Transmission Coefficient	T	0.7657
Energy	$R^2 + T^2$	0.6249

TABLE 5.8.2 Reflected and Transmitted Wave Analysis.

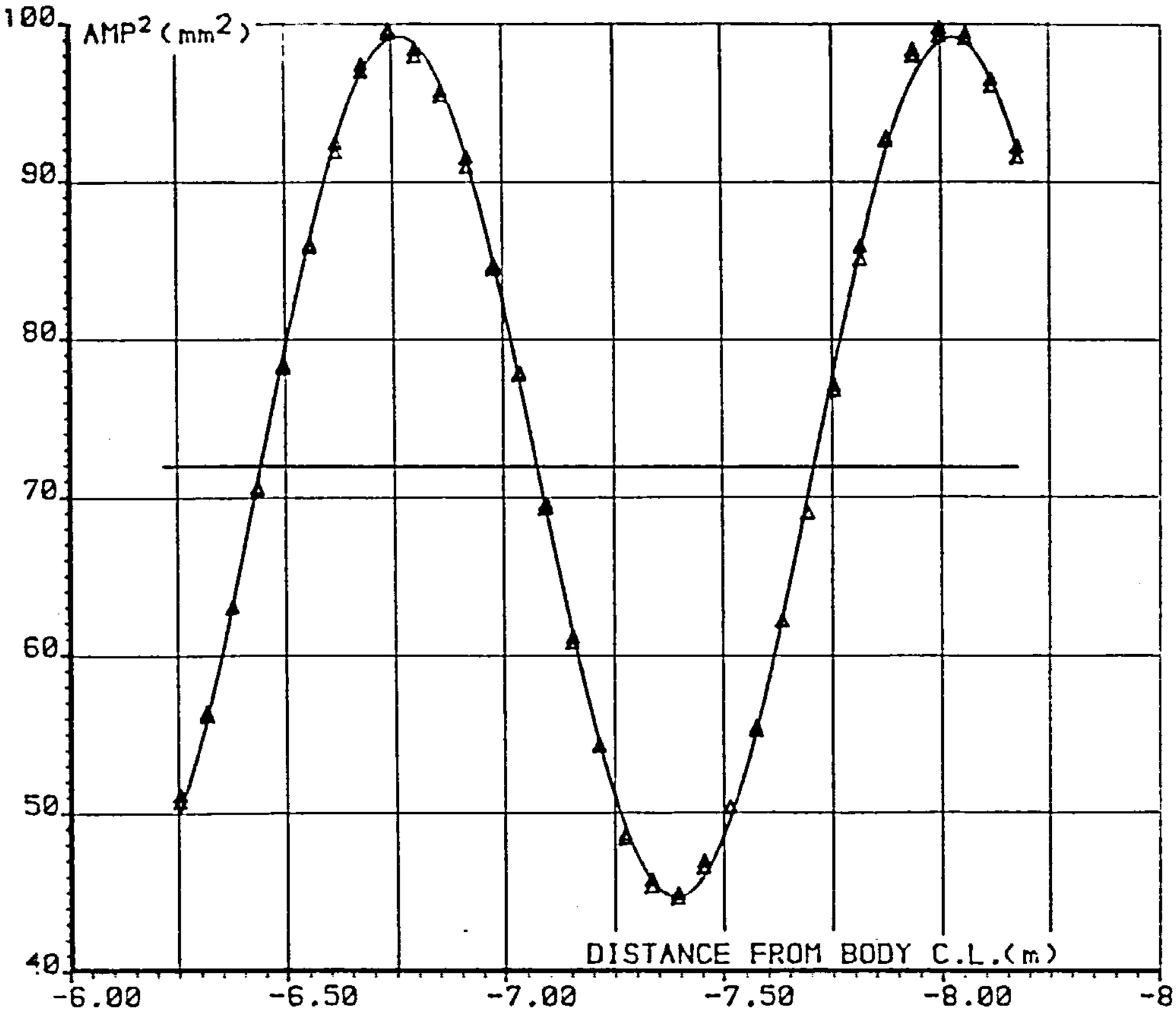

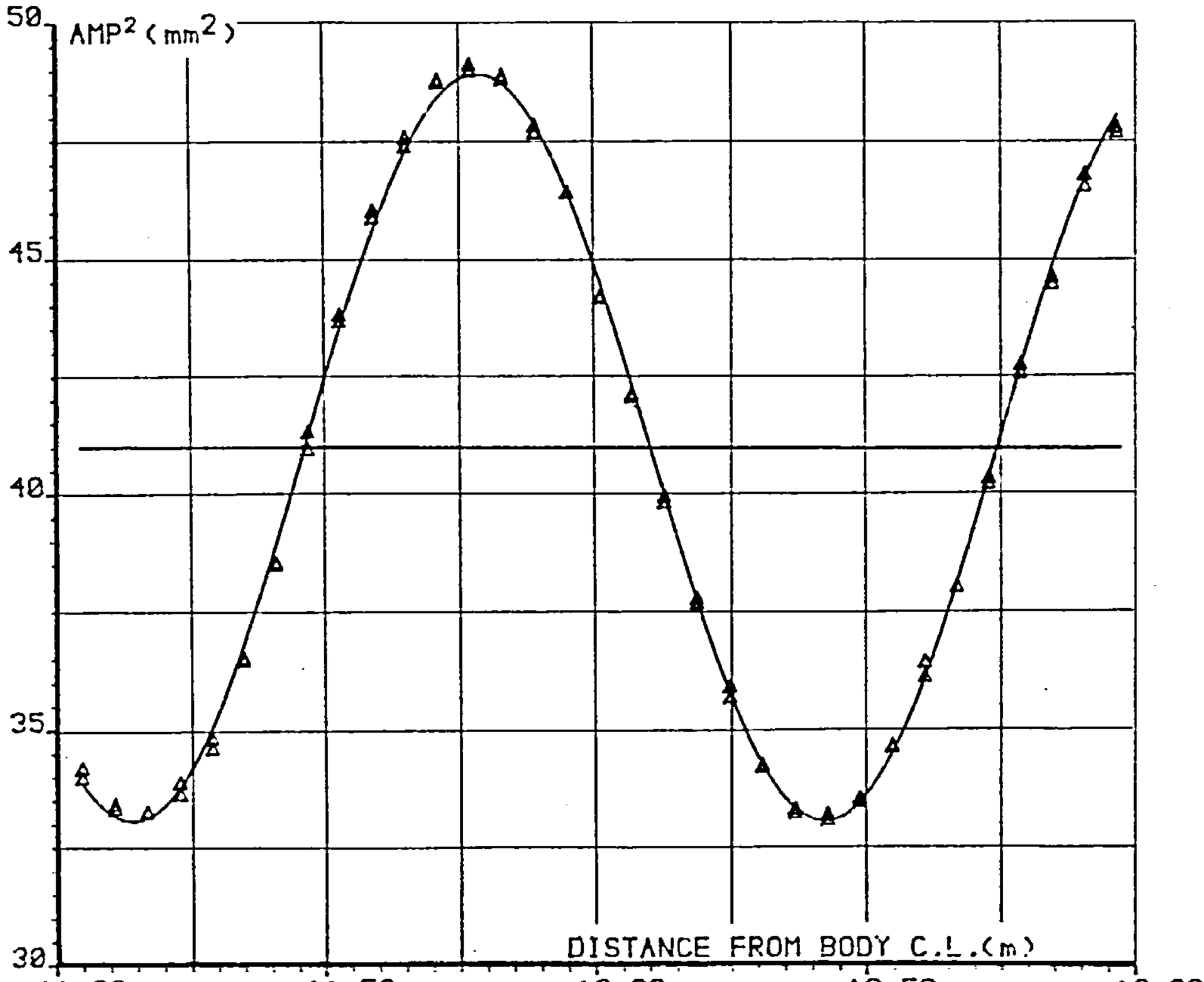

Fig.5.10 REFLECTED AND TRANSMITTED WAVE ANALYSIS

required to ensure a comparable decay of localised effects associated therewith. In order to ensure the far-field validity of reflection and transmission characteristics obtained by this method of resolution, it is a necessary requirement that surface profile measurements are abstracted from locations which remain uncontaminated by the decay of localised effects. Since the proportion of overall flume length occupied by these decay zones is a direct function of the incident wave length, it becomes immediately apparent that compliance with the above requirement imposes a limit on any investigational frequency range, below which the use of this method becomes no longer feasible. Conversely, use of this method imposes an upper limit on the frequency range such that accurate positional resolution, between individual sample points, remains possible.

In this investigation, however, the proposed range of wave frequencies (See Section 5.3.3) was encompassed by the above limits, thus imposing no restrictions on the use of this method of resolution.

A graphical representation of a typical surface profile variation with position is shown in Figure 5.10. Numerical details of the associated analysis are shown in Table 5.8.2.

5.8.3 Body Motions.

a) <u>Translatory Motions.</u>

The surge and heave motions of the floating body were separately

measured using the method described in Section 5.5.2. The peak voltage output from each transducer was determined from Fast Fourier Transform analysis of the oscillating output signal, permitting derivation of the individual motion components when used in conjunction with the appropriate static and dynamic calibration factors.

b) Rotational Motion.

Measurement of rotational motion of the floating body was achieved indirectly from the measurement of rotational acceleration, as described in Section 5.5.3. Two acceleration transducers were affixed to opposite faces of the floating body as shown in Figure 5.11.

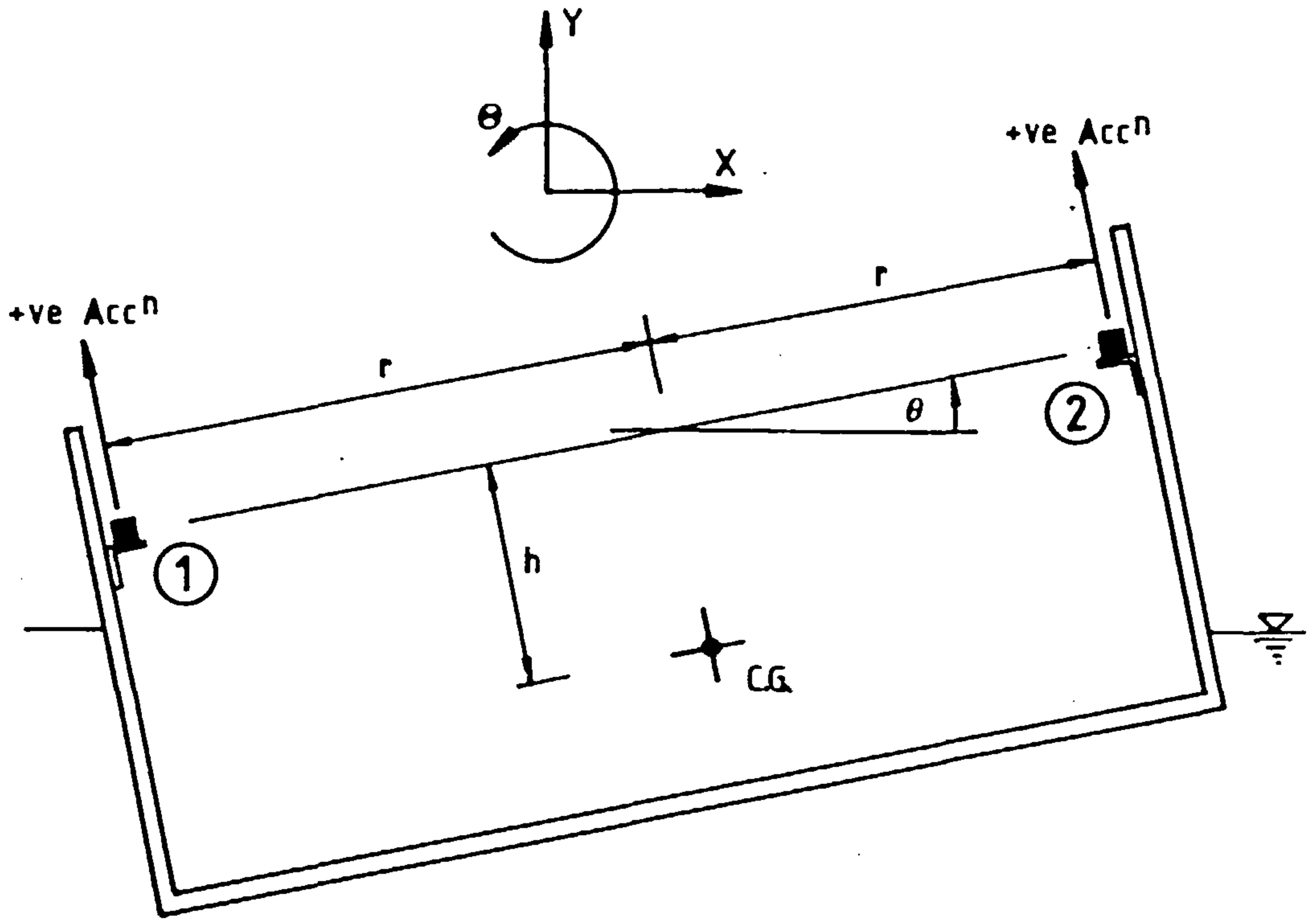

Fig. 5.11 MEASUREMENT OF PITCH ROTATION

As a consequence of the assumed rigidity of the body, the acceleration measured by each transducer consists of a linear superposition of the following components:

(i) Horizontal acceleration, a_X, resulting from surge motion of the body centroid.

(ii) Vertical acceleration, a_y, resulting from heave motion of the body centroid.

(iii) Radial and tangential accelerations, a_h and a_θ, resulting from rotation of the transducer about the body centroid.

Resolution of the components, in the direction of positively measured acceleration, yields;

$$a_1 = - a_X \text{ Sin } \theta + a_y \text{ Cos } \theta + a_h - a_\theta \text{ Cos } \beta \qquad (5.8.13a)$$

$$a_2 = - a_X \text{ Sin } \theta + a_y \text{ Cos } \theta + a_h + a_\theta \text{ Cos } \beta \qquad (5.8.13b)$$

where: a_1 = acceleration measured by transducer No.1.

a_2 = acceleration measured by transducer No.2.

θ = instantaneous angular displacement of the body.

β = $\tan^{-1}(h/r)$

Subtraction of equation (5.8.13a) from (5.8.13b) yields:

$$a_2 - a_1 = 2a_\theta \text{ Cos } \beta \qquad (5.8.14)$$

The instantaneous angular displacement may be defined:

$$\theta = \alpha_3 \text{ Cos}(\sigma t+\epsilon_3) \qquad (5.8.15)$$

where: α_3 = amplitude of angular displacement.

ϵ_3 = phase of angular displacement.

But by definition:

$$a_\Theta = (r^2 + h^2)^{1/2} \frac{\partial^2 \theta}{\partial t^2}$$

$$= - \sigma^2 (r^2 + h^2)^{1/2} \cos(\sigma t + \epsilon_3) \qquad (5.8.16)$$

Substitution in equation (5.8.14), followed by a little algebra, yields:

$$a_2 - a_1 = - 2r\sigma^2 \alpha_3 \cos(\sigma t + \epsilon_3) \qquad (5.8.17)$$

The use of Fast Fourier Transform techniques permits resolution of the transducer output signals into the following form:

$$a_1 = A_1 \cos \sigma t + B_1 \sin \sigma t \qquad (5.8.18a)$$

$$a_2 = A_2 \cos \sigma t + B_2 \sin \sigma t \qquad (5.8.18b)$$

Substitution of equations (5.8.18) into (5.8.17) yields:

$$\{A_2 - A_1\}\cos \sigma t + \{B_2 - B_1\}\sin \sigma t = -2r\sigma^2 \alpha_3 \cos(\sigma t + \epsilon_3) \qquad (5.8.19)$$

Expansion of (5.8.19) followed by equating coefficients of Cos σt and Sin σt yields:

$$A_2 - A_1 = -2r\sigma^2 \alpha_3 \cos \epsilon_3$$

$$B_2 - B_1 = 2r\sigma^2 \alpha_3 \sin \epsilon_3$$

which gives:

$$\alpha_3 = \frac{1}{2r\sigma^2}\left\{(B_2 - B_1)^2 + (A_1 - A_2)^2\right\}^{\frac{1}{2}} \qquad (5.8.20)$$

It must be noted that, in order to provide compatibility, the coefficients A and B must be derived from simultaneous observation of output from the transducers, taking into account the appropriate calibration factors.

CHAPTER 6. PRESENTATION OF RESULTS.

6.1 Introduction

As discussed in Chapter 5, the primary objective of the experimental investigation was the validation of the parameters output by a computer program constructed from the theoretical and numerical formulations detailed in Chapters 3 and 4 of this thesis.

Ideally, a complete validation would require an experimental investigation of all the output parameters but, for reasons discussed in Chapter 5, this was not possible. The lack of suitable experimental facilities limited the investigation to the measurement of wave-effects and body motions associated with the interaction of a floating obstacle and a train of regular waves. Since the computation involved the determination of the 'fixed body' potentials as described in Chapter 3, experimental measurement was also carried out of the wave-effects resulting from the equivalent fixed body interaction. The various non-dimensional parameters measured are detailed in section 5.3.2.

It was intended to investigate the validity of the theoretical formulations for various body length/draught ratios of the fixed/floating body. To this end, the aspect ratios chosen were 2, 4 and 8. Within each value of aspect ratio, it was intended to investigate the effect of different submerged transverse edge radii, both numerically and experimentally. Details are given in Table 6.1 at the end of this chapter.

In order to investigate the behaviour of the parameters over a suitable range of values of the diffraction parameter (see section 5.3.1), nine incident wave frequencies were chosen to give a diffraction parameter range of 0.17 to 0.48 approximately. These frequencies, chosen for their compatibility with the Fast Fourier Transform analysis technique (see section 5.8.1), are detailed in the various tables of experimental results presented in this chapter.

Since previous investigations in this field have demonstrated the dependence of the hydrodynamic parameters on still-water depth, it would have been desirable to carry out the above-mentioned investigations for a series of different flume depths. Owing to certain time-related limitations being imposed upon the availability of experimental facilities however, this was not possible and the investigations were consequently limited to a single flume depth. For physical reasons, this depth was chosen as a nominal 1.2m and all the theoretical predictions were computed using this value: Any slight variations arising as a result of leakage or evaporation are detailed in the tables of experimental results.

In the event, it became necessary to curtail the original experimental program owing to persistent failure of the electronic measuring equipment, resulting in the experimental investigation of Body No.9 being cancelled owing to shortage of time.

It must be noted that, for ease of inspection and consistency of format, all tables and graphs of results are presented at the end of this chapter.

6.2 Floating Body Details.

In order to facilitate possible repetition of the computations in any subsequent studies in this field, full details are given of the computational, geometric, inertial and element distribution parameters used to derive the theoretical predictions. These details are presented in Tables 6.4 to 6.11.

Physically measured geometric parameters were limited to the body length and submerged transverse edge radii. The remaining geometric and inertial parameters were calculated from the geometric properties and measured mass density of the materials used for the body and the necessary ballast to ensure the correct flotation depth. The additional horizontal mass component consisted of the measured mass of the bi-axial bearing arrangement (see section 5.4.2) since that component contributed only to the horizontal inertia of the body.

A horizontally-acting spring restraint system (see section 5.4.2) was required to counteract the effects of higher order drift forces. For various physical and economic reasons, it was not possible to provide the required restraint by means of single springs of known stiffness. As a consequence, the restraint was provided by a number of nominally identical smaller springs acting in parallel. A series of tests was performed to determine the stiffness of each spring and the results indicated a consistency of individual stiffnesses such that the overall system stiffness could be determined with reasonable accuracy by multiplying the number of springs in the system by the average individual spring stiffness as determined from the above tests. A preliminary series of tests was performed on each

body to determine the minimum number of springs necessary to ensure a substantially sinusoidal horizontal motion of the body about a constant mean position over the whole range of envisaged incident wave conditions.

In order to graphically represent the behaviour of the chosen theoretical parameters over the given range of diffraction parameter values, a vast number of solutions was required, necessitating considerable expenditure of computer processor time. Since CPU time per solution increases proportionally with the square of the number of boundary elements (see Appendix A7), it was necessary to limit the number of elements such that an acceptably accurate solution could be obtained from a minimal expenditure of CPU time. The results of a few numerical tests showed that this situation could be achieved by the use of an element length ratio (see Appendix A5) of 0.85 for each body configuration. The corresponding element distribution parameters, presented in Tables 6.4 to 6.11, are defined in Appendix A5.

6.3 Numerical Results.

Previous investigations[40] into the numerical problems associated with the solution of the three-dimensional hydrodynamic problem by the source-distribution formulation have demonstrated the considerable degree of dependence of the solution on the nature of the boundary element distribution. To the best of the author's knowledge, no similar study has been carried out for the two-dimensional case of a substantially rectangular floating body.

Using the form of element distribution detailed in Appendix A5, a series of numerical evaluations was carried out to determine the effect of varying the element length ratio (E.L.R.) while maintaining a constant number (N_c) of elements on each submerged radial edge. In order to demonstrate the effect under differing conditions of body draught and submerged edge radius and to provide a correlation with the results of the experimental investigation, the tests were carried out for Bodies 1, 4 and 7 using 4 constant length elements on each submerged and radial edge. Element distribution details are given in Table 6.2 and the test results are presented in graphical form in Figs.6.1 to 6.3, 6.7 to 6.9 and 6.13 to 6.15.

It must be noted that, for Body No.7, an element length ratio of 0.99 could not be investigated owing to the fact that available computer space limited the number of boundary elements to a maximum of 76.

A similar series of tests was performed on the same bodies to demonstrate the effect of varying the number of constant length radial edge elements whilst maintaining a constant element length ratio. To provide a correlation with the results of the experimental investigations, an element length ratio of 0.85 was used throughout. Element distribution details are given in Table 6.3 and the test results are presented in graphical form in Figs.6.4 to 6.6, 6.10 to 6.12 and 6.16 to 6.18

6.4 Fixed Body Wave-Effects.

Simultaneous measurements of the incident, reflected and transmitted wave components were made for the eight body configurations, defined in Tables 6.4 to 6.11, in the fixed mode in a train of regular waves. This enabled computation of the non-dimensional reflection and transmission coefficients R and T (see section 5.3.2) together with subsequent computation of the energy conservation characteristic (R^2+T^2).

The experimentally measured values of the Fixed Body Reflection and Transmission coefficients are presented in tabular form in Tables 6.12 to 6.19 together with the computed energy conservation characteristic. The results, together with the theoretically predicted values are presented in graphical form in Figs.6.19 to 6.26.

In order to highlight any systematic deviatory trends together between the experimental and theoretical values of the reflection and transmission coefficients, the absolute deviations between theory and experiment for these parameters are presented in graphical form in Figs.6.27 to 6.29.

It must be noted that the incident wave steepness (H/L) varied between 0.0026 and 0.0075. A brief calculation, using measured wave steepness in conjunction with measured flume depth, results in the observation that at no time did the second-order component of the incident wave velocity component exceed 0.6% of the fundamental component, thus adequately complying with the conditions imposed by linear potential theory.

6.5 Floating Body Wave-Effects.

Exactly the same procedure was carried out for the eight body configurations in the 'freely-floating' mode. The results are presented in tabular form in Tables 6.20 to 6.27 and in graphical form in Figs.6.30 to 6.37.

For the same reasons as mentioned above, the absolute deviations between theory and experiment are presented in Figs.6.38 to 6.40.

For this series of experiments, the incident wave steepness varied between 0.0047 and 0.0114 indicating a maximum second-order velocity potential component of 0.9% of the fundamental potential component, thus complying with the conditions imposed by linear potential theory.

6.6 Energy Conservation Characteristics.

The energy conservation characteristics were derived from the measured reflection and transmission coefficients obtained from the fixed and floating body wave-effect experiments described in sections 6.4 and 6.5 above.

The results pertaining to the 'fixed' mode are presented in graphical form in Fig.6.41 and those pertaining to the 'floating' mode in Fig.6.42.

6.7 Floating Body Motions.

Simultaneous measurements were made of the three body motion amplitudes: surge, heave and pitch, for the eight body configurations. In order to provide a correlation between the body motions and the floating body wave-effects, the measurements were taken concurrently with the previously detailed floating body wave effects.

In order to minimise the effect of random errors in both the measurement system and the motion of the mechanical system, ten motion measurements were consecutively taken for each incident wave condition and the computed average was taken to be the experimental value.

As detailed in Chapter 5, the translatory motions were abstracted directly from displacement transducer output and the rotational motion was computed from the body's tangential component of acceleration abstracted from the output from a pair of axi-symmetric acceleration transducers affixed to the floating body.

The results, converted into the appropriate non-dimensional parameters (see section 5.3.2) are presented in tabular form in Tables 6.28 to 6.35 and in graphical form, together with the theoretical predictions, in Figs.6.43 to 6.50.

In order to highlight any trends in deviation between theory and experiment, the absolute deviations of the non-dimensional parameters are presented in graphical form in Figs.6.51 to 6.53.

6.8 Accuracy of Experimental Results.

In order that a valid comparison be made between the experimentally measured parameters and those predicted using theoretical formulations, consideration must be given to the sources of possible errors in both the measurement system, used to abstract the raw experimental data, and the subsequent analysis techniques used to process that raw data into the form presented in the tables and graphs of results.

In general, two basic classes of parameters were experimentally measured: those pertaining to the surface profile and those pertaining to the body motions. These are considered individually and the resultant estimated error magnitudes used to evaluate the error content of the subsequently computed non-dimensional parameters.

Wherever possible, such as in the case of the linear regression analysis of raw calibration data to obtain static and dynamic calibration factors, statistical analysis techniques have been employed to assess the maximum probable errors i.e. those error magnitudes which have an exeedance probability of less than 1%. In cases where the application of such techniques is not possible, engineering judgement has been used to assess error magnitudes.

Since the primary objective of the experimental investigation was to provide a comparison between theory and actuality, a comprehensive assessment of the validity of that comparison requires consideration to be given to any source of error in the basic input parameters leading to the incurrence of systematic errors in the theoretical

hydrodynamic parameters computed therefrom.

Following assessment of the magnitudes of the above errors, an examination of the results permits the identification of genuine discrepancies between the experimentally measured parameters and the corresponding theoretical predictions.

6.8.1 Collection and Primary Analysis of Periodic Data.

Since the experimental measurement of free-surface displacement and floating body motions entailed the observation of substantially sinusoidal data, the procedures used in the collection and primary processing thereof were identical.

The procedure (see section 5.7) entailed the sampling, at known discrete time intervals, of a fluctuating voltage signal and simultaneous analogue/digital conversion of the signal samples. The application of Fast Fourier Transform techniques (see section 5.8.1) to the discretised digital signal permitted resolution of the signal into its various in-phase and quadrature components.

As a consquence of the experimental investigation being concerned largely with the validation of linear theory, all Fourier components other than those pertaining to the fundamental frequency band could be ignored. In this way, any errors resulting from the presence of high frequency electronic noise in the circuity could be completely eliminated. Similarly, any errors due to low frequency 'wandering' of the signal mean could also be eliminated subject, of course, to the signal remaining within the range of the High Speed Scanner at

all times.

The results of a comprehensive series of tests, entailing the sampling and subsequent Fourier analysis of sinusoidally fluctuating voltage signals of known amplitude and frequency, suggested that any error incurred in this operation could be regarded as insignificant for all practical and experimental purposes.

6.8.2 Free-Surface Displacement.

Experimental measurement of the surface profile (section 5.5.1) entailed the sampling of a surface-displacement related voltage signal output from a surface-piercing parallel wire wave-probe. Following analogue/digital conversion of the discretised signal, a Fourier analysis was carried out to determine the positive and negative peak values of the sinusoidal signal in terms of the digital output of the Scanner. These digital values were converted to the corresponding surface displacements by the application of static calibration factors obtained using the methods detailed in section 5.6.1. In order to account for certain amplifier-related dynamic effects, the 'static' displacements were then multiplied by the appropriate dynamic calibration factors obtained using the methods detailed in section 5.6.2. The resulting peak displacements could then be regarded as 'true' peak displacements enabling subsequent computation of the 'true' amplitude of vertical motion of the free-surface. A sinusoidal regression exercise, performed on the variation of the square of measured wave amplitude with longitudinal flume location, permitted resolution of the overall surface profile into positive and negative components (section 5.8.2).

Since the above-mentioned calibration factors were determined empirically using a 'Least-Squares' regression technique, a certain margin of error must be associated with each factor. Consideration of the individual magnitudes of these errors, together with the error incurred in the component resolution procedure, permits the estimation of the maximum probable errors which may be associated with each measured parameter.

(i) Wave Probe Static Calibration.

From some typical calibrations:

$$\text{Maximum Probable Error} = \pm\ 0.7\%\ \text{of F.S.D.} \qquad (6.1)$$

where: F.S.D. = Full Scale Deflection of Scanner.

In order that maximum scanner resolution be maintained whilst ensuring that the scanner range was not exceeded, a few preliminary wave amplitude measurements were taken prior to static calibration of the probe for each incident wave frequency. The amplifier/scanner sensitivity was adjusted according to the maximum wave amplitude encountered.

$$\text{In general: F.S.D.} = 1.5\ (\text{Maximum wave amplitude}) \qquad (6.2)$$

Thus, from expressions (6.1) and (6.2):

$$\text{Maximum Probable Error} = \pm\ 1.05\% \qquad (6.3)$$

(ii) Wave Probe Dynamic Calibration.

From examination of the calibration results:

Maximum Probable Error = ± 1.06% (6.4)

(iii) Component Resolution.

A 'Least-Squares' regression exercise performed on the variation of the square of measured wave amplitude 'A^2' with flume position 'x' yields a sinusoidal expression of the form:

$$A^2 = C_1 + C_2 \cos(2kx+\delta) \quad (6.5)$$

It can be shown (see section 5.8.2) that:

$$a_I = \left\{\frac{C_1}{2} + \left[C_1^2 - C_2^2\right]^{1/2}\right\}^{1/2} \quad (6.6a)$$

$$a_R = \frac{C_2}{2a_I} \quad (6.6b)$$

where: a_I is the amplitude of the incident or transmitted wave component.

a_R is the amplitude of the reflected wave component.

For any function of 'n' variables, $f(x_1,x_2,\ldots,x_n)$, it can be shown that:

$$\delta f = \frac{\partial f}{\partial x_1}\delta x_1 + \frac{\partial f}{\partial x_2}\delta x_2 + \ldots + \frac{\partial f}{\partial x_n}\delta x_n \quad (6.7)$$

where: δx_n represents the error associated with the n^{th} variable.

δf represents the cumulative error associated with the function as a result of the 'n' individual errors.

∂ implies partial differentiation.

Thus, from equations (6.6a) and (6.6b):

$$\delta a_I = \frac{\left[\frac{\delta C_1}{2} + C_1\delta C_1 - C_2\delta C_2\right]}{2\left[a_I(C_1^2 - C_2^2)\right]^{1/2}} \qquad (6.8a)$$

$$\delta a_R = \frac{\delta C_2}{2a_I} + \frac{C_2\delta a_I}{2a_I^2} \qquad (6.8b)$$

The results of some typical upstream and downstream regressions, used in conjunction with equations (6.8), indicate that the Maximum Probable Errors associated with component resolution are:

Incident component: ± 0.4% (6.9a)

Reflected component: ± 1.3% (6.9b)

Transmitted component: ± 0.68% (6.9c)

A combination of the individual error magnitudes, enumerated by expressions (6.3), (6.4) and (6.9), yields the following overall Maximum Probable Errors which may be associated with the experimental measurement of each surface profile parameter:

Incident wave amplitude error = ± 2.5% (6.10a)

Reflected wave amplitude error = ± 3.4% (6.10b)

Transmitted wave amplitude error = ± 2.8% (6.10c)

6.8.3 The Body Motions.

The errors associated with the experimental measurement of body motion amplitudes are similar in source to those associated with the measurement of wave amplitudes in respect of the fact that the major proportion of overall error may be attributable to instrument calibration errors. A quantitative assessment of the individual errors is given below, permitting the estimation of an overall Maximum Probable Error which may be associated with each parameter.

(i) Displacement Transducer Static Calibration (Surge/Heave).

From examination of the calibration results:

$$\text{Maximum Probable Error} = \pm 1.75\% \qquad (6.11)$$

(ii) Displacement Transducer Dynamic Calibration (Surge/Heave).

From examination ofthe calibration results:

$$\text{Maximum Probable Error} = \pm 0.55\% \qquad (6.12)$$

(iii) Acceleration Transducer Calibration (Pitch).

From examination of the calibration results:

$$\text{Maximum Probable Error in Acceleration} = \pm 0.9\% \qquad (6.13)$$

(iv) Accelerometer Cable-Flexure Error (Pitch).

As a consequence of the capacitative properties of the cables used to connect the accelerometers to the charge amplifier (see section 5.5.3), any movement or flexure of the cables resulted in the generation of a voltage additional to that generated by the motion of the accelerometers. A few preliminary tests, carried out prior to commencement of the calibration operations, indicated that this additional voltage varied in-phase with that generated by the accelerometers and would therefore be a source of possible error in the measurement of the floating body pitch motion. In this light, it was felt advisable to carry out a quantitive assessment of the effects thereof.

During the calibration operations (see section 5.6.2), voltage fluctuation measurements were taken from a dummy cable affixed to the cable connecting the charge amplifier to the accelerometer under investigation. Since cable motion was identical in both cases, it was not unreasonable to assume that cable flexure generated voltages would be identical in both cables. The 'dummy' voltages were subsequently compared with the adjacent accelerometer generated voltages to give an indication of the relative magnitude of cable flexure error.

From examination of the calibration results:

Maximum Probable Cable Flexure Error = ± 0.35% (6.14)

(v) Errors of Means (Surge/Heave/Pitch).

As detailed in section 6.7, the experimentally measured amplitude of body motion was taken to be the mean of 10 consecutively measured amplitudes of motion.

From consideration of the spread of the individual results, the errors of the means of those results are:

Surge amplitude: ± 2.28% (6.15a)

Heave amplitude: ± 2.60% (6.15b)

Pitch amplitude: ± 0.88% (6.15c)

A combination of the individual errors, enumerated in expressions (6.11) to (6.15), yields the following overall Maximum Probable Errors which may be associated with the experimental measurement of each body motion amplitude:

Surge amplitude error: ± 4.6% (6.16a)

Heave amplitude error: ± 5.0% (6.16b)

Pitch amplitude error: ± 3.4% (6.16c)

6.8.4 Non-dimensional Parameters.

Using the expressions for the various non-dimensional parameters defined in section 5.3.2, the Maximum Probable Errors which may be associated with each parameter have been estimated using equation

(6.7) in conjunction with the previously computed component errors:

Reflection Coefficient, R: ± 5.9%

Transmission Coefficient, T: ± 5.3%

Non-dimensional Surge amplitude, $\bar{a}_1$: ± 7.1%

Non-dimensional Heave amplitude, $\bar{a}_2$: ± 7.5%

Non-dimensional Pitch amplitude, $\bar{a}_3$: ± 5.6%

6.8.5 Systematic Errors.

In this particular instance, systematic errors are regarded as those which may be associated with the input parameters used to derive the theoretical predictions. These errors, together with their effect on the resultant theoretical predictions, are considered in turn.

(i) Still Water Depth.

For ease of computation and to maintain theoretical continuity, the same flume depth of 1.2m was assumed for all theoretical predictions. In reality, however, the flume depth varied by up to 10mm either side of that value due mainly to evaporation and subsequent over-filling. The results of a comprehensive series of numerical evaluations showed the effect of such a depth variation on the resultant theoretical predictions to be insignificant for practical and experimental purposes.

(ii) Horizontal Spring Restraint System.

As detailed previously, the horizontal spring restraint system consisted of up to 32 nominally identical springs. Tests were carried out to determine the strength of each spring and the overall strength of the system was computed from the average strength of all the tested springs multiplied by the number of springs in the system at any particular time. A subsequent statistical analysis of the spread of individual spring strengths, however, indicated that the overall strength of the system could vary up to 10% either side of the computed strength. A series of numerical evaluations, performed for each body configuration, demonstrated that a spring strength variation of up to 20% could be tolerated before any significant change in the theoretical behaviour of the floating body could be observed. It can thus be reasonably concluded that, in this instance, the spring restraint system was not a source of significant systematic error.

(iii) Body Rotational Inertia.

As discussed previously, the rotational moment of inertia of each body configuration was computed from the measured mass density of the materials used in the body and the necessary ballast. However, as a consequence of non-uniformity of construction materials, ingress of water into construction joints in the course of the experiment and unavoidably inaccurate placing of ballast materials, it was adjudged that the computed value of the body's moment of inertia was subject to a confidence limit of ± 5%. The effect of such a variation is presented in Figs.6.54 to 6.59.

6.8.6 Abnormal Experimental Errors.

Up to now, experimental errors have been quantified from a general point of view using 'typical' sets of results. However, as with many investigations of this nature, certain physical conditons give rise to experimental errors which must be regarded as atypical.

A series of preliminary tests, performed in still water prior to commencement of the experimental investigation, elucidated the fact that the level of the wave-probe trolley support railing varied significantly over the length of the flume. Whilst in the normal course of events this would have had no effect on the accuracy of measurement of wave amplitudes, it presented the possibility of the scanner range being exceeded if maximum sensitivity was to be maintained for small amplitude waves. Consequently, a lower limit had to be imposed on the range of displacements over which the wave probes were statically calibrated, irrespective of the amplitude of the wave to be measured. This resulted in a relatively coarse wave probe static calibration for small amplitude waves leading to an increased magnitude of Probable Error. An examination of the results shows that this situation pertains to approximately 10% of transmitted waves and does not, therfore, affect the measurement accuracy of either the upstream wave components or the non-dimensional body motion parameters. An examination of the relevant cases indicates that the resultant error in transmission coefficient may be as great as 12% in some cases.

A feature of wave behaviour in closed basins is the possibility of wave resonance. It can be shown that a resonant condition pertains in an essentially two-dimensional experimental wave flume if the

distance between the wave generator and the vertical end wall is equal to an integer number of wavelengths of the generated wave. Such a condition is equally likely to occur if a fixed, surface-piercing obstacle, of width equal to that of the flume, is located at an integer number of wavelengths from the wave generator. Owing to a certain lack of forethought on the part of the author, this possibility was not considered when the location of the body support structure was decided upon. It was only after everything had been set up and the investigation was underway, that it was discovered that the location of the 'fixed' body was such that a resonant condition pertained at one particular investigative frequency. Such a condition was characterised by an inherent lack of stability of the upstream wave train. This lack of stability, indicated by a distinct reluctance of the upstream wave train to achieve an equilibrium condition, was exacerbated by the fact that the fixed body Reflection Coefficient was extremely high for all the body configurations at this frequency. The effect of such a condition is graphically illustrated in Fig.6.60 which clearly shows the abnormal behaviour of the upstream and downstream wavetrains. A few calculations, using the appropriate sinusoidal regression results, indicate that the error associated with measurement of the reflection and transmission parameters in these cases is likely to be as much as 20 to 30%.

Body Number	Nominal Length/Draught	Nominal Length/Radius	Nominal Draught/Radius
1	2	8	4
2		16	8
3		32	16
4	4	16	4
5		32	8
6		64	16
7	8	32	4
8		64	8
9		128	16

Table 6.1 Experimental Body Configurations

Body Number	Element Length Ratio				
	0.50	0.60	0.70	0.85	0.99
1	17	19	21	27	37
4	19	23	25	33	55
7	21	25	29	41	87

Table 6.2 Number of Boundary Elements with Varying Element Length Ratio

Body Number	No. of Elements per Radial Edge			
	2	4	6	8
1	15	27	37	45
4	21	33	43	53
7	27	41	51	62

Table 6.3 Number of Boundary Elements with Varying Number of Radial Edge Elements

BODY NO. 1

COMPUTATION DATA

Greens Function Accuracy	99.990	(%)

GEOMETRICAL DATA (RADIAL EDGES)

Body Length	0.9600	(m)
Edge Radius	0.1200	(m)
Length/Draught Ratio	1.9835	
Draught	0.4840	(m)
Centroidal Y-Coordinate	-0.28300	(m)
Metacentric Height	0.20790	(m)

INERTIAL DATA PER M.WIDTH (NON-HOMOGENEOUS)

Mass	458.458	(Kg)
Horizontally acting Mass Component	39.383	(Kg)
Mass Moment of Pitching Inertia	26.590	($Kg.m^2$)

SPRING RESTRAINT DATA N/M (PER M.WIDTH)

Surge	371.900
Heave	FREE
Pitch	FREE

ELEMENT DISTRIBUTION DATA

Nominal Element Length Ratio	0.85	
No.of Side Elements	5	
No.of Base Elements	9	
No.of Radial Elements	4	
Total No.of Elements	27	
Min.Element Length	0.047124	(m)
Max.Side Element Length	0.094234	(m)
Max.Base Element Length	0.116119	(m)
Side Element Length Ratio	0.870576	
Base Element Length Ratio	0.834964	

TABLE 6.4 Floating Body Details

BODY NO. 2

COMPUTATION DATA

Greens Function Accuracy	99.990	(%)

GEOMETRICAL DATA (RADIAL EDGES)

Body Length	0.9600	(m)
Edge Radius	0.0600	(m)
Length/Draught Ratio	1.9926	
Draught	0.4818	(m)
Centroidal Y-Coordinate	-0.28100	(m)
Metacentric Height	0.20161	(m)

INERTIAL DATA PER M.WIDTH (NON-HOMOGENEOUS)

Mass	460.977	(Kg)
Horizontally acting Mass Component	39.383	(Kg)
Mass Moment of Pitching Inertia	26.995	($Kg.m^2$)

SPRING RESTRAINT DATA N/M (PER M.WIDTH)

Surge	371.900
Heave	FREE
Pitch	FREE

ELEMENT DISTRIBUTION DATA

Nominal Element Length Ratio	0.85	
No.of Side Elements	8	
No.of Base Elements	15	
No.of Radial Elements	4	
Total No.of Elements	39	
Min.Element Length	0.023562	(m)
Max.Side Element Length	0.087217	(m)
Max.Base Element Length	0.102900	(m)
Side Element Length Ratio	0.849085	
Base Element Length Ratio	0.831715	

TABLE 6.5 Floating Body Details

BODY NO. 3

COMPUTATION DATA

Greens Function Accuracy	99.990	(%)

GEOMETRICAL DATA (RADIAL EDGES)

Body Length	0.9600	(m)
Edge Radius	0.0300	(m)
Length/Draught Ratio	1.9948	
Draught	0.4812	(m)
Centroidal Y-Coordinate	-0.28100	(m)
Metacentric Height	0.20050	(m)

INERTIAL DATA PER M.WIDTH (NON-HOMOGENEOUS)

Mass	461.606	(Kg)
Horizontally acting Mass Component	39.383	(Kg)
Mass Moment of Pitching Inertia	27.133	($Kg.m^2$)

SPRING RESTRAINT DATA N/M (PER M.WIDTH)

Surge	371.900
Heave	FREE
Pitch	FREE

ELEMENT DISTRIBUTION DATA

Nominal Element Length Ratio	0.85	
No.of Side Elements	12	
No.of Base Elements	23	
No.of Radial Elements	4	
Total No.of Elements	55	
Min.Element Length	0.011781	(m)
Max.Side Element Length	0.077223	(m)
Max.Base Element Length	0.087994	(m)
Side Element Length Ratio	0.854974	
Base Element Length Ratio	0.845721	

TABLE 6.6 Floating Body Details

BODY NO. 4

COMPUTATION DATA

Greens Function Accuracy	99.990	(%)

GEOMETRICAL DATA (RADIAL EDGES)

Body Length	0.9600	(m)
Edge Radius	0.0600	(m)
Length/Draught Ratio	3.9563	
Draught	0.2427	(m)
Centroidal Y-Coordinate	-0.11800	(m)
Metacentric Height	0.31681	(m)

INERTIAL DATA PER M.WIDTH (NON-HOMOGENEOUS)

Mass	231.400	(Kg)
Horizontally acting Mass Component	39.383	(Kg)
Mass Moment of Pitching Inertia	14.142	($Kg.m^2$)

SPRING RESTRAINT DATA N/M (PER M.WIDTH)

Surge	278.900
Heave	FREE
Pitch	FREE

ELEMENT DISTRIBUTION DATA

Nominal Element Length Ratio	0.85	
No.of Side Elements	5	
No.of Base Elements	15	
No.of Radial Elements	4	
Total No.of Elements	33	
Min.Element Length	0.023562	(m)
Max.Side Element Length	0.047375	(m)
Max.Base Element Length	0.102900	(m)
Side Element Length Ratio	0.869626	
Base Element Length Ratio	0.831715	

TABLE 6.7 Floating Body Details

BODY NO. 5

COMPUTATION DATA

Greens Function Accuracy	99.990	(%)

GEOMETRICAL DATA (RADIAL EDGES)

Body Length	0.9600	(m)
Edge Radius	0.0300	(m)
Length/Draught Ratio	3.9653	
Draught	0.2421	(m)
Centroidal Y-Coordinate	-0.11800	(m)
Metacentric Height	0.31509	(m)

INERTIAL DATA PER M.WIDTH (NON-HOMOGENEOUS)

Mass	232.030	(Kg)
Horizontally acting Mass Component	39.383	(Kg)
Mass Moment of Pitching Inertia	14.661	($Kg.m^2$)

SPRING RESTRAINT DATA N/M (PER M.WIDTH)

Surge	278.900
Heave	FREE
Pitch	FREE

ELEMENT DISTRIBUTION DATA

Nominal Element Length Ratio	0.85	
No.of Side Elements	8	
No.of Base Elements	23	
No.of Radial Elements	4	
Total No.of Elements	47	
Min.Element Length	0.011781	(m)
Max.Side Element Length	0.043982	(m)
Max.Base Element Length	0.087994	(m)
Side Element Length Ratio	0.848181	
Base Element Length Ratio	0.845721	

TABLE 6.8 Floating Body Details

BODY NO. 6

COMPUTATION DATA

Greens Function Accuracy	99.990	(%)

GEOMETRICAL DATA (RADIAL EDGES)

Body Length	0.9600	(m)
Edge Radius	0.0150	(m)
Length/Draught Ratio	3.9676	
Draught	0.2420	(m)
Centroidal Y-Coordinate	-0.11800	(m)
Metacentric Height	0.31466	(m)

INERTIAL DATA PER M.WIDTH (NON-HOMOGENEOUS)

Mass	232.187	(Kg)
Horizontally acting Mass Component	39.383	(Kg)
Mass Moment of Pitching Inertia	14.697	($Kg.m^2$)

SPRING RESTRAINT DATA N/M (PER M.WIDTH)

Surge	278.900
Heave	FREE
Pitch	FREE

ELEMENT DISTRIBUTION DATA

Nominal Element Length Ratio	0.85	
No.of Side Elements	12	
No.of Base Elements	31	
No.of Radial Elements	4	
Total No.of Elements	63	
Min.Element Length	0.005890	(m)
Max.Side Element Length	0.038945	(m)
Max.Base Element Length	0.083133	(m)
Side Element Length Ratio	0.854362	
Base Element Length Ratio	0.847517	

TABLE 6.9 Floating Body Details

BODY NO. 7

COMPUTATION DATA

Greens Function Accuracy	99.990	(%)

GEOMETRICAL DATA (RADIAL EDGES)

Body Length	0.9600	(m)
Edge Radius	0.0300	(m)
Length/Draught Ratio	8.0356	
Draught	0.1195	(m)
Centroidal Y-Coordinate	0.03400	(m)
Metacentric Height	0.55166	(m)

INERTIAL DATA PER M.WIDTH (NON-HOMOGENEOUS)

Mass	114.304	(Kg)
Horizontally acting Mass Component	39.383	(Kg)
Mass Moment of Pitching Inertia	10.802	($Kg.m^2$)

SPRING RESTRAINT DATA N/M (PER M.WIDTH)

Surge	185.900
Heave	FREE
Pitch	FREE

ELEMENT DISTRIBUTION DATA

Nominal Element Length Ratio	0.85	
No.of Side Elements	5	
No.of Base Elements	23	
No.of Radial Elements	4	
Total No.of Elements	41	
Min.Element Length	0.011781	(m)
Max.Side Element Length	0.022955	(m)
Max.Base Element Length	0.087994	(m)
Side Element Length Ratio	0.875104	
Base Element Length Ratio	0.845721	

TABLE 6.10 Floating Body Details

BODY NO. 8

COMPUTATION DATA

Greens Function Accuracy	99.990	(%)

GEOMETRICAL DATA (RADIAL EDGES)

Body Length	0.9600	(m)
Edge Radius	0.0150	(m)
Length/Draught Ratio	8.0531	
Draught	0.1192	(m)
Centroidal Y-Coordinate	0.03400	(m)
Metacentric Height	0.55128	(m)

INERTIAL DATA PER M.WIDTH (NON-HOMOGENEOUS)

Mass	114.344	(Kg)
Horizontally acting Mass Component	39.383	(Kg)
Mass Moment of Pitching Inertia	10.812	($Kg.m^2$)

SPRING RESTRAINT DATA N/M (PER M.WIDTH)

Surge	185.900
Heave	FREE
Pitch	FREE

ELEMENT DISTRIBUTION DATA

Nominal Element Length Ratio	0.85	
No.of Side Elements	8	
No.of Base Elements	31	
No.of Radial Elements	4	
Total No.of Elements	55	
Min.Element Length	0.005890	(m)
Max.Side Element Length	0.021421	(m)
Max.Base Element Length	0.083133	(m)
Side Element Length Ratio	0.850971	
Base Element Length Ratio	0.847517	

TABLE 6.11 Floating Body Details

Body Number: 1

F - Incident Wave Frequency (Hz)
B - Body Length (m)
L - Incident Wave Length (m)
D - Still Water Depth (m)
R - Reflection Coefficient
T - Transmission Coefficient

F	D	B/L	R	T	$R^2 + T^2$
0.4883	1.201	0.1688	0.8270	0.4306	0.8693
0.5371	1.201	0.1948	0.9067	0.3541	0.9475
0.5859	1.201	0.2239	0.9246	0.2705	0.9281
0.6348	1.201	0.2567	1.0000	0.2348	1.0551
0.6836	1.201	0.2931	1.0000	0.1417	1.0201
0.7324	1.201	0.3333	1.0000	0.1340	1.0180
0.7813	1.201	0.3772	0.9280	0.1034	0.8719
0.8301	1.201	0.4248	0.7676	0.1271	0.6054
0.8789	1.201	0.4755	0.8374	0.0648	0.7054

TABLE 6.12 Fixed Body Reflection and Transmission

Body Number: 2

F - Incident Wave Frequency (Hz)
B - Body Length (m)
L - Incident Wave Length (m)
D - Still Water Depth (m)
R - Reflection Coefficient
T - Transmission Coefficient

F	D	B/L	R	T	$R^2 + T^2$
0.4883	1.199	0.1689	0.8304	0.4158	0.8625
0.5371	1.199	0.1949	1.0000	0.3581	1.1282
0.5859	1.199	0.2240	1.0000	0.2679	1.0718
0.6348	1.199	0.2567	1.0000	0.2208	1.0488
0.6836	1.199	0.2932	1.0000	0.1251	1.0157
0.7324	1.199	0.3334	1.0000	0.1350	1.0182
0.7813	1.199	0.3773	1.0000	0.0907	1.0082
0.8301	1.199	0.4248	0.7867	0.1215	0.6337
0.8789	1.199	0.4755	0.8343	0.0609	0.6998

TABLE 6.13 Fixed Body Reflection and Transmission

Body Number: 3

F - Incident Wave Frequency (Hz)
B - Body Length (m)
L - Incident Wave Length (m)
D - Still Water Depth (m)
R - Reflection Coefficient
T - Transmission Coefficient

F	D	B/L	R	T	$R^2 + T^2$
0.4883	1.210	0.1685	0.8163	0.4021	0.8280
0.5371	1.210	0.1945	0.9420	0.3244	0.9926
0.5859	1.210	0.2237	1.0000	0.2521	1.0636
0.6348	1.205	0.2566	1.0000	0.2474	1.0612
0.6836	1.210	0.2929	1.0000	0.1273	1.0162
0.7324	1.205	0.3333	1.0000	0.1045	1.0109
0.7813	1.205	0.3772	0.9265	0.1063	0.8697
0.8301	1.205	0.4247	0.8102	0.1061	0.6677
0.8789	1.205	0.4755	0.8430	0.0532	0.7135

TABLE 6.14 Fixed Body Reflection and Transmission

Body Number: 4

F - Incident Wave Frequency (Hz)
B - Body Length (m)
L - Incident Wave Length (m)
D - Still Water Depth (m)
R - Reflection Coefficient
T - Transmission Coefficient

F	D	B/L	R	T	$R^2 + T^2$
0.4883	1.199	0.1689	0.6885	0.6512	0.8981
0.5371	1.199	0.1949	0.7624	0.5979	0.9387
0.5859	1.200	0.2240	0.8498	0.4796	0.9522
0.6348	1.200	0.2567	0.8457	0.4604	0.9272
0.6836	1.200	0.2931	0.9308	0.3067	0.9605
0.7324	1.200	0.3334	0.9023	0.2969	0.9023
0.7813	1.200	0.3773	0.9394	0.2292	0.9350
0.8301	1.200	0.4248	0.8646	0.1597	0.7730
0.8789	1.200	0.4755	0.8235	0.1207	0.6927

TABLE 6.15 Fixed Body Reflection and Transmission

Body Number: 5

F - Incident Wave Frequency (Hz)
B - Body Length (m)
L - Incident Wave Length (m)
D - Still Water Depth (m)
R - Reflection Coefficient
T - Transmission Coefficient

F	D	B/L	R	T	$R^2 + T^2$
0.4883	1.200	0.1688	0.7377	0.6129	0.9198
0.5371	1.200	0.1948	0.7832	0.5667	0.9346
0.5859	1.200	0.2240	0.8559	0.4724	0.9557
0.6348	1.200	0.2567	0.9003	0.5322	1.0938
0.6836	1.200	0.2931	0.9362	0.3102	0.9727
0.7324	1.200	0.3334	1.0000	0.2572	1.0662
0.7813	1.200	0.3773	0.9485	0.2196	0.9479
0.8301	1.200	0.4248	0.8869	0.1556	0.8108
0.8789	1.200	0.4755	0.8491	0.1264	0.7369

TABLE 6.16 Fixed Body Reflection and Transmission

Body Number: 6

F - Incident Wave Frequency (Hz)
B - Body Length (m)
L - Incident Wave Length (m)
D - Still Water Depth (m)
R - Reflection Coefficient
T - Transmission Coefficient

F	D	B/L	R	T	$R^2 + T^2$
0.4883	1.203	0.1687	0.7534	0.6278	0.9617
0.5371	1.203	0.1947	0.7907	0.5442	0.9214
0.5859	1.203	0.2239	0.8332	0.4537	0.9001
0.6348	1.203	0.2566	0.8650	0.4504	0.9511
0.6836	1.203	0.2931	0.9057	0.2879	0.9032
0.7324	1.203	0.3333	0.9485	0.2851	0.9809
0.7813	1.203	0.3772	1.0000	0.2206	1.0487
0.8301	1.203	0.4247	0.8635	0.1423	0.7659
0.8789	1.203	0.4755	0.8552	0.0868	0.7389

TABLE 6.17 Fixed Body Reflection and Transmission

Body Number: 7

F - Incident Wave Frequency (Hz)
B - Body Length (m)
L - Incident Wave Length (m)
D - Still Water Depth (m)
R - Reflection Coefficient
T - Transmission Coefficient

F	D	B/L	R	T	$R^2 + T^2$
0.4883	1.200	0.1688	0.6425	0.7322	0.9489
0.5371	1.200	0.1948	0.6690	0.6687	0.8947
0.5859	1.200	0.2240	0.7485	0.5976	0.9174
0.6348	1.200	0.2567	0.7620	0.5750	0.9113
0.6836	1.200	0.2931	0.8117	0.4785	0.8878
0.7324	1.200	0.3334	0.8273	0.4757	0.9107
0.7813	1.200	0.3773	0.8695	0.3882	0.9067
0.8301	1.200	0.4248	0.8721	0.3235	0.8652
0.8789	1.200	0.4755	0.8597	0.2223	0.7885

TABLE 6.18 Fixed Body Reflection and Transmission

Body Number: 8

F - Incident Wave Frequency (Hz)
B - Body Length (m)
L - Incident Wave Length (m)
D - Still Water Depth (m)
R - Reflection Coefficient
T - Transmission Coefficient

F	D	B/L	R	T	$R^2 + T^2$
0.4883	1.198	0.1689	0.6299	0.7091	0.8996
0.5371	1.198	0.1949	0.6593	0.6993	0.9237
0.5859	1.198	0.2240	0.7485	0.6164	0.9402
0.6348	1.198	0.2568	0.7857	0.5928	0.9687
0.6836	1.198	0.2932	0.8249	0.4870	0.9176
0.7324	1.198	0.3334	0.8722	0.4812	0.9923
0.7813	1.198	0.3773	0.8757	0.3875	0.9170
0.8301	1.198	0.4248	0.8551	0.2908	0.8158
0.8789	1.198	0.4755	0.8900	0.2149	0.8383

TABLE 6.19 Fixed Body Reflection and Transmission

Body Number: 1

F - Incident Wave Frequency (Hz)
B - Body Length (m)
L - Incident Wave Length (m)
D - Still Water Depth (m)
R - Reflection Coefficient
T - Transmission Coefficient

F	D	B/L	R	T	$R^2 + T^2$
0.4883	1.199	0.1689	0.2911	0.8944	0.8847
0.5371	1.199	0.1949	0.6330	0.6479	0.8205
0.5859	1.199	0.2240	1.0000	0.1340	1.0180
0.6348	1.199	0.2567	1.0000	0.1366	1.0187
0.6836	1.199	0.2932	1.0000	0.1202	1.0144
0.7324	1.199	0.3334	0.8727	0.1306	0.7787
0.7813	1.199	0.3773	0.5904	0.5376	0.6376
0.8301	1.199	0.4248	0.0793	0.7207	0.5257
0.8789	1.199	0.4755	0.5189	0.6975	0.7558

TABLE 6.20 Floating Body Reflection and Transmission

Body Number: 2

F - Incident Wave Frequency (Hz)
B - Body Length (m)
L - Incident Wave Length (m)
D - Still Water Depth (m)
R - Reflection Coefficient
T - Transmission Coefficient

F	D	B/L	R	T	$R^2 + T^2$
0.4883	1.199	0.1689	0.3422	0.8587	0.8545
0.5371	1.199	0.1949	0.7090	0.5520	0.8074
0.5859	1.199	0.2240	1.0000	0.0313	1.0010
0.6348	1.199	0.2567	1.0000	0.1729	1.0299
0.6836	1.199	0.2932	1.0000	0.0748	1.0056
0.7324	1.199	0.3334	0.7479	0.3537	0.6845
0.7813	1.199	0.3773	0.1965	0.7657	0.6249
0.8301	1.199	0.4248	0.3268	0.7258	0.6336
0.8789	1.199	0.4755	0.6312	0.6000	0.7584

TABLE 6.21 Floating Body Reflection and Transmission

Body Number: 3

F - Incident Wave Frequency (Hz)
B - Body Length (m)
L - Incident Wave Length (m)
D - Still Water Depth (m)
R - Reflection Coefficient
T - Transmission Coefficient

F	D	B/L	R	T	$R^2 + T^2$
0.4883	1.205	0.1686	0.3209	0.8704	0.8606
0.5371	1.205	0.1946	0.7181	0.5295	0.7960
0.5859	1.205	0.2238	0.9092	0.0331	0.8277
0.6348	1.205	0.2566	1.0000	0.1795	1.0322
0.6836	1.205	0.2930	0.9687	0.0329	0.9395
0.7324	1.205	0.3333	0.6238	0.5384	0.6790
0.7813	1.205	0.3772	0.1113	0.8200	0.6848
0.8301	1.205	0.4247	0.4009	0.6739	0.6149
0.8789	1.205	0.4755	0.7020	0.5796	0.8287

TABLE 6.22 Floating Body Reflection and Transmission

Body Number: 4

F - Incident Wave Frequency (Hz)
B - Body Length (m)
L - Incident Wave Length (m)
D - Still Water Depth (m)
R - Reflection Coefficient
T - Transmission Coefficient

F	D	B/L	R	T	$R^2 + T^2$
0.4883	1.200	0.1688	0.0587	0.9514	0.9086
0.5371	1.200	0.1948	0.1333	0.9071	0.8406
0.5859	1.200	0.2240	0.2074	0.8816	0.8202
0.6348	1.200	0.2567	0.4161	0.7778	0.7781
0.6836	1.200	0.2931	0.5458	0.6733	0.7512
0.7324	1.200	0.3334	0.6892	0.4670	0.6931
0.7813	1.200	0.3773	0.7620	0.4845	0.8154
0.8301	1.200	0.4248	0.3801	0.6578	0.5772
0.8789	1.200	0.4755	0.4034	0.6680	0.6090

TABLE 6.23 Floating Body Reflection and Transmission

Body Number: 5

F - Incident Wave Frequency (Hz)
B - Body Length (m)
L - Incident Wave Length (m)
D - Still Water Depth (m)
R - Reflection Coefficient
T - Transmission Coefficient

F	D	B/L	R	T	$R^2 + T^2$
0.4883	1.200	0.1688	0.0704	0.9530	0.9132
0.5371	1.200	0.1948	0.1197	0.9076	0.8381
0.5859	1.200	0.2240	0.2175	0.8739	0.8110
0.6348	1.200	0.2567	0.4558	0.7762	0.8102
0.6836	1.200	0.2931	0.5757	0.6537	0.7588
0.7324	1.200	0.3334	0.7371	0.4679	0.7622
0.7813	1.200	0.3773	0.6773	0.4974	0.7061
0.8301	1.200	0.4248	0.1605	0.7398	0.5731
0.8789	1.200	0.4755	0.5308	0.6332	0.6827

TABLE 6.24 Floating Body Reflection and Transmission

Body Number: 6

F - Incident Wave Frequency (Hz)
B - Body Length (m)
L - Incident Wave Length (m)
D - Still Water Depth (m)
R - Reflection Coefficient
T - Transmission Coefficient

F	D	B/L	R	T	$R^2 + T^2$
0.4883	1.200	0.1688	0.0535	0.9480	0.9016
0.5371	1.200	0.1948	0.1249	0.9087	0.8413
0.5859	1.200	0.2240	0.2111	0.8767	0.8132
0.6348	1.200	0.2567	0.4520	0.7578	0.7786
0.6836	1.200	0.2931	0.5747	0.6524	0.7559
0.7324	1.200	0.3334	0.7220	0.4623	0.7350
0.7813	1.200	0.3773	0.6017	0.5527	0.6675
0.8301	1.200	0.4248	0.1318	0.7410	0.5665
0.8789	1.200	0.4755	0.6061	0.5782	0.7017

TABLE 6.25 Floating Body Reflection and Transmission

Body Number: 7

F - Incident Wave Frequency (Hz)
B - Body Length (m)
L - Incident Wave Length (m)
D - Still Water Depth (m)
R - Reflection Coefficient
T - Transmission Coefficient

F	D	B/L	R	T	$R^2 + T^2$
0.4883	1.200	0.1688	0.0952	0.9464	0.9047
0.5371	1.200	0.1948	0.0613	0.9242	0.8579
0.5859	1.200	0.2240	0.0272	0.9038	0.8176
0.6348	1.200	0.2567	0.0925	0.8936	0.8071
0.6836	1.200	0.2931	0.0996	0.8622	0.7533
0.7324	1.200	0.3334	0.2047	0.8490	0.7627
0.7813	1.200	0.3773	0.1259	0.8259	0.6980
0.8301	1.200	0.4248	0.3307	0.6898	0.5852
0.8789	1.200	0.4755	0.6996	0.4006	0.6499

TABLE 6.26 Floating Body Reflection and Transmission

Body Number: 8

F - Incident Wave Frequency (Hz)
B - Body Length (m)
L - Incident Wave Length (m)
D - Still Water Depth (m)
R - Reflection Coefficient
T - Transmission Coefficient

F	D	B/L	R	T	$R^2 + T^2$
0.4883	1.200	0.1688	0.0750	0.9457	0.9000
0.5371	1.200	0.1948	0.0629	0.9211	0.8524
0.5859	1.200	0.2240	0.0588	0.9161	0.8427
0.6348	1.200	0.2567	0.0927	0.9046	0.8269
0.6836	1.200	0.2931	0.1186	0.8949	0.8149
0.7324	1.200	0.3334	0.1962	0.8682	0.7923
0.7813	1.200	0.3773	0.1042	0.8090	0.6653
0.8301	1.200	0.4248	0.3710	0.6194	0.5213
0.8789	1.200	0.4755	0.7072	0.2702	0.5731

TABLE 6.27 Floating Body Reflection and Transmission

Body Number: 1

F	-	Incident Wave Frequency	(Hz)
B	-	Body Length	(m)
L	-	Incident Wave Length	(m)
D	-	Still Water Depth	(m)
η	-	Incident Wave Amplitude	(mm)
a1	-	Body Surge Amplitude	(mm)
a2	-	Body Heave Amplitude	(mm)
a3	-	Body Pitch Amplitude	(Rad)

F	D	B/L	η	a1/η	a2/η	a3*B/η
0.4883	1.199	0.1689	20.571	0.947	1.631	1.260
0.5371	1.199	0.1949	15.911	0.827	1.843	1.556
0.5859	1.199	0.2240	14.971	0.785	1.527	1.947
0.6348	1.199	0.2567	12.918	0.717	0.870	2.393
0.6836	1.199	0.2932	9.740	0.731	0.430	3.192
0.7324	1.199	0.3334	10.211	0.549	0.265	4.224
0.7813	1.199	0.3773	14.556	0.276	0.149	4.644
0.8301	1.199	0.4248	10.684	0.053	0.074	3.760
0.8789	1.199	0.4755	8.351	0.134	0.055	2.783

TABLE 6.28 Floating Body Motions

Body Number: 2

F	-	Incident Wave Frequency	(Hz)
B	-	Body Length	(m)
L	-	Incident Wave Length	(m)
D	-	Still Water Depth	(m)
η	-	Incident Wave Amplitude	(mm)
a1	-	Body Surge Amplitude	(mm)
a2	-	Body Heave Amplitude	(mm)
a3	-	Body Pitch Amplitude	(Rad)

F	D	B/L	η	a1/η	a2/η	a3*B/η
0.4883	1.199	0.1689	21.637	0.909	1.763	1.342
0.5371	1.199	0.1949	14.843	0.815	1.909	1.592
0.5859	1.199	0.2240	15.396	0.768	1.306	2.008
0.6348	1.199	0.2567	14.071	0.718	0.821	2.642
0.6836	1.199	0.2932	9.516	0.718	0.390	3.812
0.7324	1.199	0.3334	8.883	0.408	0.232	4.876
0.7813	1.199	0.3773	8.323	0.082	0.141	4.646
0.8301	1.199	0.4248	8.628	0.189	0.184	3.049
0.8789	1.199	0.4755	8.538	0.214	0.111	1.987

TABLE 6.29 Floating Body Motions

Body Number: 3

F	-	Incident Wave Frequency	(Hz)
B	-	Body Length	(m)
L	-	Incident Wave Length	(m)
D	-	Still Water Depth	(m)
η	-	Incident Wave Amplitude	(mm)
a1	-	Body Surge Amplitude	(mm)
a2	-	Body Heave Amplitude	(mm)
a3	-	Body Pitch Amplitude	(Rad)

F	D	B/L	η	a1/η	a2/η	a3*B/η
0.4883	1.205	0.1686	16.265	0.945	1.753	1.285
0.5371	1.205	0.1946	12.455	0.813	1.936	1.551
0.5859	1.205	0.2238	10.452	0.756	1.226	2.001
0.6348	1.205	0.2566	13.974	0.731	0.678	3.009
0.6836	1.205	0.2930	7.729	0.739	0.360	4.274
0.7324	1.205	0.3333	8.529	0.374	0.178	5.591
0.7813	1.205	0.3772	7.509	0.040	0.148	4.002
0.8301	1.205	0.4247	8.251	0.232	0.117	2.681
0.8789	1.205	0.4755	8.323	0.222	0.073	1.775

TABLE 6.30 Floating Body Motions

Body Number: 4

F	-	Incident Wave Frequency	(Hz)
B	-	Body Length	(m)
L	-	Incident Wave Length	(m)
D	-	Still Water Depth	(m)
η	-	Incident Wave Amplitude	(mm)
a1	-	Body Surge Amplitude	(mm)
a2	-	Body Heave Amplitude	(mm)
a3	-	Body Pitch Amplitude	(Rad)

F	D	B/L	η	a1/η	a2/η	a3*B/η
0.4883	1.200	0.1688	24.281	0.979	1.109	1.155
0.5371	1.200	0.1948	16.378	0.880	1.126	1.320
0.5859	1.200	0.2240	16.409	0.778	1.237	1.499
0.6348	1.200	0.2567	10.356	0.681	1.371	1.771
0.6836	1.200	0.2931	13.763	0.654	1.162	2.122
0.7324	1.200	0.3334	7.685	0.568	0.852	2.541
0.7813	1.200	0.3773	11.395	0.521	0.658	4.330
0.8301	1.200	0.4248	10.193	0.230	0.444	4.613
0.8789	1.200	0.4755	6.636	0.132	0.257	4.342

TABLE 6.31 Floating Body Motions

Body Number: 5

F	-	Incident Wave Frequency	(Hz)
B	-	Body Length	(m)
L	-	Incident Wave Length	(m)
D	-	Still Water Depth	(m)
η	-	Incident Wave Amplitude	(mm)
a1	-	Body Surge Amplitude	(mm)
a2	-	Body Heave Amplitude	(mm)
a3	-	Body Pitch Amplitude	(Rad)

F	D	B/L	η	a1/η	a2/η	a3*B/η
0.4883	1.200	0.1688	24.600	0.994	1.086	1.192
0.5371	1.200	0.1948	13.226	0.882	1.092	1.391
0.5859	1.200	0.2240	15.838	0.769	1.250	1.599
0.6348	1.200	0.2567	11.388	0.708	1.320	1.965
0.6836	1.200	0.2931	12.980	0.665	1.081	2.465
0.7324	1.200	0.3334	10.375	0.634	0.827	3.537
0.7813	1.200	0.3773	9.191	0.459	0.447	5.027
0.8301	1.200	0.4248	10.263	0.083	0.260	5.555
0.8789	1.200	0.4755	6.133	0.199	0.377	3.844

TABLE 6.32 Floating Body Motions

Body Number: 6

F	-	Incident Wave Frequency	(Hz)
B	-	Body Length	(m)
L	-	Incident Wave Length	(m)
D	-	Still Water Depth	(m)
η	-	Incident Wave Amplitude	(mm)
a1	-	Body Surge Amplitude	(mm)
a2	-	Body Heave Amplitude	(mm)
a3	-	Body Pitch Amplitude	(Rad)

F	D	B/L	η	a1/η	a2/η	a3*B/η
0.4883	1.200	0.1688	15.982	1.000	1.091	1.187
0.5371	1.200	0.1948	13.276	0.897	1.110	1.399
0.5859	1.200	0.2240	13.157	0.786	1.257	1.599
0.6348	1.200	0.2567	10.464	0.696	1.310	1.933
0.6836	1.200	0.2931	9.989	0.690	1.086	2.566
0.7324	1.200	0.3334	10.370	0.665	0.846	3.753
0.7813	1.200	0.3773	11.297	0.446	0.551	5.632
0.8301	1.200	0.4248	7.193	0.091	0.349	5.420
0.8789	1.200	0.4755	6.094	0.215	0.374	3.584

TABLE 6.33 Floating Body Motions

Body Number: 7

F	-	Incident Wave Frequency	(Hz)
B	-	Body Length	(m)
L	-	Incident Wave Length	(m)
D	-	Still Water Depth	(m)
η	-	Incident Wave Amplitude	(mm)
a1	-	Body Surge Amplitude	(mm)
a2	-	Body Heave Amplitude	(mm)
a3	-	Body Pitch Amplitude	(Rad)

F	D	B/L	η	a1/η	a2/η	a3*B/η
0.4883	1.200	0.1688	14.940	0.973	0.747	1.256
0.5371	1.200	0.1948	17.511	0.850	0.942	1.469
0.5859	1.200	0.2240	14.019	0.753	0.970	1.672
0.6348	1.200	0.2567	12.411	0.656	1.039	1.892
0.6836	1.200	0.2931	15.243	0.663	0.910	2.510
0.7324	1.200	0.3334	8.759	0.609	0.913	3.427
0.7813	1.200	0.3773	9.010	0.503	0.804	4.912
0.8301	1.200	0.4248	11.575	0.245	0.657	5.740
0.8789	1.200	0.4755	7.777	0.085	0.617	4.855

TABLE 6.34 Floating Body Motions

Body Number: 8

F	-	Incident Wave Frequency	(Hz)
B	-	Body Length	(m)
L	-	Incident Wave Length	(m)
D	-	Still Water Depth	(m)
η	-	Incident Wave Amplitude	(mm)
a1	-	Body Surge Amplitude	(mm)
a2	-	Body Heave Amplitude	(mm)
a3	-	Body Pitch Amplitude	(Rad)

F	D	B/L	η	a1/η	a2/η	a3*B/η
0.4883	1.200	0.1688	15.336	0.942	0.798	1.262
0.5371	1.200	0.1948	15.148	0.841	0.845	1.459
0.5859	1.200	0.2240	16.933	0.747	0.987	1.692
0.6348	1.200	0.2567	12.440	0.657	1.050	1.987
0.6836	1.200	0.2931	14.805	0.680	0.956	2.695
0.7324	1.200	0.3334	9.248	0.617	0.929	3.765
0.7813	1.200	0.3773	9.316	0.476	0.795	5.238
0.8301	1.200	0.4248	8.871	0.226	0.705	6.023
0.8789	1.200	0.4755	5.945	0.141	0.566	4.249

TABLE 6.35 Floating Body Motions

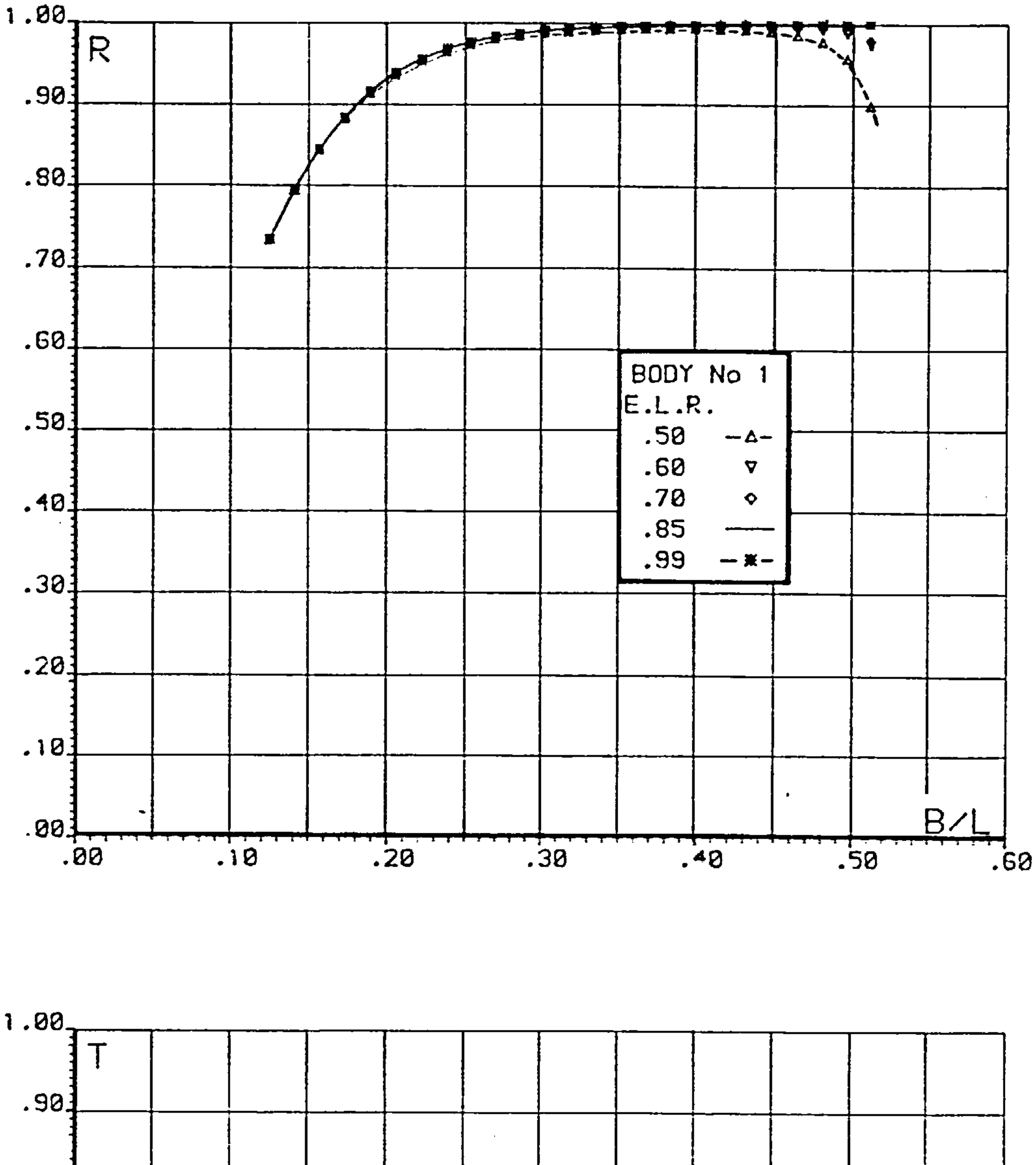

Fig. 6.1 FIXED BODY REFLECTION AND TRANSMISSION

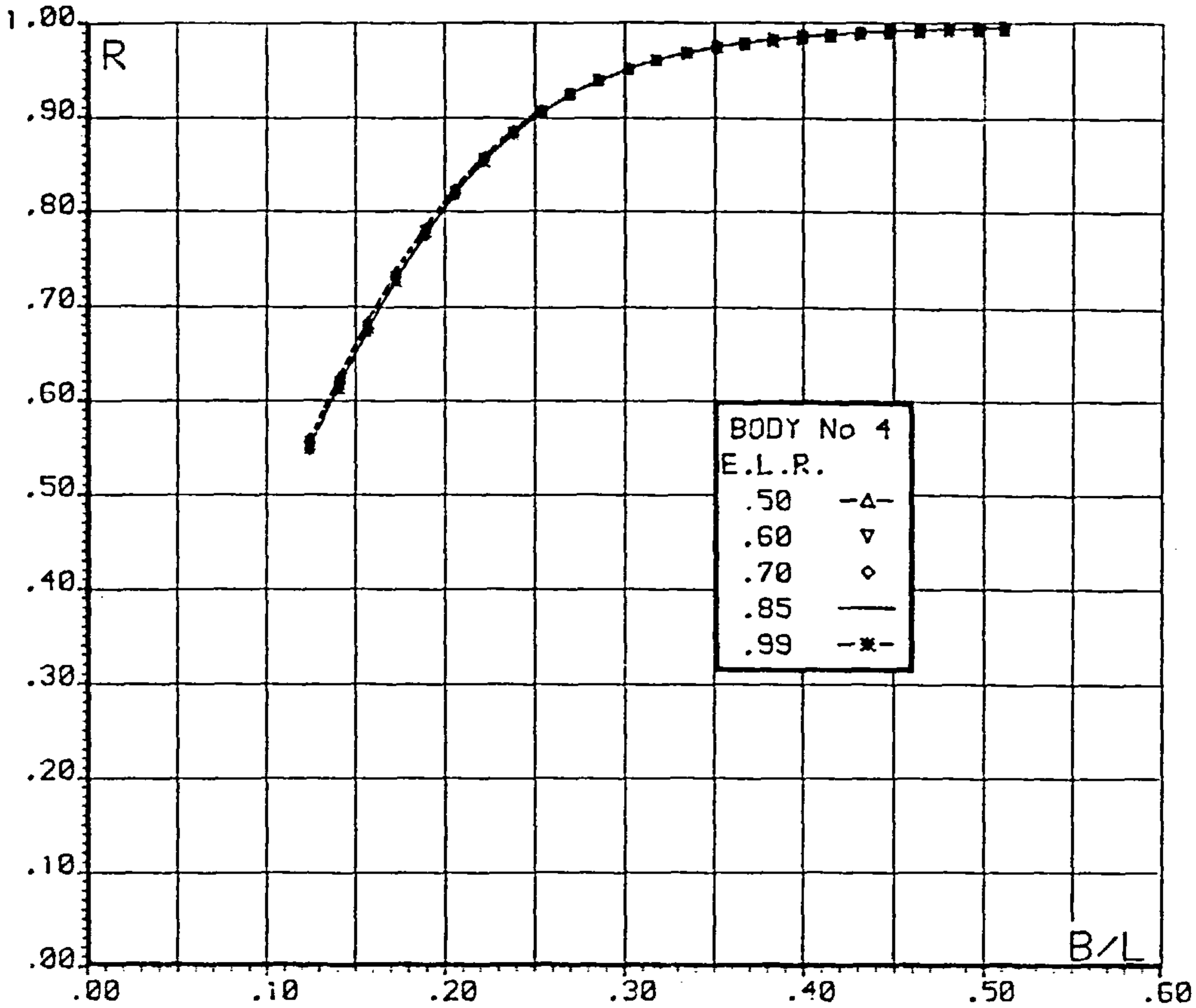

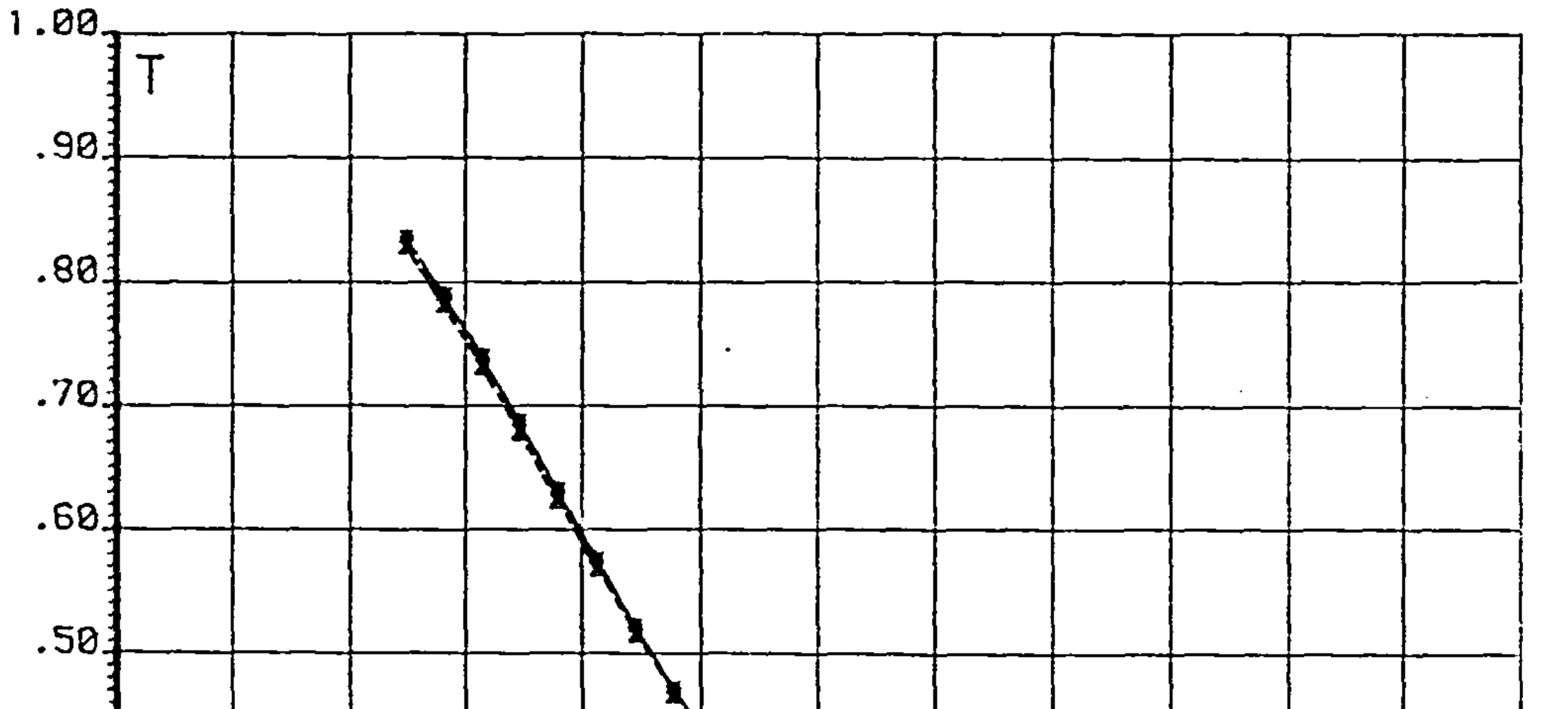

Fig.6.2 FIXED BODY REFLECTION AND TRANSMISSION

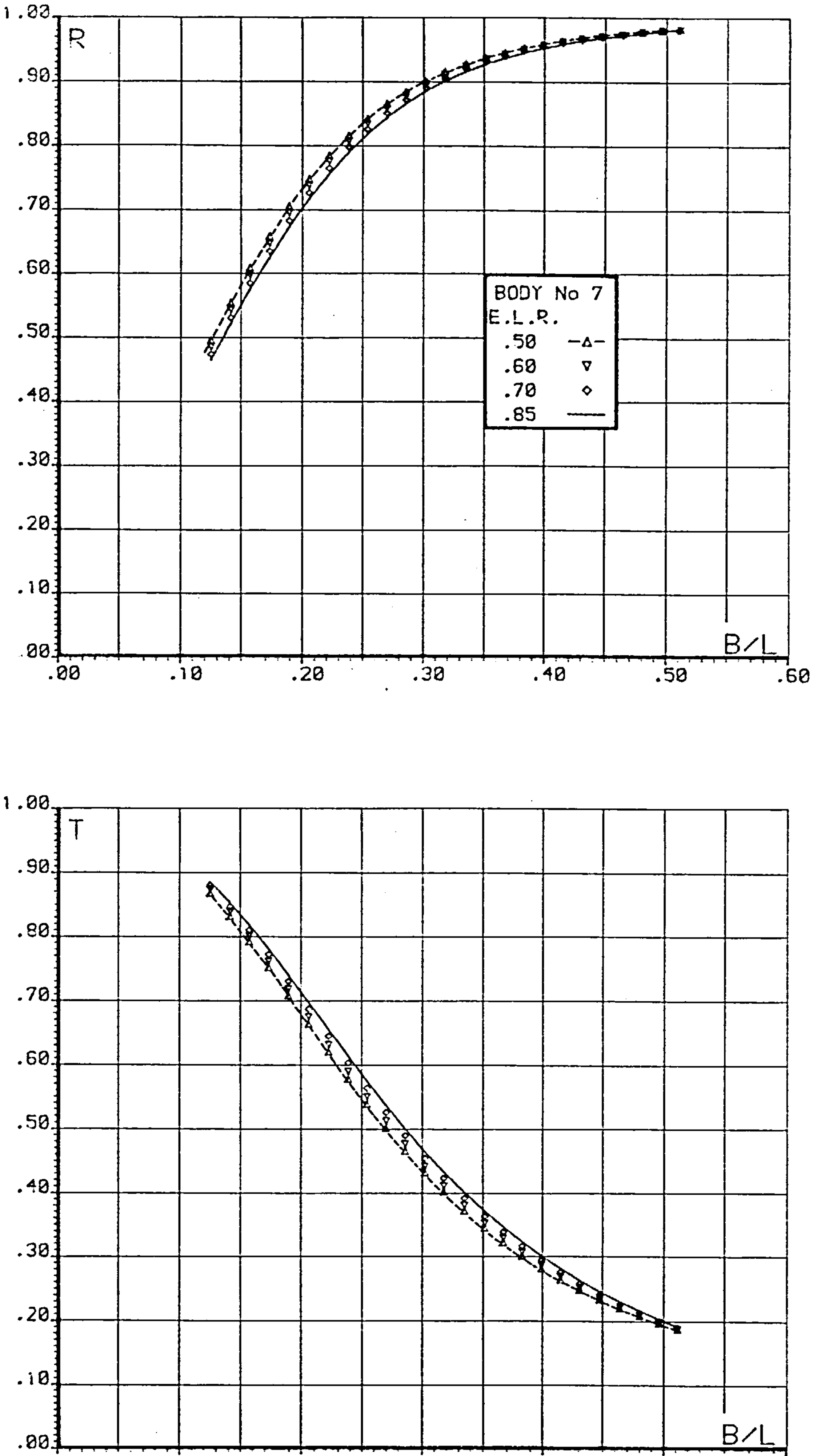

Fig.6.3 FIXED BODY REFLECTION AND TRANSMISSION

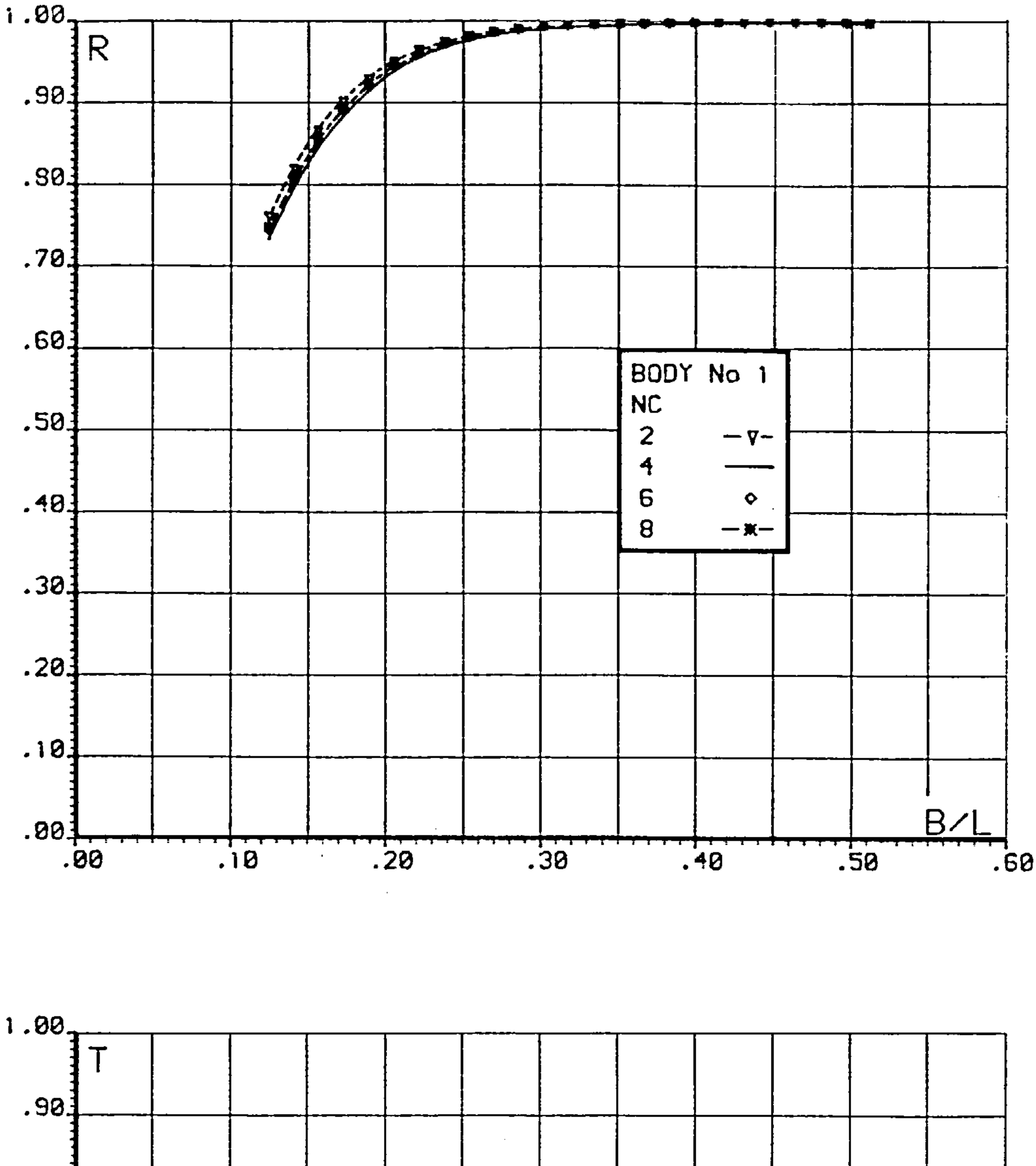

Fig.6.4 FIXED BODY REFLECTION AND TRANSMISSION

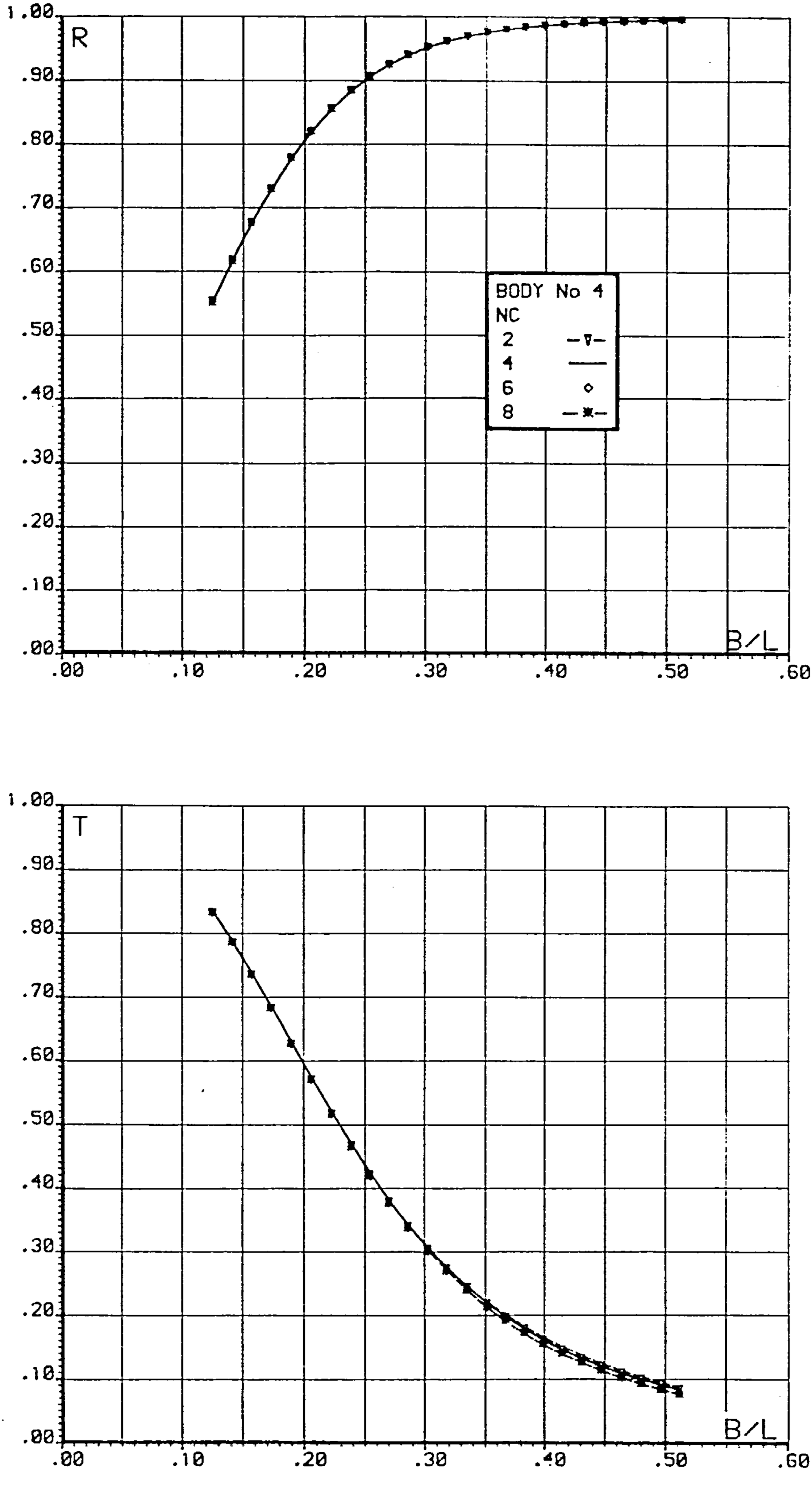

Fig.6-5 FIXED BODY REFLECTION AND TRANSMISSION

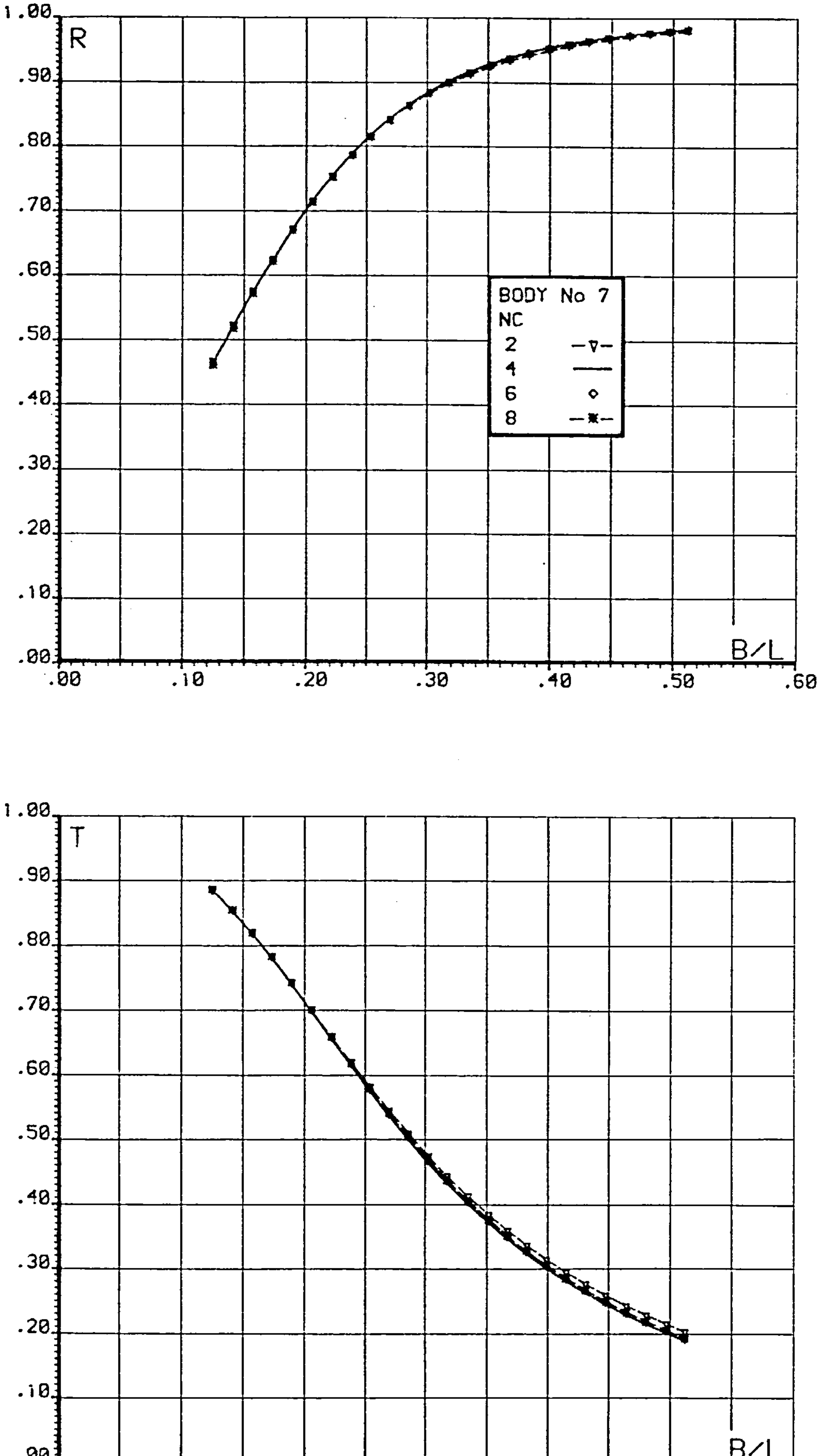

Fig.6.6 FIXED BODY REFLECTION AND TRANSMISSION

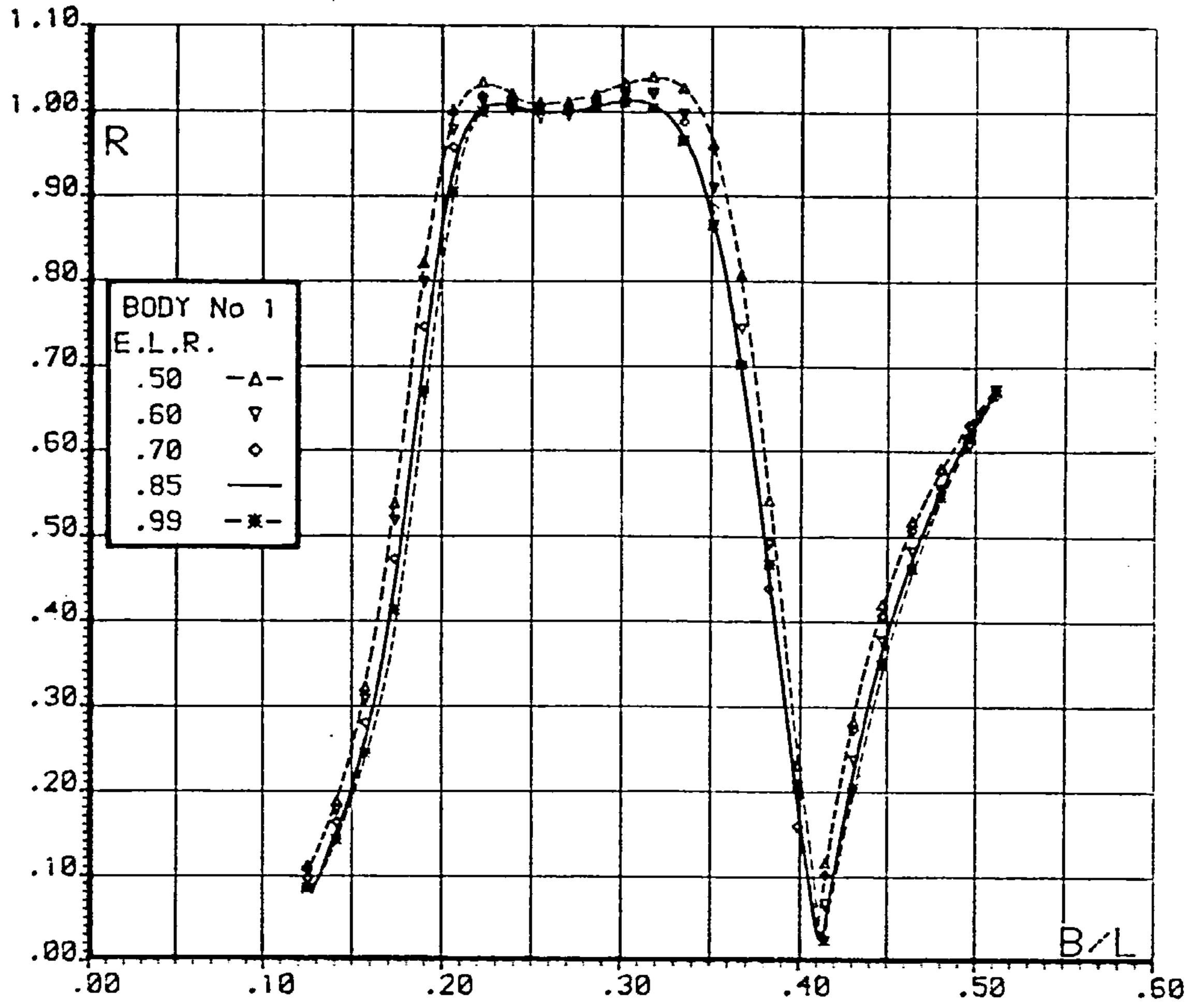

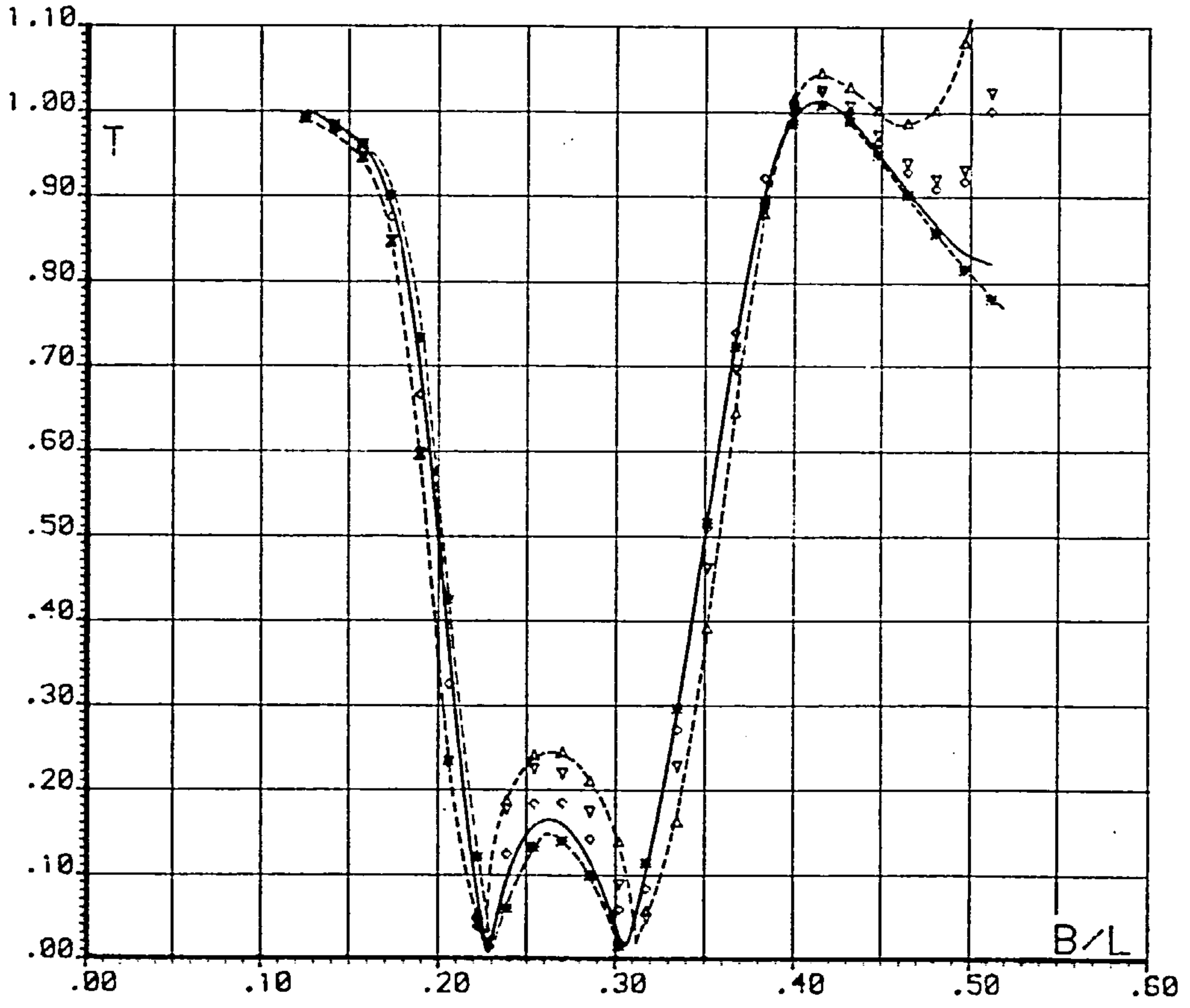

Fig.6.7 FLOATING BODY REFLECTION AND TRANSMISSION

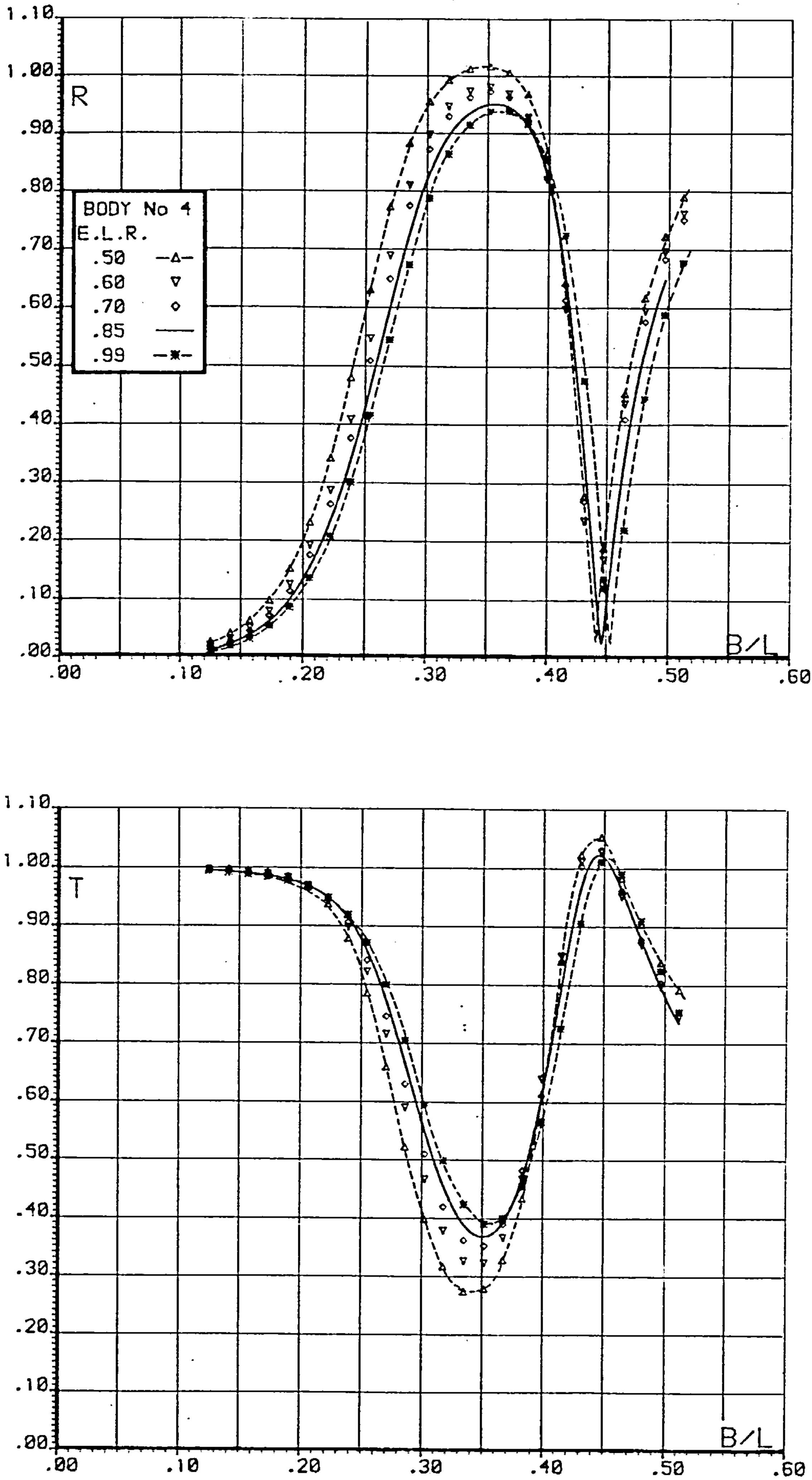

Fig.6.8 FLOATING BODY REFLECTION AND TRANSMISSION

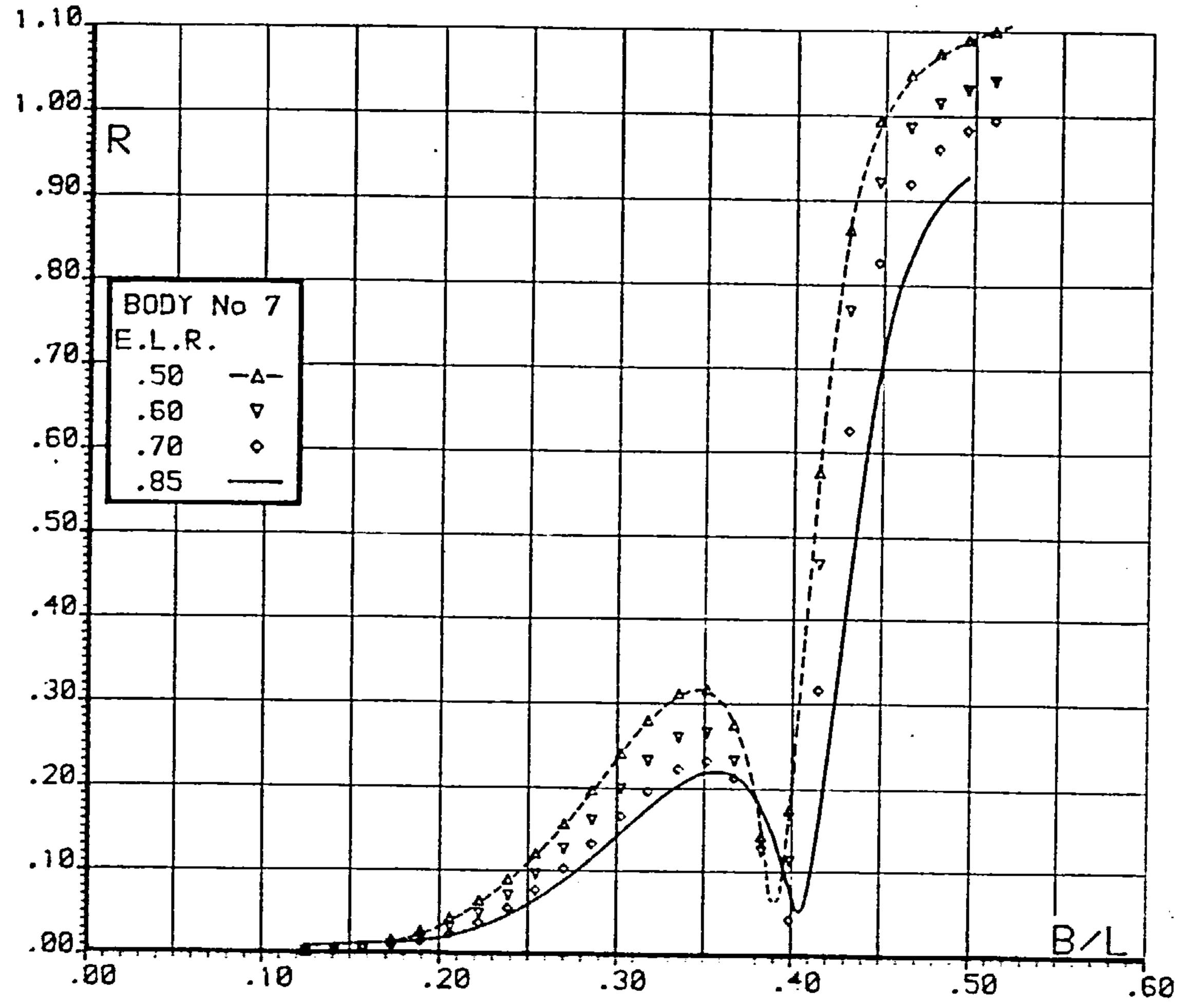

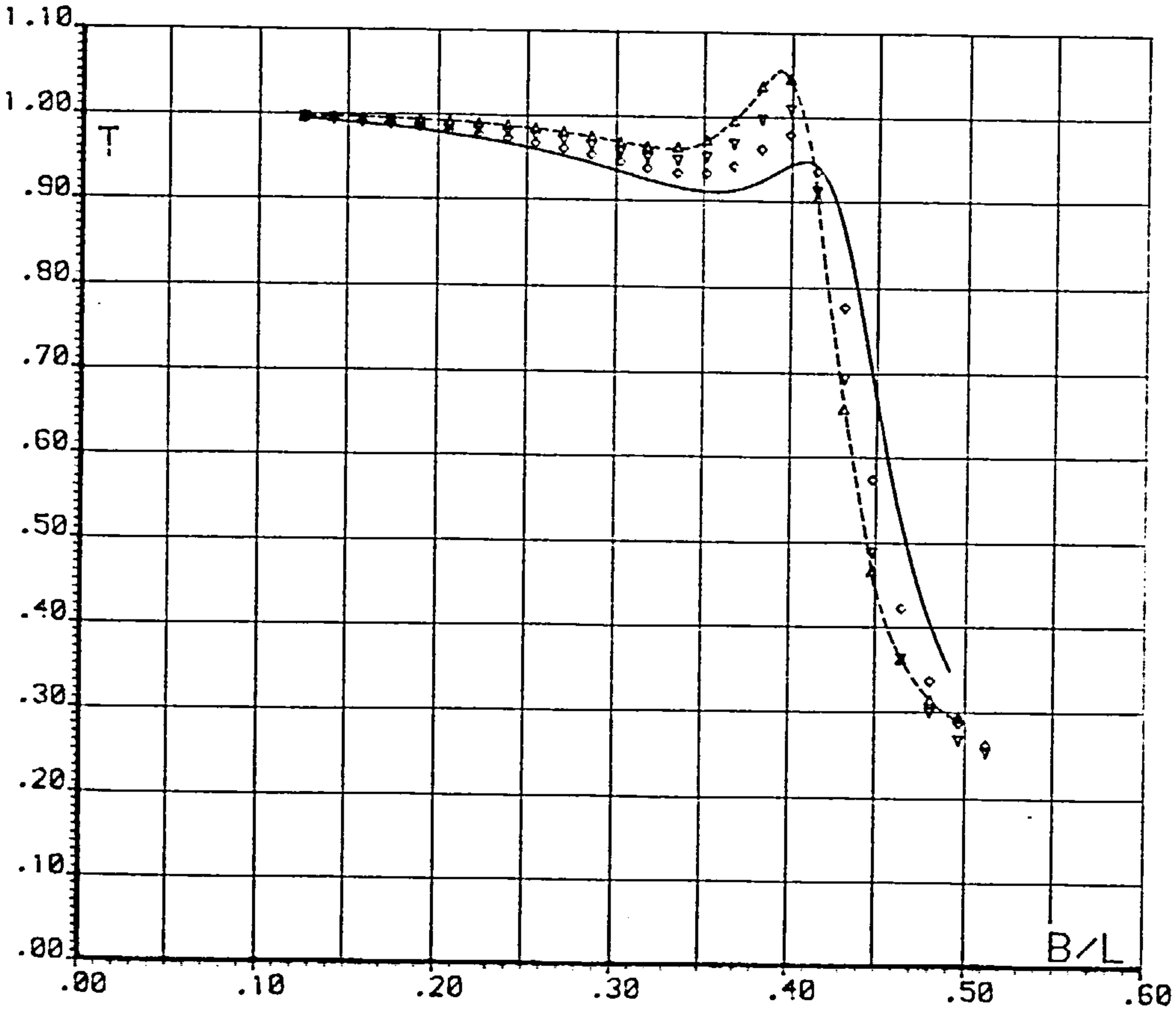

Fig.6.9 FLOATING BODY REFLECTION AND TRANSMISSION

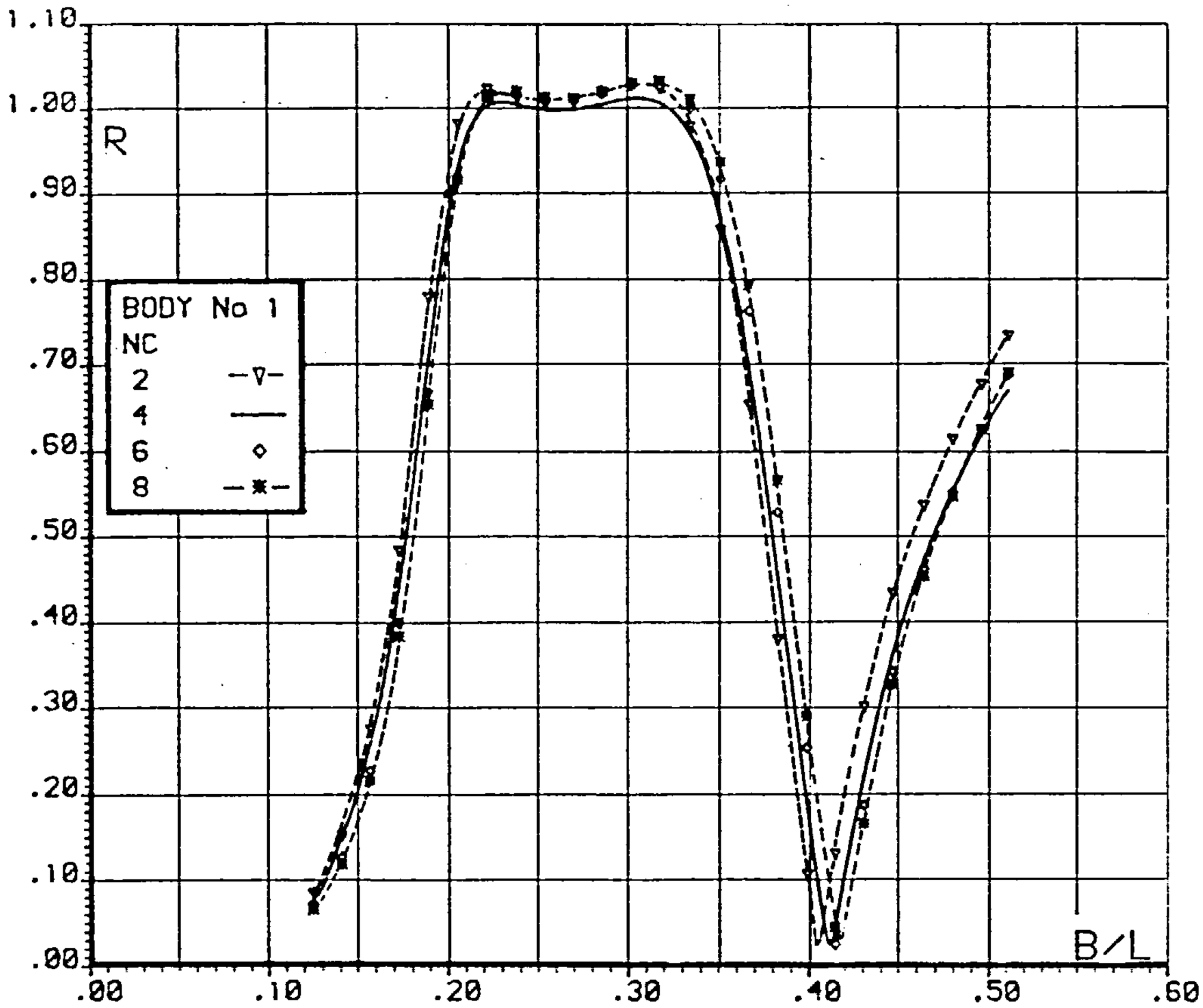

Fig.6.10 FLOATING BODY REFLECTION AND TRANSMISSION

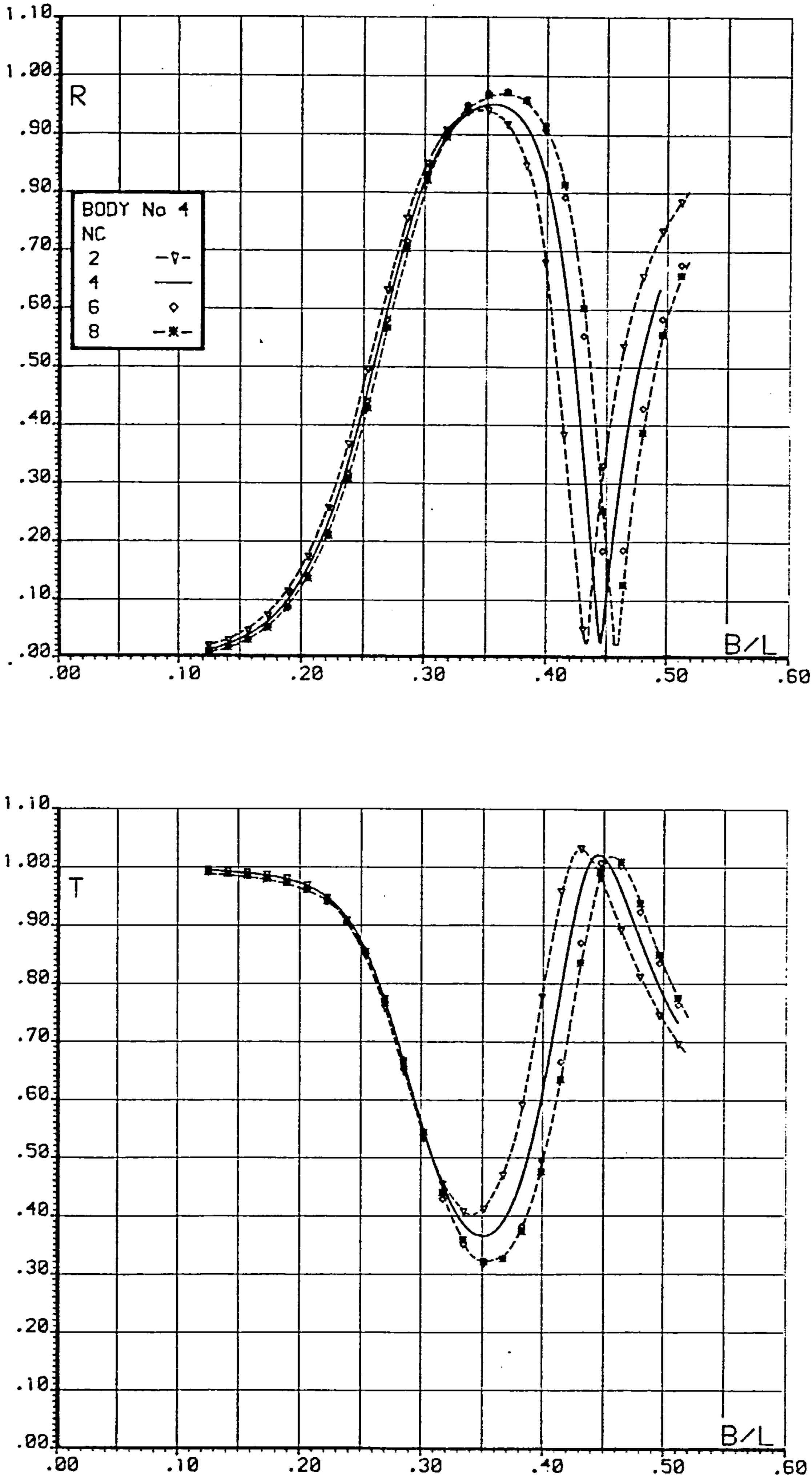

Fig.6.11 FLOATING BODY REFLECTION AND TRANSMISSION

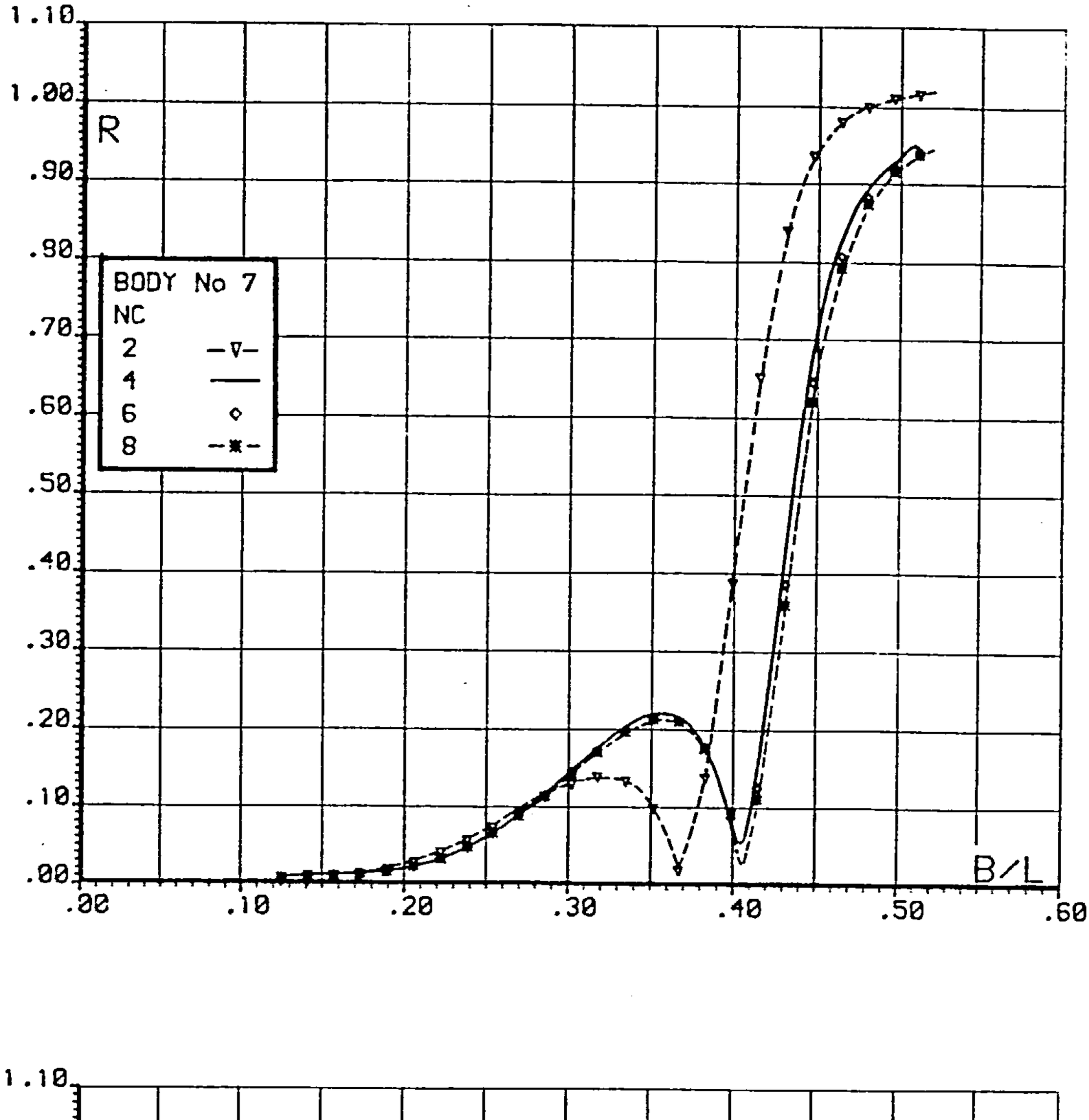

Fig.6.12 FLOATING BODY REFLECTION AND TRANSMISSION

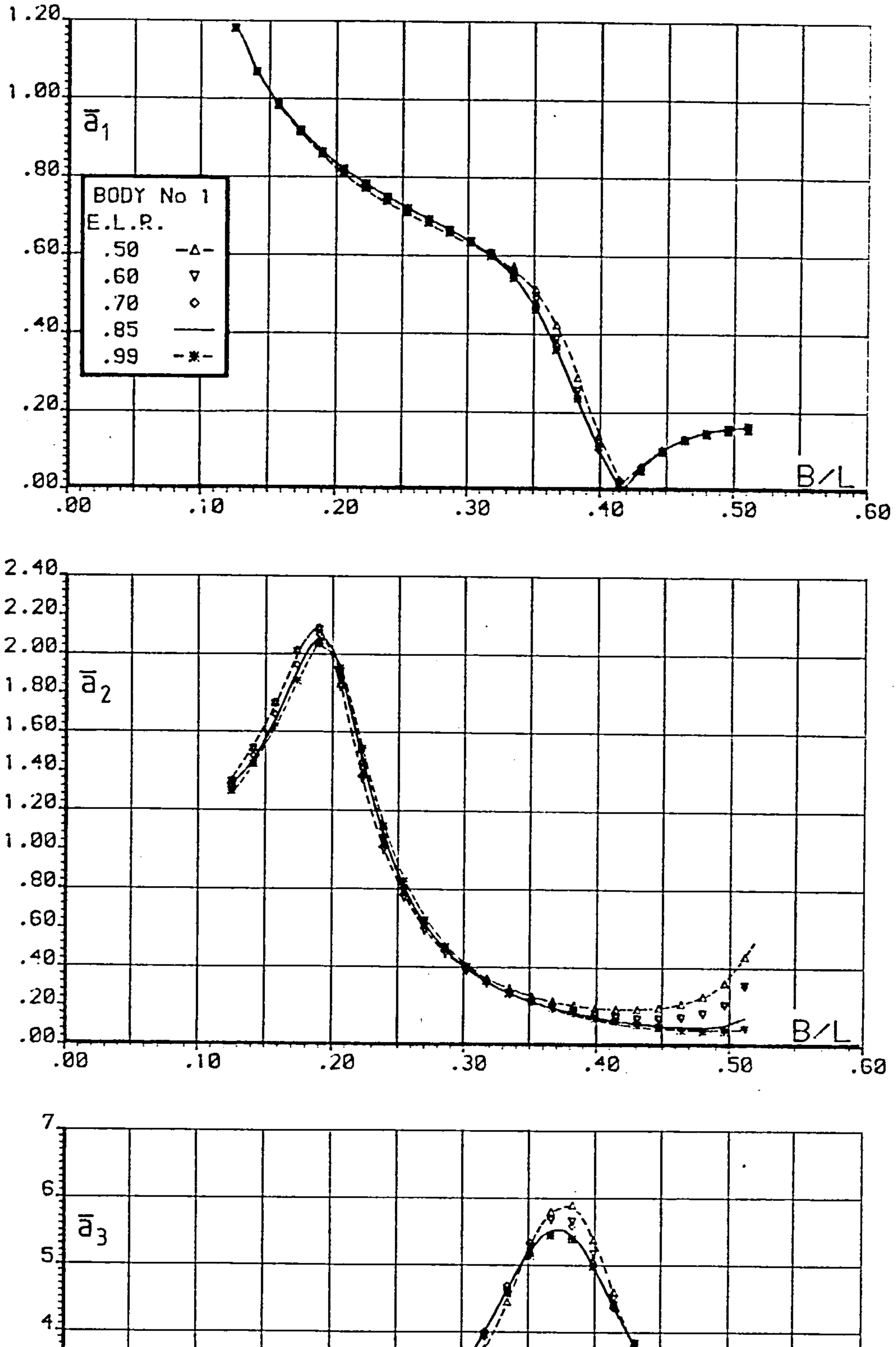

Fig.6.13 FLOATING BODY MOTIONS

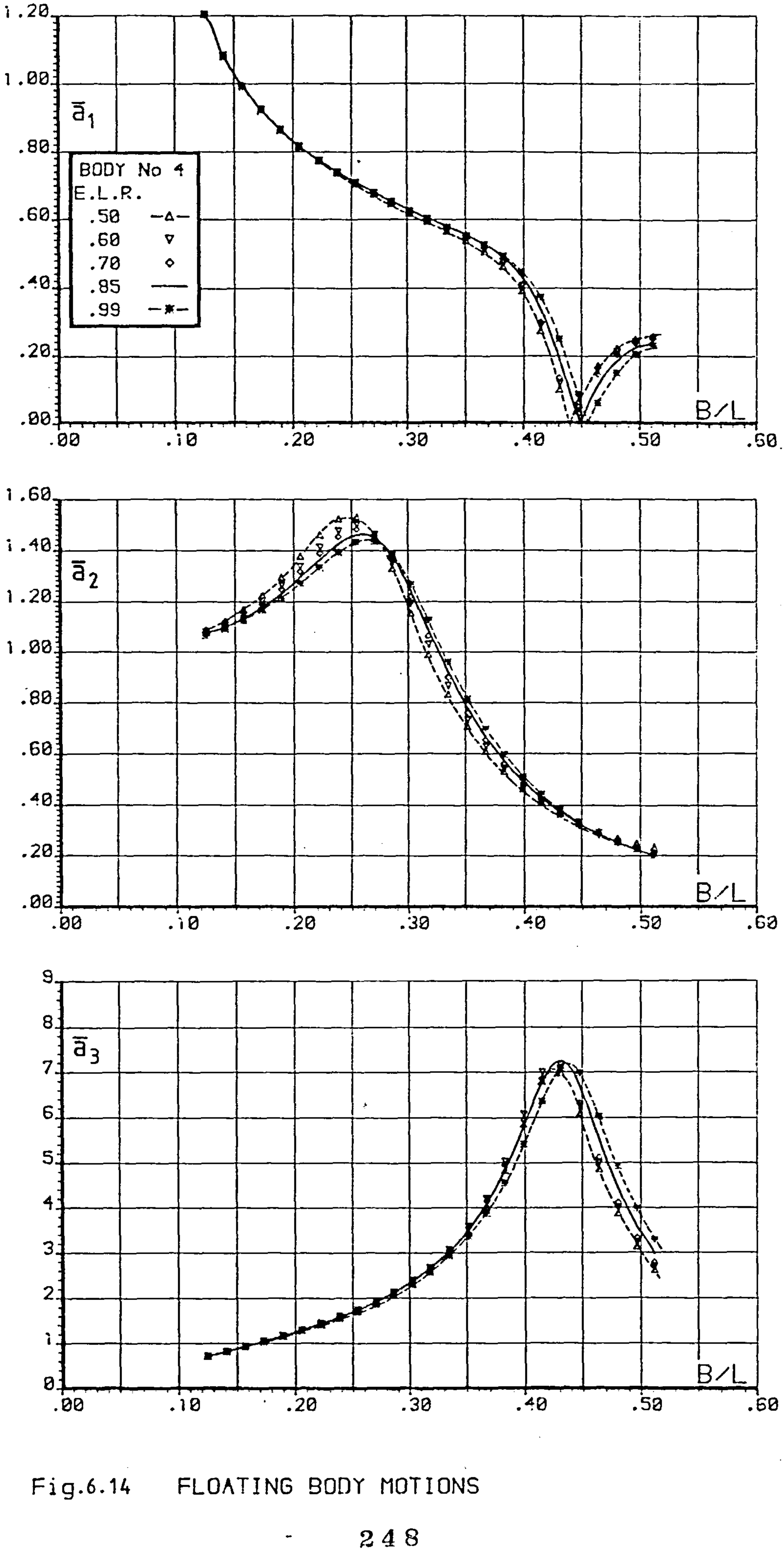

Fig.6.14 FLOATING BODY MOTIONS

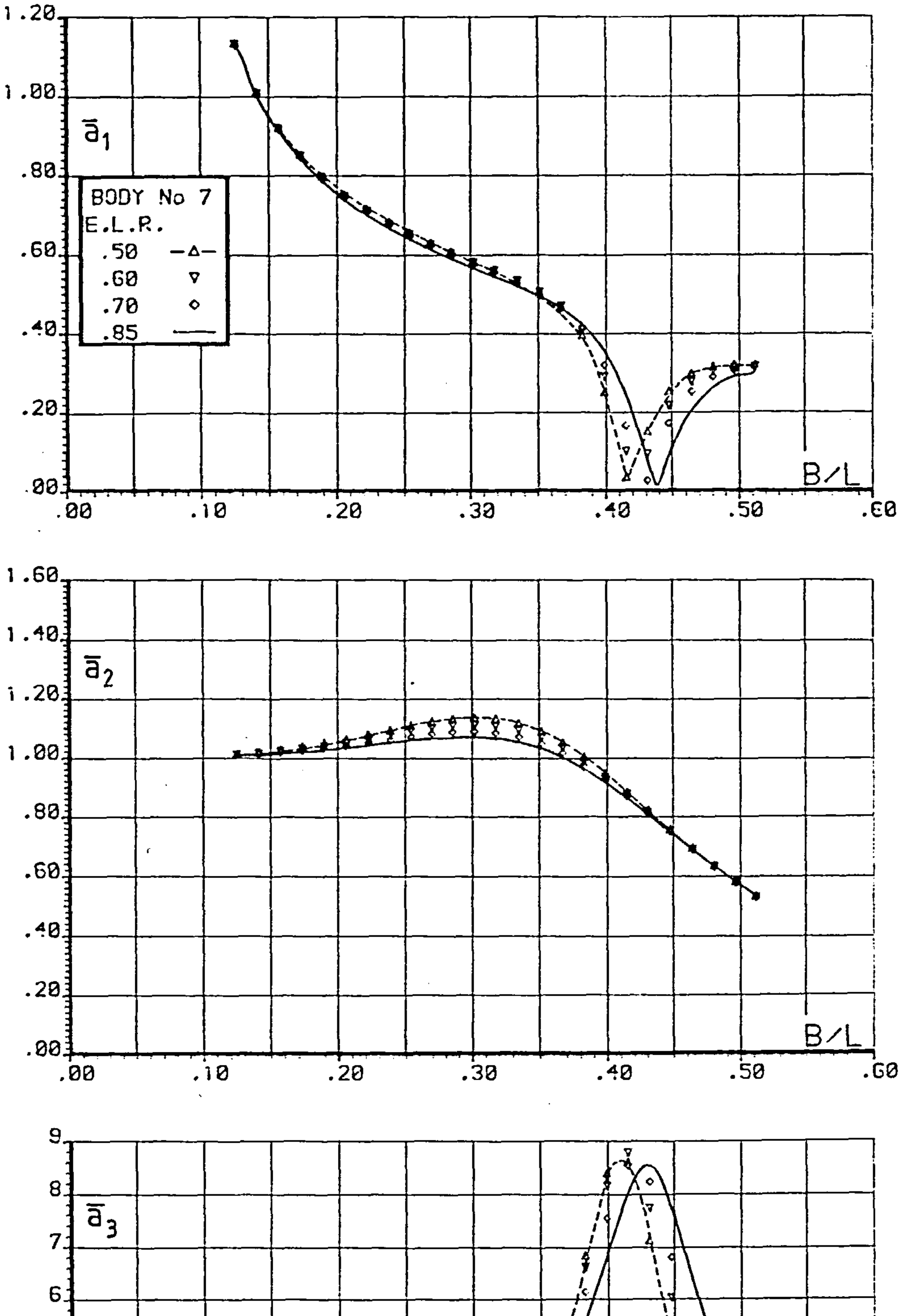

Fig.6.15 FLOATING BODY MOTIONS

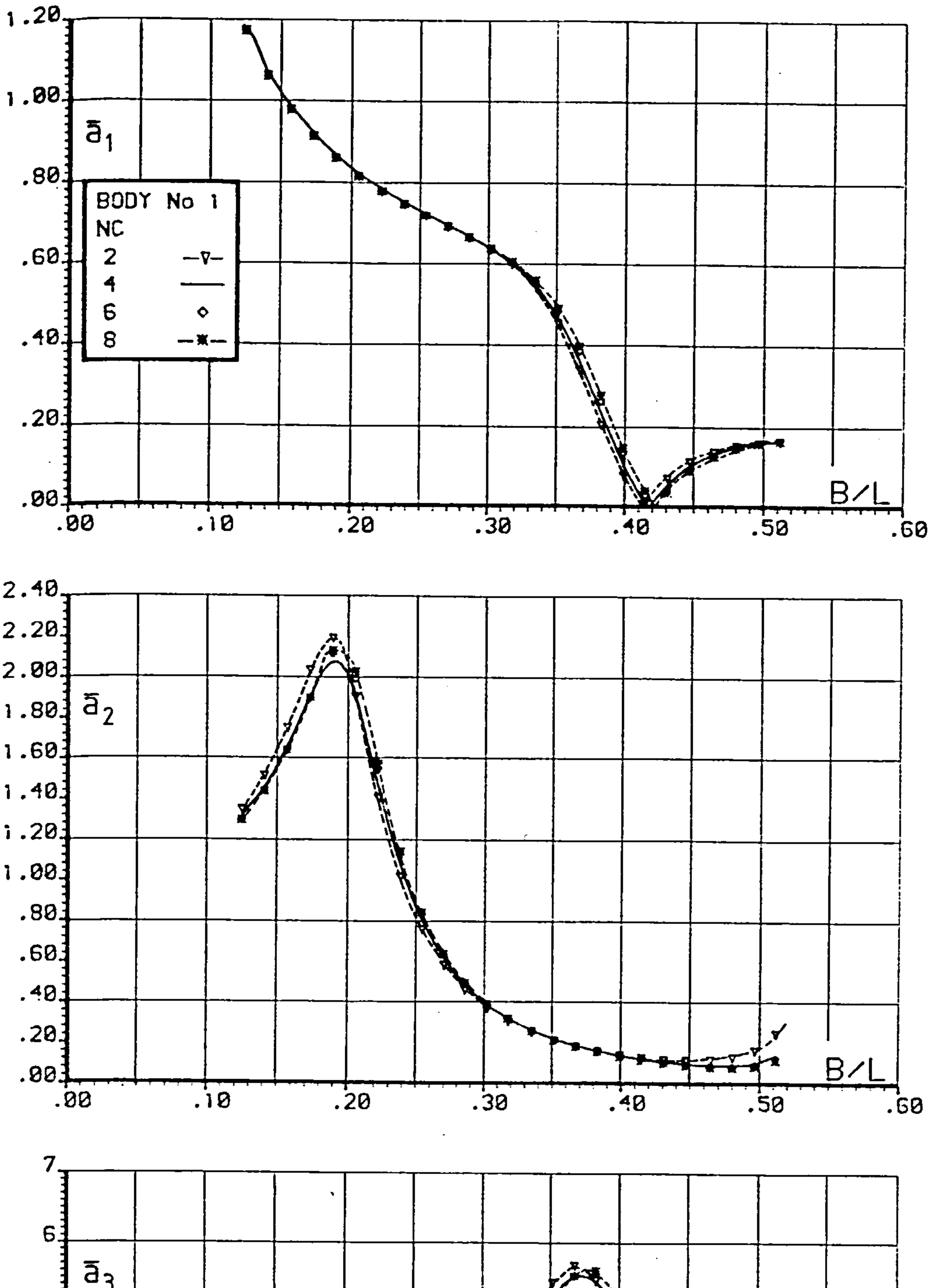

Fig.6.16 FLOATING BODY MOTIONS

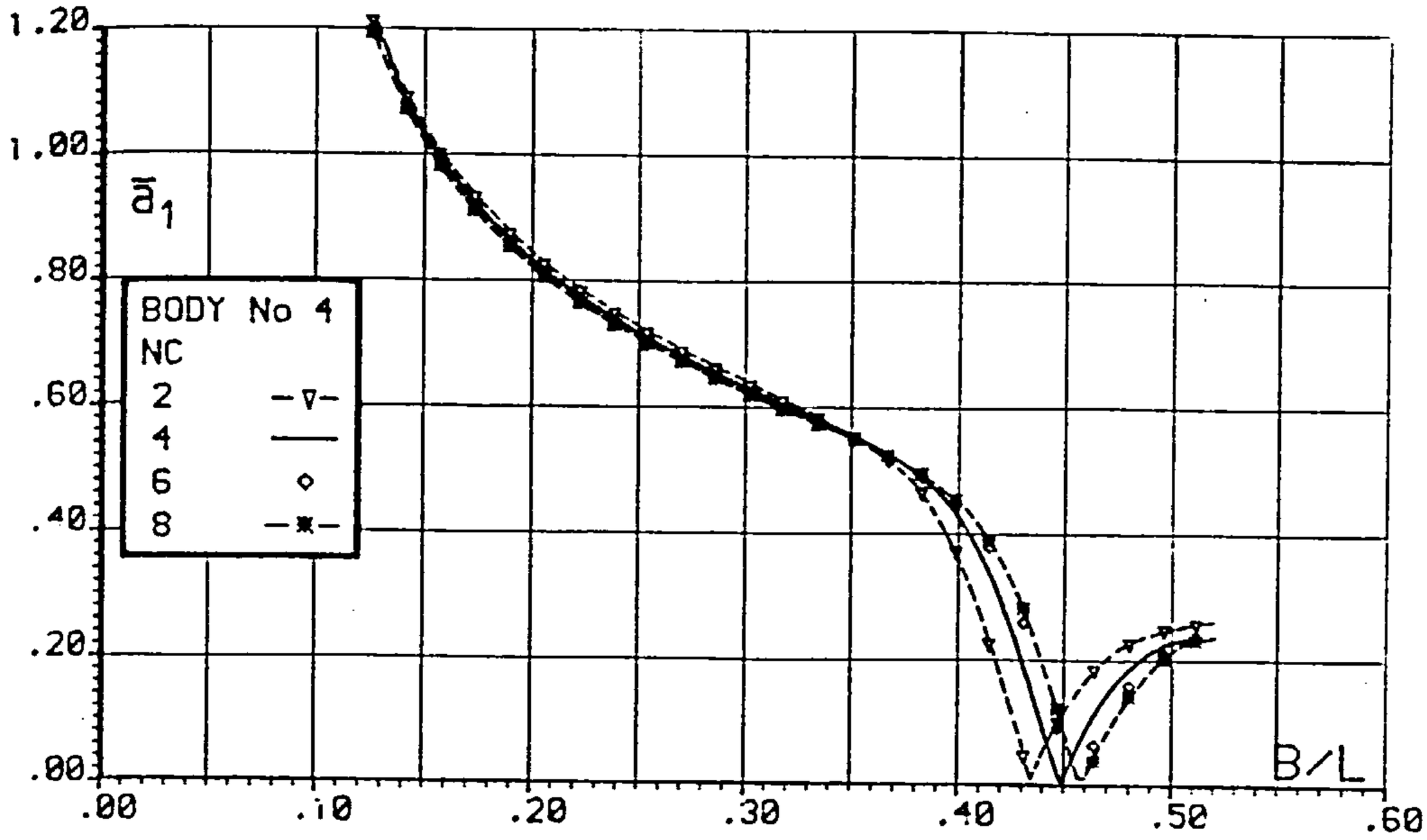

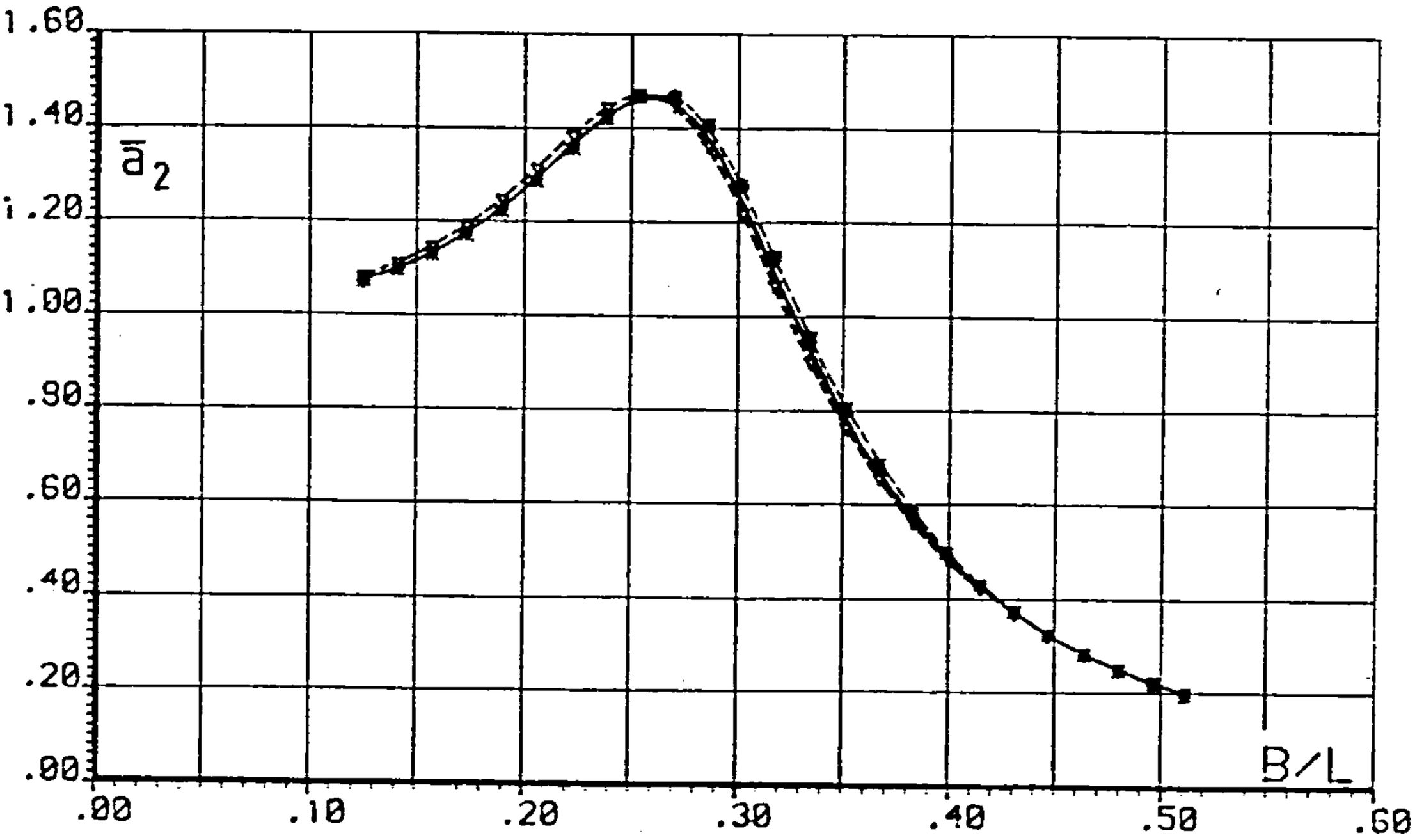

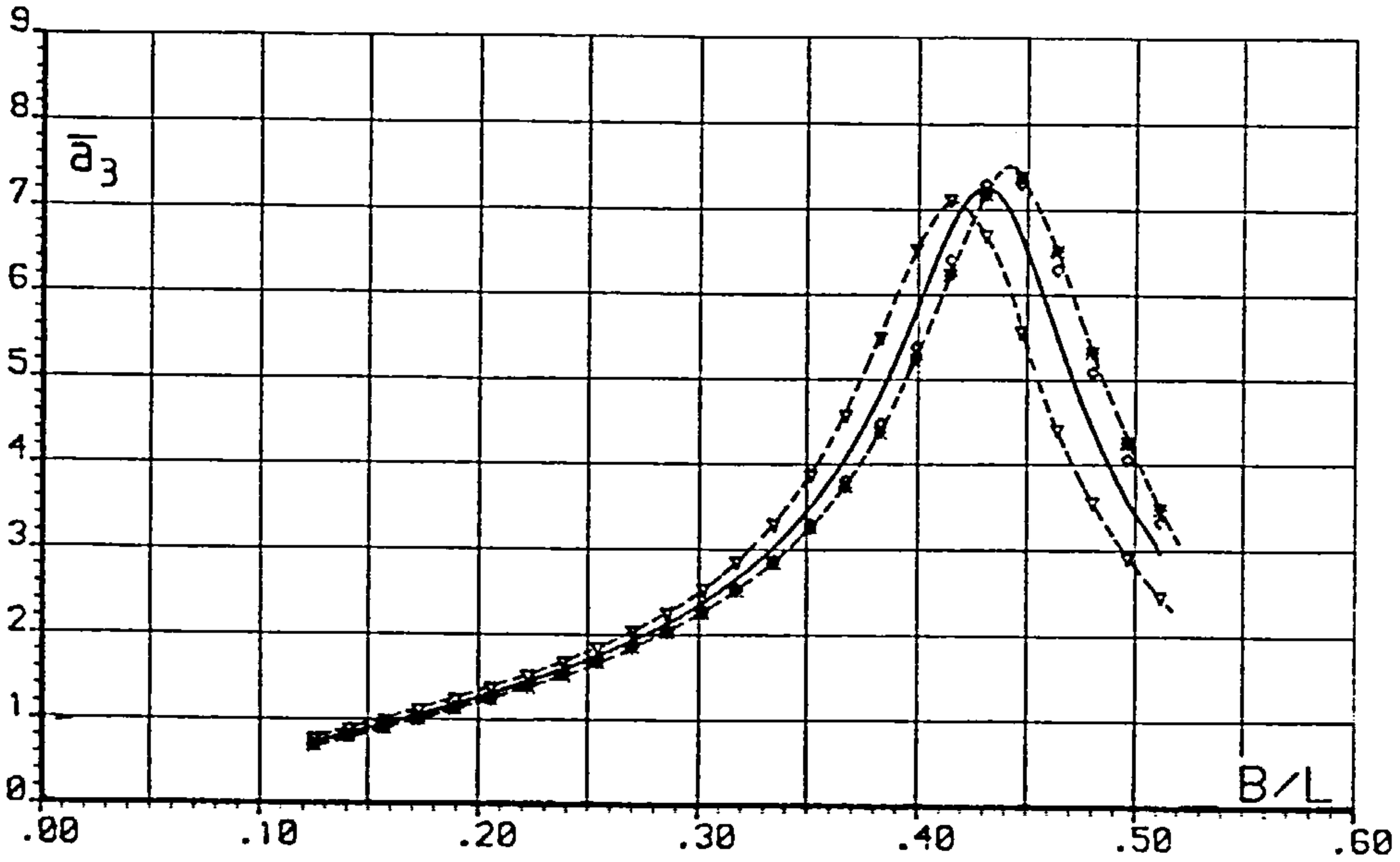

Fig.6.17 FLOATING BODY MOTIONS

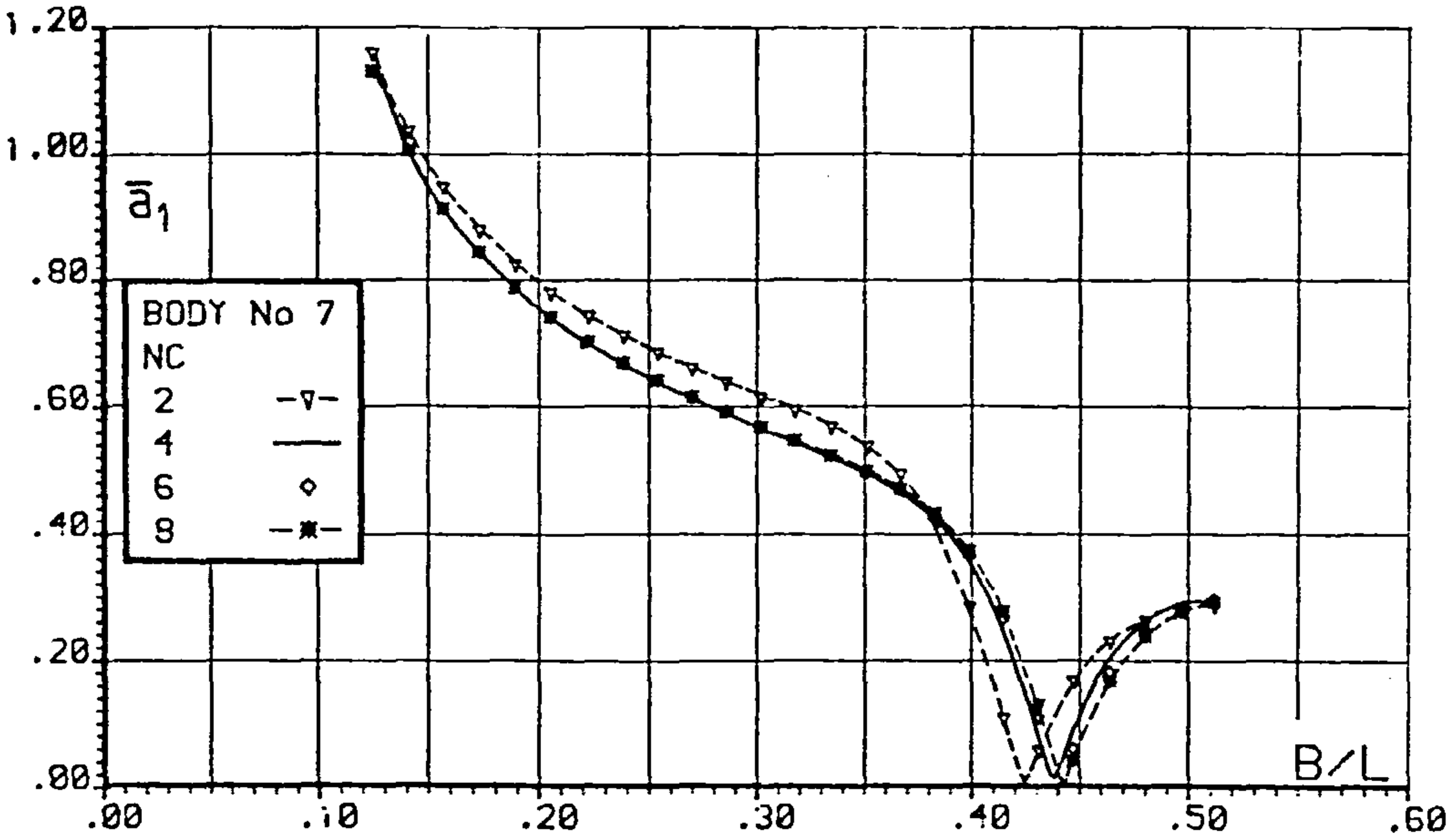

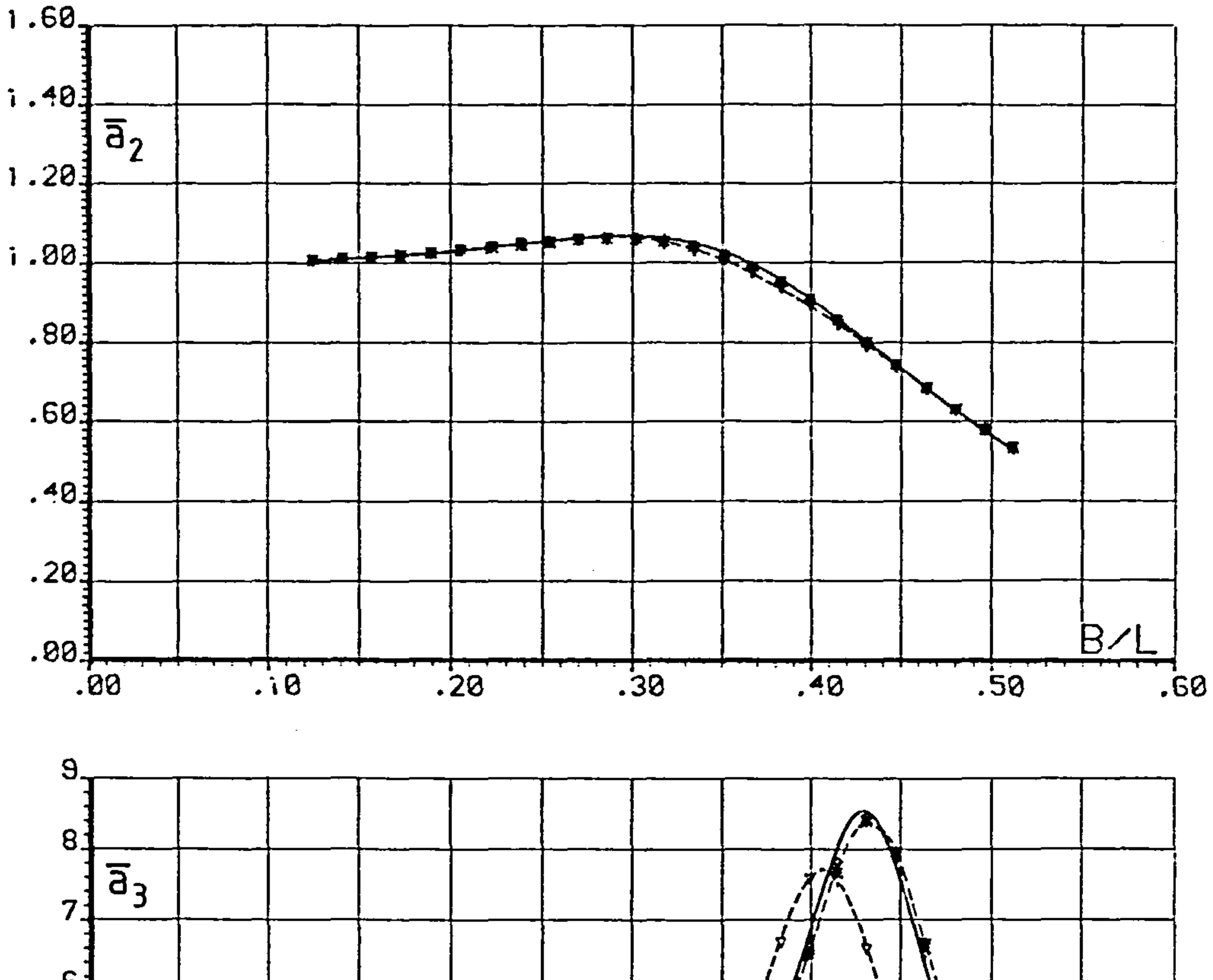

Fig.6.18 FLOATING BODY MOTIONS

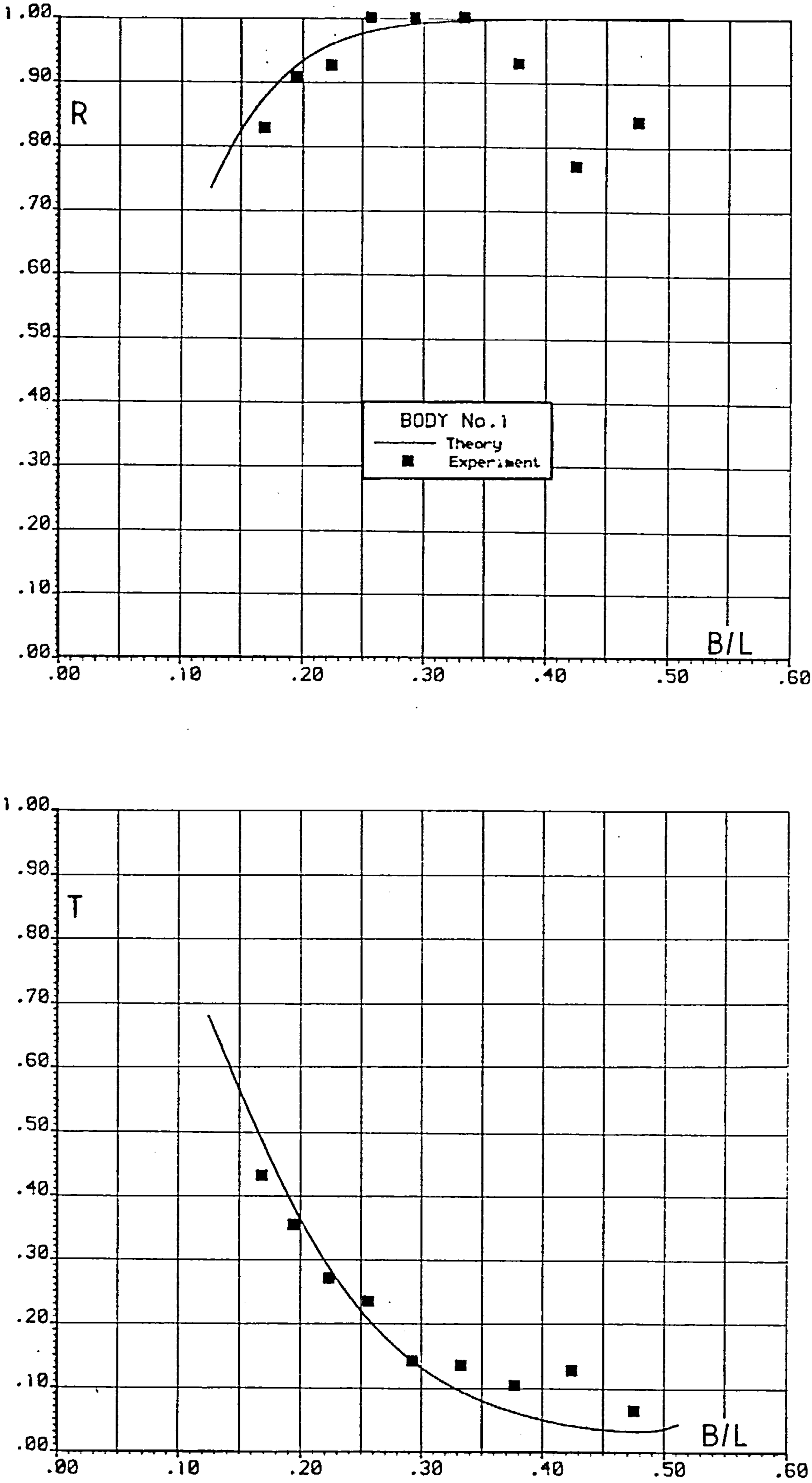

Fig.6.19 FIXED BODY REFLECTION AND TRANSMISSION

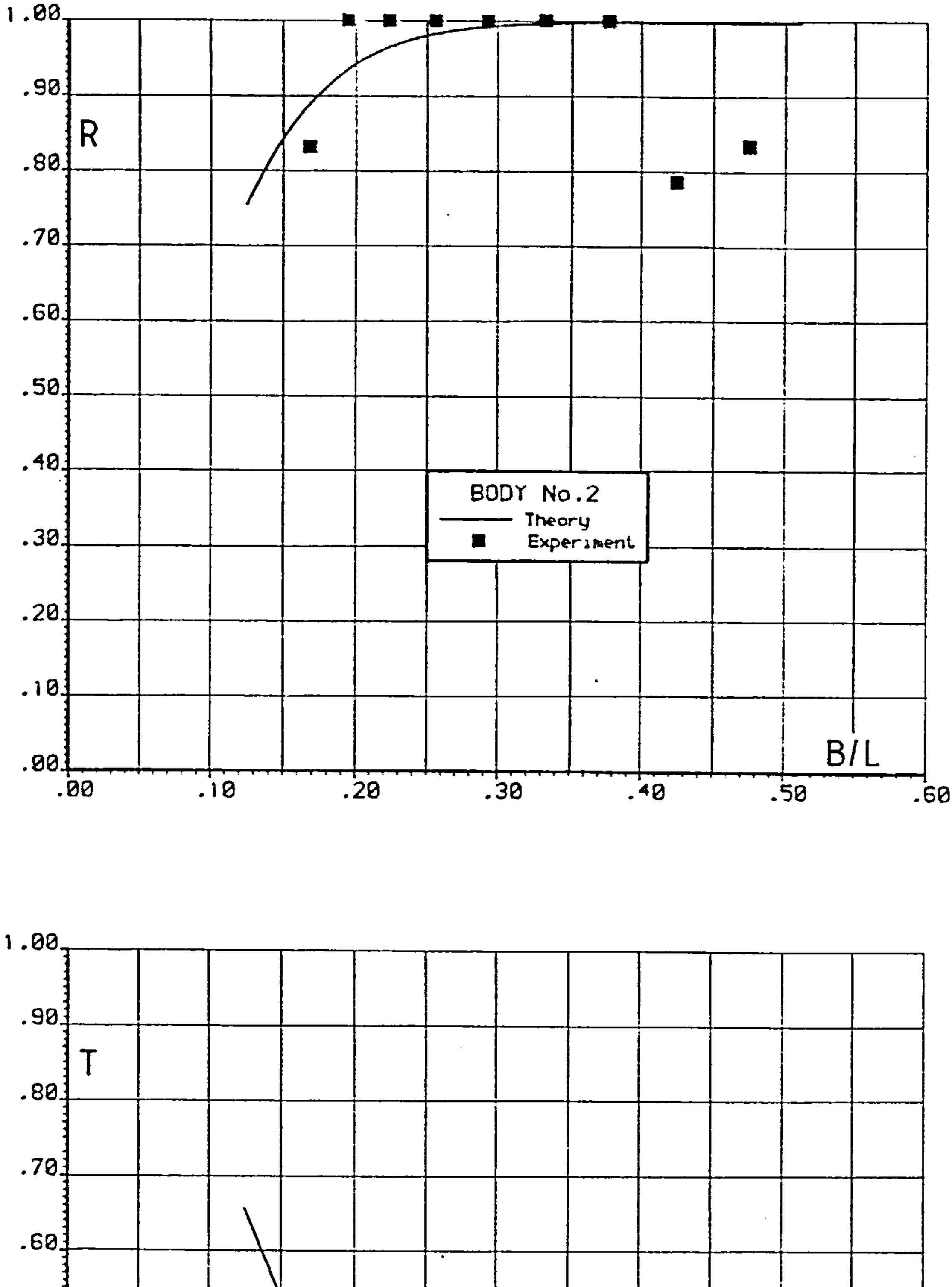

Fig.6.20 FIXED BODY REFLECTION AND TRANSMISSION

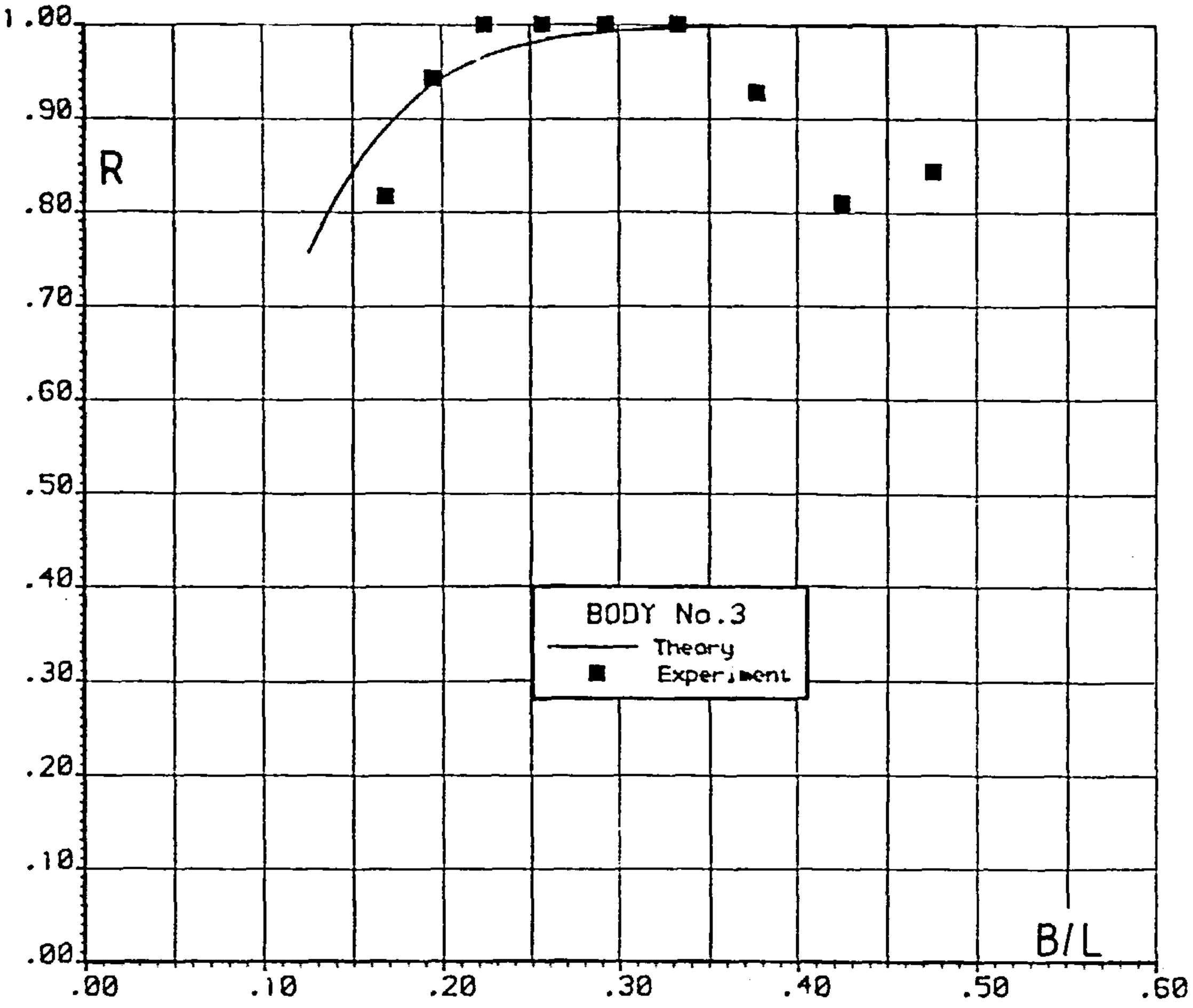

Fig.6.21 FIXED BODY REFLECTION AND TRANSMISSION

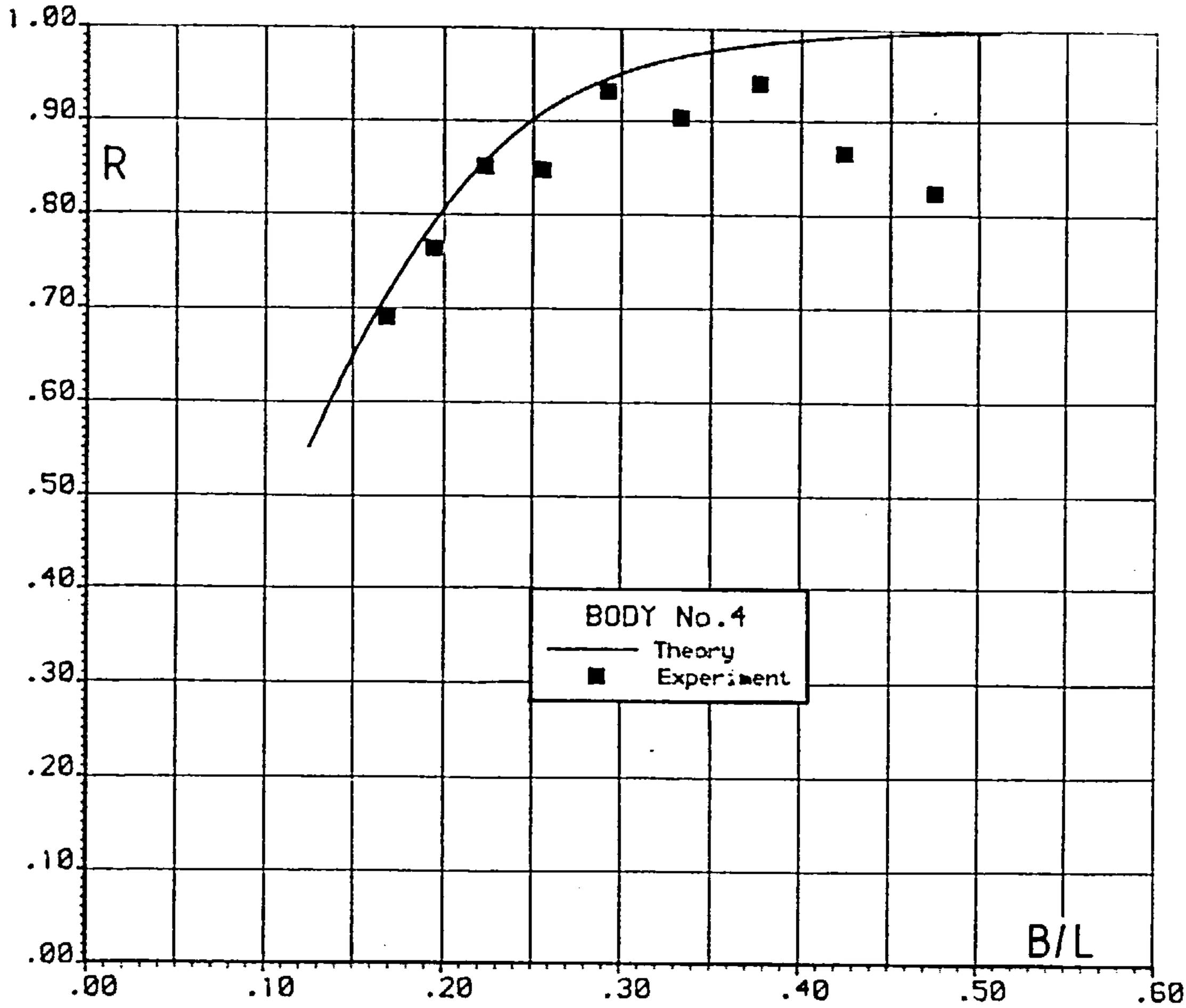

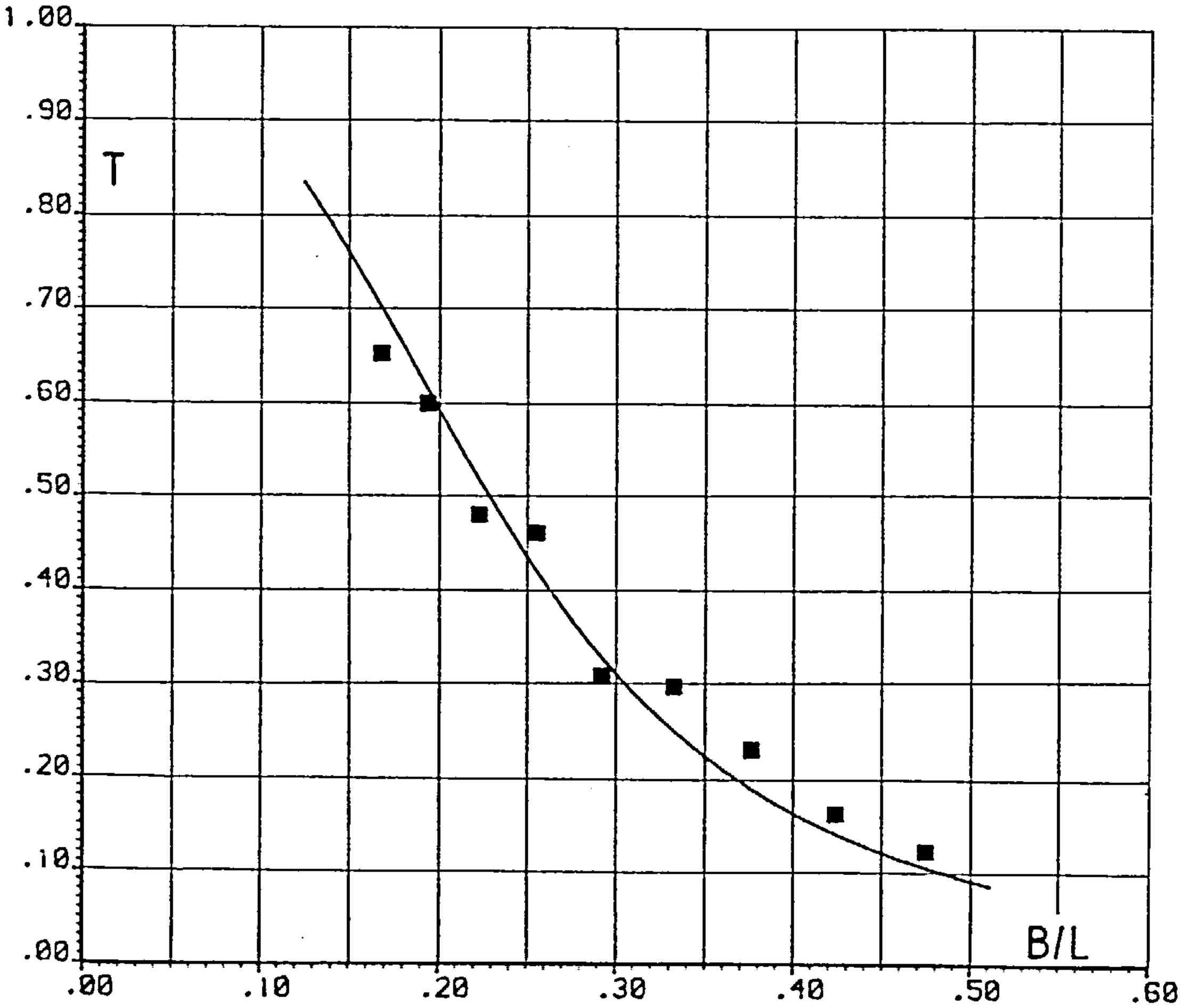

Fig.6.22 FIXED BODY REFLECTION AND TRANSMISSION

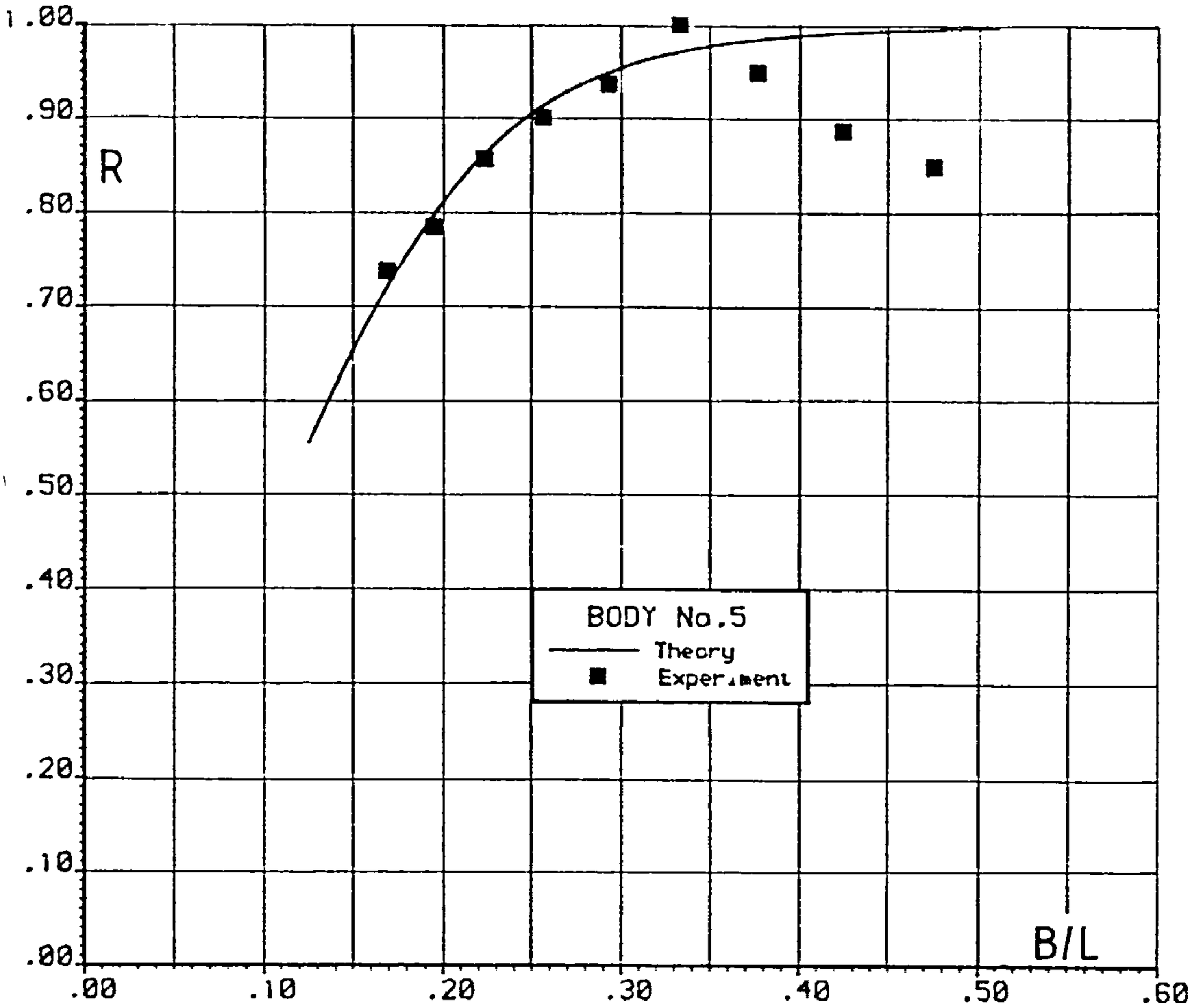

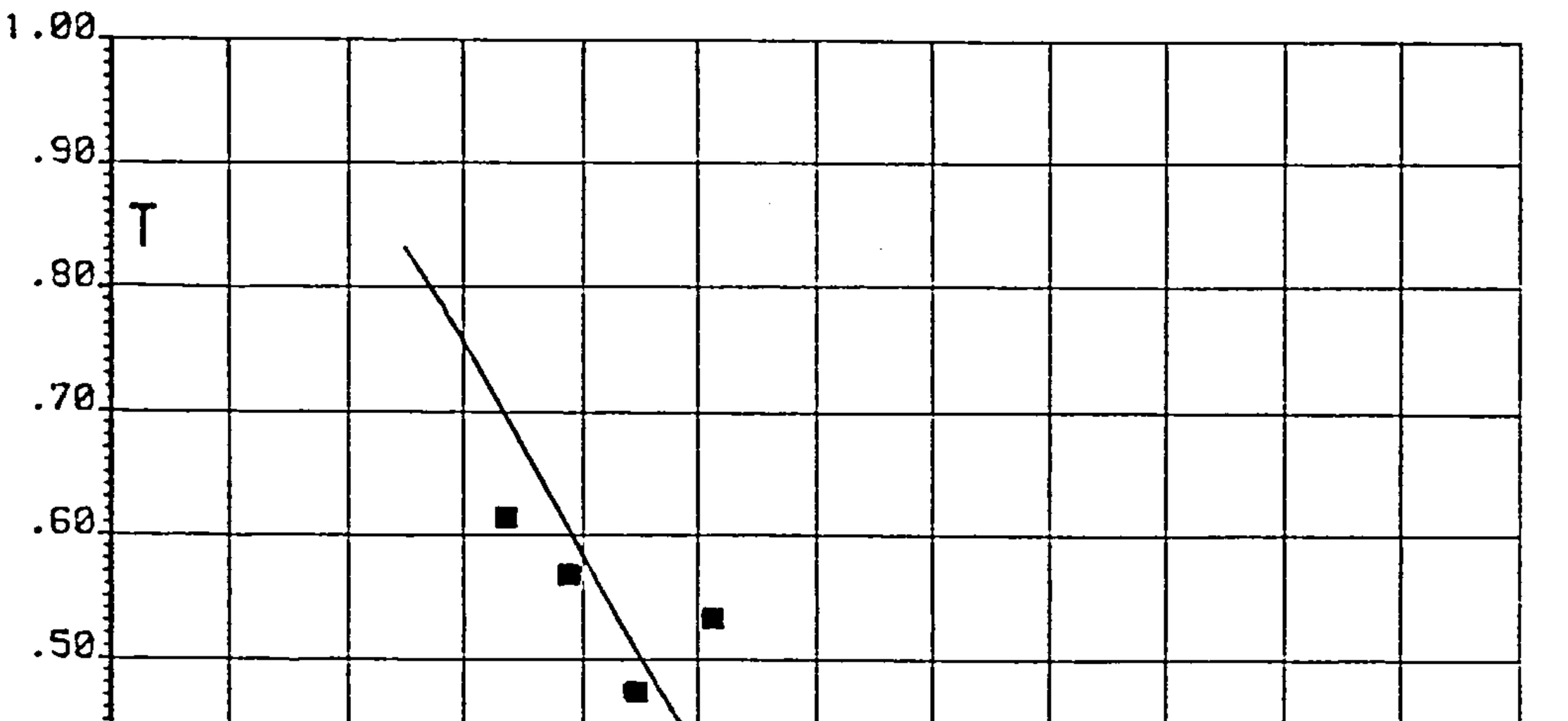

Fig.6.23 FIXED BODY REFLECTION AND TRANSMISSION

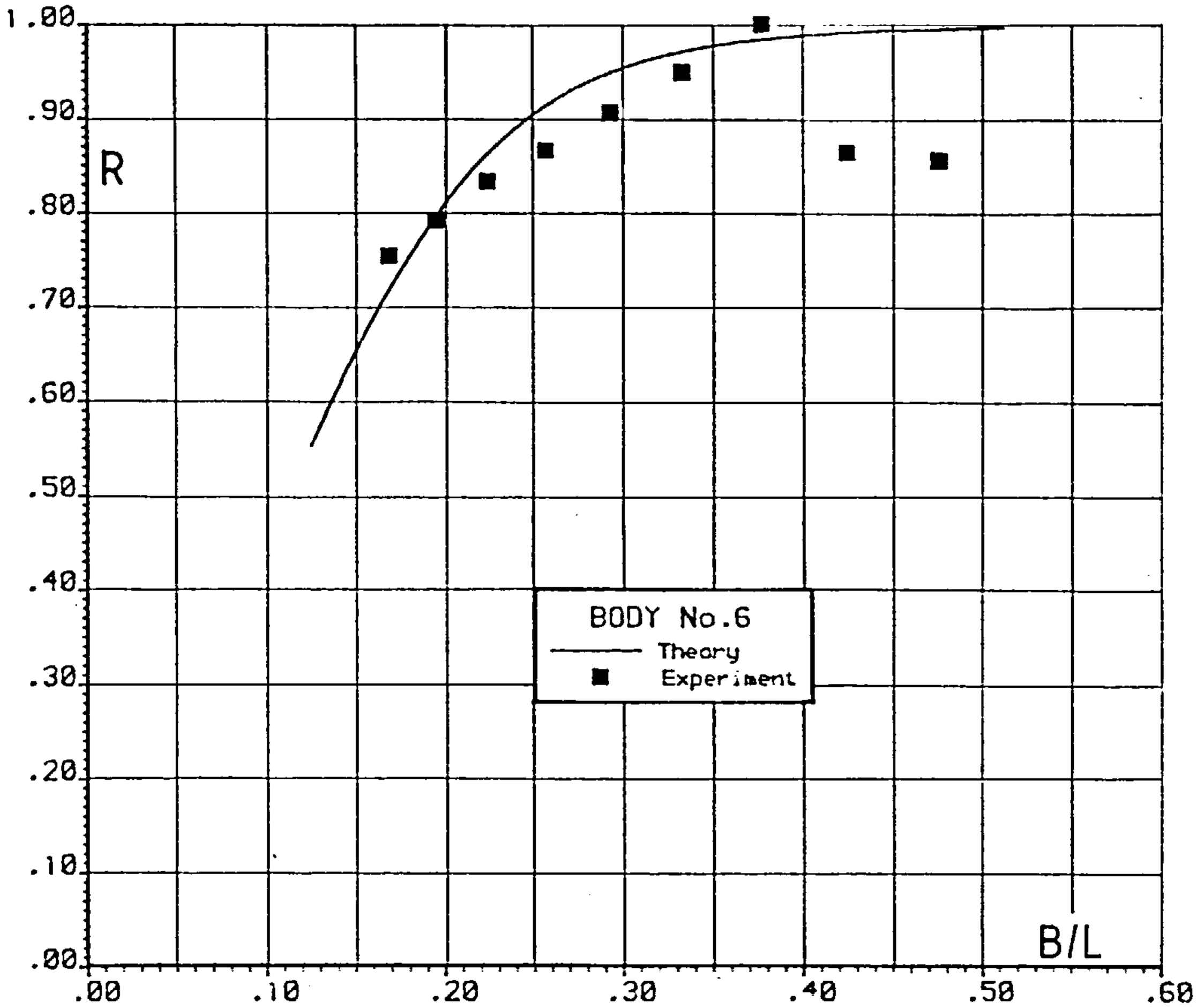

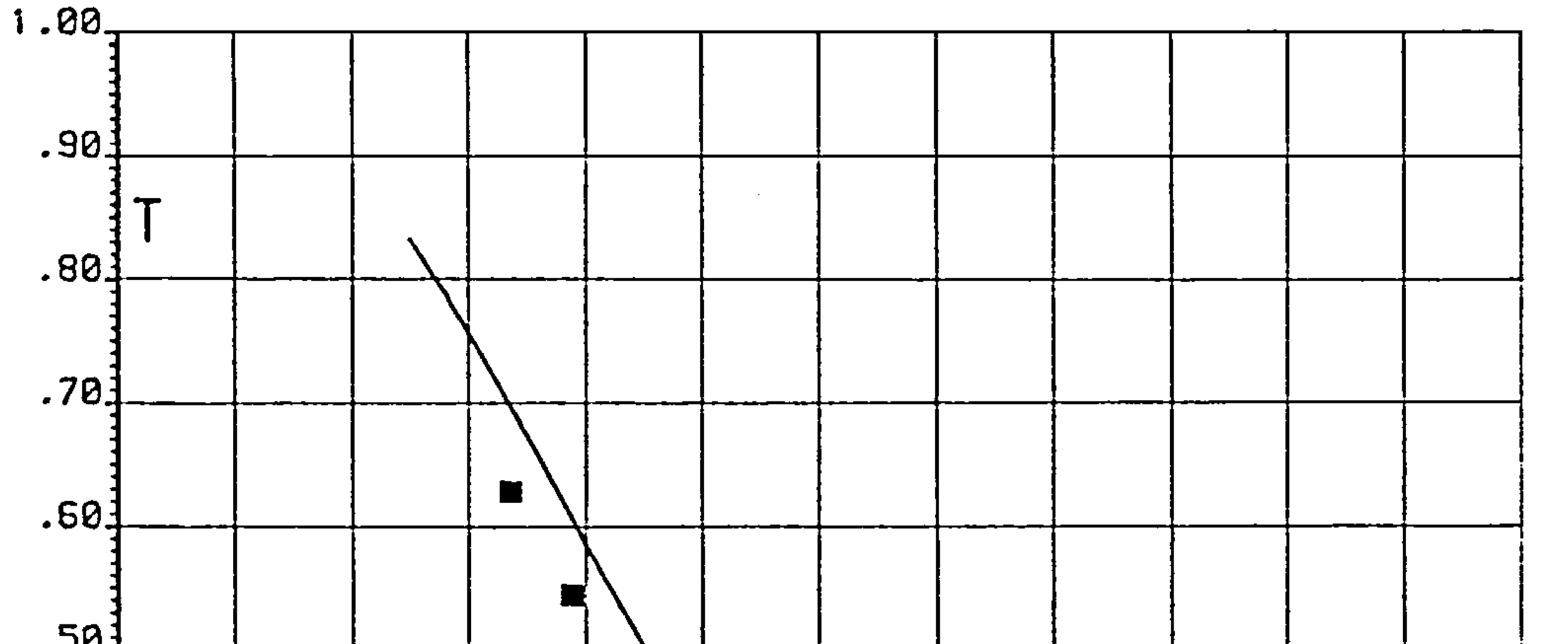

Fig.6.24 FIXED BODY REFLECTION AND TRANSMISSION

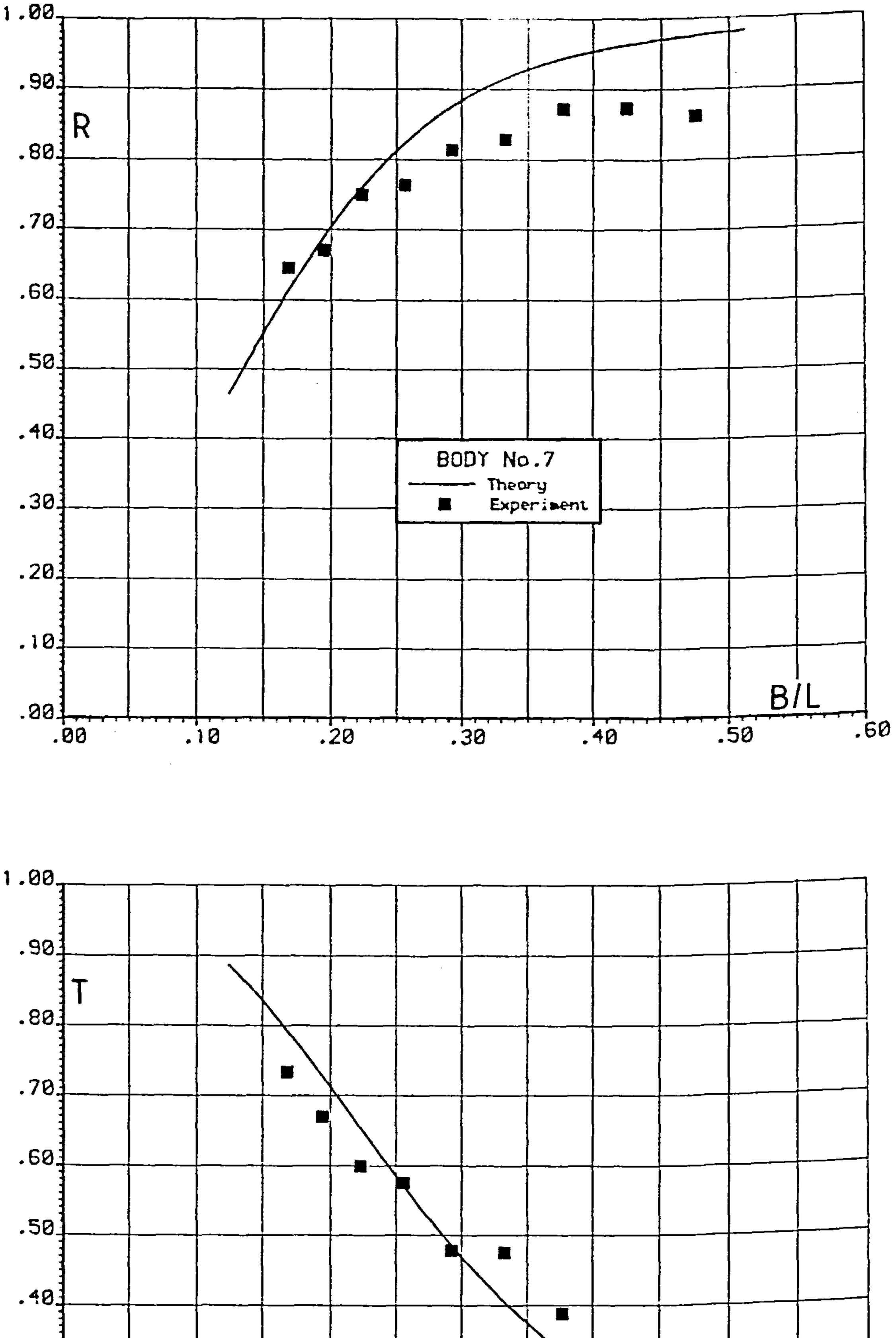

Fig. 6.25 FIXED BODY REFLECTION AND TRANSMISSION

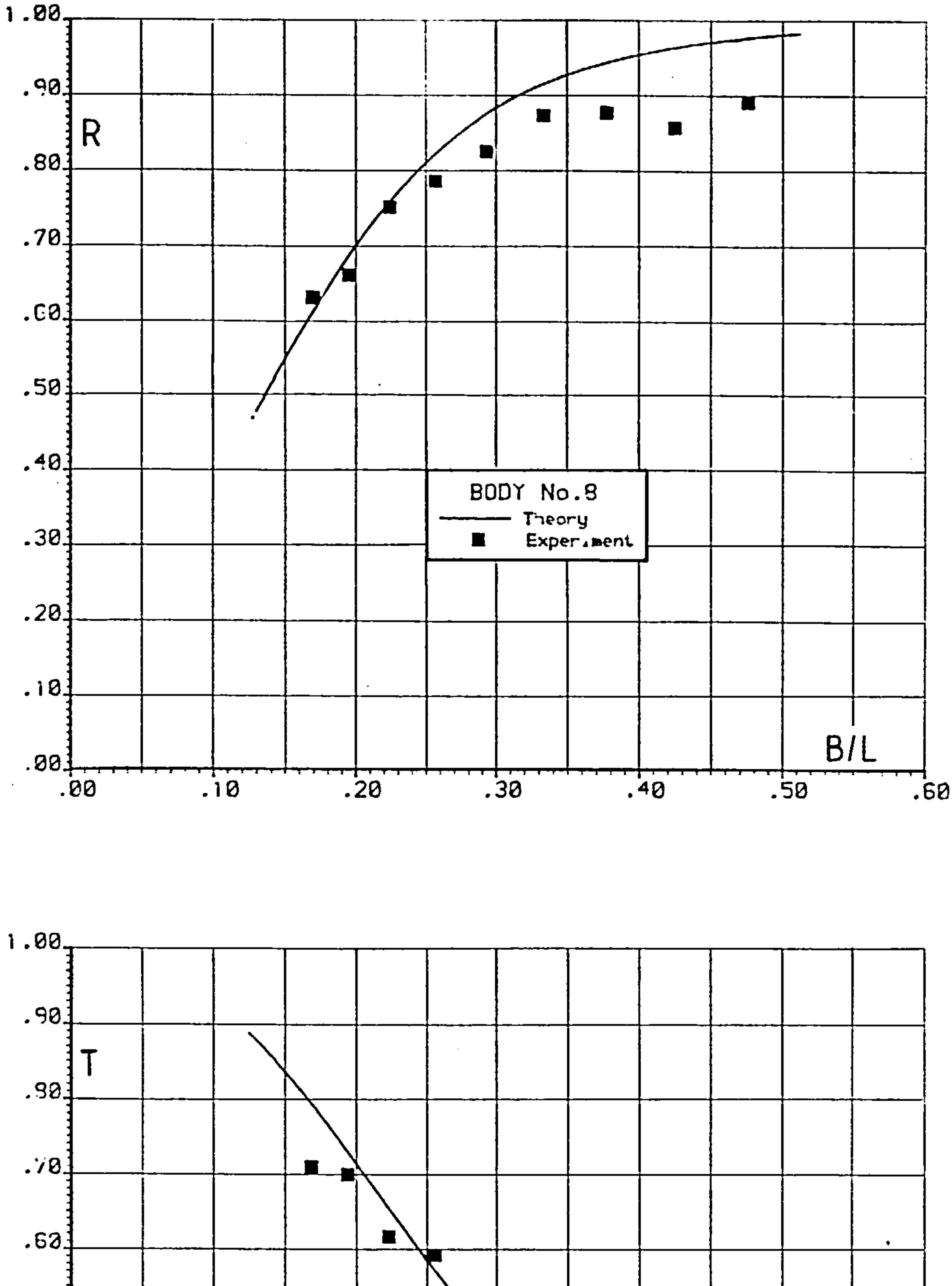

Fig. 6.26 FIXED BODY REFLECTION AND TRANSMISSION

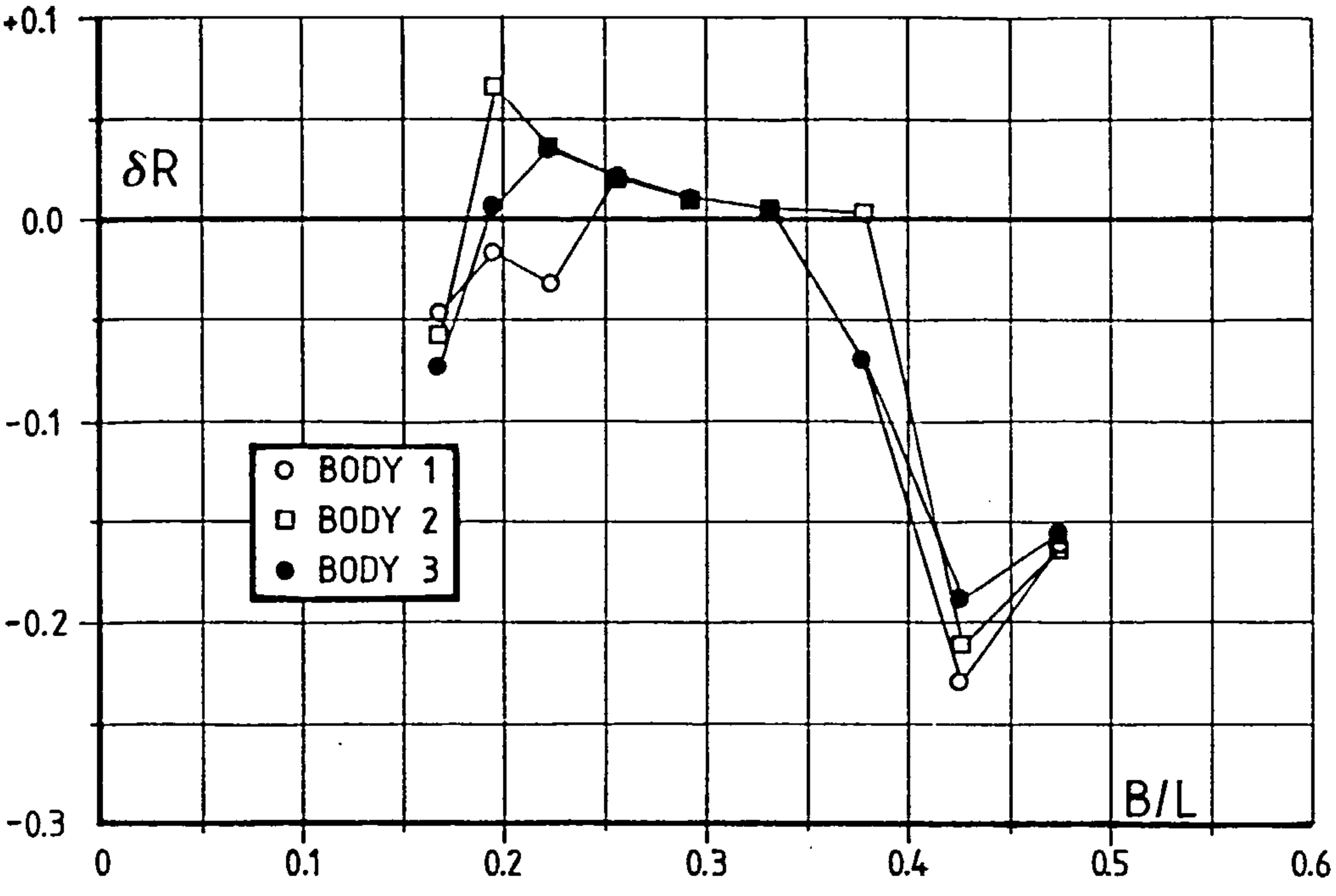

δ = Experiment - Theory

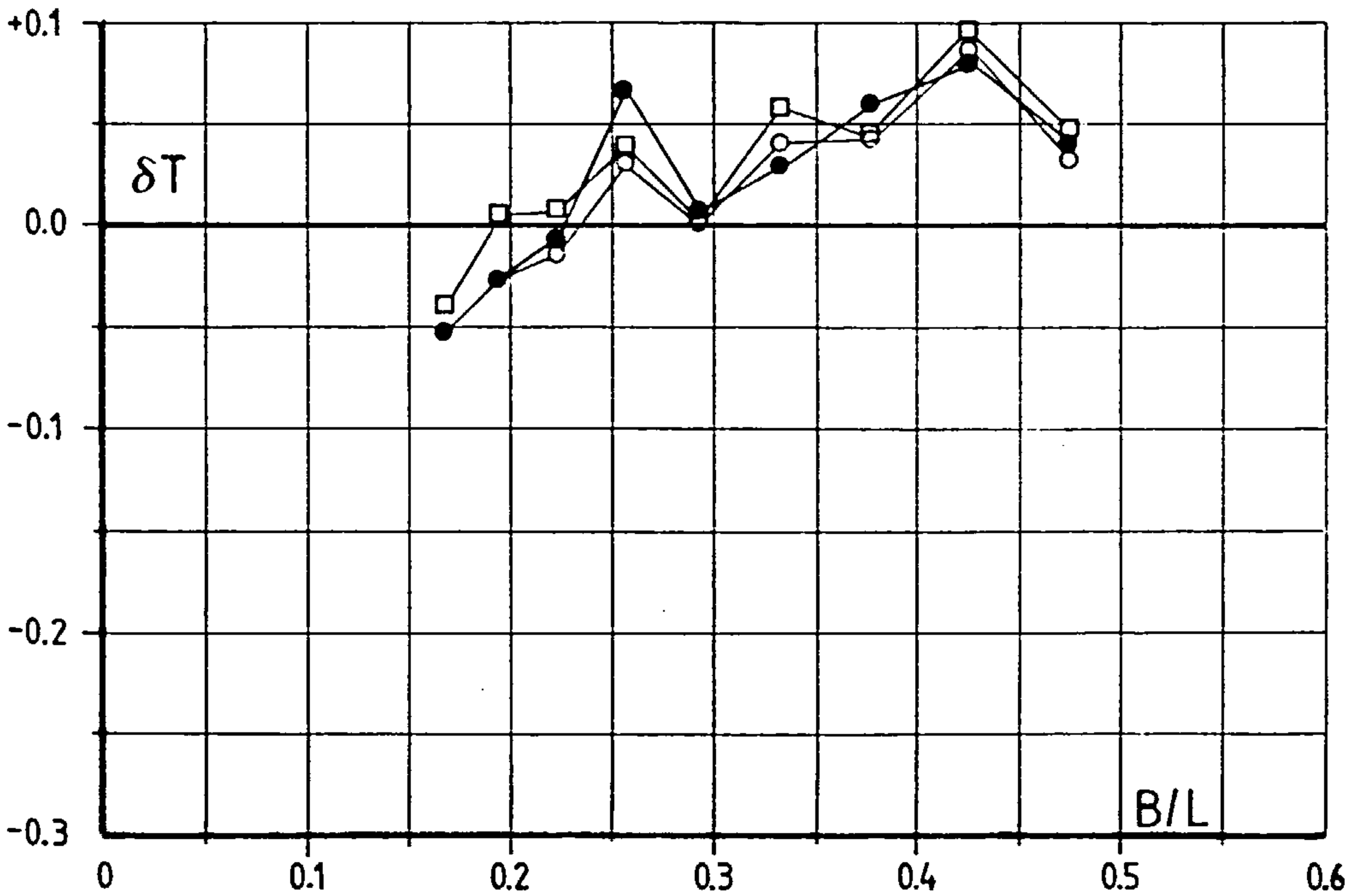

Fig. 6.27 FIXED BODY REFLECTION AND TRANSMISSION ERRORS

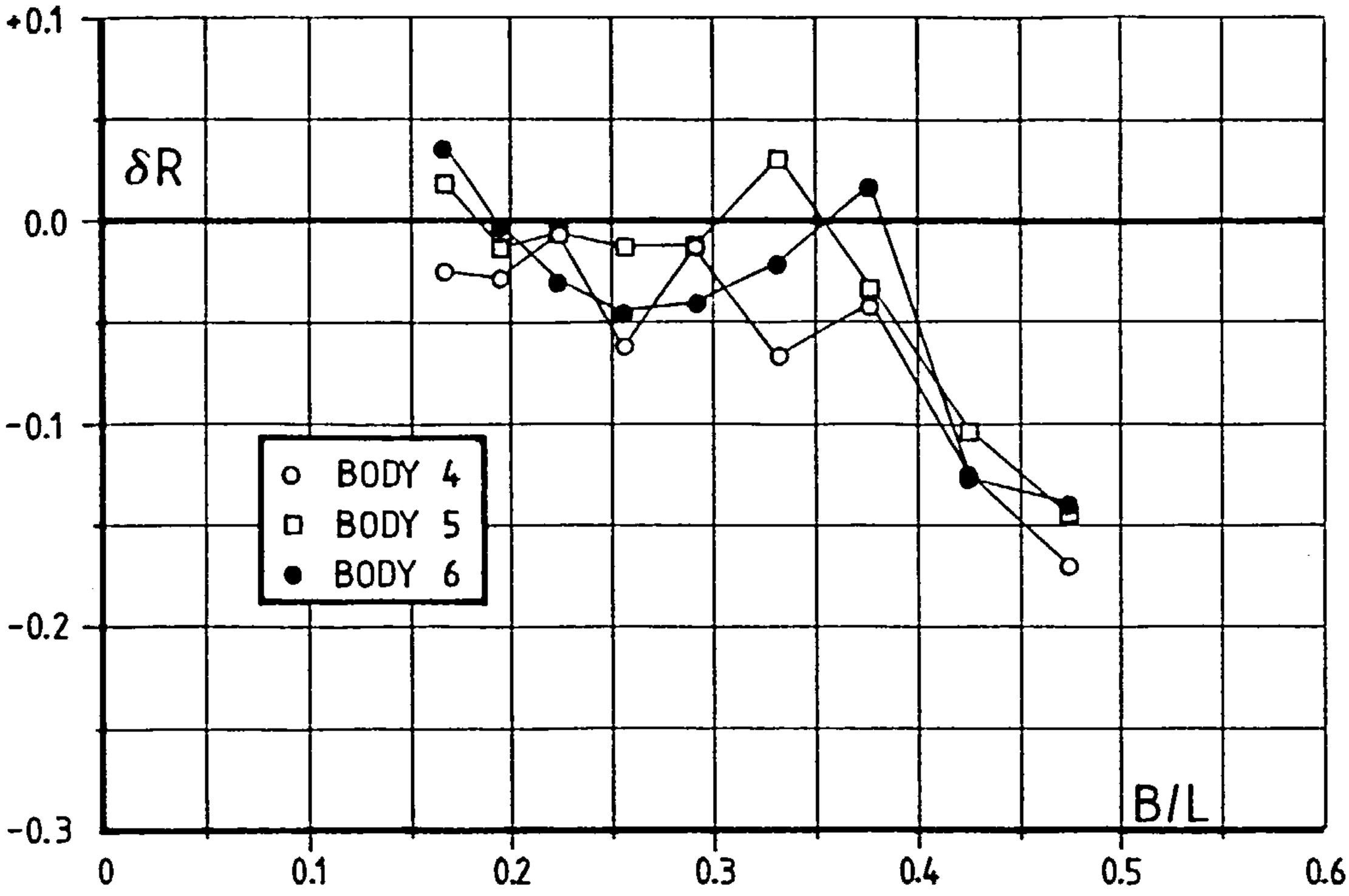

δ = Experiment - Theory

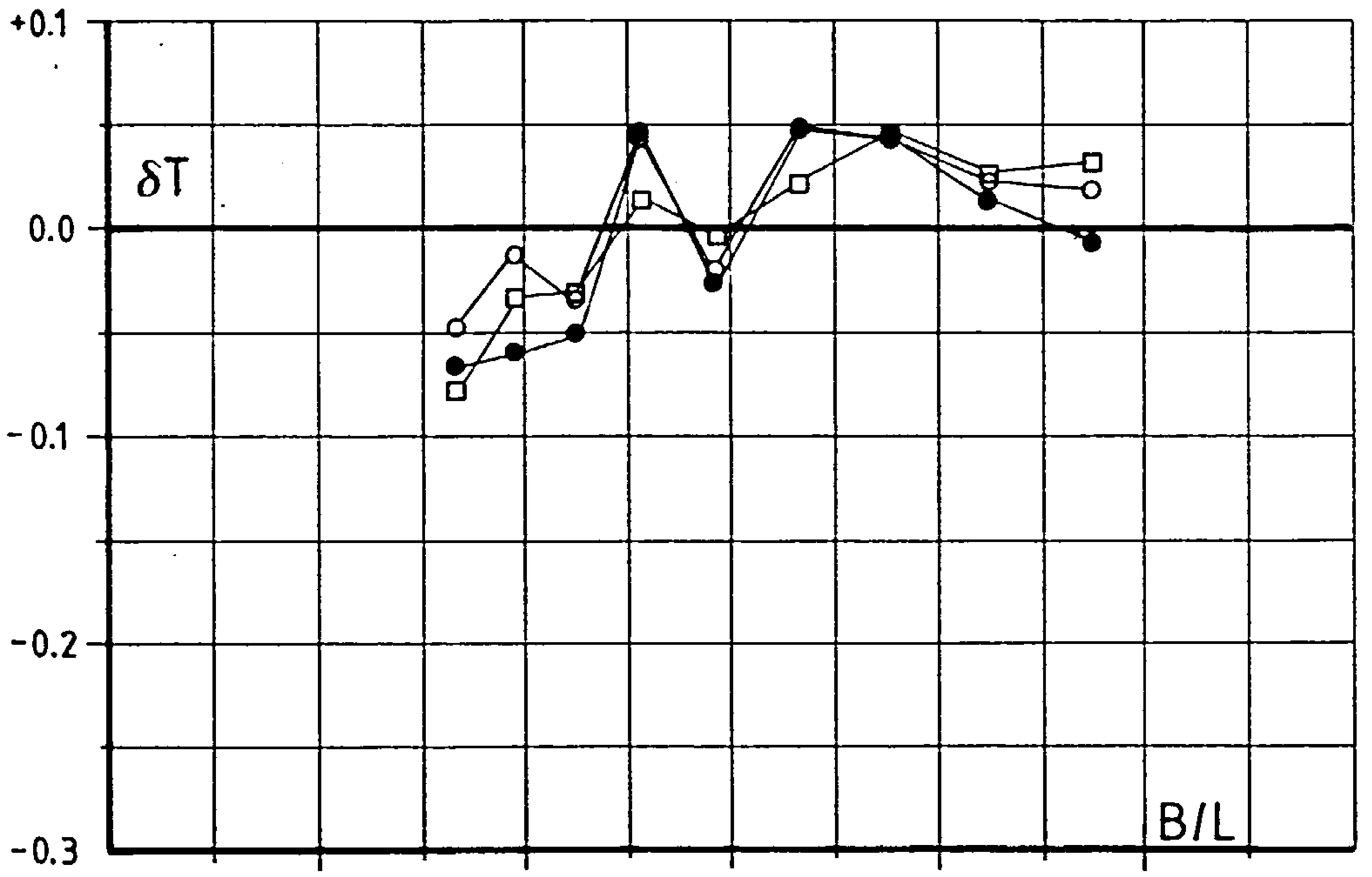

Fig. 6.28 FIXED BODY REFLECTION AND TRANSMISSION ERRORS

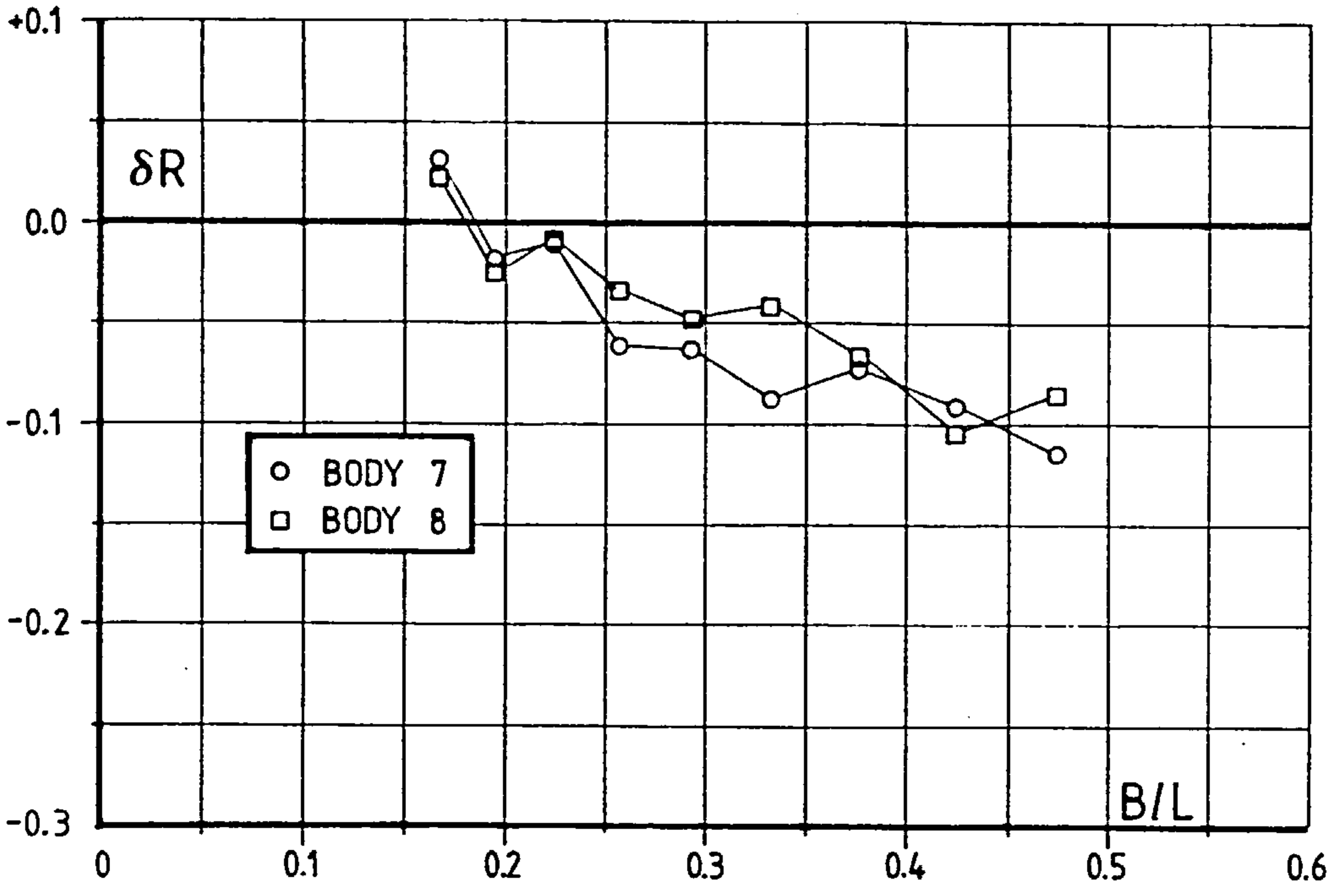

δ = Experiment - Theory

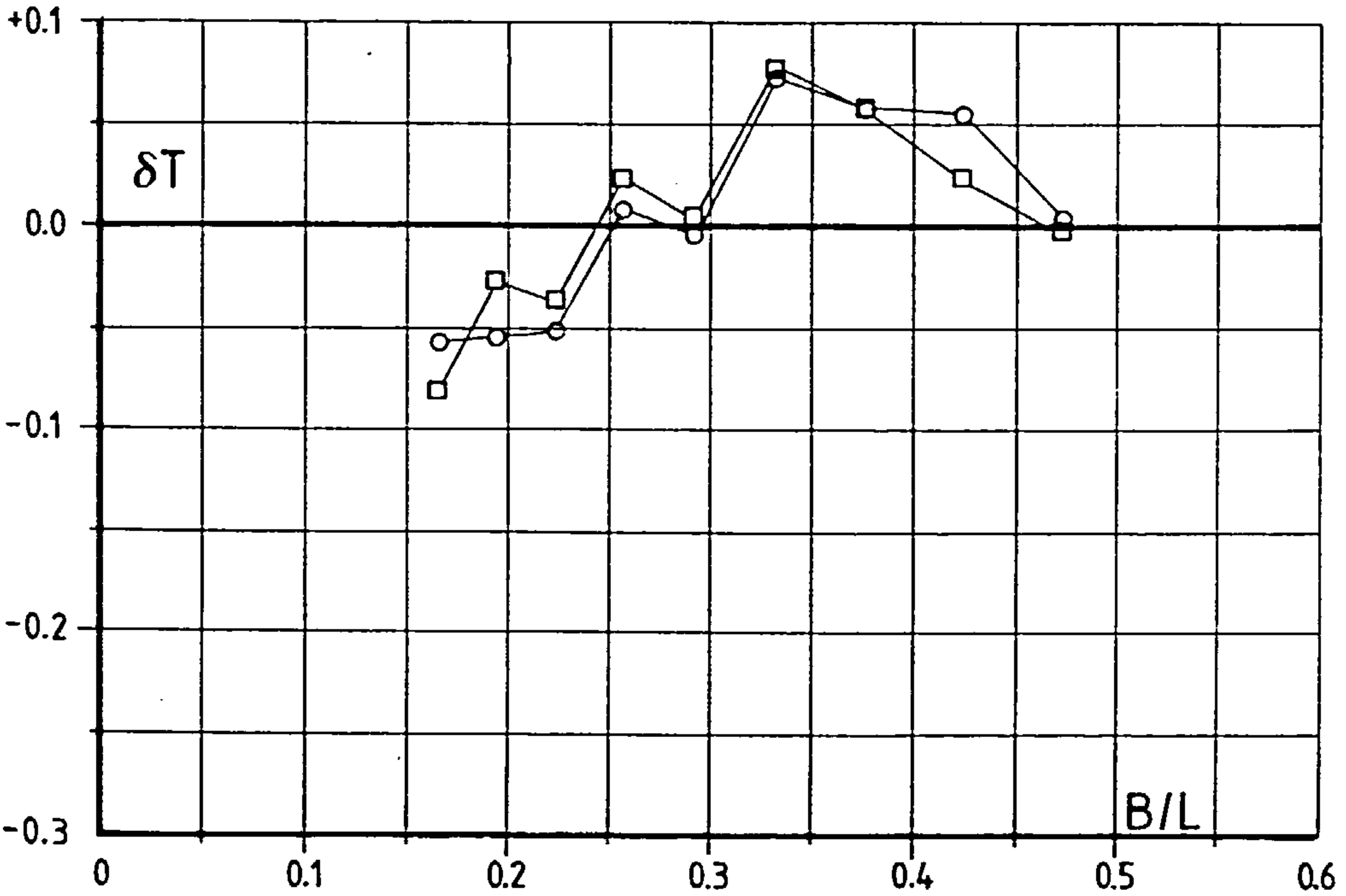

Fig. 6.29 FIXED BODY REFLECTION AND TRANSMISSION ERRORS

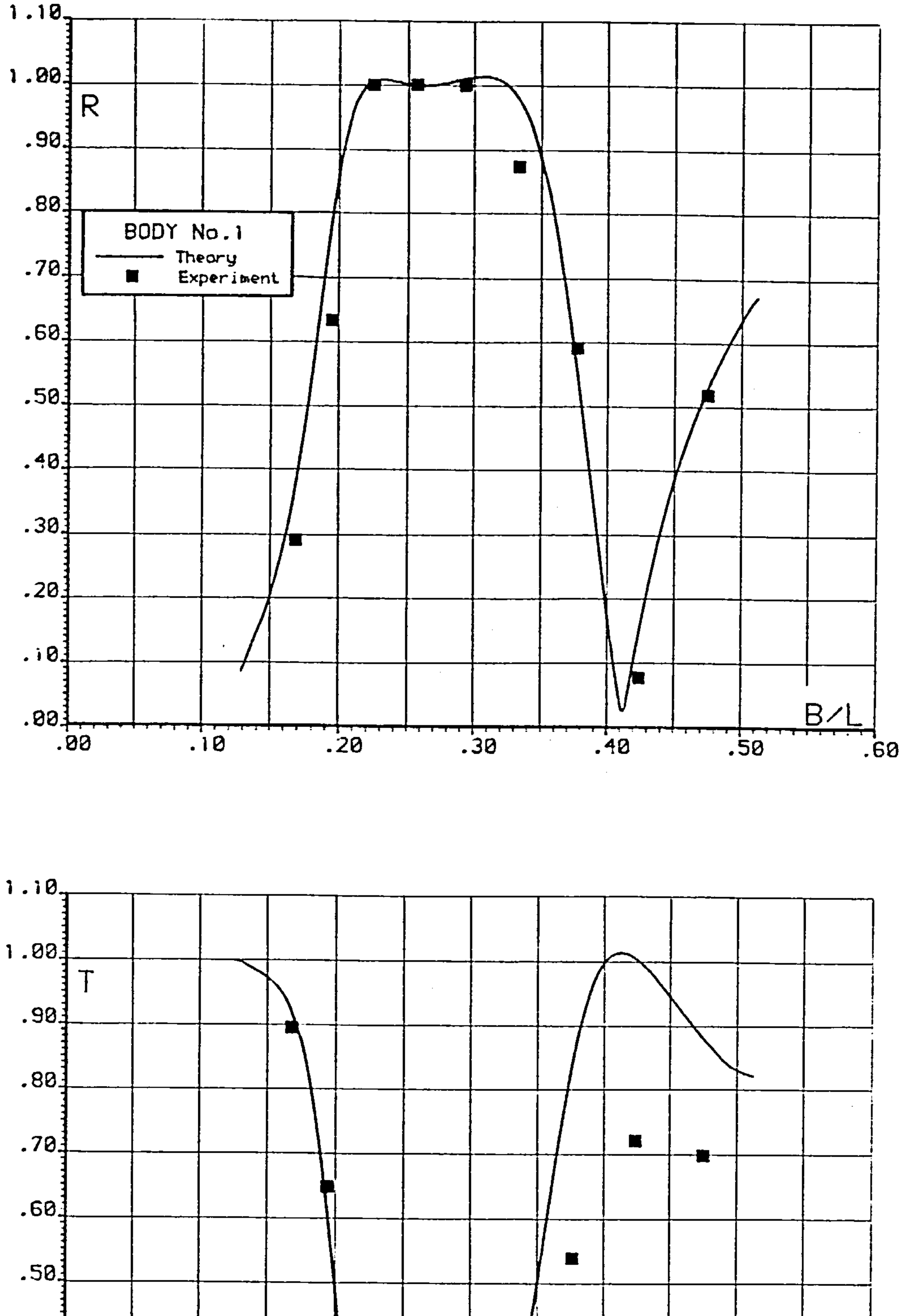

Fig. 6.30 FLOATING BODY REFLECTION AND TRANSMISSION

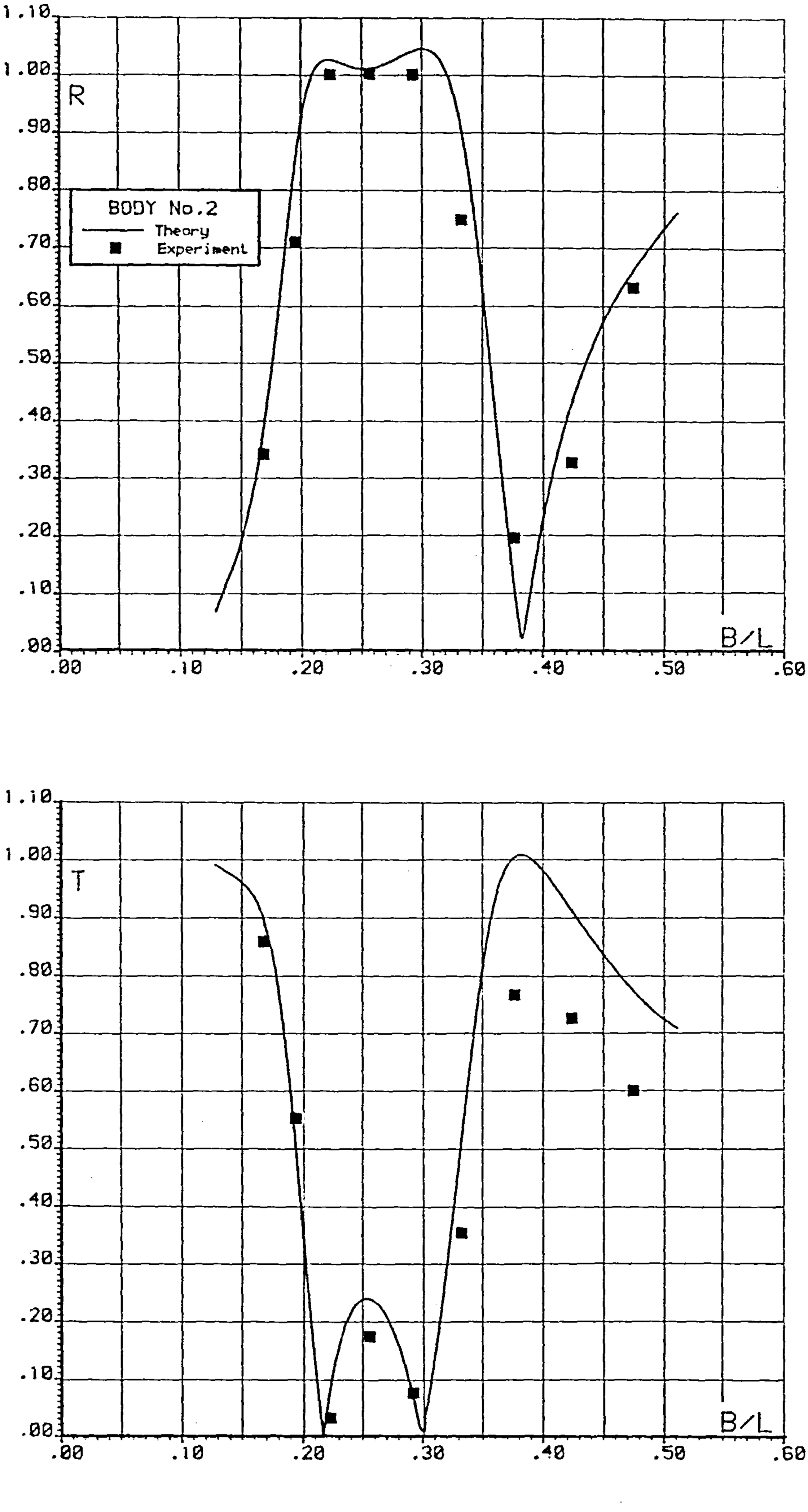

Fig. 6.31 FLOATING BODY REFLECTION AND TRANSMISSION

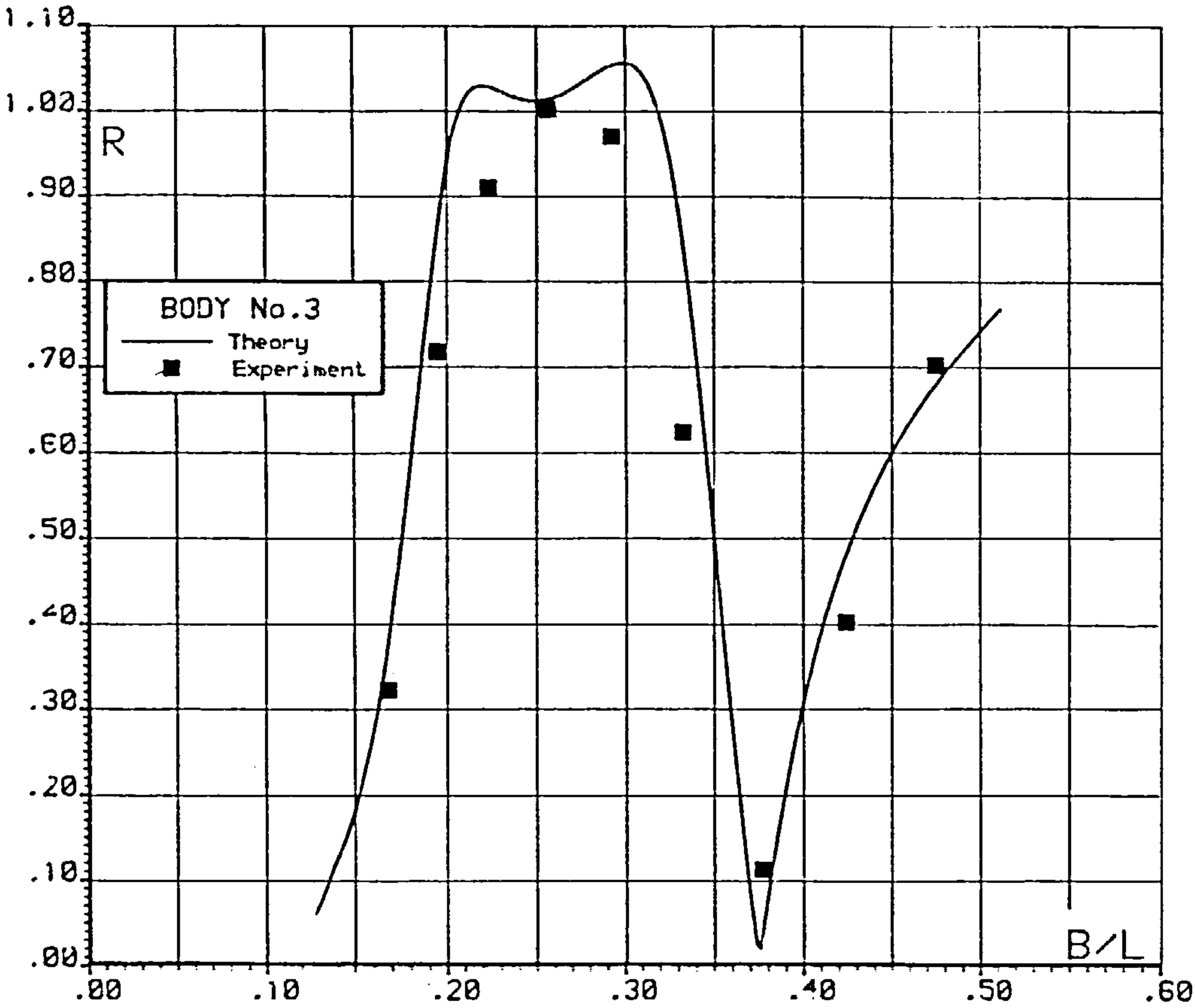

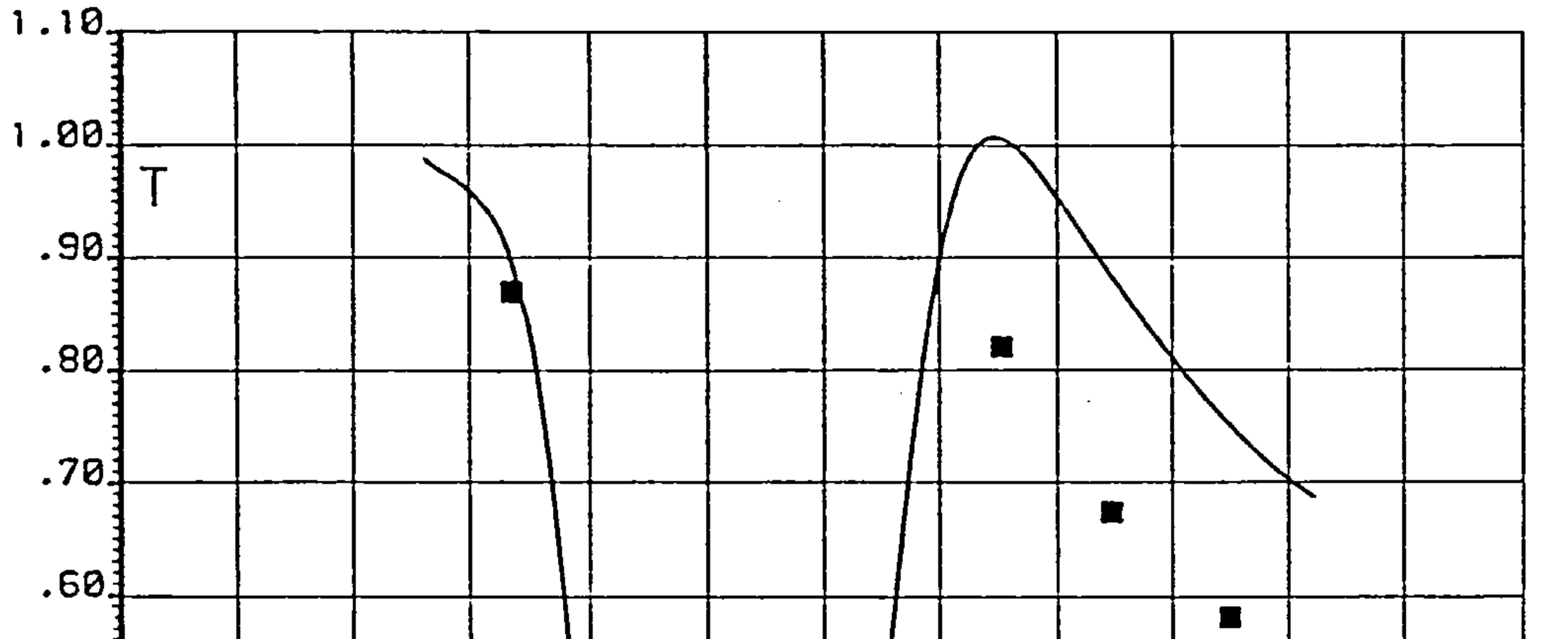

Fig. 6.32 FLOATING BODY REFLECTION AND TRANSMISSION

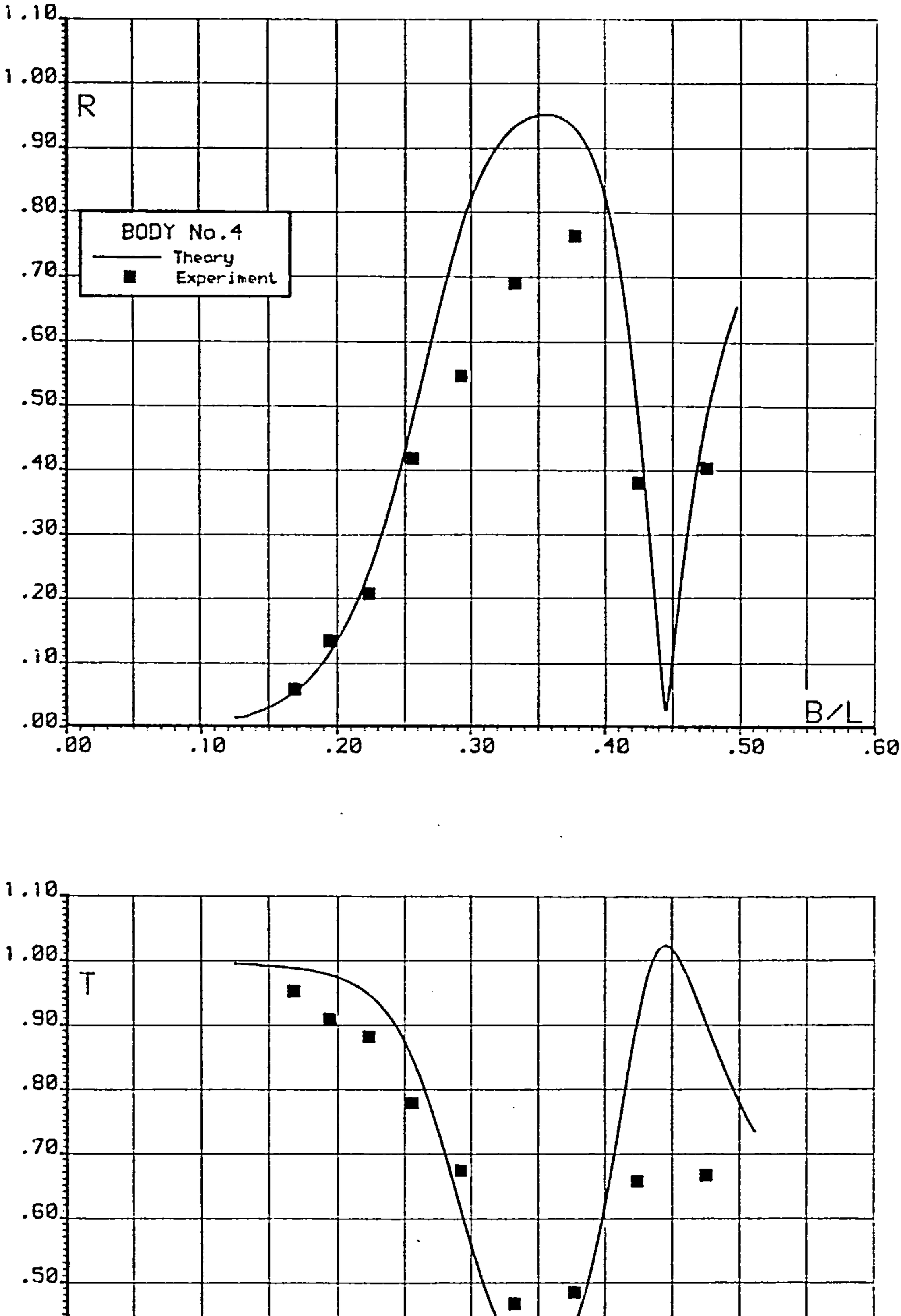

Fig. 6.33 FLOATING BODY REFLECTION AND TRANSMISSION

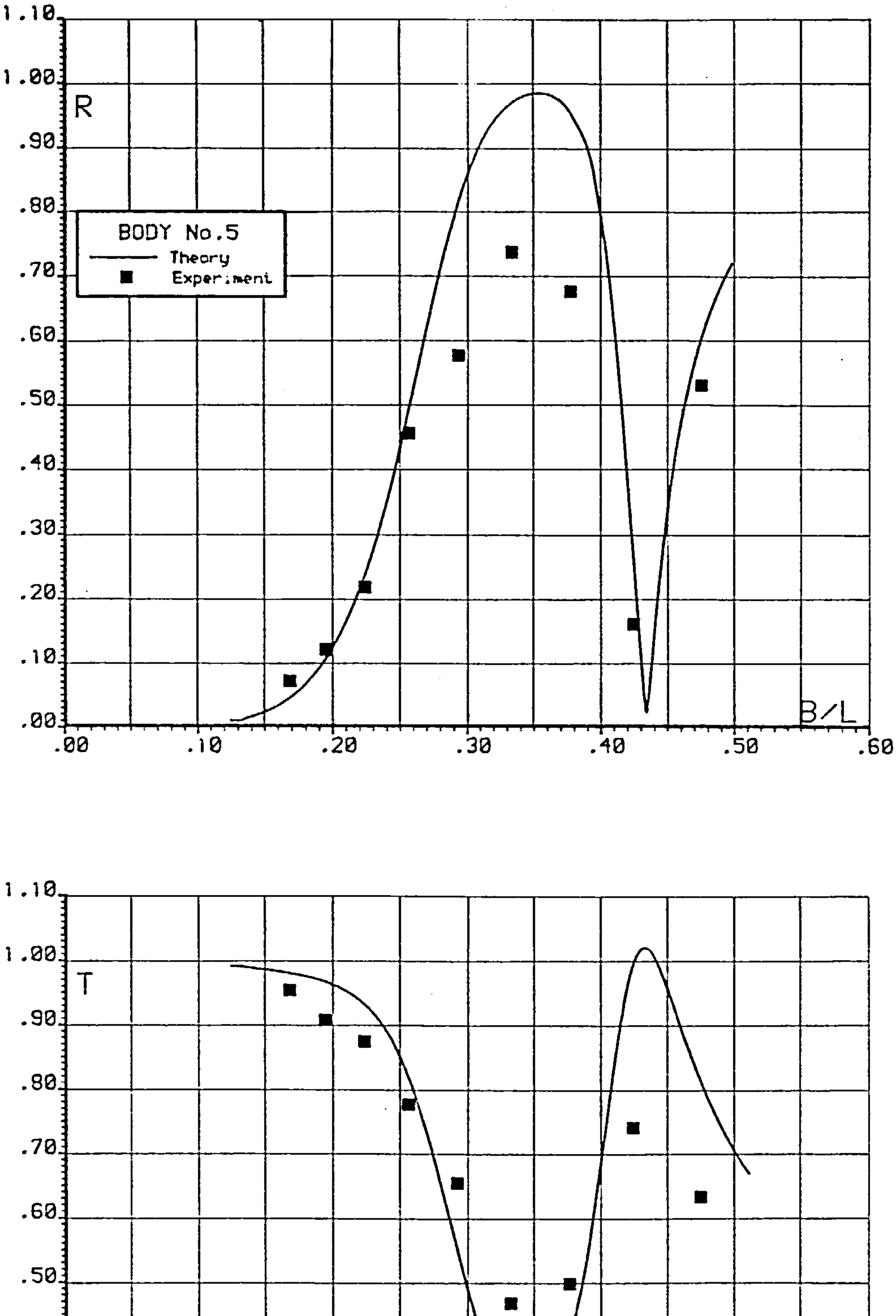

Fig. 6.34 FLOATING BODY REFLECTION AND TRANSMISSION

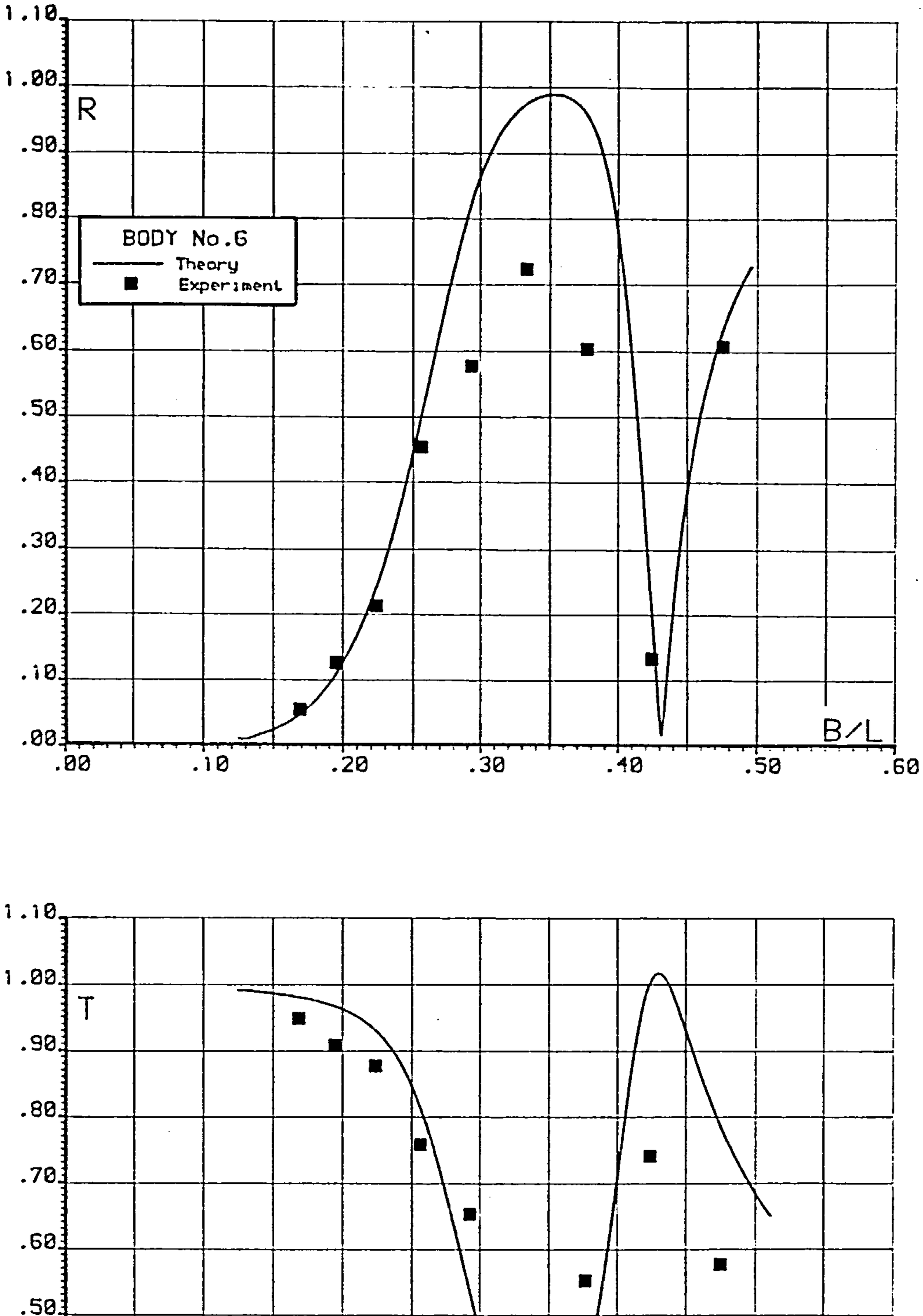

Fig. 6.35 FLOATING BODY REFLECTION AND TRANSMISSION

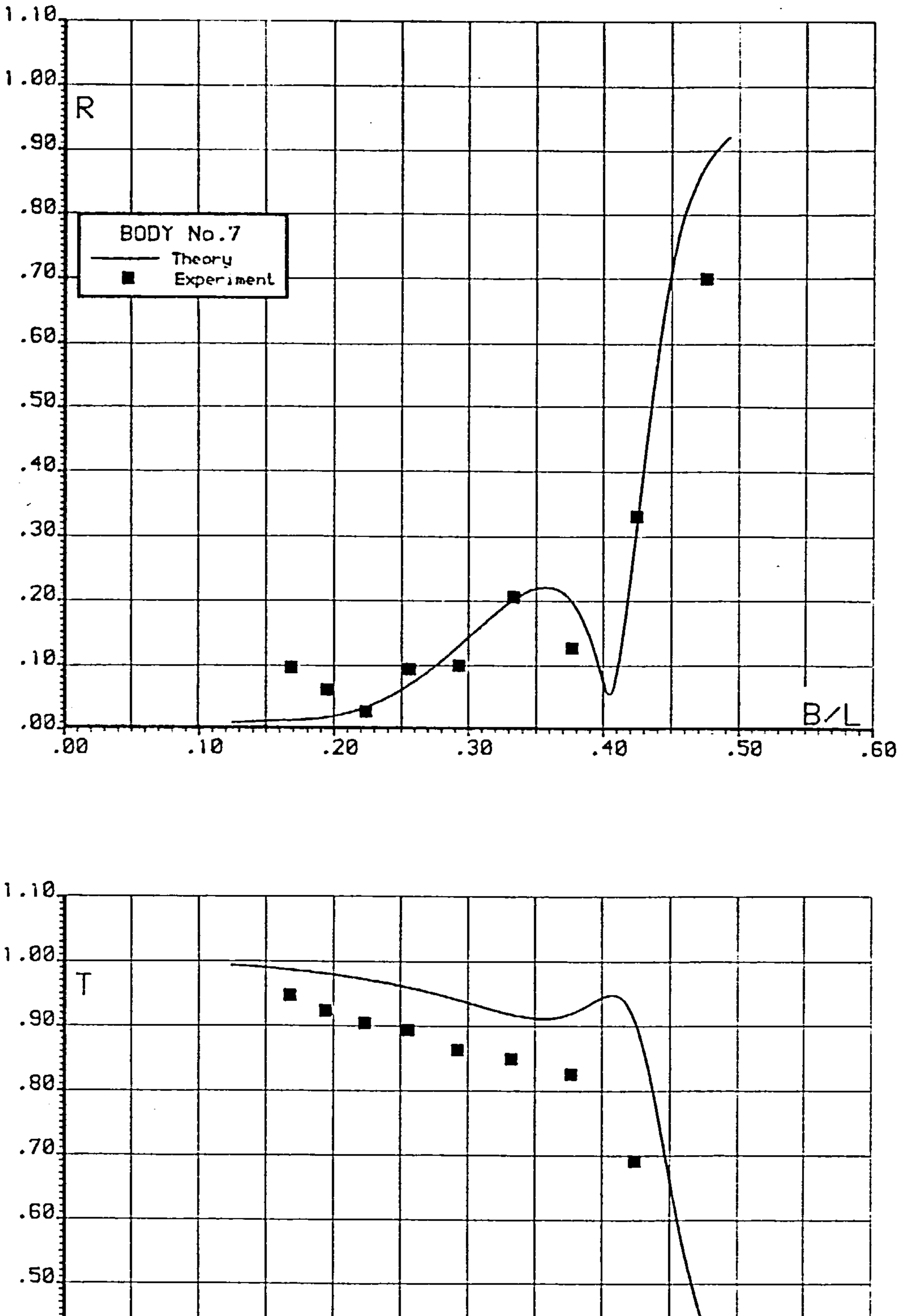

Fig. 6.36 FLOATING BODY REFLECTION AND TRANSMISSION

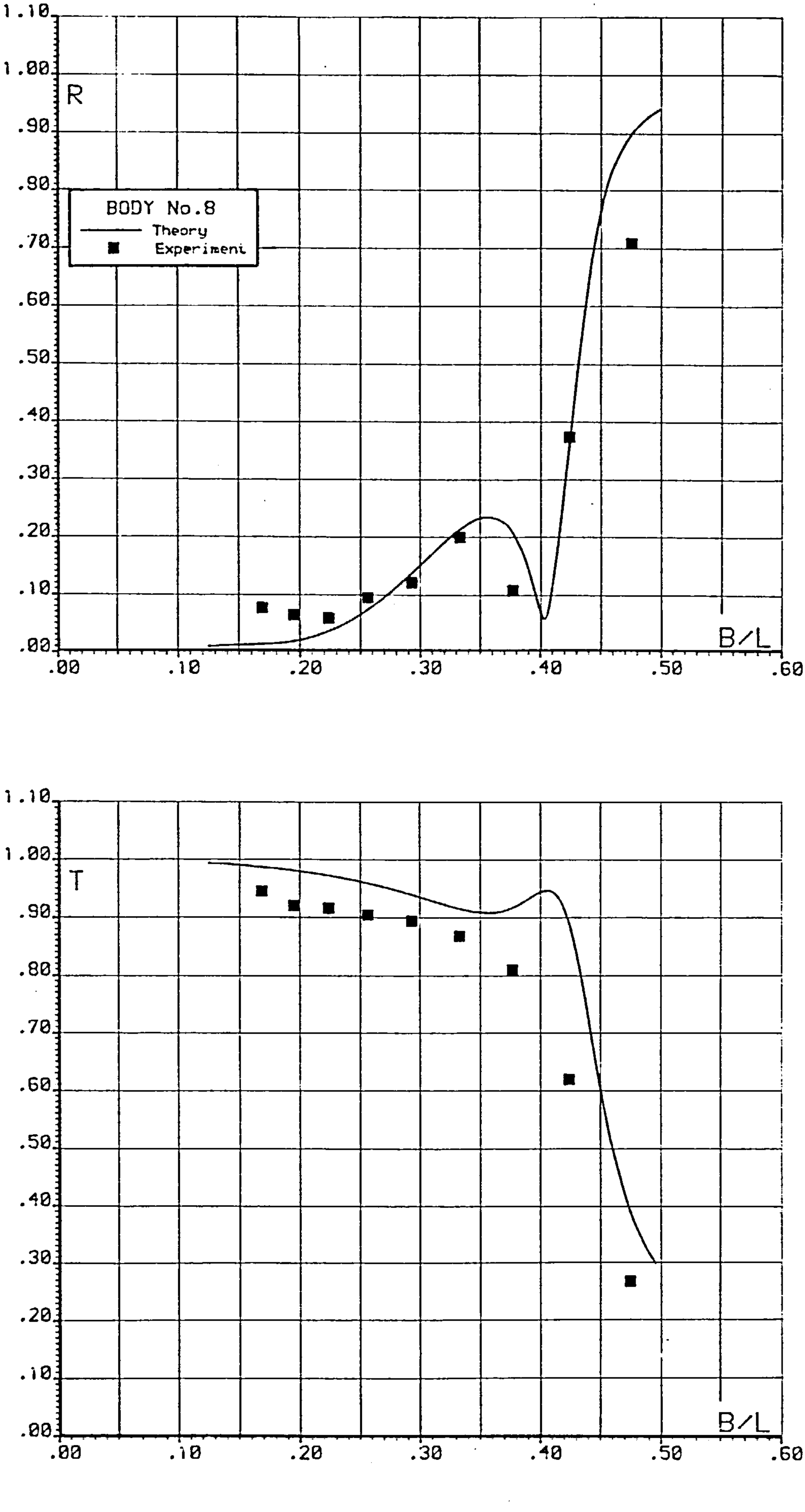

Fig. 6.37 FLOATING BODY REFLECTION AND TRANSMISSION

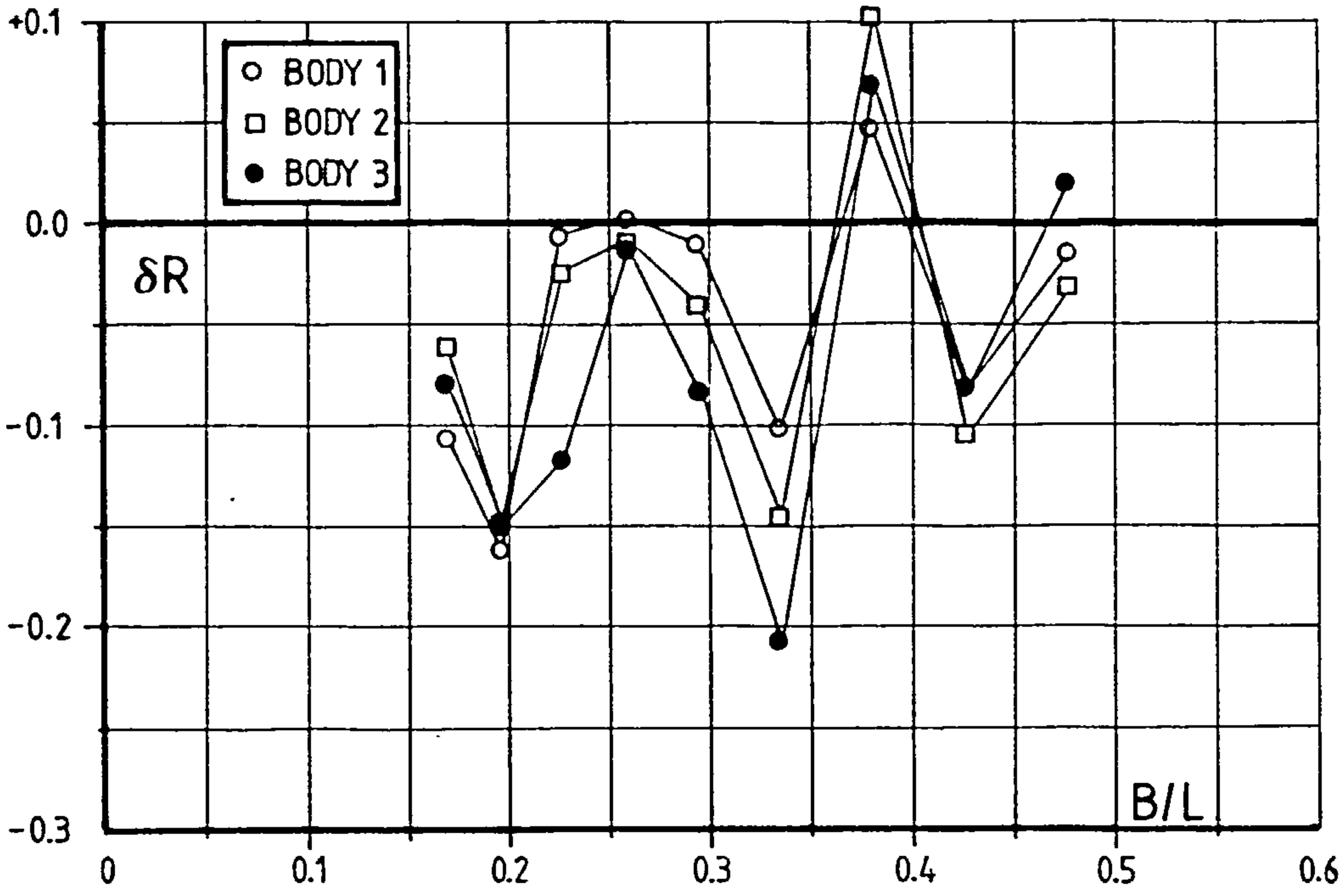

δ = Experiment - Theory

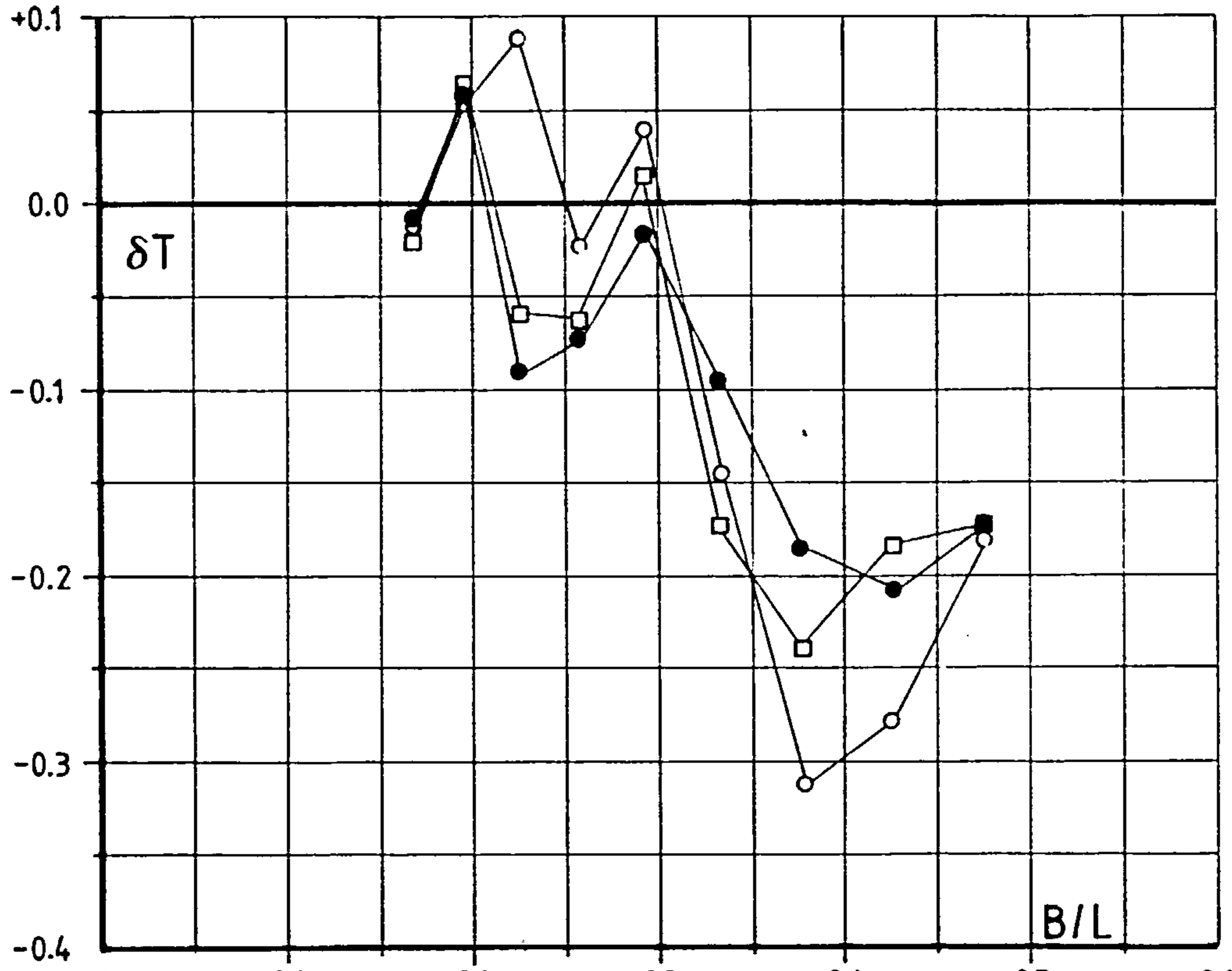

Fig. 6.38 FLOATING BODY REFLECTION AND TRANSMISSION ERRORS

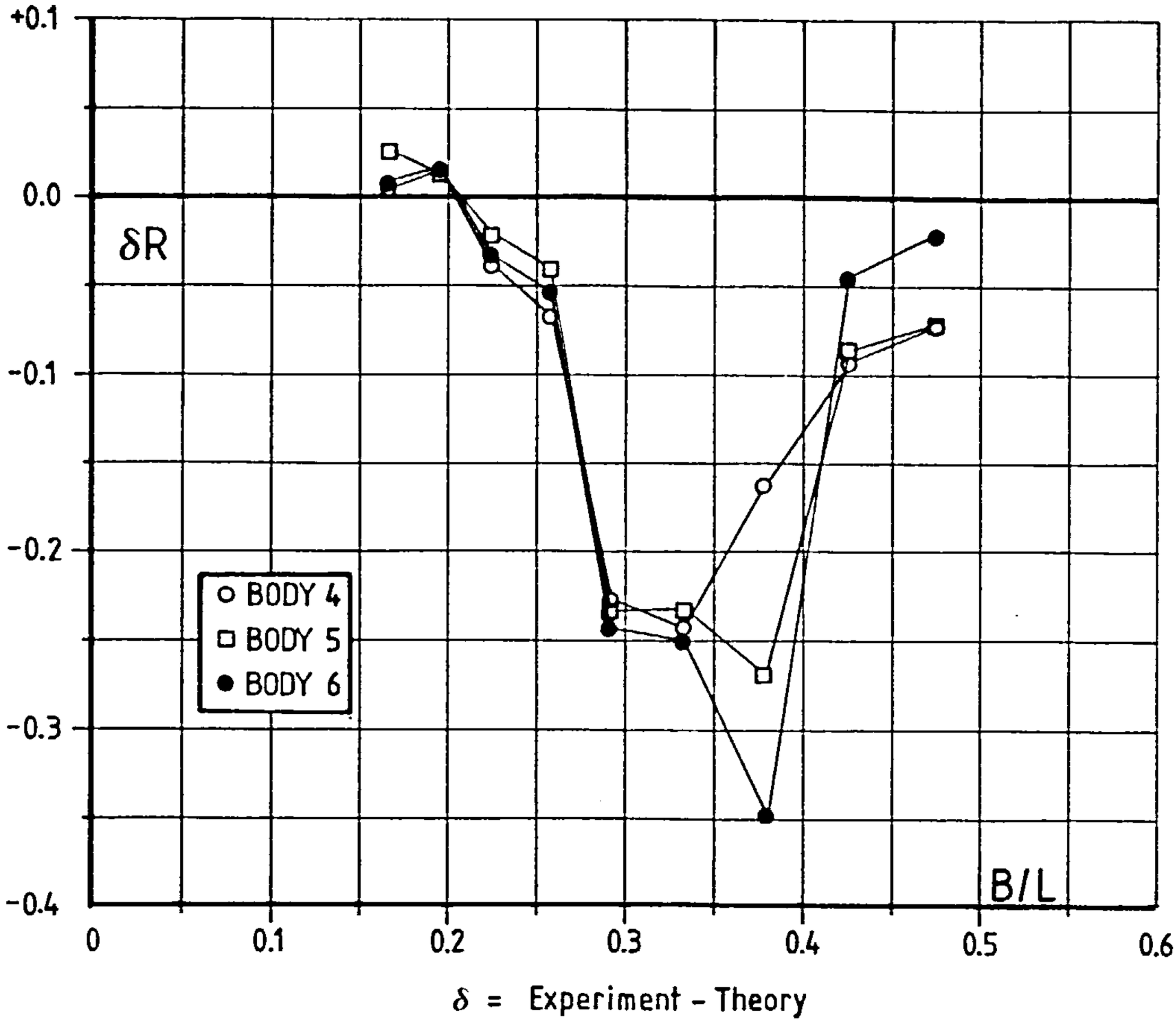

δ = Experiment - Theory

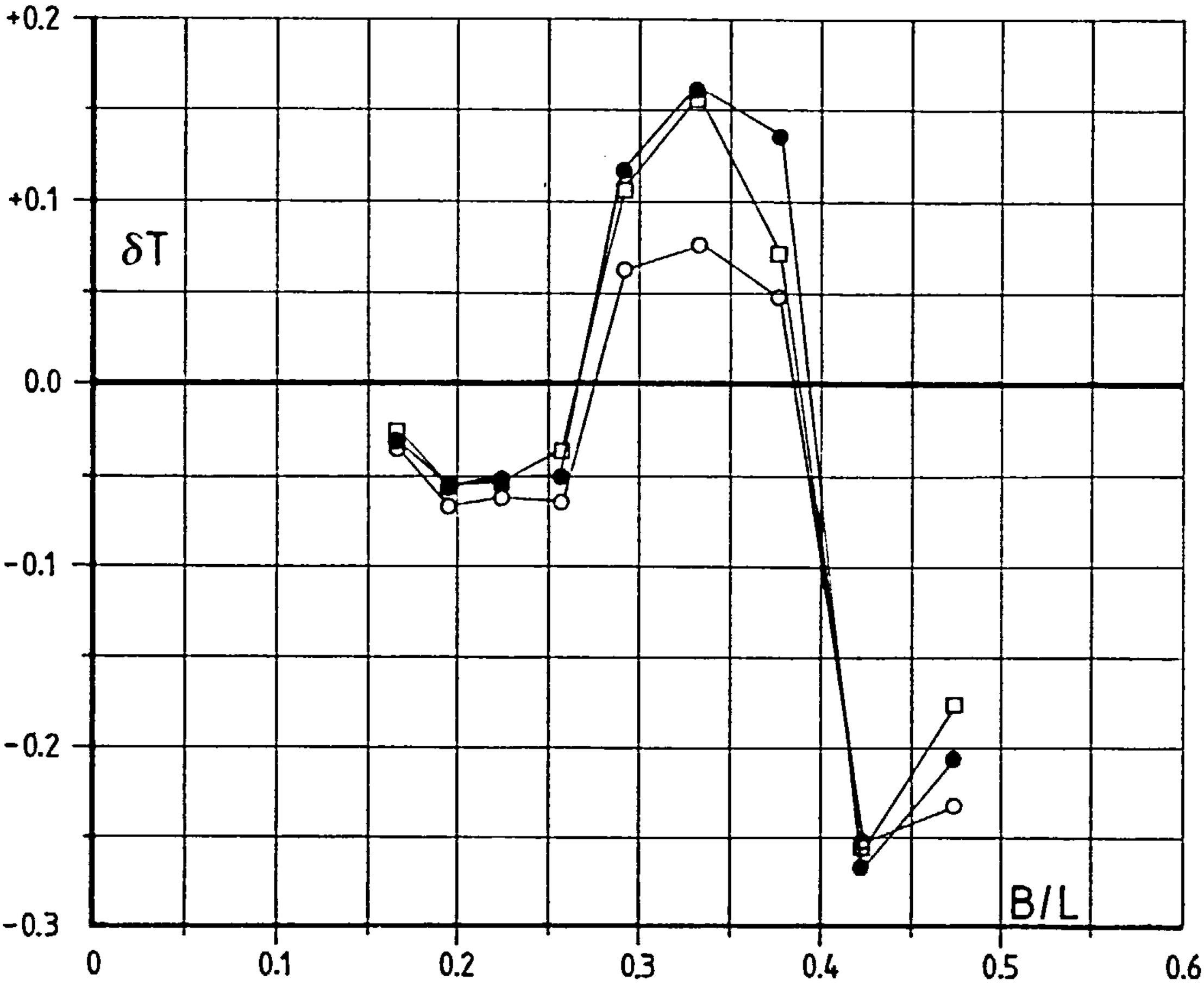

Fig. 6.39 FLOATING BODY REFLECTION AND TRANSMISSION ERRORS

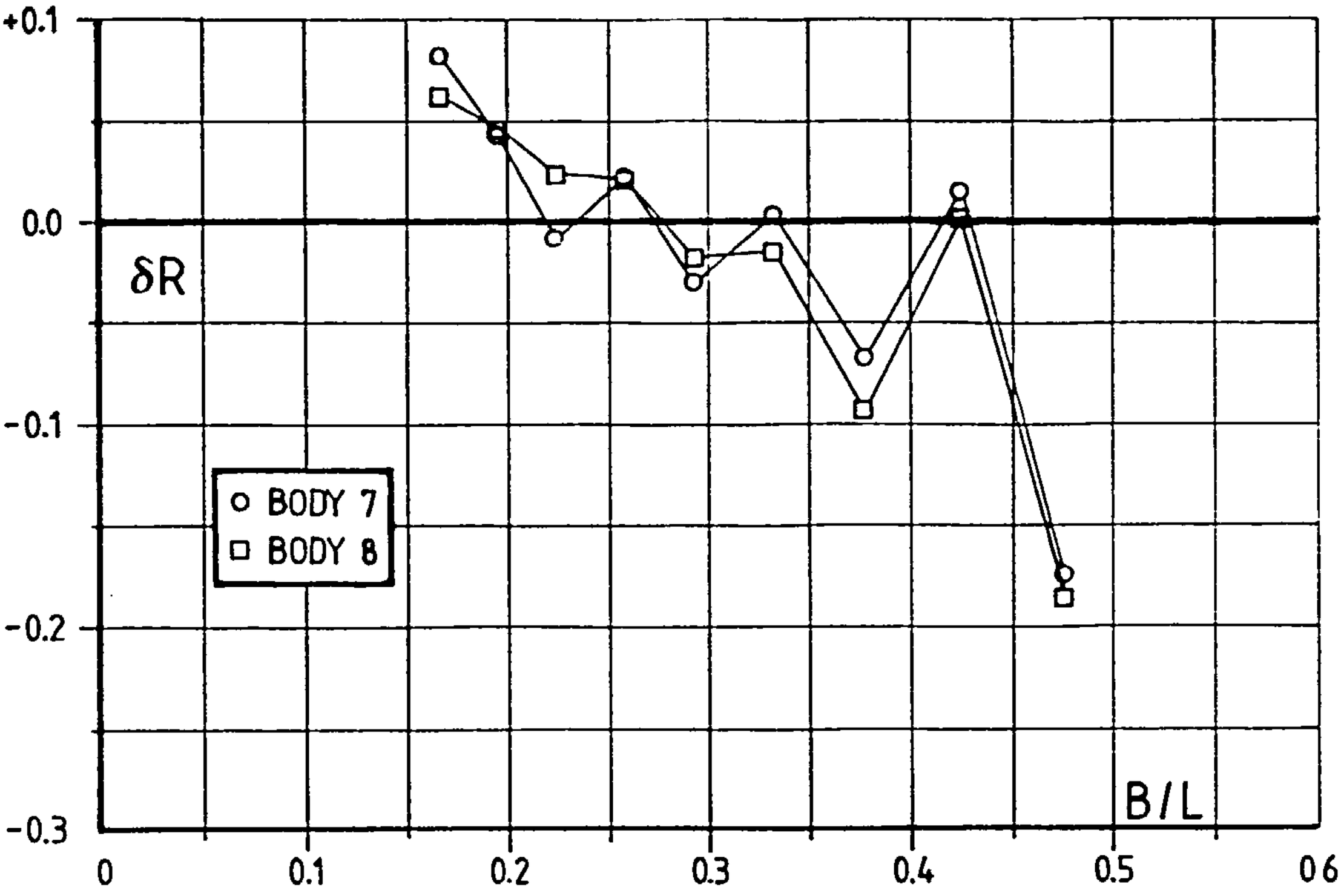

δ = Experiment - Theory

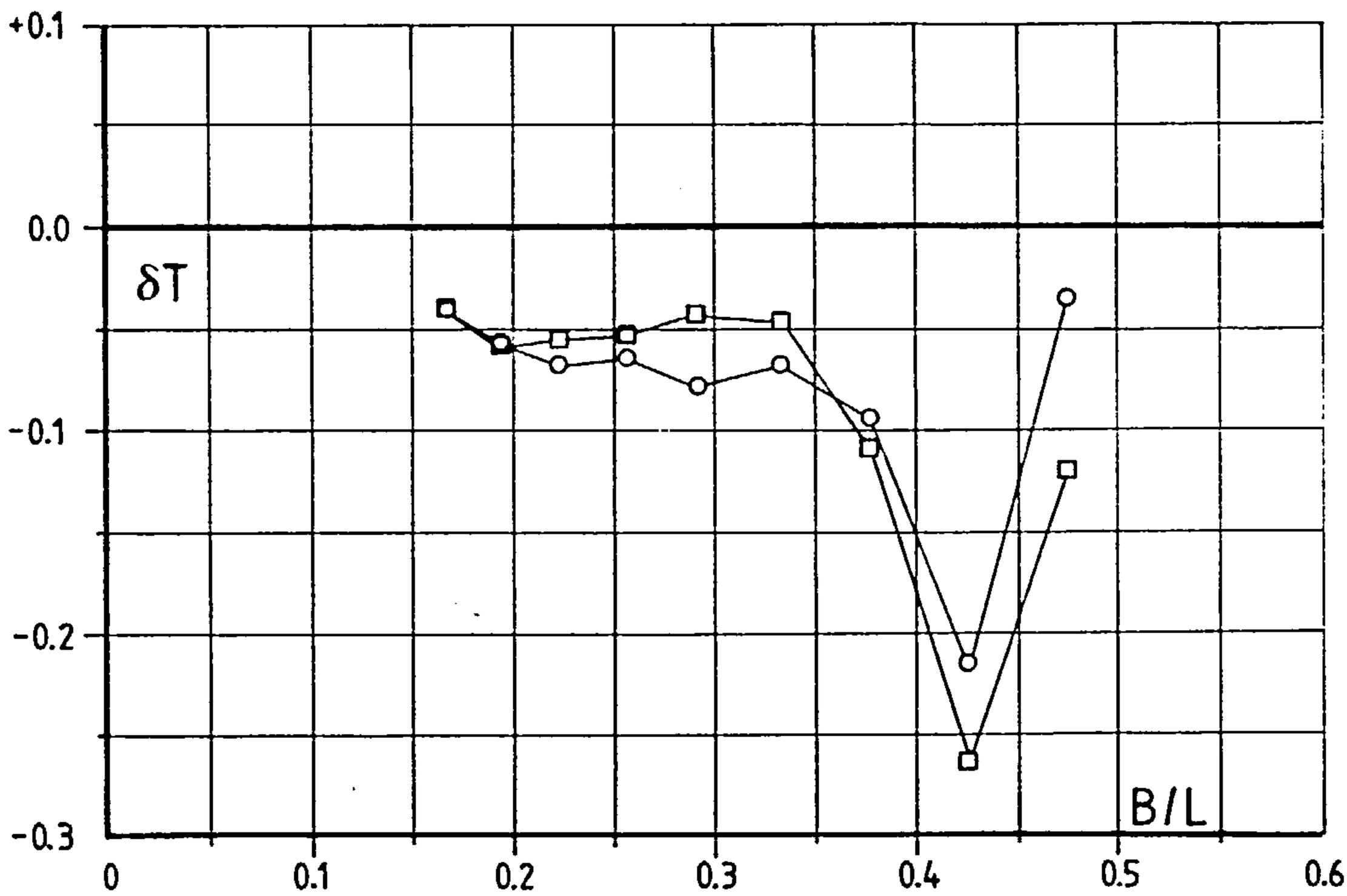

Fig. 6.40 FLOATING BODY REFLECTION AND TRANSMISSION ERRORS

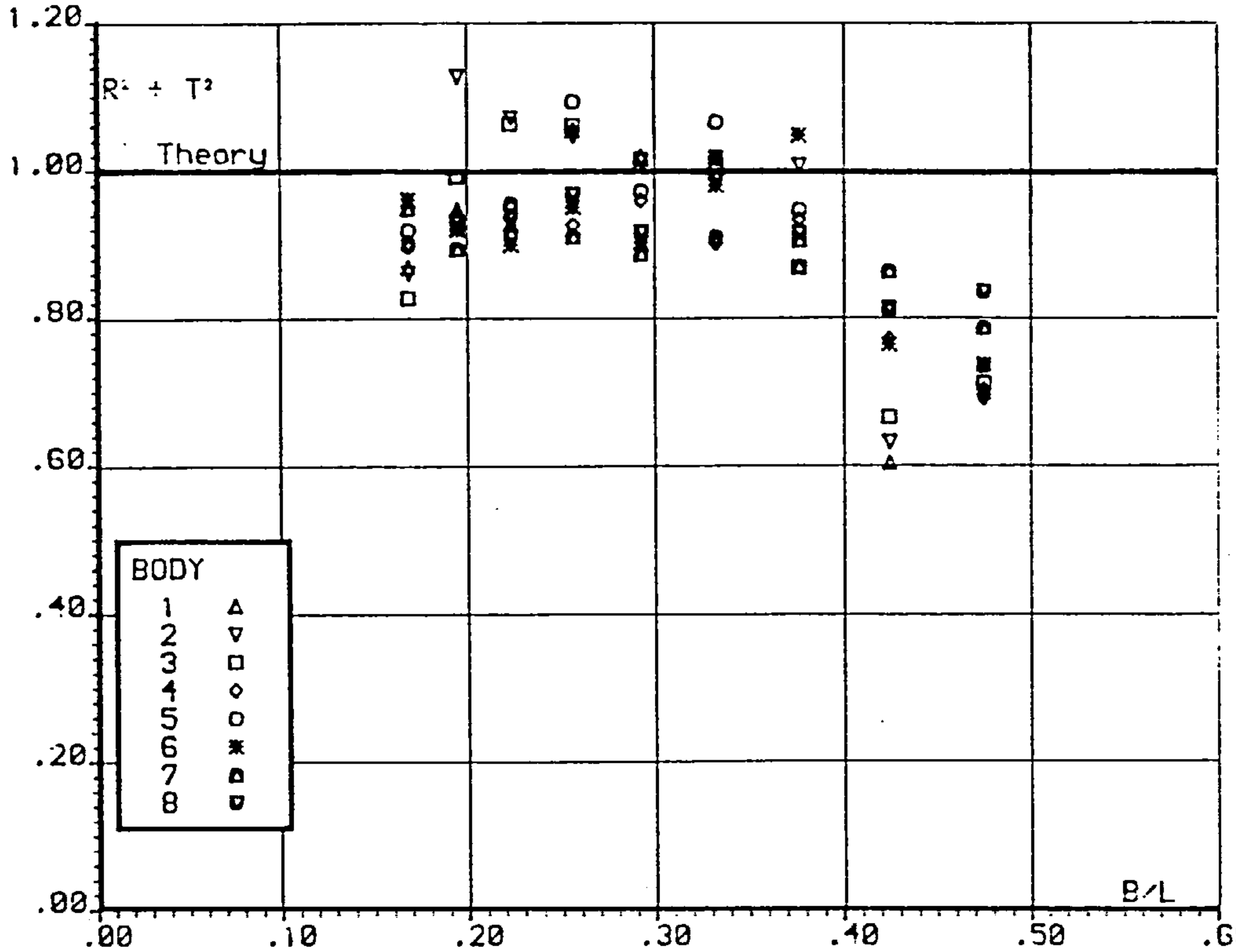

Fig. 6.41 FIXED BODY ENERGY CONSERVATION

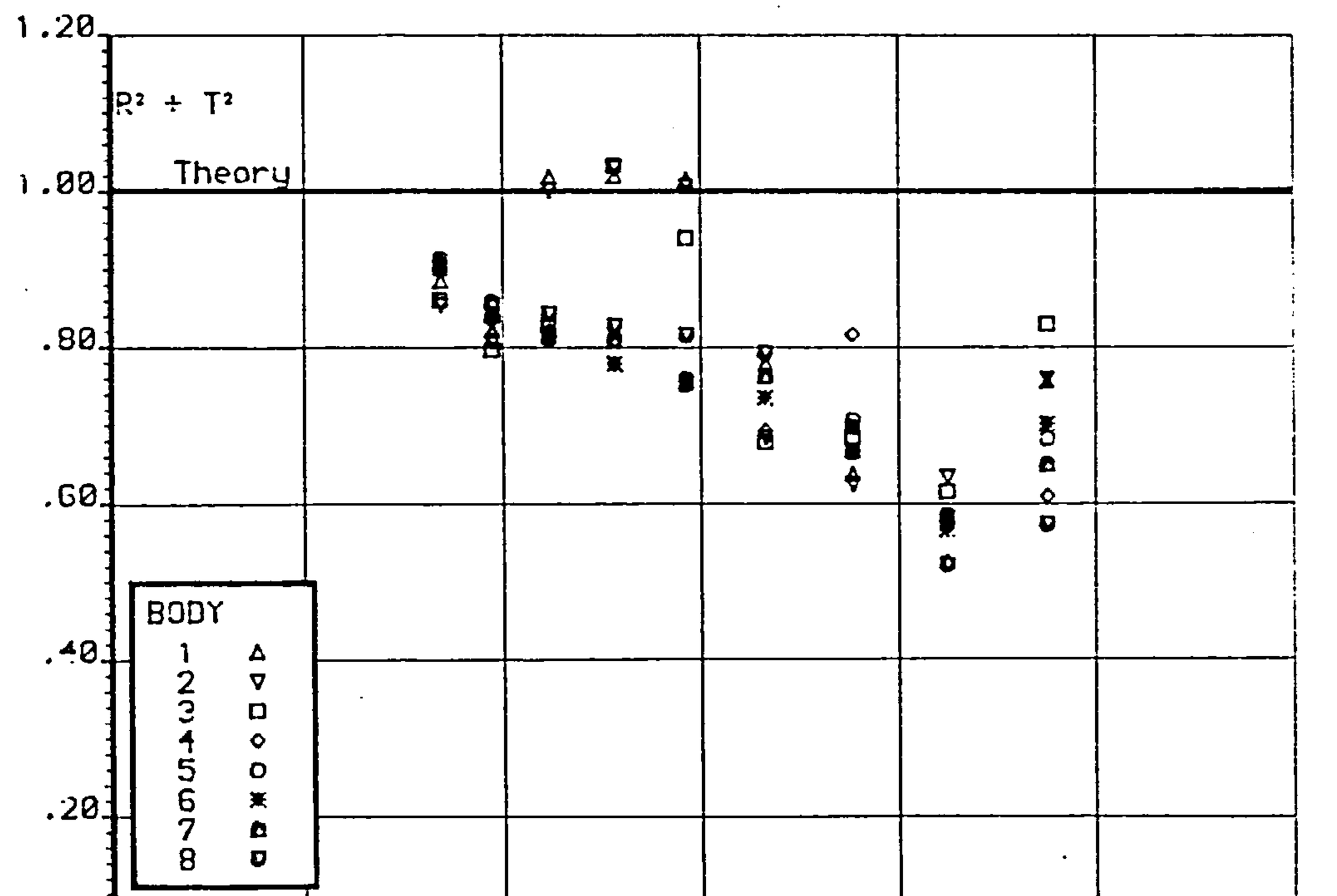

Fig. 6.42 FLOATING BODY ENERGY CONSERVATION

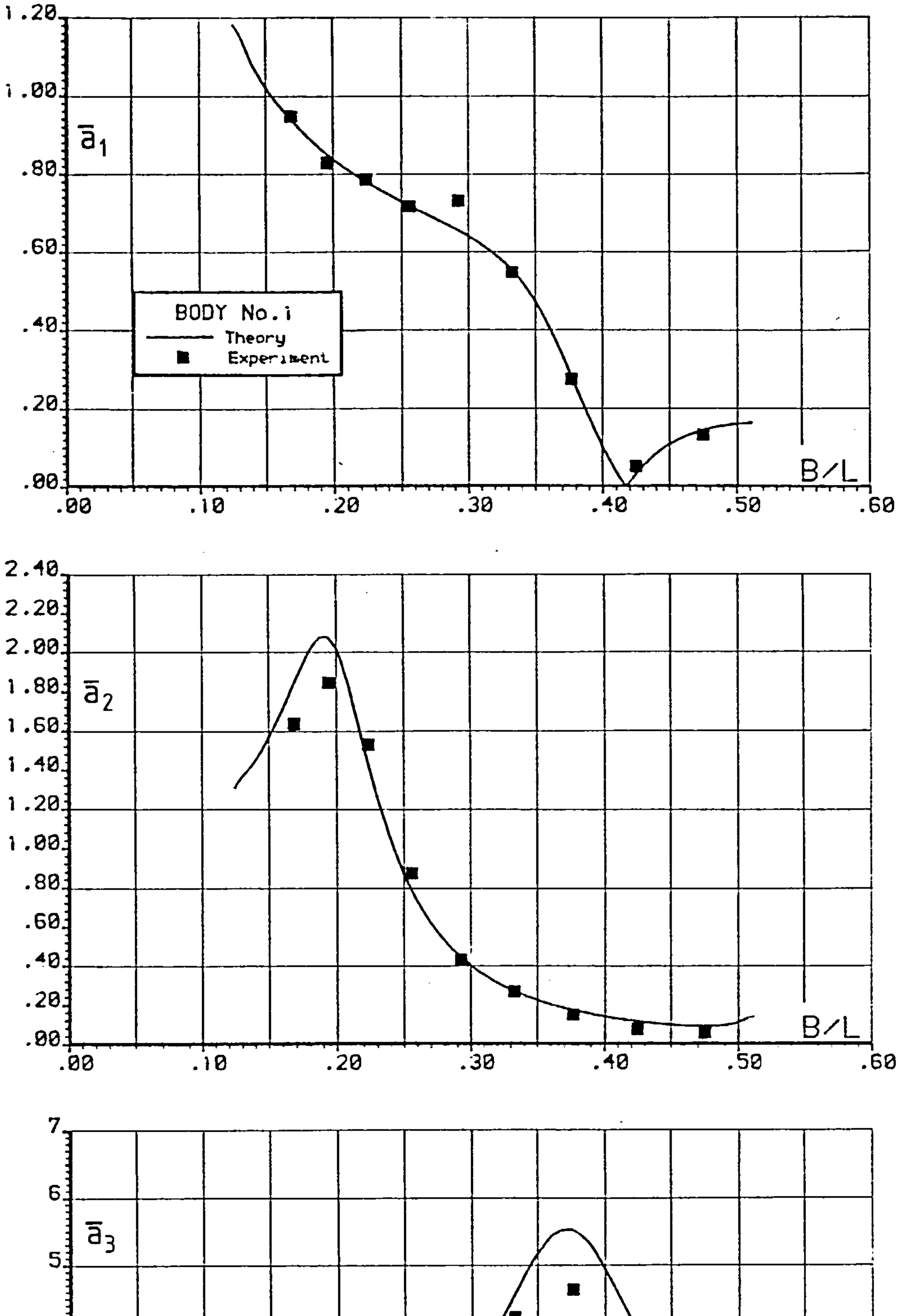

Fig. 6.43 FLOATING BODY MOTIONS

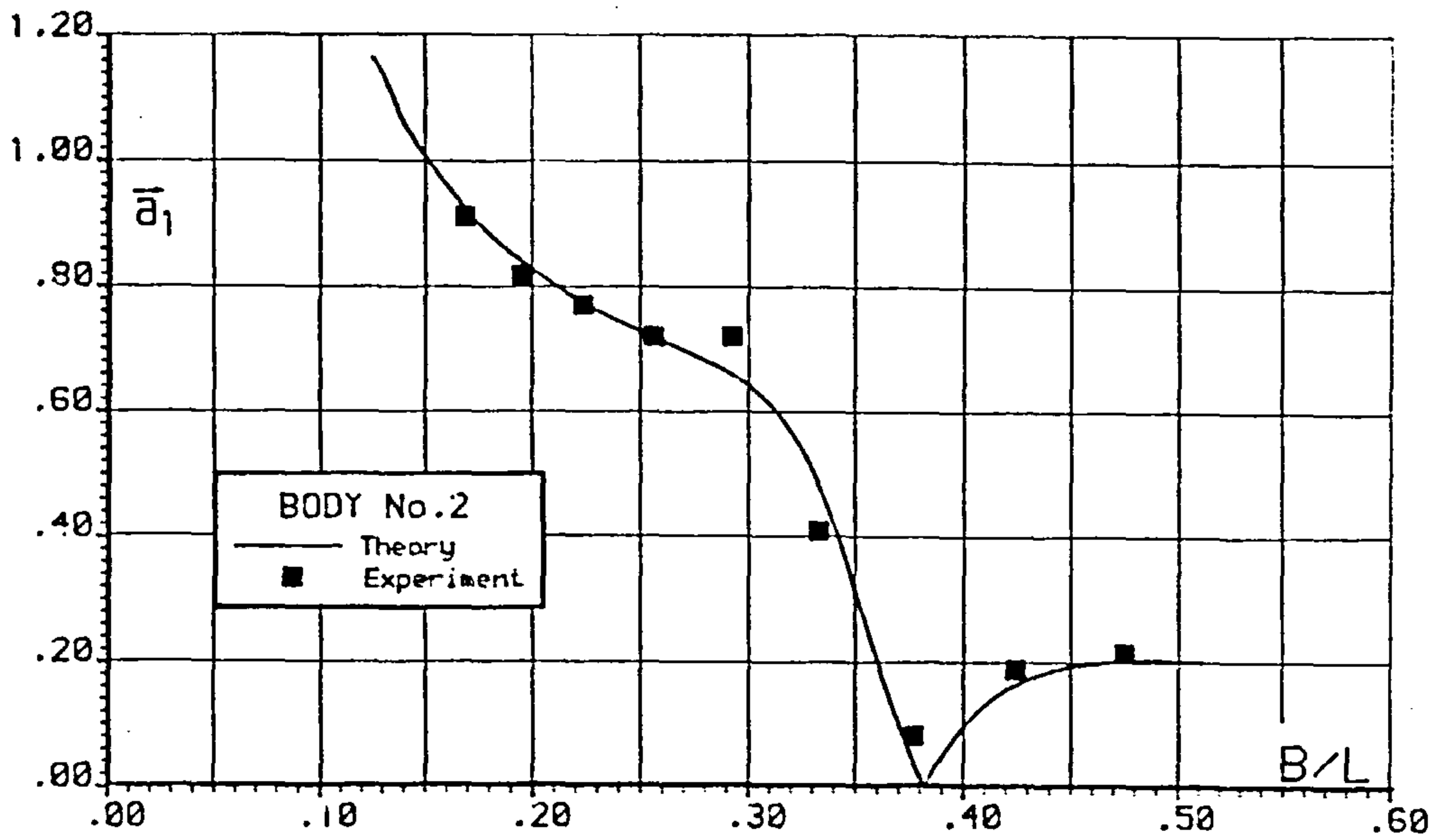

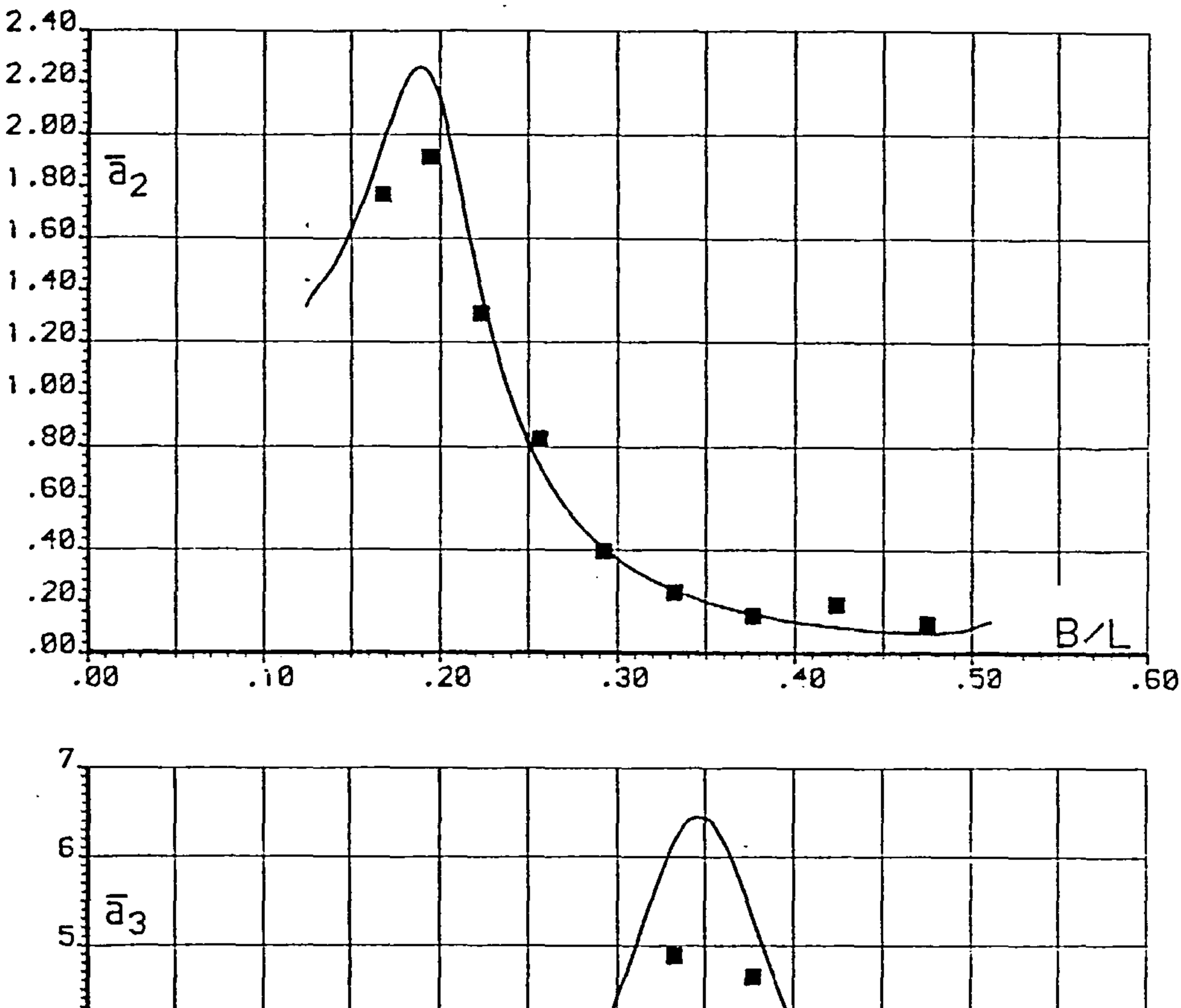

Fig. 6.44 FLOATING BODY MOTIONS

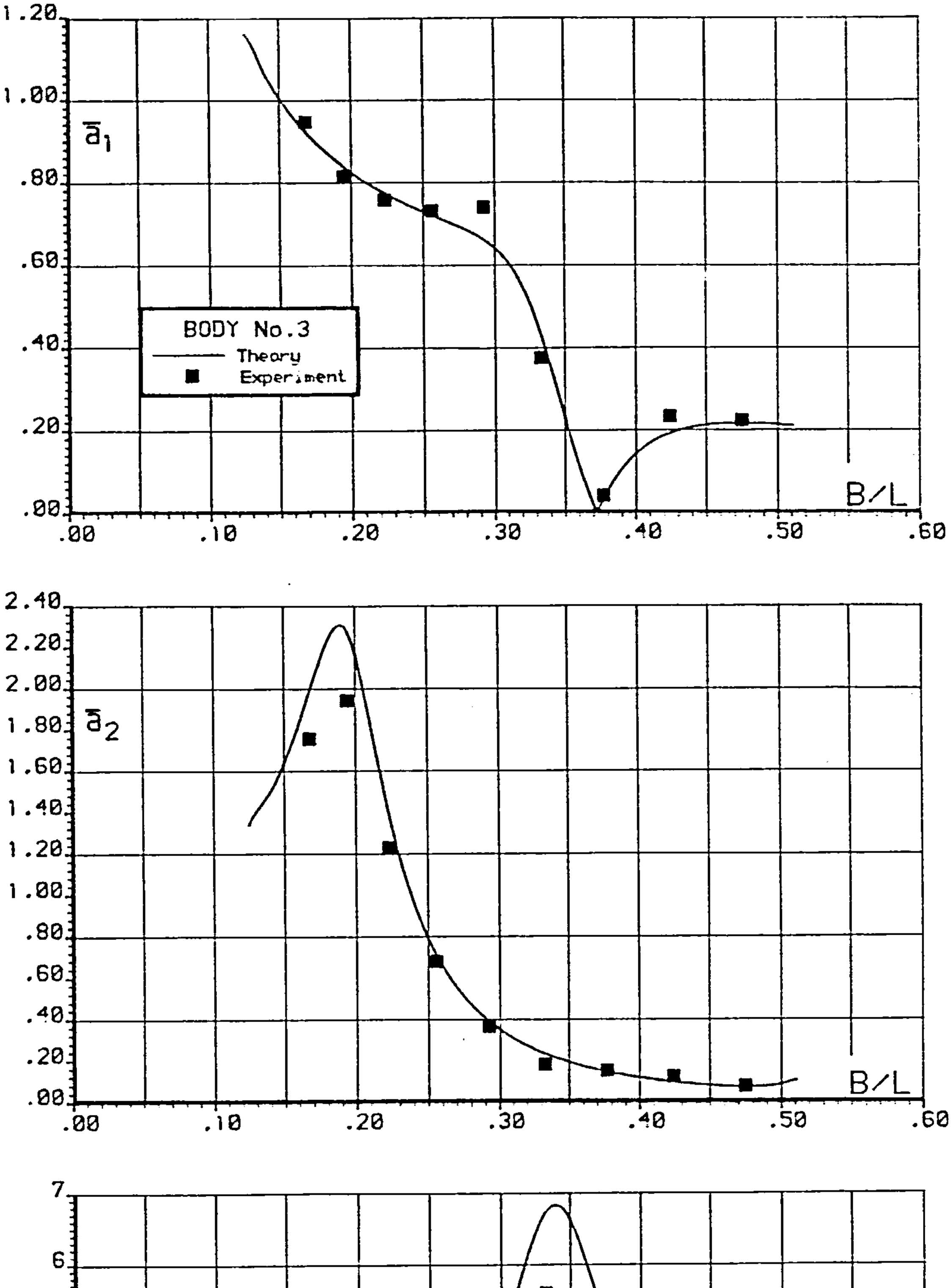

Fig. 6.45 FLOATING BODY MOTIONS

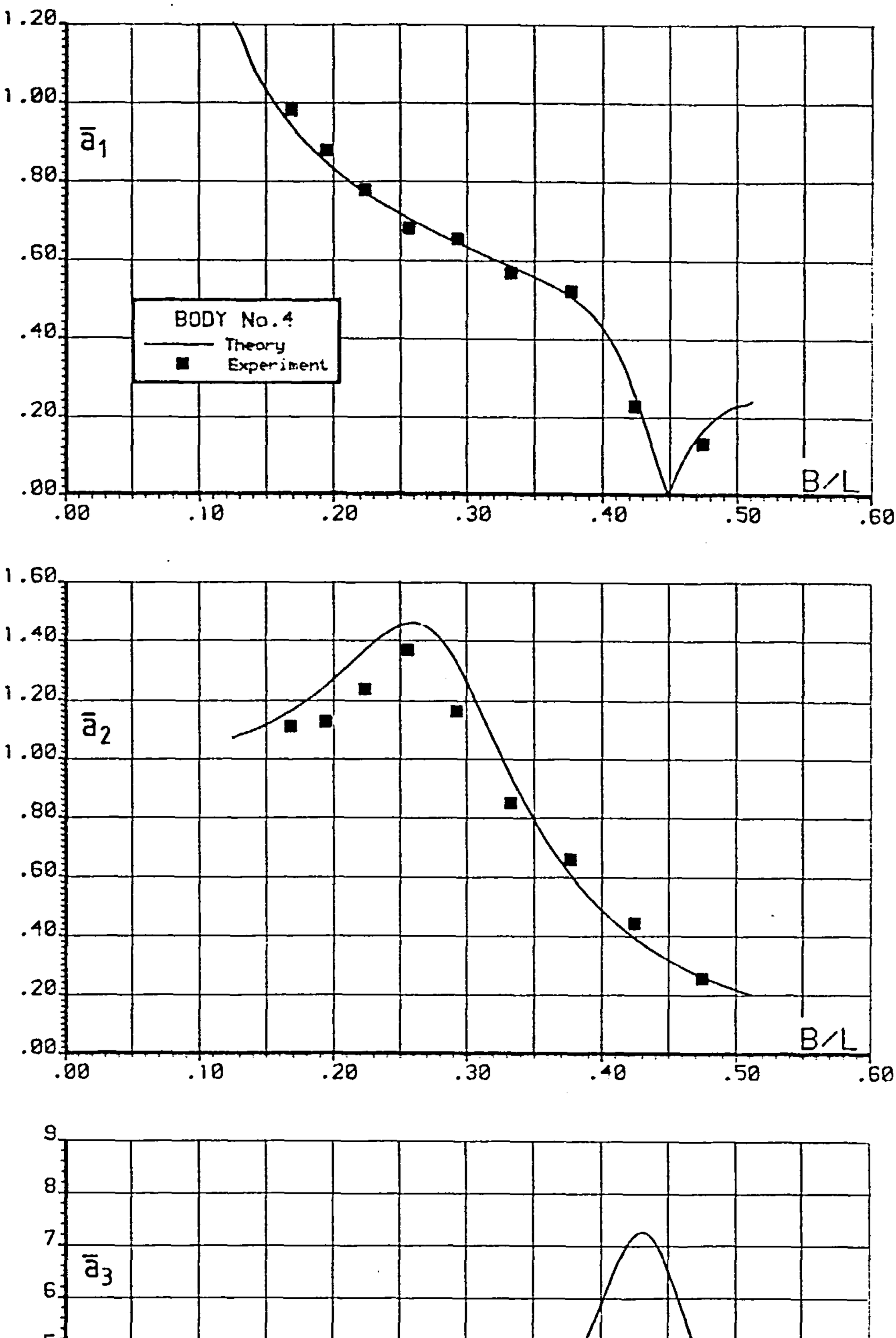

Fig. 6.46 FLOATING BODY MOTIONS

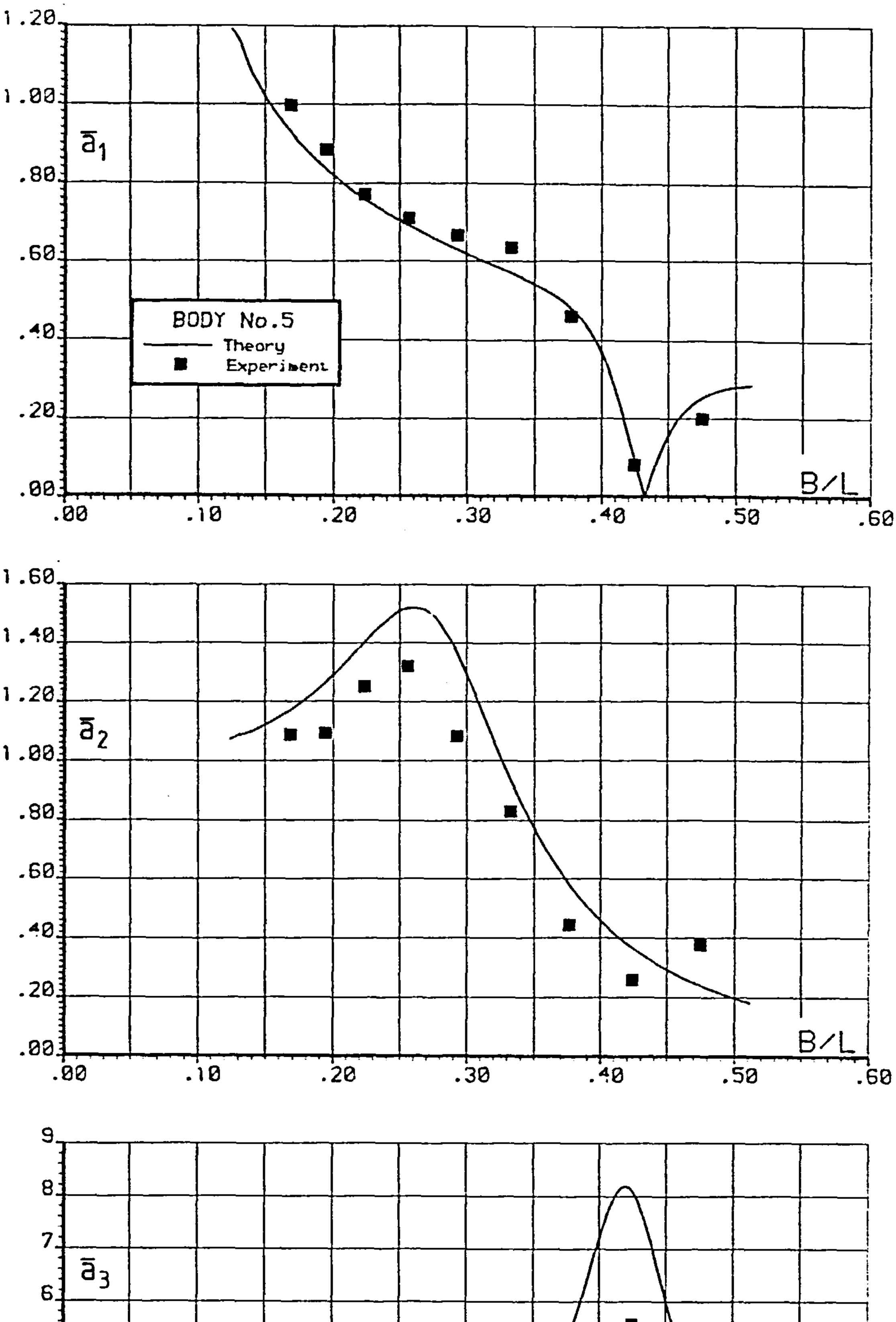

Fig. 6.47 FLOATING BODY MOTIONS

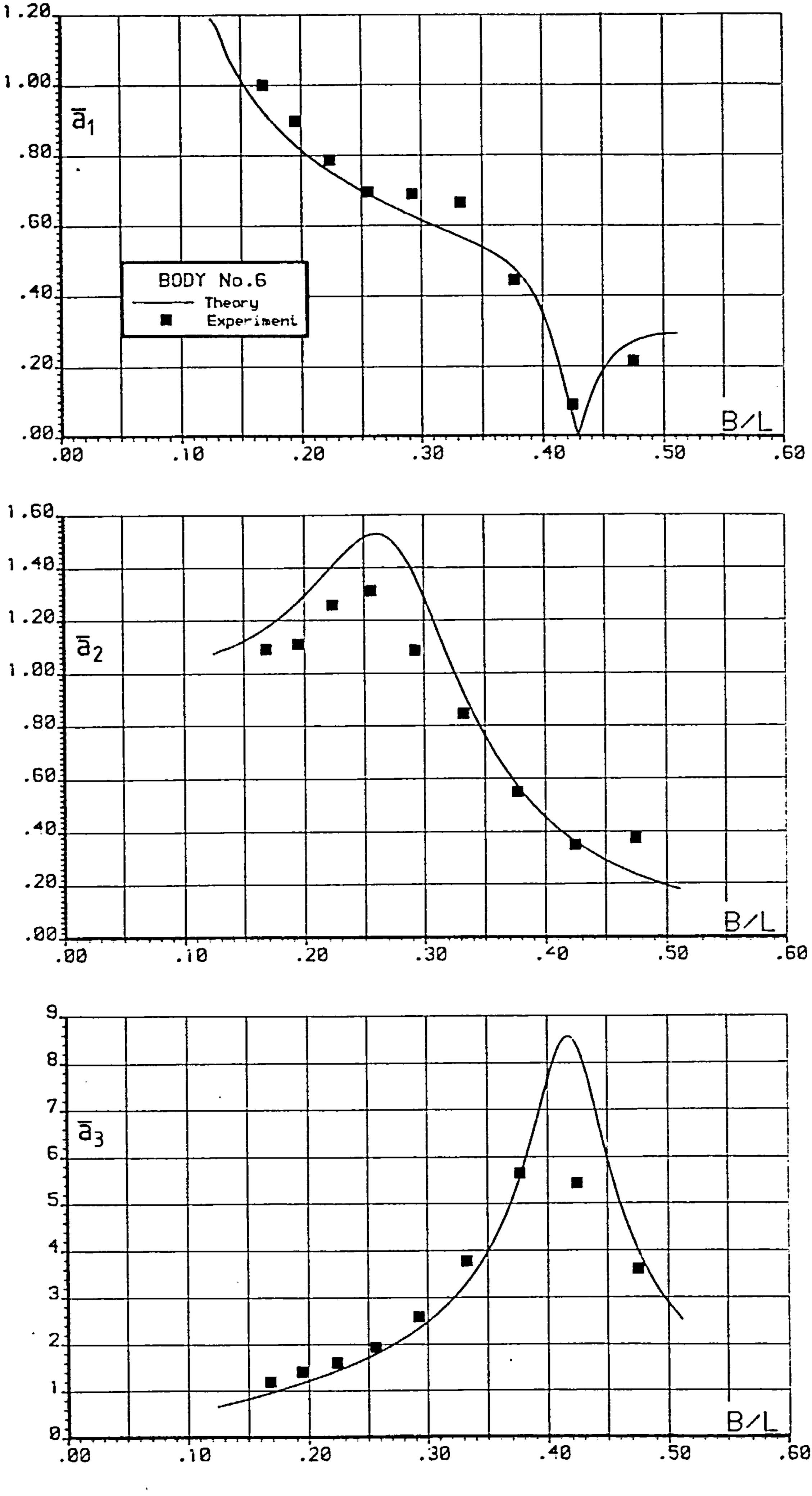

Fig. 6.48 FLOATING BODY MOTIONS

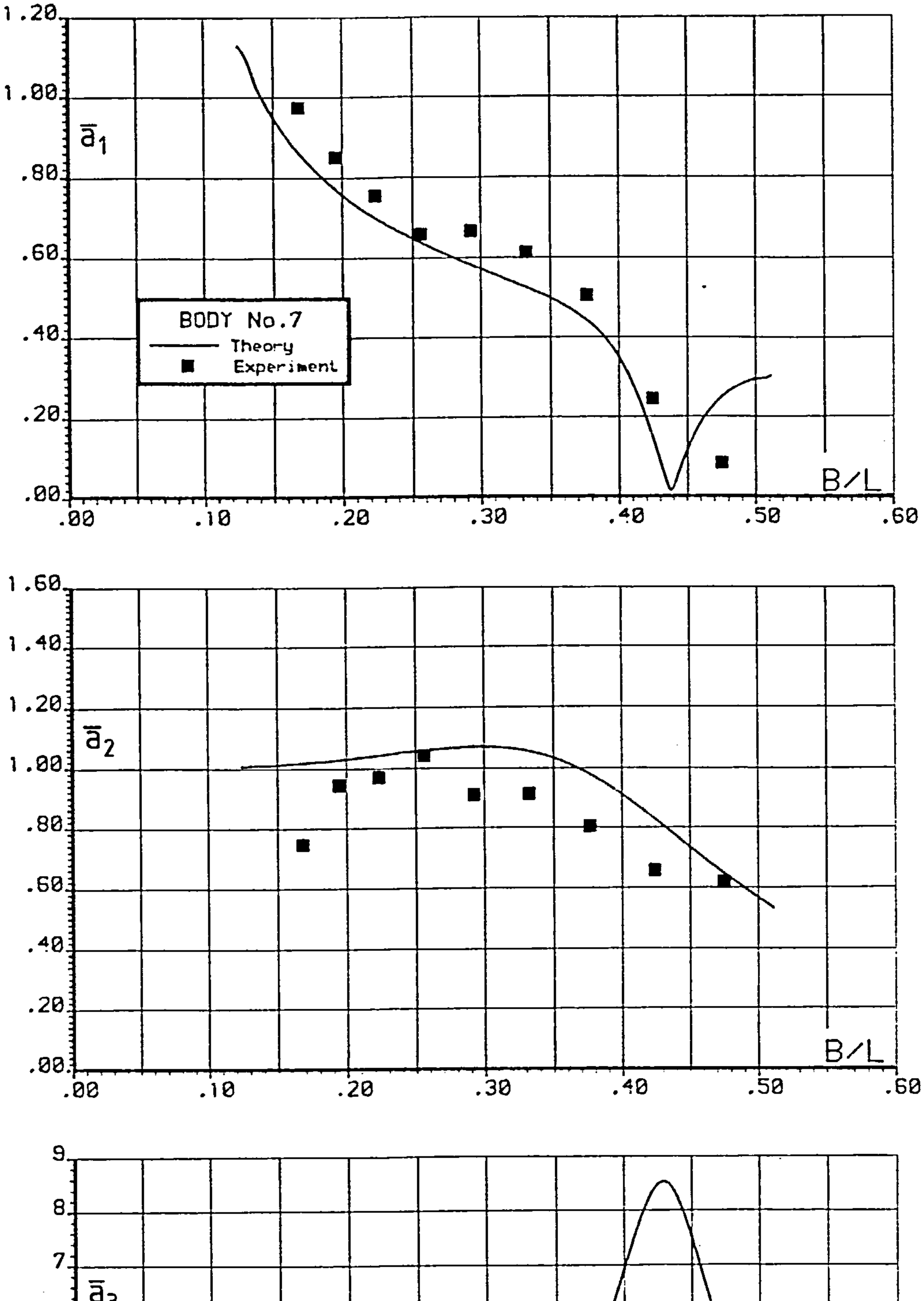

Fig. 6.49 FLOATING BODY MOTIONS

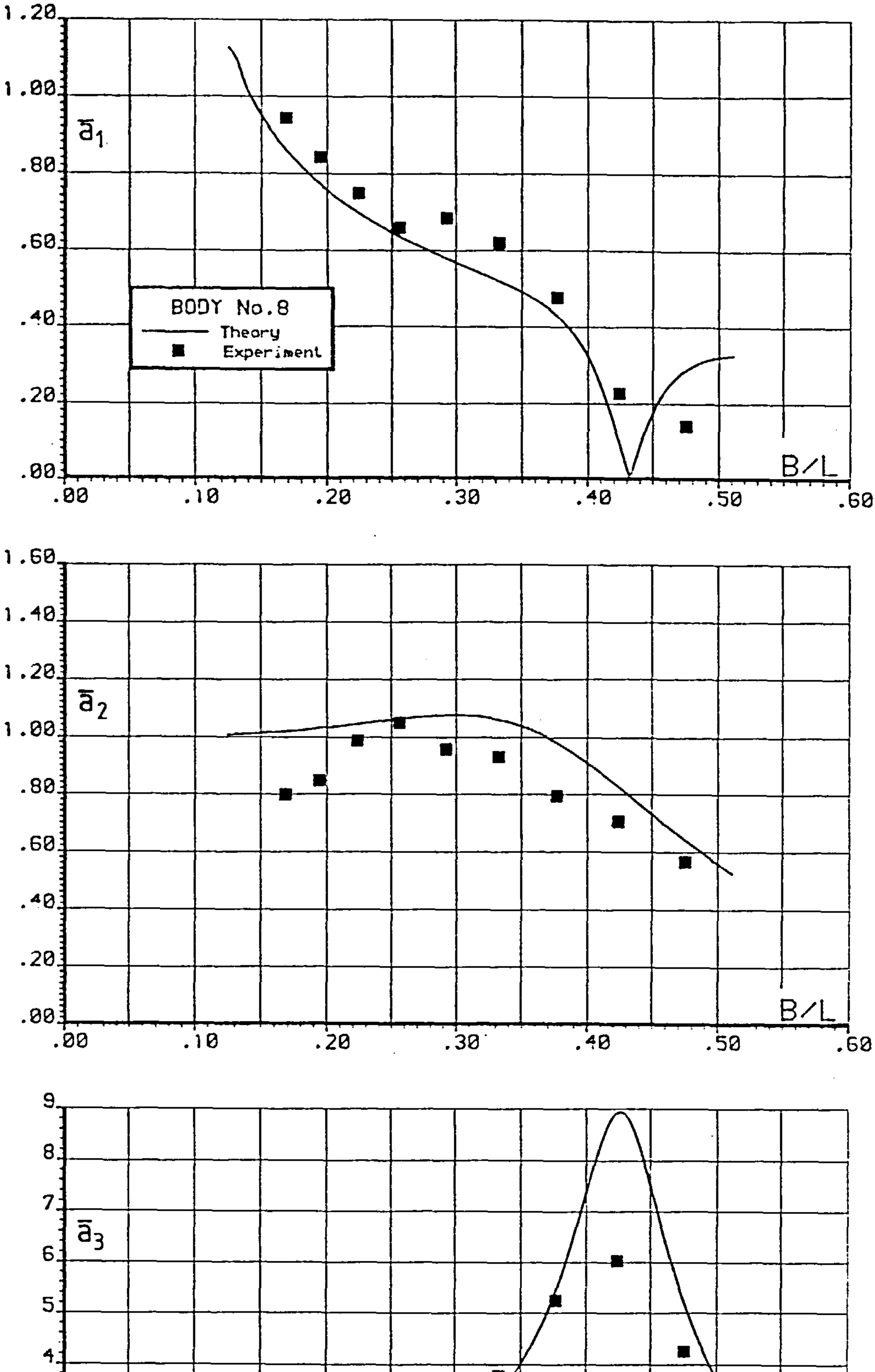

Fig. 6.50 FLOATING BODY MOTIONS

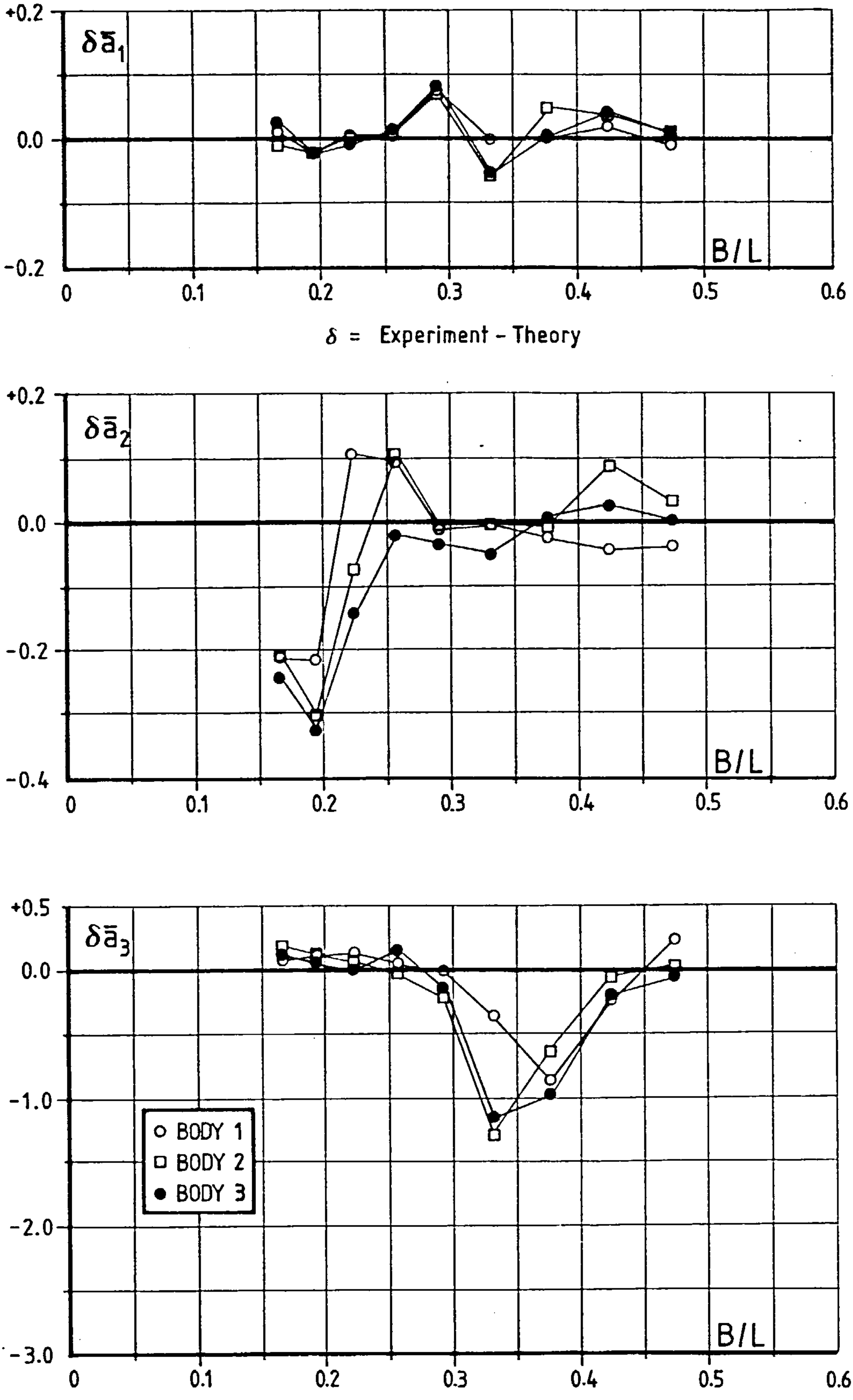

Fig. 6.51 FLOATING BODY MOTION ERRORS

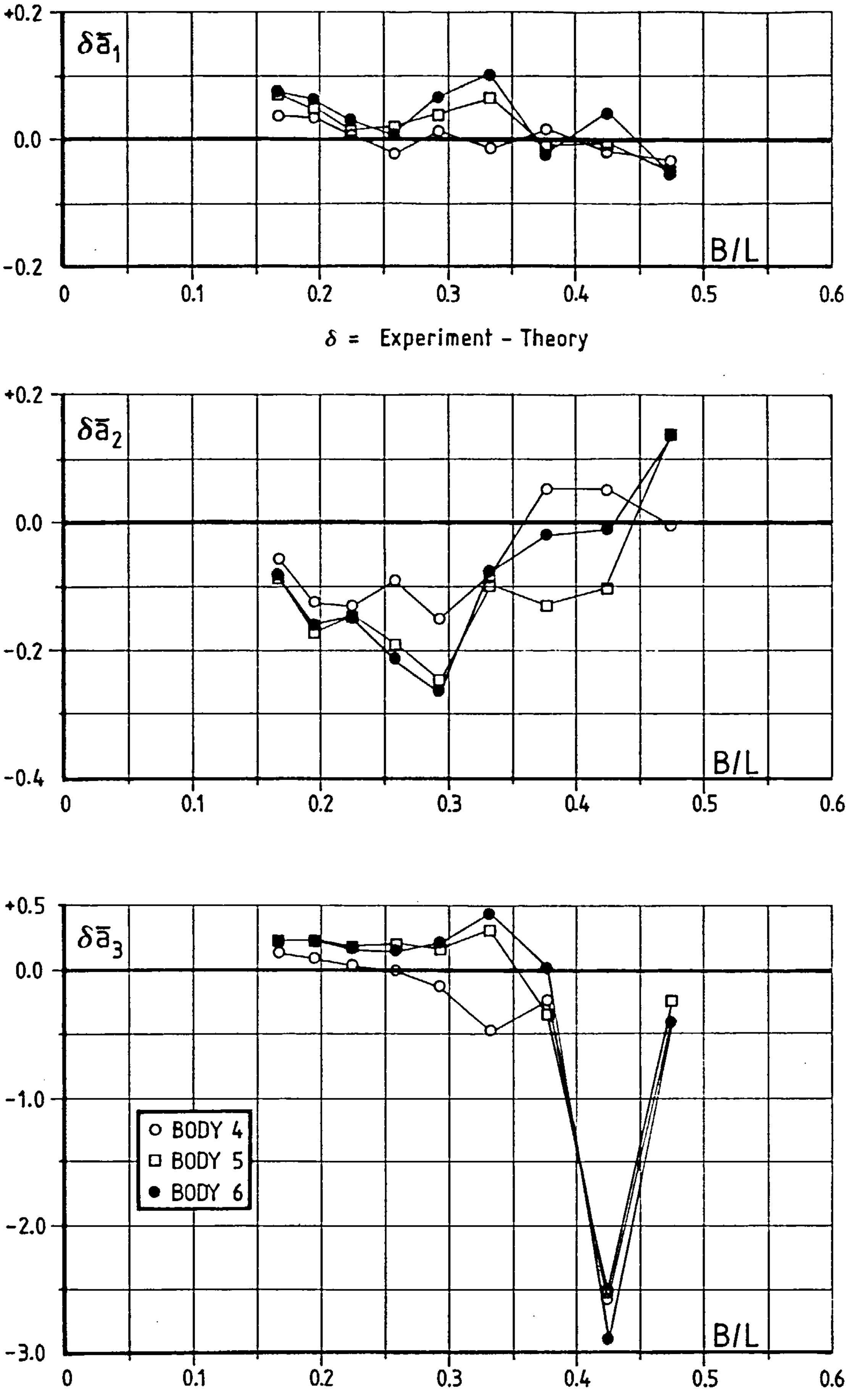

Fig. 6.52 FLOATING BODY MOTION ERRORS

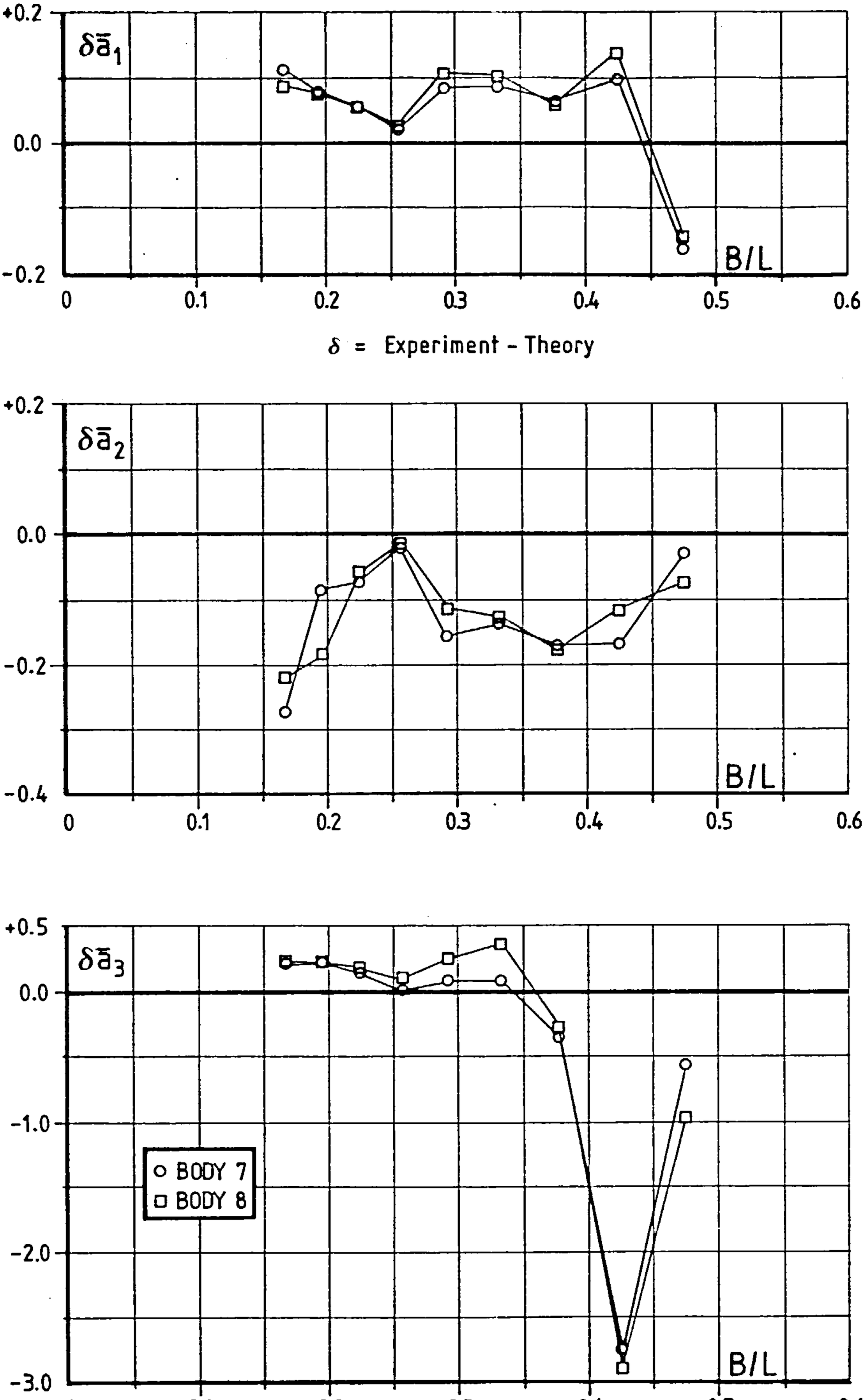

Fig. 6.53 FLOATING BODY MOTION ERRORS

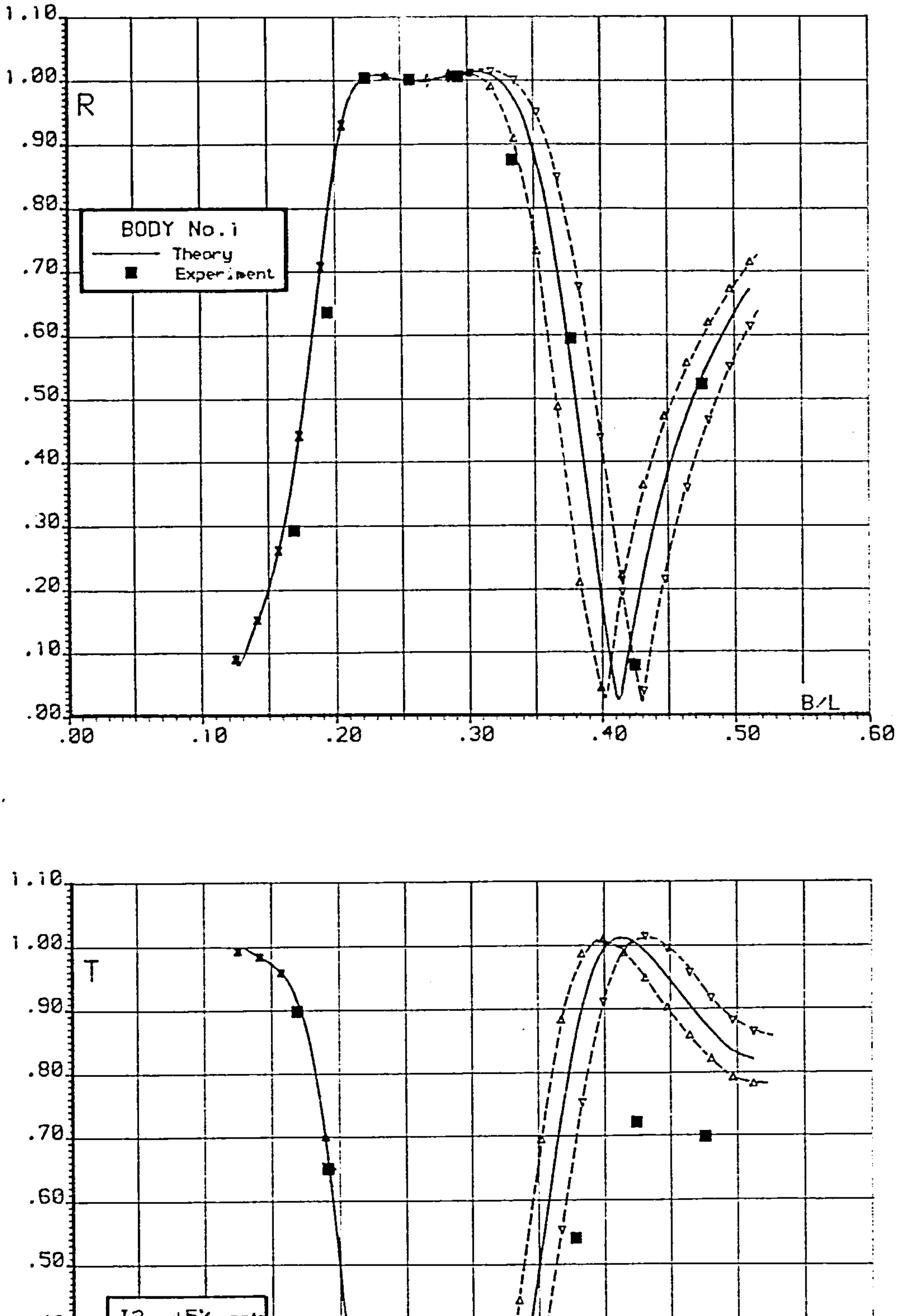

Fig. 6.54 FLOATING BODY REFLECTION AND TRANSMISSION

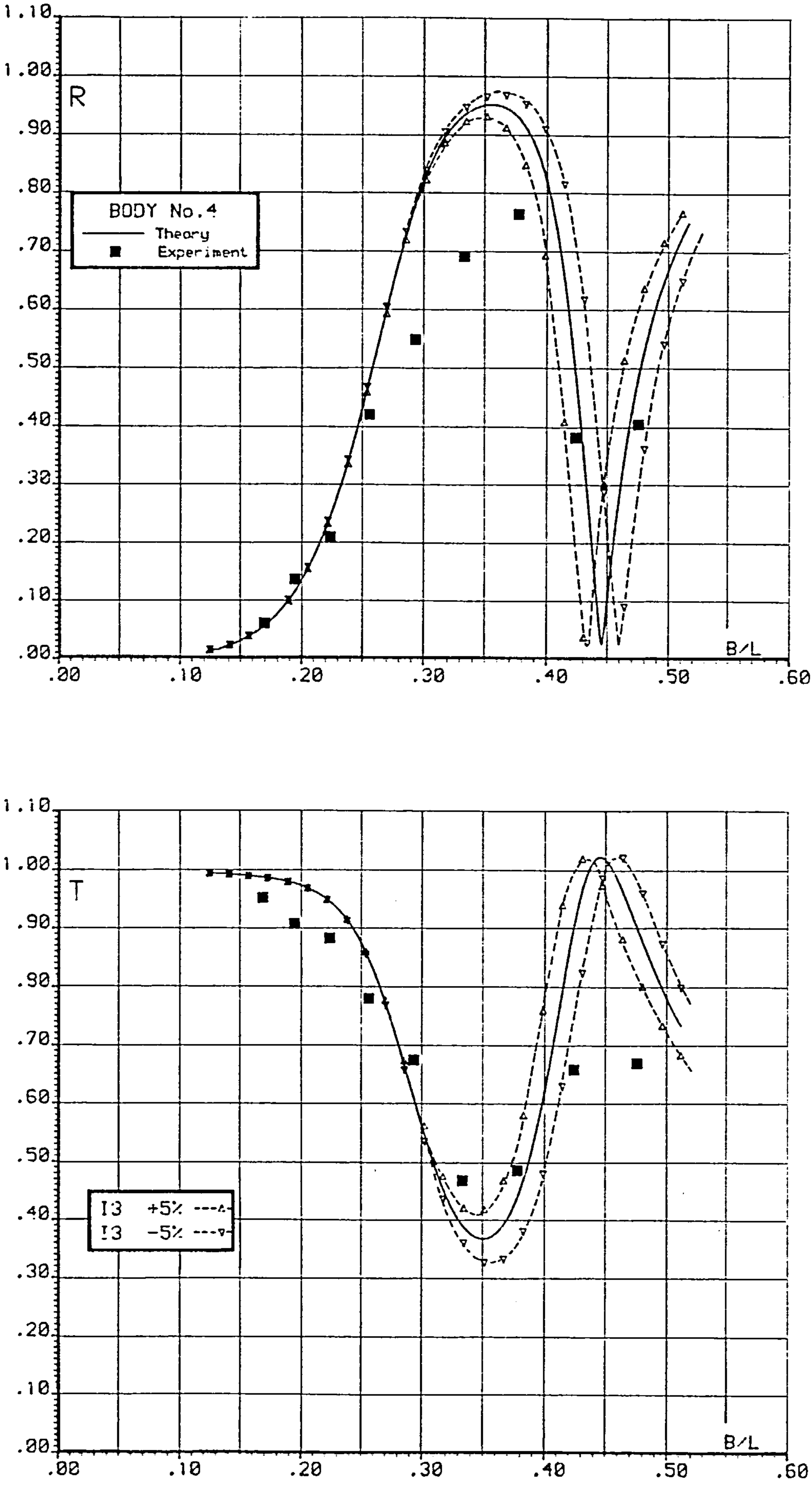

Fig. 6.55 FLOATING BODY REFLECTION AND TRANSMISSION

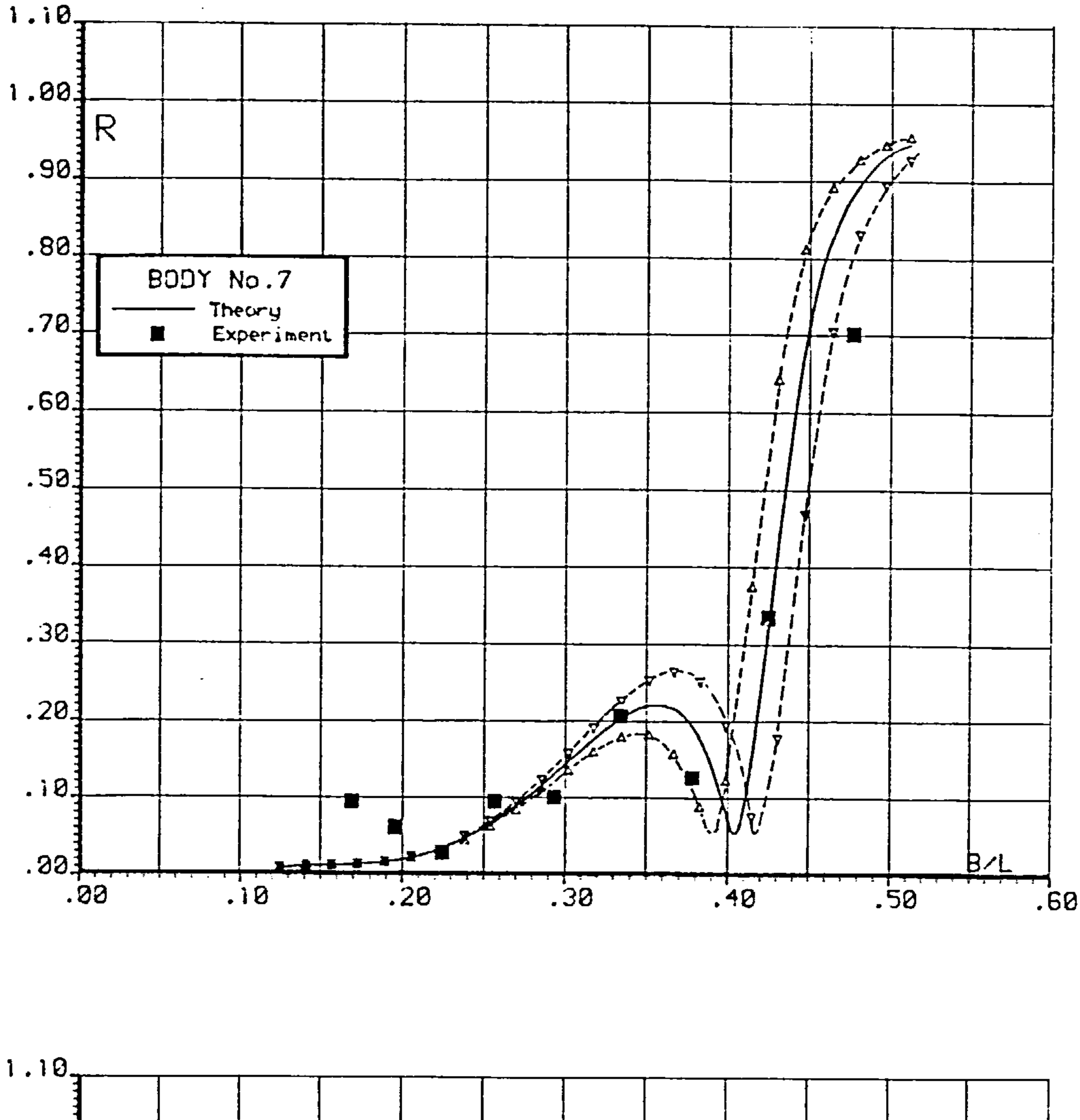

Fig. 6.56 FLOATING BODY REFLECTION AND TRANSMISSION

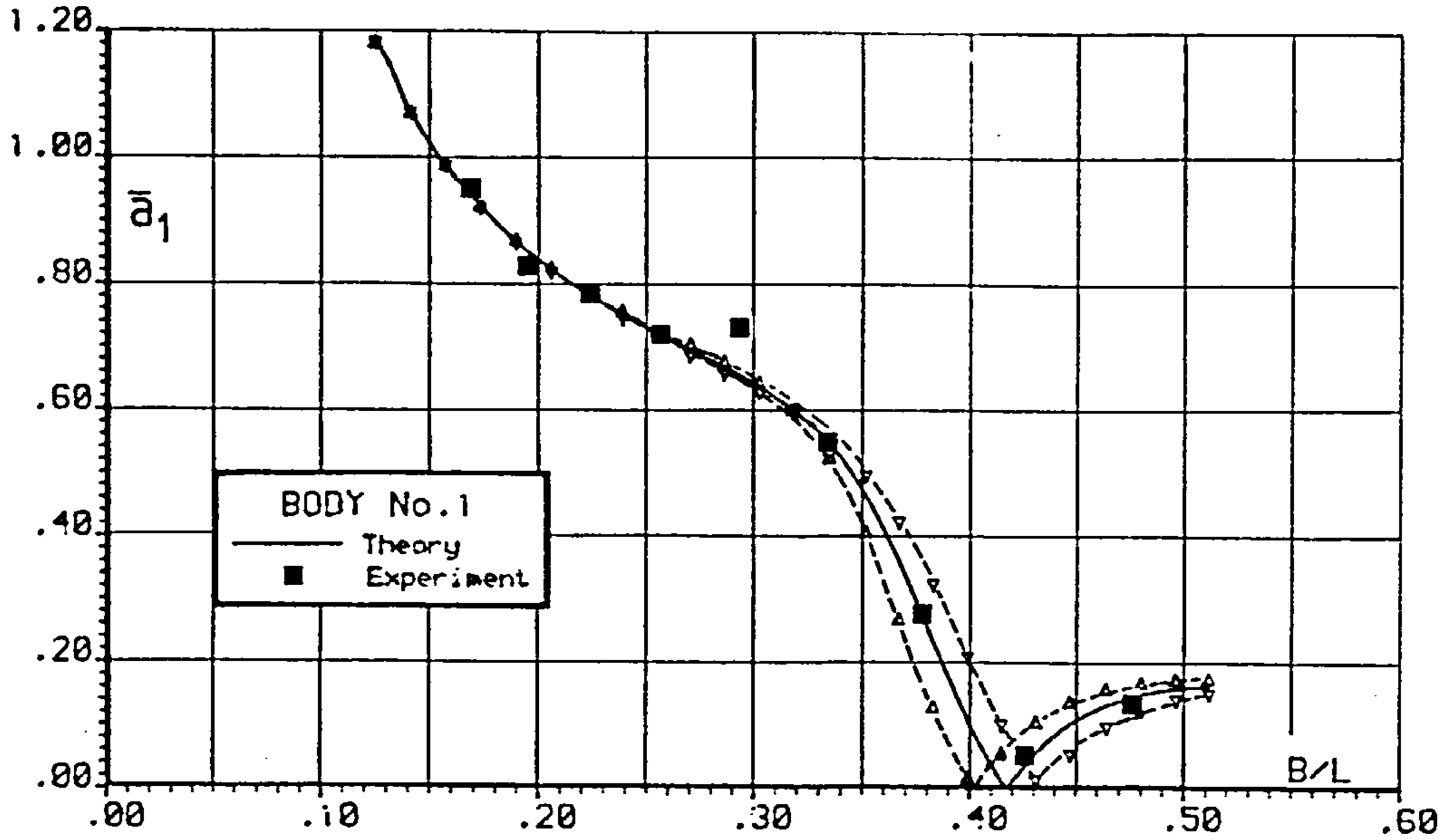

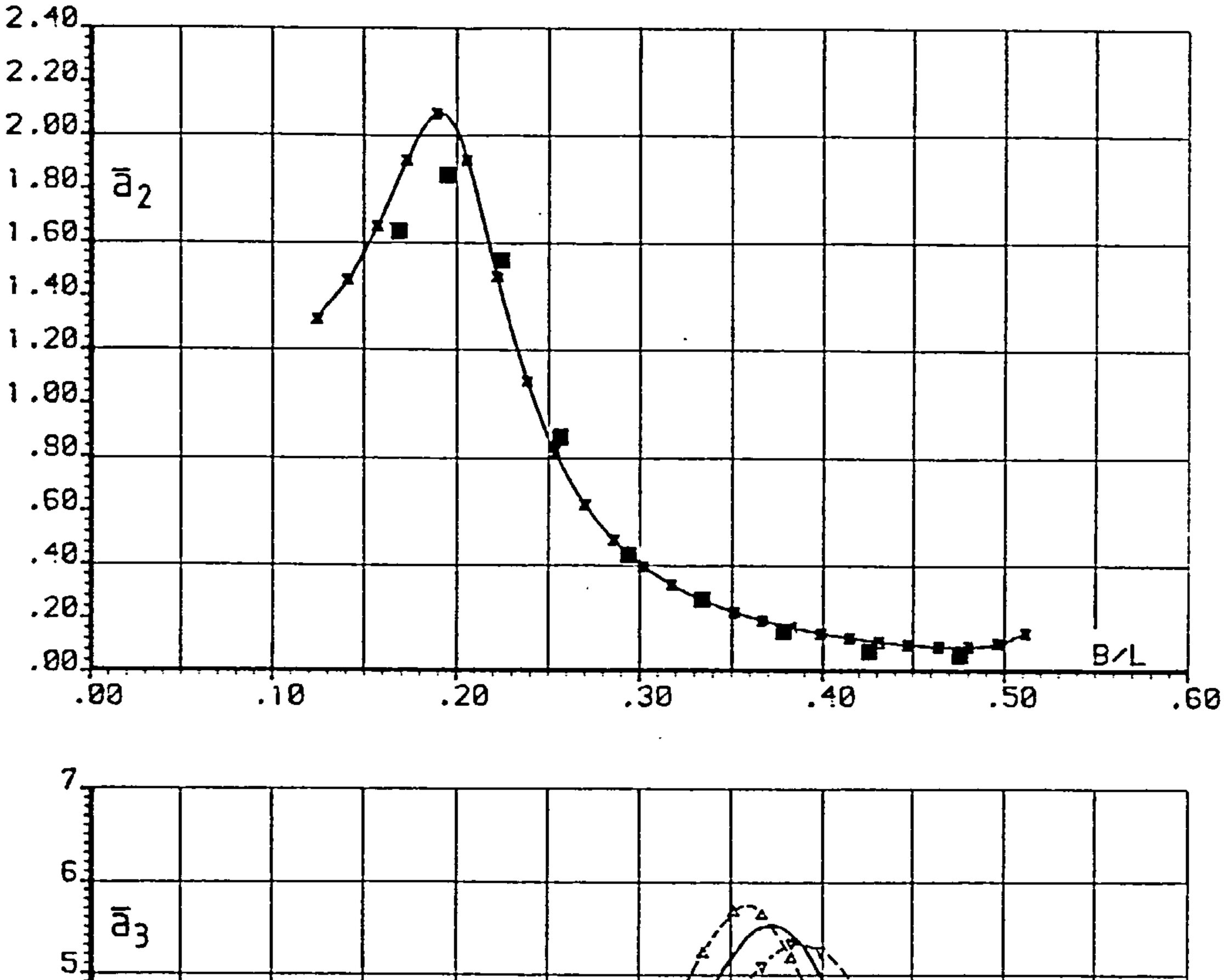

Fig. 6.57 FLOATING BODY MOTIONS

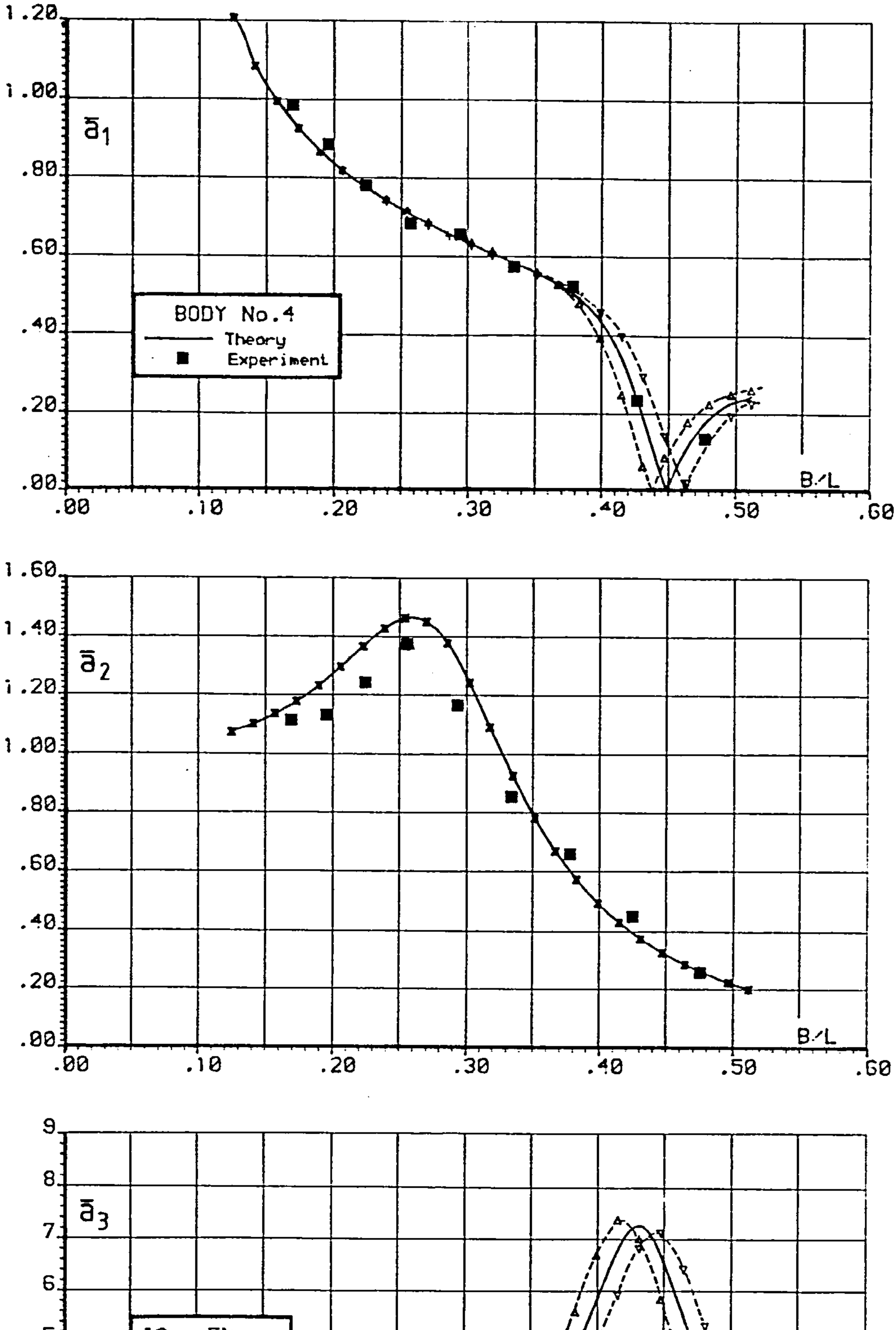

Fig. 6.58 FLOATING BODY MOTIONS

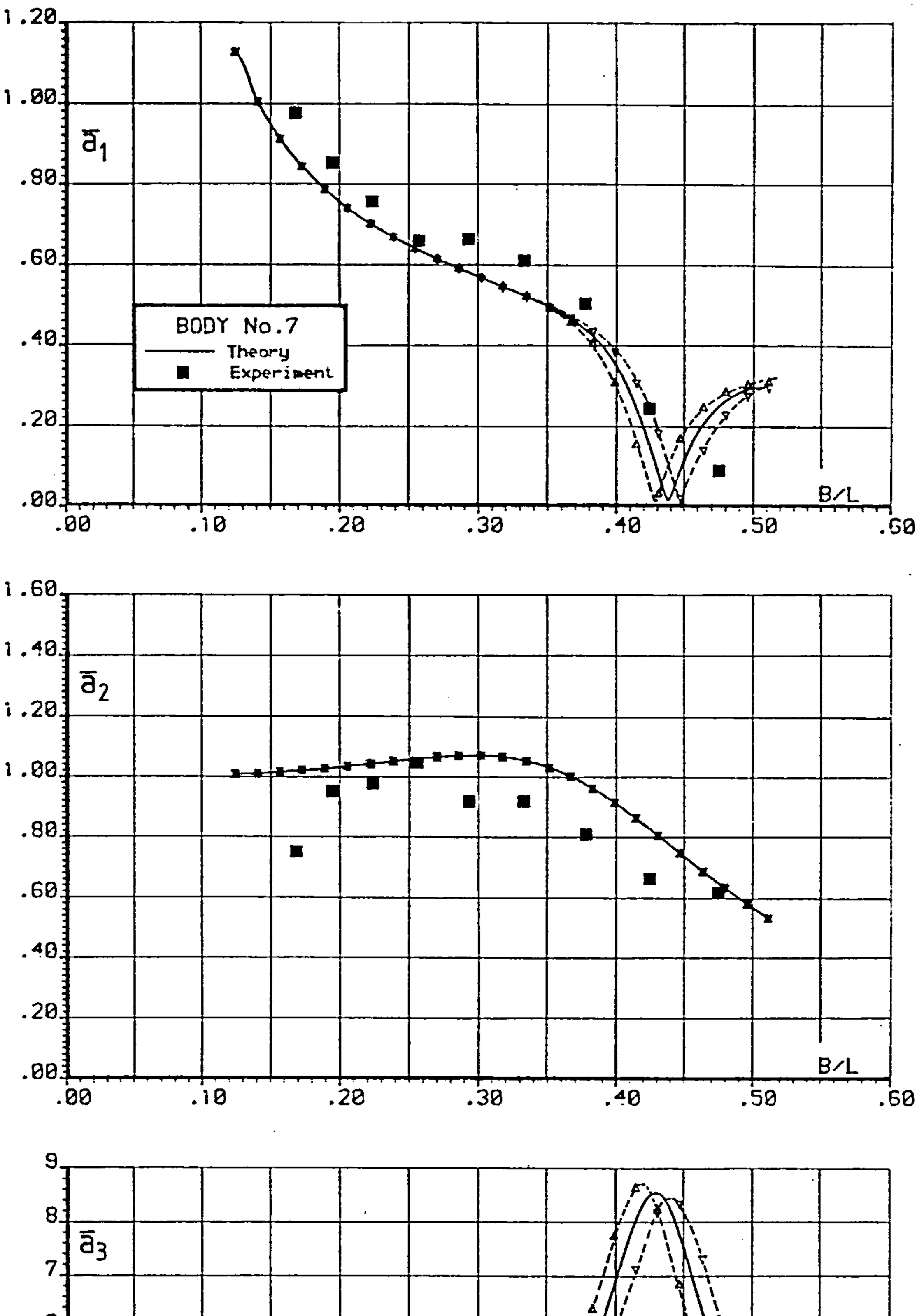

Fig. 6.59 FLOATING BODY MOTIONS

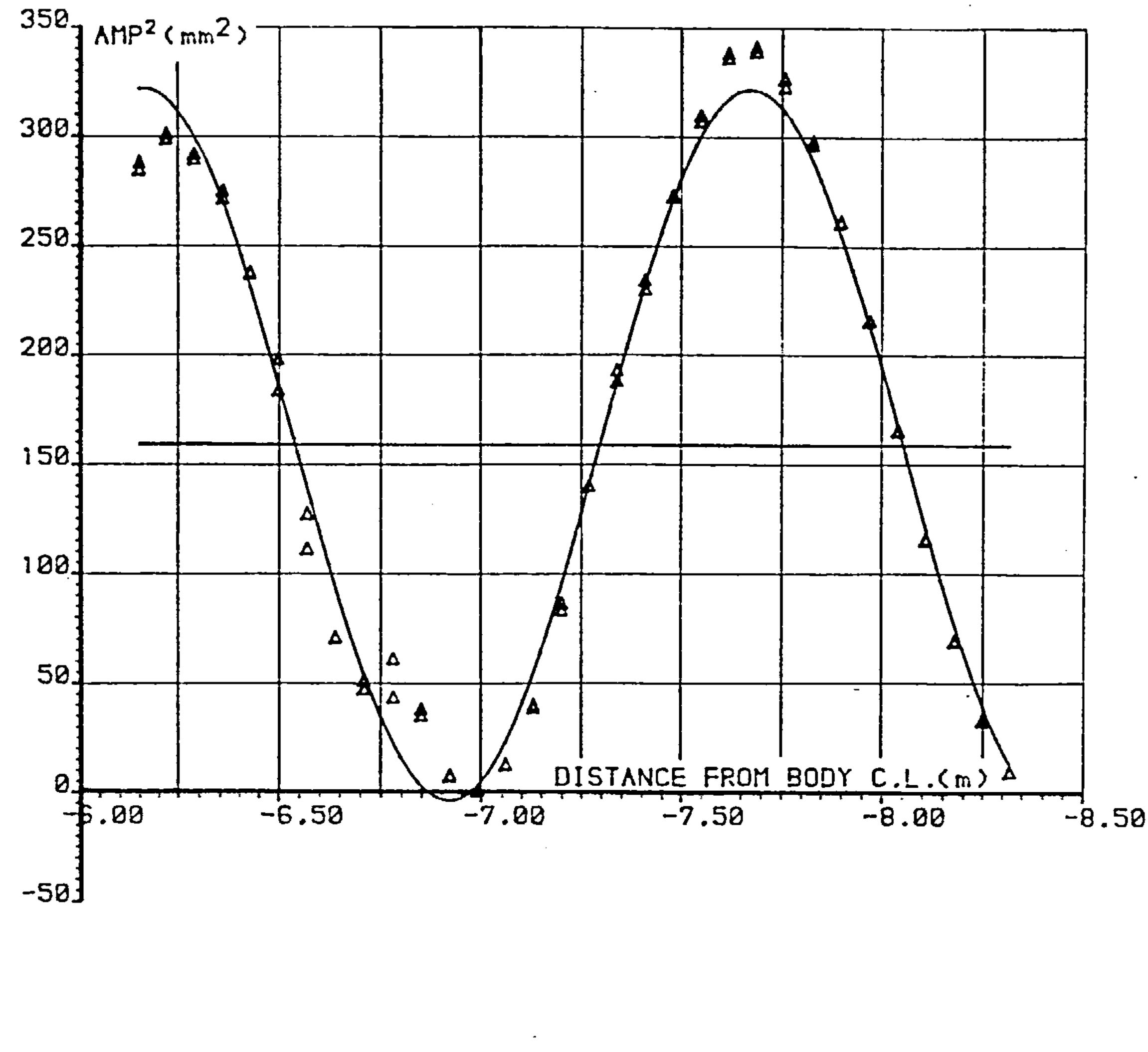

Fig.6.60 REFLECTED AND TRANSMITTED WAVE ANALYSIS

CHAPTER 7. DISCUSSION OF RESULTS.

7.1 Introduction.

The discussion of the main results of the investigation reported in this thesis commences with a consideration, in general terms, of the suitability of the various formulations available for the numerical solution of the generalised hydrodynamic interaction problem. In particular, the various integral equation formulations are considered in terms of their applicability to certain specific problems, together with the specific advantages and disadvantages associated therewith.

In view of the importance of achieving an efficient procedure for the solution evaluation, in terms of both accuracy and expenditure of time, a discussion is presented of the various computational aspects contributing thereto. Particular attention is paid to the problems associated with the discretisation of the immersed surface, for which numerical results have been presented as illustration.

The validation of linearised potential theory results, under controlled experimental conditions, is necessary if numerical methods are to be used with any degree of confidence. The experimental investigation reported in this thesis has been limited to the hydrodynamic interaction between a train of regular, small amplitude waves and a substantially rectangular obstacle which may be fixed or freely floating, and attempts have been made to determine how well the actual physics of the interaction can be predicted by linear diffraction theory. Physical mechanisms which

are not accommodated in the diffraction model are considered in an attempt to explain discrepancies between theory and experiment.

The dicussion of results is concluded by considering further improvements which may be made in the numerical formulations and procedures, both with regard to computational efficiency and the applicability of the method to generalised hydrodynamic integration problems. A discussion is also presented with regard to future investigations, both experimental and theoretical, which are recommended to enable the inclusion of non-linear effects in the theoretical formulations, with a view to improving the accuracy with which the actual hydrodynamic interaction can be predicted by theory.

7.2 The Numerical Results.

7.2.1 General Aspects.

If a solution is required for the potential theory problem of the interaction of a floating body with small amplitude waves in an essentially two-dimensional environment, there are a number of alternative numerical formulations which are available in this regard. The Finite Element Method, the Multipole Method, the Integral Equation methods and the Hybrid Element Method have all been used to varying extents and each has certain associated advantages and disadvantages which must be considered when assessing its suitability to any particular problem.

The most obvious disadvantage associated with the use of the

Multipole Method is the constraint imposed on obstacle geometry by the use of conformal mapping techniques. Such techniques limit the application of the method to solutions for simple axi-symmetric obstacle profiles which may be conformally mapped onto a circle (in the case of submerged bodies) or a semi-circle (in the case of partially submerged bodies), thus precluding the method's suitability for generalised solutions. Whilst no such constraints are imposed on the use of the Finite Element Method, the fact that the entire fluid domain must be considered gives rise to certain difficulties in obtaining a solution for problems in which the fluid domain extends to infinity in any direction. Unless such a formulation is used as part of a Hybrid Element scheme, it would appear that its usefulness is limited to domains of finite extent i.e. closed basins. It is therefore not unreasonable to suggest that the Integral Equation methods, in which the unknown velocity potential is represented by a distribution of fluid singularities over the domain boundary, are the most suitable for obtaining the generalised solution of the hydrodynamics problem. This suggestion is reinforced by the extensive use of such methods in research and design.

If the integral equation methods are to be regarded as the most suitable for the numerical solution of wave/obstacle interaction problems, it is relevent to consider which of the various formulations is to be preferred. Six possible formulations are available, these formulations being dependent on the choice of fluid singularity, the method of solution and the location of the source distribution boundary relative to the obstacle boundary. The earliest published solutions were for the wave-source 'indirect' formulation but subsequent investigations have included solutions

derived from the wave-source and simple-source 'direct' formulations. Most authors have preferred the wave-source (Green's Function) formulations, however, since their use results in a smaller system of equations.

This derives from the fact that automatic satisfaction of the free-surface, bottom boundary and radiation conditions by the Green's Functions precludes the necessity of considering the entire domain boundary. The automatic satisfaction of the far-field radiation conditions provides the additional facility of a solution check using the Principle of Conservation of Energy. Whilst several comparatively recent studies have investigated the use of the regular kernel integral equation method, in which the source distribution boundary is separate from the obstacle boundary, the majority of authors have indicated a preference for the singular kernel method in which the two boundaries are coincident. This preference is supported by the susceptibility of the regular kernel approach to numerical instability resulting from matrix ill-conditioning, particularly in the case of irregularly shaped profiles containing abrupt changes of geometry.

Further refinements include the use of linear and higher order elemental source strength distributions, as opposed to the more conventionally used constant elemental source strength, but results have indicated that no significant advantage can be derived therefrom.

For the above reasons, together with those detailed in Chapter 2, the numerical method chosen for this investigation was the 'indirect' Green's Function formulation using a source distribution

boundary coincident with the obstacle boundary.

7.2.2 Green's Function Evaluation.

One of the computational features associated with the use of the Green's Function Integral Equation method is that the vast bulk of CPU time, as a proportion of that required for the overall solution, is consumed in evaluating the Green's Function expressions for inclusion in the matrices required for the discretised solution of the unknown velocity potential. For an immersed surface subdivided into N boundary elements, whether the direct or indirect formulation is used, the overall solution requires the evaluation of $3N^2$ Green's Function expressions. It can therefore be seen that the efficiency with which each function is evaluated has a direct bearing on the overall solution efficiency, a feature which must be taken into account when assessing the viability of the method. For this reason, considerable effort has been devoted to achieving maximum efficiency in respect of Green's Function evaluation, resulting in a substantial reduction in overall computation time. Additionally, a considerable saving in CPU time has been effected by taking into account the axi-symmetry of the immersed surface and, hence, the symmetry of the Green's Functions. Full details can be seen in Chapter 4 of this thesis.

One of the factors directly affecting the efficiency and precision of Green's Function evaluation is the correct specification of convergence criteria to determine the point at which a sufficient number of iterations have been carried out to produce an acceptably precise evaluation. The importance of correctly specifying such

criteria is further emphasised by the fact that, in general, each iterative value is itself the result of a series of intermediate iterative procedures each of which has its own convergence criterion. Whilst considerable attention has been given to the investigation of convergence, it must be said that the relevant tests were performed on what was adjudged to be a representative sample of source/field point locations. The resultant criteria were taken to be those pertaining to 'worst-case' instances to ensure that all possible future evaluations would be sufficiently precise. It might be reasonably suggested, therefore, that a considerable number of function evaluations were computed from an excessive number of iterations, resulting in a somewhat spurious degree of accuracy. In order to minimise function evaluation time whilst maintaining acceptable precision, it is therefore suggested that further investigations are warranted in this regard using an exhaustive combination of the appropriate variables such as source/field point locations, still water depth, incident wave length etc.

Since the computer program described herein was constructed to provide theoretical predictions of the parameters associated with a particular range of experimental conditions, all of which may be classified as pertaining to intermediate depth, no account was taken of the approximate forms of the Green's Functions relating to deep and shallow water conditions. Since any future investigation would entail solutions pertaining to both conditions, it is felt that inclusion of the appropriate modifications in the relevant routines would be advantageous.

7.2.3 Element Distribution.

The continuous formulation of the problem indicates that the resultant integral equation be satisfied at all points on the source distribution boundary. In order to obtain a discretised solution, it is necessary to relax this requirement and apply the condition at a discrete number of control points, those points being the centroids of the boundary elements. As a consequence of this relaxation, together with certain assumptions made in regard of the elemental variation of the source strength and Green's Function, the eventual solution is an approximation. As indicated by previous authors, the closeness of this approximation to the 'true' solution is highly dependent on the efficiency of discretisation of the source distribution boundary.

In the case of a substantially rectangular immersed profile, two factors have the most significant effect on the efficiency of discretisation: the precision with which the submerged radial edges are modelled and the relative dimensions of adjacent elements. The former factor is determined by the number of constant length elements (N_C) on each submerged radial edge and the latter by the nominal element length ratio (E.L.R.) as defined in Appendix A5. Both factors are considered separately for the fixed and floating modes of the obstacle.

a) <u>Fixed Mode</u>

It can be seen from Fig.6.1, pertaining to the fixed mode reflection and transmission characteristics of body No.1, that the sensitivity

of the solution to changes in element length ratio increases dramatically with increasing values of the diffraction parameter. This behaviour may be attributed to the proximity of the first 'irregular' frequency (see section 4.9.1) associated with this particular body configuration which, using equation 4.9.2, is equivalent to a diffraction parameter value of 0.545. It can clearly be seen that, as suggested in section 4.9.1, both the magnitude and extent of the effects associated with the irregular frequency are substantially reduced by employing a more precise boundary discretisation. It must be noted however that, for relatively coarse levels of discretisation, the onset of numerical instability is more gradual than previously suggested in section 4.9.1. In the case of solutions which are less well-behaved than those illustrated, this could result in a failure to identify the occurrence of an irregular frequency, particularly if the body configuration is sufficiently complex to preclude prior evaluation of the irregular frequency, leading to an erroneous interpretation of results.

It is fortunate, however,that application of the Principle of Energy Conservation provides a check on the accuracy of the solution. The proximity of an irregular frequency can be readily identified by inspection of the energy residual $(1-R^2-T^2)$ which dramatically increases in magnitude in the event of numerical instability, emphasising the inadvisability of considering individual solutions in isolation.

The results presented in Fig.6.4, pertaining to a change in submerged radial edge discretisation for the same body configuration, indicate little or no evidence of the proximity of an irregular frequency. Comparison with the corresponding results in

Fig.6.1, however, suggests that the initial level of discretisation is sufficiently precise to minimise numerical instability and that any further increase in discretistion precision is superfluous in this regard.

As detailed in section 4.4, the secondary regular component of the Green's Function oscillates in value with a wavelength of comparable magnitude to that of the incident wave, enabling the simplifying assumption to be made that the function remains virtually constant over the extent of any particular boundary element. This, of course, is subject to the proviso that the element dimension is small in comparison to the incident wavelength. It would, therefore, be reasonable to expect higher frequency solutions to exhibit greater sensitivity to increasingly precise discretisation than lower frequency solutions. Notwithstanding the effects of irregular frequency proximity, the results presented in Figs.6.1 to 6.6 exhibit no consistent pattern in this regard suggesting that, at this level of discretisation, the above assumption may be regarded as valid for all practical and experimental purposes.

An interesting feature, associated with the variation of solution sensitivity to increasing levels of discretisation over a range of values of the diffraction parameter, is illustrated in Fig.6.3 and, to a lesser extent, in Fig.6.2. In these cases, contrary to logical expectations, the sensitivity actually <u>decreases</u> with increasing values of the diffraction parameters. The results presented in Fig.6.4 exhibit a similar pattern of behaviour compounded with a variation of results inconsistent with an increased precision of discretisation. Examination of results, not presented herein, shows that this behavioral inconsistency is reflected by a similar

variation of associated energy residuals. It is reasonable to suggest, therefore, that the solution inaccuracies may be associated with variations in numerical conditioning of the matrix equations used to derive the discretised source strength distribution function. However, it can be seen that, for the fixed body configurations investigated, any inaccuracies resulting therefrom are small and may be regarded as insignificant for all practical and experimental purposes.

It can be seen from Fig.6.3 that solution sensitivity to changes in discretisation is markedly increased for shallow draught bodies. However, it is not clear from the results whether the increased sensitivity derives from the large aspect ratio of the body or the proximity of the body to the free-surface. Nevertheless, the results provide a clear indication of the necessity for further investigation to be carried out in respect of the discretisation of shallow draught immersed surfaces.

b) Floating Mode

Comparison between the results presented in Figs.6.1 to 6.6 and those presented in Figs.6.7 to 6.12 demonstrates clearly that, notwithstanding the difference in overall behavioral trends, the reflection and transmission characteristics pertaining to the floating body mode are significantly more sensitive to discretisation changes than the equivalent fixed body mode results. Since the discretised solution of the integral equation (see sections 4.2.1 and 4.2.2) requires the use of identical coefficient matrices for both modes, the difference in sensitivity must be

attributable to the three degrees of motional freedom associated with the floating mode.

As with the fixed body case, for reasons connected with the oscillation of the regular part of the Green's Function, it would be reasonable to expect a gradual increase in discretisation related solution sensitivity with increasing values of the diffraction parameter. As a consequence of the similarity of all three function expressions, it would also be reasonable to expect this gradual increase in sensitivity to be equally evident in all three modes of motion. Figs.6.13 to 6.18 show that, whilst the surge and pitch motion solutions appear to exhibit such a trend, the corresponding heave motion solutions only demonstrate a significant degree of sensitivity in the vicinity of the body's resonant frequency pertaining to that mode. Additionally it can be seen that, notwithstanding the effects of numerical instability induced by the proximity of an irregular frequency, the heave solutions exhibit little or no sensitivity to changes in discretisation precision at comparatively high incident wave frequency conditions. It would therefore be reasonable to conclude that, for the cases investigated, it is perfectly valid to assume that the Green's Function is constant over the extent of any individual element.

It must therefore be suggested by process of elimination that, within certain ranges of value of the diffraction parameter, the spacial variation of the source strength distribution function is such that it is no longer valid to assume a constant source strength over the extent of each boundary element. On the basis of the results presented, however, it is not possible to assess whether the invalidity of the assumption applies to all boundary elements or,

perhaps, merely to those in the vicinity of abrupt variations in the geometry of the immersed surface. Although the solutions for all three modes of motion exhibit increased sensitivity to discretisation in the vicinity of the modal reasonant frequency, the scope of the numerical investigation is insufficiently comprehensive to determine whether the two factors are related or whether the connection is merely fortuitous.

An interesting feature arising from a comparative evaluation of the body motion solutions is the fact that the sensitivity of the surge and pitch solutions increases for shallow draught bodies whilst the sensitivity of the corresponding heave solutions appears to be unrelated to changes in draught. Since the heave motion of the body is dependent on a distribution of potential sources only over those sections of the immersed surface having horizontal orientation components, and is independent of both surge and pitch motion, the conclusion must be reached that the spacial rate of change of source strength over these parts of the surface does not significantly change with increasing proximity to the free-surface. In this light, therefore, it is logical to suggest that increasing proximity to the free-surface induces an increase in the rate of spacial variation of the source strength distribution function over those regions of the immersed surface having vertical orientation components, such that the assumption of a constant elemental source strength no longer remains valid. This suggestion is supported by the dependence of both surge and pitch motions on the distribution of sources thereon.

In the case of substantially rectangular bodies of the type investigated herein, this would indicate the need at shallow draughts for a higher level of discretisation precision on the vertical sides of the immersed surface than on the horizontal base.

7.3 The Experimental Results.

7.3.1 Fixed Body Reflection and Transmission.

A major feature of wave/obstacle interaction, pertaining to the fixed body mode, may be seen in Fig.6.41 which shows the variation of the experimentally measured energy conservation characteristic (R^2+T^2) with respect to the diffraction parameter. The pattern of results clearly demonstrates that a loss of energy is incurred in the interactive process, the magnitude of which systematically increases with increasing values of the diffraction parameter.

It can be seen from Figs.6.19 to 6.26 that, in general, the experimentally measured transmission coefficients agree acceptably with theoretical prediction throughout the whole range of values of the diffraction parameter. The agreement between theory and experiment of the corresponding reflection coefficients is, at the lower end of the diffraction parameter range, of a lesser order but can nevertheless be regarded as acceptable for practical purposes. At the higher end of the diffraction parameter range, however, the experimentally measured reflection coefficients become substantially less than the theoretical predictions to an extent far in excess of that which might be attributable to normal experimental error. It is therefore reasonable to conclude that the above-mentioned overall energy loss is largely attributable to substantial energy losses incurred in the wave reflection process. It is worth noting that this concurs with the conclusion reached by Dean and Ursell[15] following a similar form of investigation carried out on a fixed, semi-immersed circular cylinder.

In view of the above conclusion, the comparative magnitudes of the appropriate reflection and transmission coefficients indicate that an increase in energy loss may be associated with an increase of wave amplitude. Similarly, the variation of the energy conservation characteristic with respect to the diffraction parameter suggests that energy loss increases with increasing wave frequency. A combination of these two variational dependencies indicates an implied relationship between energy loss and wave particle velocity. As a consequence, it is reasonable to suggest that the loss of energy may be attributed to the onset of viscous flow separation, induced by high wave particle velocities and resulting in the shedding of vortices at body locations with high curvature, i.e. sharp corners or edges. The validity of this suggested source of energy loss is supported by the observed presence of free-surface vortices in the immediate vicinity of the body. Although the density of these observed vortices increased with higher incident wave frequency conditions, it must be suggested that their structure and location indicated possible emanation from the sharp vertical end corners of the body.

The results of previous investigations[7], on the effects of vortex shedding by sharp cornered fixed bodies in oscillatory flow, have indicated that vortex shedding is not only dependent on wave particle velocity but also on the degree of sharpness and included-angle of the body edges. It would be reasonable, therefore, to expect the discrepancy beween experimentally measured and theoretically predicted values of reflection and transmission coefficients to increase with decreasing radius of the submerged radial edges of the body. It can be seen from Figs.6.27 to 6.29 that no consistent trend is exhibited in this regard. It is therefore

reasonable to suggest that the relationship between vortex shedding and edge sharpness is highly non-linear and that, at this level of edge rounding, the rate of change of vortex shedding with respect to edge sharpness is sufficiently small to preclude identification of the effects of differing edge radii by the experimental techniques described herein.

Notwithstanding the absence of any detectable dependence on submerged edge radius, the deviation between theory and experiment of the reflection coefficients exhibits a noticeable dependence on body draught. It can be seen from Figs.6.19 to 6.29 that the experimentally measured reflection coefficients start to deviate from theoretical prediction at wave frequencies which become progressively lower as body draught decreases, giving a clear indication of the increase in interactive energy loss with increasing proximity to the free-surface. Since wave particle velocity increases non-linearly with proximity to the free-surface, this behavioral trend provides further support for the suggestion that the deviation between theory and experiment is attributable to the effects of vortex shedding. It might also be suggested that a proportion of the deviation is attributable to a violation of linear boundary conditions in the highly non-linear free-surface zone.

Figs.6.27 to 6.29 illustrate an interesting trend of deviation between theory and experiment pertaining to the transmission characteristics of the fixed body. It can be seen that, irrespective of submerged edge radius and body draught, the experimentally measured transmission coefficients exceed the corresponding theoretical predictions by a magnitude which systematically increases with increasing frequency of wave motion. In the absence

of any other obvious cause associated with the hydrodynamic interaction, and notwithstanding any increase in measurement error of the small amplitude transmitted waves (see section 6.8.6), intuitive reasoning suggests that such a trend would result from slight horizontal body movements attributable to a lack of rigidity of the body support structure. Such movements were observed in the course of the investigation, although it was felt at the time that they would not be a significant source of error.

7.3.2 Floating Body Reflection and Transmission.

It can be seen from Fig.6.42, showing the variation of energy conservation characteristic with respect to the diffraction parameter, that the same trend of energy loss is demonstrated with the floating body as with the fixed body, namely an increase of energy loss with increasing wave frequency. Comparision of Fig.6.42 with Fig.6.41 demonstrates, however, that the general magnitude of energy loss associated with the floating body/wave interaction is significantly greater than that associated with the fixed body. Since the floating mode possesses three additional degrees of motional freedom, it is not unreasonable to expect such a phenomenon.

Comparison of the numerical results presented in Figs.6.7 to 6.12 with those presented in Figs.6.13 to 6.18 demonstrates that, for a given change in discretisation precision, the variation of reflection and transmission is disproportionately greater than the variation in corresponding body motions. This serves to illustrate the high degree of sensitivity of the reflection and transmission

coefficients to minor variations in body motion. The inference may be drawn that comparatively small discrepancies between the experimentally measured and theoretically predicted body motions would result in substantially larger discrepancies in the corresponding reflection and transmission characteristics. It is therefore suggested that no meaningful conclusion may be derived from a comparison between fixed and floating body results in terms of the relative magnitude and trend of discrepancy between theoretical and experimental values of the reflection and transmission characteristics.

In deriving the theoretical predictions of the wave-effects associated with the interaction between a floating body and a train of regular waves, a fundamental assumption is made that the overall wave-effect consists of a linear superposition of the effects associated with the fixed mode and those associated with each degree of motional freedom. Using the theoretically derived generated wave ratios in conjunction with the experimentally measured values of amplitude and phase of each motion, it is possible to predict the wave-effects associated with the actual motions, thus permitting a more meaningful conclusion to be reached from examination of the discrepancies. In view of the localised wave effects associated with the interactive process, however, experimental measurement of the phase of each motion relative to the incident wave would require a comparison of body motion phase with that of the wave train at some distance from the floating body. It was felt that, as a consequence of irregularities in flume dimensions, the error associated with the extrapolated phase difference would be too large to enable derivation of an acceptably accurate, and therefore meaningful, prediction of reflection and transmission. Aside from that, however,

there exists no method of experimentally analysing the overall wave profile to enable resolution of the various components associated with each mode. As a consequence, it would not be possible to make an assessment of the relative discrepancies between theory and experiment associated with each mode of motion, thereby rendering the exercise largely pointless.

Notwithstanding the above shortcomings, however, the experimental results presented in Figs.6.30 to 6.37 show a distinct conformity with theoretical predictions in terms of variational trend, if not in magnitude, throughout the whole range of values of the diffraction parameter. Of the reflection and transmission characteristics, the only parameter of practical significance is the transmission coefficient in the context of floating breakwater design. If the results presented in Figs.6.30 to 6.37 are examined in this context, it is encouraging to note that, where significant discrepancies exist between theory and experiment, the experimentally measured transmission coefficients are generally lower than those predicted by theory.

7.3. Floating Body Motions.

a) Surge Motion

It can be seen from Figs.6.43 to 6.45 that, for the body configurations pertaining to an immersed surface aspect ratio of 2, the experimentally measured amplitudes of surge motion agree excellently with the theoretically predicted values throughout the entire range of values of the diffraction parameter. It can be seen

from Fig.6.57, in conjunction with Figs.6.13 and 6.16, that any discrepancies between theory and experiment are within the acceptable limits associated with measurement error, systematic errors resulting from variations in rotational inertia, and discretisation-related inaccuracies in the theoretical predictions.

A noticeable exception to this trend of agreement is the experimentally measured amplitude of surge motion pertaining to a diffraction parameter value of 0.293. It can be seen from Figs.6.43 to 6.45 that, in comparison with adjacent results, the discrepancy between theory and experimental appears to be somewhat abnormal. Fig.6.51 shows that, for each body configuration within the immersed surface aspect ratio grouping, the discrepancy is virtually identical thereby precluding the possibility of a random error. Additionally, the wave analysis results and raw surge measurement data (not presented herein) display no evidence of instability in either the wave regime or body motions. It is particularly interesting to note that, despite the coupling effect between pitch and surge, the corresponding pitch motions are apparently unaffected. In this light, it is not unreasonable to suggest that the discrepancy is related in some way to the inherent resonant frequency characteristics of the mechanical system in the horizontal mode of motion, as opposed to the hydrodynamic interaction between the wave train and the floating body.

The results presented in Figs.6.46 to 6.50 show that the experimentally measured surge motions pertaining to those body configurations having immersed surface aspect ratios of 4 and 8 demonstrate less good agreement with theoretical predictions. Nevertheless, it can be seen that the general trend of deviation

between theory and experiment is consistent within each immersed surface aspect ratio grouping. Examination of Figs.6.52 and 6.53 shows that the general magnitude of the deviations increases with decreasing body draught, suggesting the source of deviation to be associated with proximity to the free-surface. Furthermore, Fig.6.52 illustrates a distinct pattern of deviation, for body configurations having an immersed surface aspect ratio of 4, consistent with decreasing radius of the submerged edge of the body. The same trend is exhibited in Fig.6.53 although the absence of a third body configuration within this aspect ratio group must give rise to a certain degree of uncertainty over the continuity of the trend. Notwithstanding this uncertainty however, it is reasonable to conclude that the deviation between experimentally measured and theoretically predicted surge motion increases with increasing 'sharpness' of the immersed edges of the floating body and also with increasing proximity to the free-surface.

As with the fixed body case, this deviatory trend indicates the presence of vortex shedding effects induced by viscous flow separation at the body edges. However, intuitive reasoning suggests that vortex shedding effects, as a consequence of the surge motion of the body, would result in the experimentally measured surge being somewhat less than the theoretical prediction. It can be seen from Figs.6.46 to 6.50 that this is not the case, the experimentally measured amplitude of motion being generally greater than theory to an extent which increases with edge sharpness and proximity to the free-surface. In the absence of any other feasible explanation for this behavior, it must be suggested that the deviation between experiment and theory is, by virtue of cross-coupling effects, largely attributable to the theoretical and experimental deviation

of the corresponding pitch motions of the body. This suggestion is supported by the fact that, with the exception of results pertaining to frequencies in the immediate vicinity of the pitch resonant frequency, the deviations between theory and experiment for pitch and surge exhibit distinctly similar trends. Examination of Figs.6.57 to 6.59 suggests, however, that the surge deviations are far greater than would be expected from cross-coupled pitch deviations alone. In this light, it is not unreasonable to conclude that the actual cross-coupling parameters are significantly different from those predicted by theory.

b) Heave Motion

The results presented in Figs.6.43 to 6.45, pertaining to body configurations having an immersed surface aspect ratio of 2, show that the experimentally measured heave motions of the body agree excellently with those predicted by theory over a substantial proportion of the diffraction parameter range. It can be seen, however, that significant deviations between theory and experiment occur in the vicinity of the diffraction parameter value pertaining to the body's resonant frequency in the heave mode, the experimentally measured heave motion always being less than theoretically predicted. Figs.6.46 to 6.50 show that, whilst this deviatory trend is maintained for body configurations having immersed surface aspect ratios of 4 and 8, a decrease in body draught has the effect of increasing the range of diffraction parameter values over which this 'localised' increased deviation occurs. It must be suggested, however, that this is probably related to the fact that a decrease in body draught results in a more gradual increase of heave motion as the frequency of motion

approaches the modal resonant frequency. Examination of Figs.6.51 to 6.53, illustrating the trends of deviation between theory and experiment with respect to the diffraction parameter, shows that within each immersed surface aspect ratio grouping, the magnitude of deviation in the vicinity of the modal resonant frequency increases consistently with increasing 'sharpness' of the submerged radial edge. It is therefore reasonable to suggest that the deviations are attributable to viscous flow separation, and consequence vortex shedding, induced by severe velocity gradients in the immediate vicinity of the submerged edges of the body.

A feature of interest arises from examination of Figs.6.49 and 6.50. It can be seen that, at relatively low frequencies, the experimentally measured heave motions are substantially lower than the theoretical predictions despite the fact that the heave amplitude of the body is of a similar order of magnitude to the amplitude of the incident wave. This deviation is explained by the fact that the heave motion of the body, within this frequency domain, is approximately 180° out of phase with the incident wave, resulting in high velocity gradients in the immediate vicinity of the body/fluid interface, thus supporting the suggestion that vortex shedding effects are a function of the <u>relative</u> velocity of the body and adjacent fluid.

c) <u>Pitch Motion</u>

It has generally been accepted, from the results of a considerable number of experimental studies in this field, that the effects of vortex shedding induced by viscous flow separation are more significant in the context of rotational body motions than in the

context of translatory motions. Previous studies have further indicated that the most significant deviations between theory and experiment, due to this phenomenon, occur in the vicinity of the modal resonant frequency. The results presented in Figs.6.43 to 6.50 confirm this behaviour and demonstrate that the amplitude of pitch motion at the modal resonant frequency can be reduced by as much as 35% by the effects of viscous flow separation.

Apart from these localised deviations, however, the experimental results over the remaining range of values of the diffraction parameter demonstrate excellent agreement with theory. It must also be stated that, unlike the results pertaining to the surge and heave body motions, no significant draught-related general increase in deviation is evident. As a consequence of the relatively coarse frequency distribution of results over the range within which the localised large deviations occur, the deviations presented in Figs.6.51 to 6.53 do not exhibit any obvious behavioral trends consistent with a decrease of submerged edge radius. It would, therefore, be unwise to infer such a relationship from the results presented herein.

Notwithstanding the fact that the deviations between theory and experiment, outwith the immediate vicinity of the modal natural frequency, are within the acceptable limits of measurement error, inertial variation and discretisation-related numerical inaccuracies in the theoretical predictions, the trend of deviations illustrated in Figs.6.51 to 6.53 suggests the experimental results are consistently greater than the theoretical predictions. Since this trend pertains to all of the body configurations investigated, the presence of a systematic error is indicated. In order to comply with

the assumptions made in connection with the simplified equations of motion, each body was constrained to rotate about a transverse axis passing through the centroid of the body. As a consequence of the size and mass of the body, it was not possible to physically check the centroidal axis as computed from the mass and relative location of the constituent components of the body and ballast. It can be reasonably suggested, therefore, that the body was constrained to rotate about an axis marginally lower than the true centroidal axis. This may have been due to a computation error or, alternatively, a systematic physical error associated with the precise location of the pitch rotation bearings.

An interesting feature, pertaining to the magnitude of the theoretically predicted amplitude of pitch motion at the modal natural frequency, can be seen from comparison of Figs.6.43, 6.44 and 6.57. The results presented in Fig.6.57 show that, for body configuration No.1, a 5% increase of inertia without a change of body geometry results in an increase of resonant pitch amplitude of a comparable order of magnitude. However, comparison of the theortical predictions presented in Figs.6.43 and 6.44 shows that a reduction in submerged edge radius from 120mm to 60mm, equivalent to an increase in rotational inertia of 1.5%, results in a 17% increase in resonant pitch amplitude for the same immersed surface aspect ratio. It may therefore be concluded that the increase in resonant pitch amplitude, associated with a decreased edge radius, is attributable to the change in body geometry rather than the associated inertial increase. This sensitivity is displayed by the corresponding experimental results, thereby emphasising the importance of precise geometric construction of the body in the context of future experimental investigations in this field.

7.4 Conclusions and Recommendations.

The results of the numerical investigation, and subsequent discussion thereof, have shown that the singular kernel, indirect solution of the Green's Function Integral Equation formulation is a suitable method for obtaining the numerical solution to the hydrodynamic problem of the interaction between a fixed or freely floating body and a train of regular waves.

Notwithstanding the considerable improvements in computational efficiency which have been achieved without significant loss of solution accuracy, it is felt that additional improvements may be made, in this regard, following the results of further investigations as recommended hereunder. For purposes of clarity, the recommendations are presented in list format.

(1) The most significant factor affecting the efficiency and accuracy of evaluation of the Green's Function expressions, with consequent effect on the overall solution, is that pertaining to numerical convergence of the integral and series form thereof. It is recommended that further numerical tests be carried out, using a comprehensive range of combinations of the appropriate variables, to determine the convergence criteria which would result in an optimised function evaluation in terms of computation time and precision.

(2) In order to improve the efficiency of solution for a comprehensive range of incident wave and flume conditions,it is recommended that routines be included in the computer program to facilitate use of the appropriate deep and shallow water

approximations of the Green's Function expressions. It is further recommended that tests be performed, for a comprehensive range of flume conditions and body configurations, to determine the range of validity of these approximations.

(3) It has been shown that the numerical solutions are, under certain conditions, extremely sensitive to variations in the level of discretisation of the immersed body surface. Whilst considerable improvements have been achieved with regard to the efficiency of discretistion by the use of the element distribution format described herein, it is suggested that further investigation be carried out in respect of the validity of assuming a constant source strength distribution over the extent of each boundary element. For the particular case of substantially rectangular bodies, it is recommended that a series of numerical evaluations of the source strength distribution function be carried out, for a comprehensive range of body aspects, flume depths and diffraction parameter values, to determine the variation of source strength with respect to the immersed body surface. It is felt that the results of such tests will enable the determination of more precise rules of element distribution such that the above assumption is valid under all conditions.

(4) It has been suggested that the overall solution accuracy is adversely affected by the effects of matrix ill-conditioning, the occurrence of which is related to the discretisation of the immersed body surface. It is therefore recommended that the matrix solution routines in the computer program be extended to include facilities for computing a 'conditioning number',

details of which can be found in a number of texts on matrix operations, to assist in the identification of unsuitable discretisation schemes.

(5) It has been demonstrated that the sensitivity of solutions to different levels of discretisation varies for each mode of motion of the floating body. Owing to the cross-coupling of certain motions, together with the method of simultaneous solution for the appropriate velocity potential components, the use of separate discretisation schemes for each mode of motion is <u>not</u> recommended for a freely floating body.

The experimental study was designed primarily to examine the validity of the theoretically predicted parameters, derived from the formulations detailed in this thesis, pertaining to the interaction between a train of small amplitude regular waves and a substantially rectangular body in fixed and/or floating mode. By investigating the behaviour of the body over a suitable range of values of the diffraction parameter, it was additionally intended to examine the extent of validity of linearised potential theory within regimes where diffraction effects predominate.

The results obtained indicate that the theoretical formulations provide a good representation of the wave refection and transmission characteristics of the body at the lower end of the diffraction parameter range. As the body dimension increases with respect to the incident wave length and diffraction effects become increasingly dominant, a progressively increasing loss of energy is incurred in the system. The general magnitude of the energy loss is significantly greater in the case of the floating body than in the

case of the fixed body.

In the case of the fixed body, the general trend of results indicates this energy loss to largely associated with the wave reflection process, resulting in singificant deviations between the experimentally measured reflection coefficients and those predicted by theory for values of the diffraction parameter greater than about 0.3. The experimentally measured transmission coefficients, however, demonstrated good agreement with theory, within the limits of practical significance, throughout the entire range of values of the diffraction parameter.

As a consquence of the high degree of dependance of the floating body reflection and transmission characteristics on the motions of the body, together with an inability to resolve the combined wave profile into the individual components associated with each degree of freedom, a firm conclusion cannot be reached with regard to the limits of validity of the theoretically-predicted wave effects with respect to the diffraction parameter.

It would be reasonable, however, to assume that the theoretical predictions pertaining to the individual generated wave components are valid over a similar range to that associated with the corresponding body motions.

The agreement between theoretical and experimental surge motion amplitudes is excellent, over the entire range of values of the diffraction parameter, for substantially-draughted bodies but gradually deteriorates with decreasing body draught. For body configurations of constant draught, the deviation between theory and

experiment increases with increasing sharpness of the submerged edges of the body. It is suggested, however, that these deviations may be largely associated with cross-coupling effects between pitch and surge motions, rather than effects associated with surge motion *per se*.

The standard of agreement between theoretical and experimental heave motions is generally of the same order as that pertaining to surge motion although the deterioration associated with decreasing body draught is more rapid. The most significant deviations between theory and experiment occur in the vicinity of the resonant frequency of the body in the heave mode and are substantially greater than would be acceptable for practical purposes.

In general, the agreement between theoretically-predicted and experimentally-measured amplitudes of pitch motion is excellent and exhibits no draught-related deterioration. As with the heave motions, however, unacceptably large deviations between theory and experiment are incurred in the immediate vicinity of the modal resonant frequency.

For reasons discussed in the preceding sections, it is suggested that the major discrepancies between theory and experiment, for both fixed and floating bodies, may be directly attributed to the effects of vortex shedding induced by viscous flow separation at locations of abrupt changes, in geometry of the immersed surface of the body. It must therefore be stated that, notwithstanding any improvements in solution techniques which may results from further numerical investigation, the application of linear diffraction theory to the solution of hydrodynamic interaction problems is of somewhat

questionable validity unless such effects are considered in the derivation of the theoretical formulations.

The significance of vortex shedding, in the context of rotational body motions in the vicinity of the modal resonant frequency, has long been recognised. Previous investigators in this field, noting the damping effect of vortex-shedding forces on rotational motions, have corrected for this effect by including an additional component in the potential damping term in the equations of motion, resulting in a marked improvement in agreement between theory and experiment for the particular model under consideration. Although the application of this correction factor has the desired effect, its magnitude can only be determined *a posteriori* by empirical means from the results of model testing, suggesting its somewhat limited validity in the context of theoretical prediction. Notwithstanding the fact that it is no doubt possible, from the results of an exhaustive series of model tests, eventually to derive an empirical relationship between the magnitude of this corrective term and factors such as the fluid viscosity, the velocity of body motion and the geometry of the body, the highly probable existence of non-linear scale effects must raise certain doubts regarding the validity of this approach in terms of the derivation of a generalised viscous damping correction.

The results of this study indicate that vortex shedding effects are not limited entirely to rotational body motions. It has been demonstrated that the effects are equally significant in regard to the heave motions and also in regard of the interaction between a wave train and a fixed body. The apparent ubiquity of such a phenomenon provides further emphasis of the unsuitability of the

above-mentioned empirical approach and suggest the urgent necessity for a more fundamental examination of the problem. It is felt that such an investigation should initially take the form of a theoretical examination, reinforced by suitable experimentation, of the fluid particle velocity distribution within the region immediately adjacent to the interface between the fluid and the immersed body surface. It is suggested that such an approach, in possible conjunction with the accepted concepts relating to boundary-layer theory, would provide a better understanding of the cause of the phenomenon and, in view of its applicability to fixed and floating bodies alike, would serve to pave the way towards the derivation of a truly generalised solution to the hydrodynamic interaction problem.

APPENDIX A1. THE TWO-DIMENSIONAL SOURCE STRENGTH DISTRIBUTION EQUATION.

Consider a simple source with velocity potential Φ. (see Lamb[62])

Then the flux across any surface = $-\iint \frac{\partial \Phi}{\partial r}\, ds$

where: r represents the radial vector;

ds represents the area of a surface element;

If m is called the source strength and represents the flux travelling outward across a small closed spherical surface surrounding the source, it can be stated that:

$$m = -\iint \frac{\partial \Phi}{\partial r}\, ds$$

By analogy, for a two-dimensional source:

$$m = -\int \frac{\partial \Phi}{\partial r}\, dr \qquad (A1.1)$$

where: dr represents the length of a two-dimensional element.

But: $dr = r d\theta$

Substitution in equation (A1.1) gives:

$$m = -\int_0^{2\pi} \frac{\partial \Phi}{\partial r}\, r\, d\theta$$

Thus:

$$\frac{m}{r} = -\int_0^{2\pi} \frac{\partial \Phi}{\partial r}\, d\theta = -2\pi \frac{\partial \Phi}{\partial r}$$

Integrating both sides gives:

$$m \log r = -2\pi\Phi$$

Thus:

$$\Phi = -\frac{m \log r}{2\pi} \qquad \text{(A1.2)}$$

APPENDIX A2. THE GREEN'S FUNCTION FORMULATIONS.

The Green's Function may be expressed thus:

$$G(x,y;a,b;t) = g(x,y;a,b)e^{-i\sigma t} \qquad (A2.1)$$

Since the parameter g is complex, it may be expressed as:

$$g(x,y;a,b) = g_1(x,y;a,b) + ig_2(x,y;a,b) \qquad (A2.2)$$

A2.1 The Normal Gradient.

From equation (A2.2):

$$\frac{\partial g}{\partial n} = \frac{\partial g_1}{\partial n} + i\frac{\partial g_2}{\partial n} \qquad (A2.3)$$

where: $\frac{\partial g_1}{\partial n} = \frac{\partial g_1}{\partial x}(n_x) + \frac{\partial g_1}{\partial y}(n_y)$

$\frac{\partial g_2}{\partial n} = \frac{\partial g_2}{\partial x}(n_x) + \frac{\partial g_2}{\partial y}(n_y)$

n_x, n_y are the direction cosines of the normal with respect to the positive x and y axes and have been defined in Chapter 3.

A2.2 The Imaginary Part.

From Naftzger & Chakrabarti[72], the imaginary part of the

two-dimensional finite depth Green's Function may be expressed as:

$$g_z = - g_o \text{ Cos } k(x-a) \qquad \text{(A2.4)}$$

where: $g_o = \frac{2\pi\nu}{k} \frac{\text{Cosh } k(d+b) \text{ Cosh } k(d+y)}{\nu d + \text{Sinh}^2 kd}$

$$\nu = \frac{\sigma^2}{g}$$

The x and y gradients, and hence the normal gradient, may be obtained by straightforward differentiation.

A2.3 The Integral Form of the Real Part.

In integral form, the real part may be expressed as:

$$g_1 = \text{Log}_e \frac{r}{d} + \text{Log}_e \frac{r_2}{d} - 2I_1 \qquad \text{(A2.5)}$$

where: $I_1 = \int_0^\infty \left\{ \frac{\mu+\nu}{\mu} \cdot \frac{e^{-\mu d} \text{Cosh } \mu(d+b) \text{Cosh } \mu(d+y) \text{Cos } \mu(x-a)}{\mu \text{ Sinh } \mu d - \nu \text{ Cosh } \mu d} + \frac{e^{-\mu d}}{\mu} \right\} d\mu$

$$r^2 = (x-a)^2 + (y-b)^2$$

$$r_2^2 = (x-a)^2 + (y+2d+b)^2$$

$\int$ denotes the Cauchy Principal Value Integral

A little algebra shows that the expression

$$\frac{e^{-\mu d} \text{ Cosh } \mu(d+b) \text{ Cosh } \mu(d+y)}{\mu \text{ Sinh } \mu d - \nu \text{ Cosh } \mu d} \qquad \text{(A2.6a)}$$

may be alternatively expressed as:

$$\frac{\frac{1}{2}e^{\mu(b+y)}\{1 + e^{-2\mu(b+d)}\}\{1 + e^{-2\mu(d+y)}\}}{(\mu-\nu) - (\mu+\nu)e^{-2\mu d}} \qquad \text{(A2.6b)}$$

Hogben and Standing[43] have shown that expression (A2.6a) tends to be badly behaved in deep water ($kd \geqslant 5$) whereas expression (A2.6b) is well behaved at any depth.

Using the alternative expression, the Principal Value Integral in (A2.5) may be re-expressed as:

$$I_1 = \int_0^{\mu_{max}} \left\{ \frac{F_1 . F_2 . F_3 . \text{Cos } \mu(x-a)}{(\mu-\nu) - (\mu+\nu)e^{-2\mu d}} + \frac{e^{-\mu d}}{\mu} \right\} d\mu \qquad \text{(A2.7)}$$

where: $F_1 = \frac{1}{2}\left\{\frac{\mu+\nu}{\mu}\right\}e^{\mu(b+y)}$

$F_2 = 1 + e^{-2\mu(b+d)}$

$F_3 = 1 + e^{-2\mu(d+y)}$

μ_{max} is an arbitrarily chosen point at which the contribution to the integral becomes insignificant.

By applying the linear dispersion equation $\nu = k \text{ Tanh } kd$, it can be seen that the denominator of the P.V. integrand in (A2.7) becomes zero at $\mu = k$. This may be resolved by adopting the following procedure:

In general, if a function $f(\mu)$ has a simple pole at $\mu = k$, it may be written thus:

$$f(\mu) = \frac{g(\mu)}{h(\mu)} \qquad \text{(A2.8)}$$

Then:

$$\int_0^{\mu_1} f(\mu)\, d\mu = \int_0^{\mu_1} \left\{ f(\mu) - \frac{g(k)}{h'(k)\ (\mu-k)} \right\} d\mu + \frac{g(k)}{h'(k)} \mathrm{Log}_e \left| \frac{\mu_1 - k}{k} \right| \qquad \text{(A2.9)}$$

where: h' implies $\partial h/\partial \mu$

μ_1 is an arbitrarily chosen point $k \leqslant \mu_1 \leqslant \mu_{max}$.

It can clearly be seen from Figs (A2.1) to (A2.3) that the effect of the singularity is removed. It is important to note that the modified integrand in (A2.9) is indeterminate at $\mu = k$ and that this ordinate must be avoided in any numerical integration procedure.

The functions $f(\mu)$, $g(\mu)$ and $h(\mu)$ can be derived from expression (A2.7) together with their derivatives.

A2.4 The Series Form of the Real Part.

The real part of the Green's Function expression may be

alternatively expressed in series form thus:

$$g_1 = g_o \text{ Sin } k|x-a| - 2\pi \sum_{m=1}^{\infty} \frac{1}{\mu_m} . C_m . \text{Cos } \mu_m(d+y) . \text{Cos } \mu_m(b+d) . e^{-\mu_m|x-a|} \qquad \text{(A2.10)}$$

where: $\mu_m (m \leqslant 1)$ are the positive real roots of $\mu_m \text{Tan } \mu_m d + \nu = 0$

$$C_m = \frac{\mu_m^2 + \nu^2}{\mu_m^2 d + \nu^2 d - \nu}$$

g_o is defined in equation (A2.4).

The x and y derivatives may easily be obtained from straightforward differentiation.

The solution of the modified dispersion equation above is detailed in Appendix A4.1

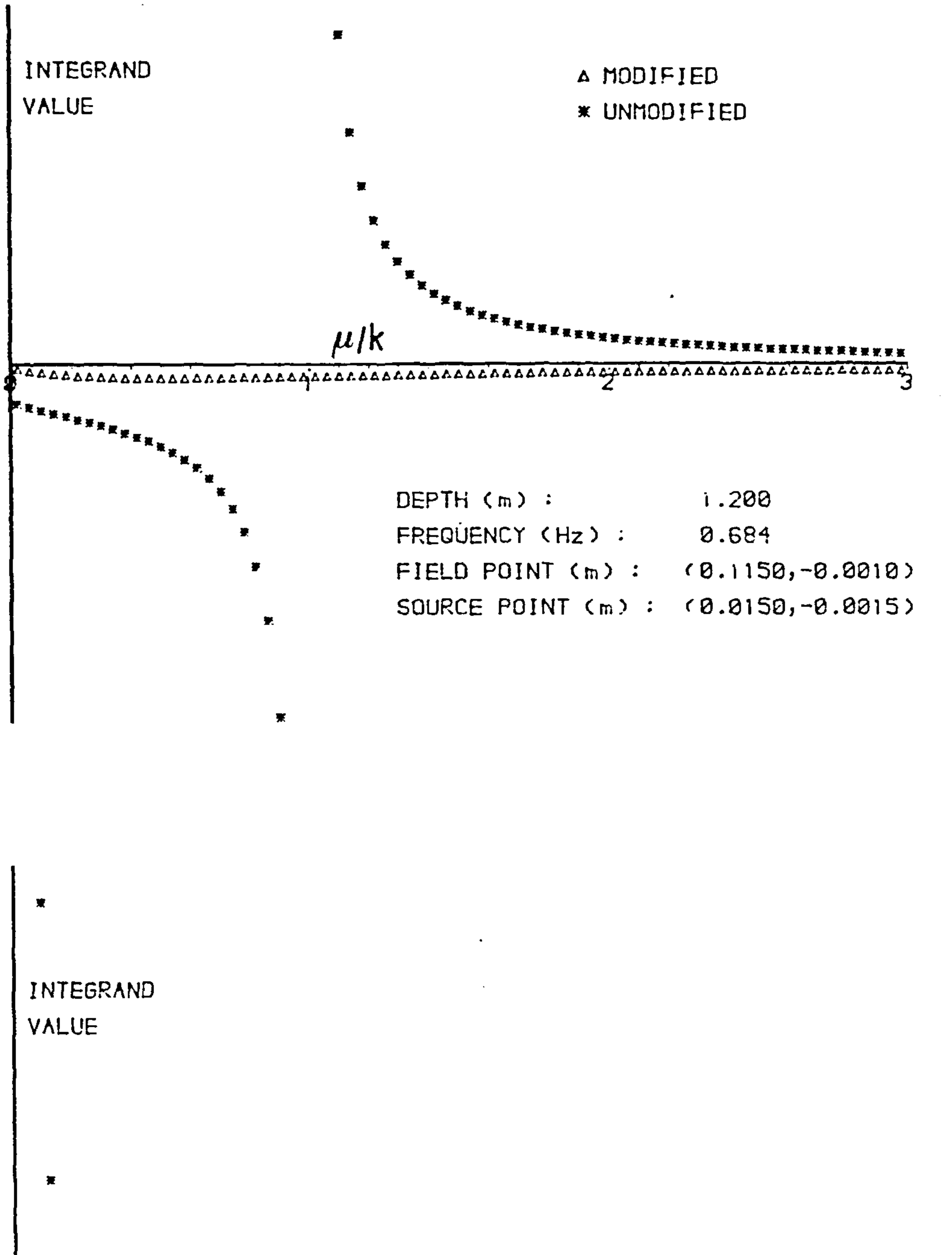

Fig.A2.1 2-DIMENSIONAL GREEN'S FUNCTION
TYPICAL BEHAVIOUR OF THE P.V.INTEGRAND

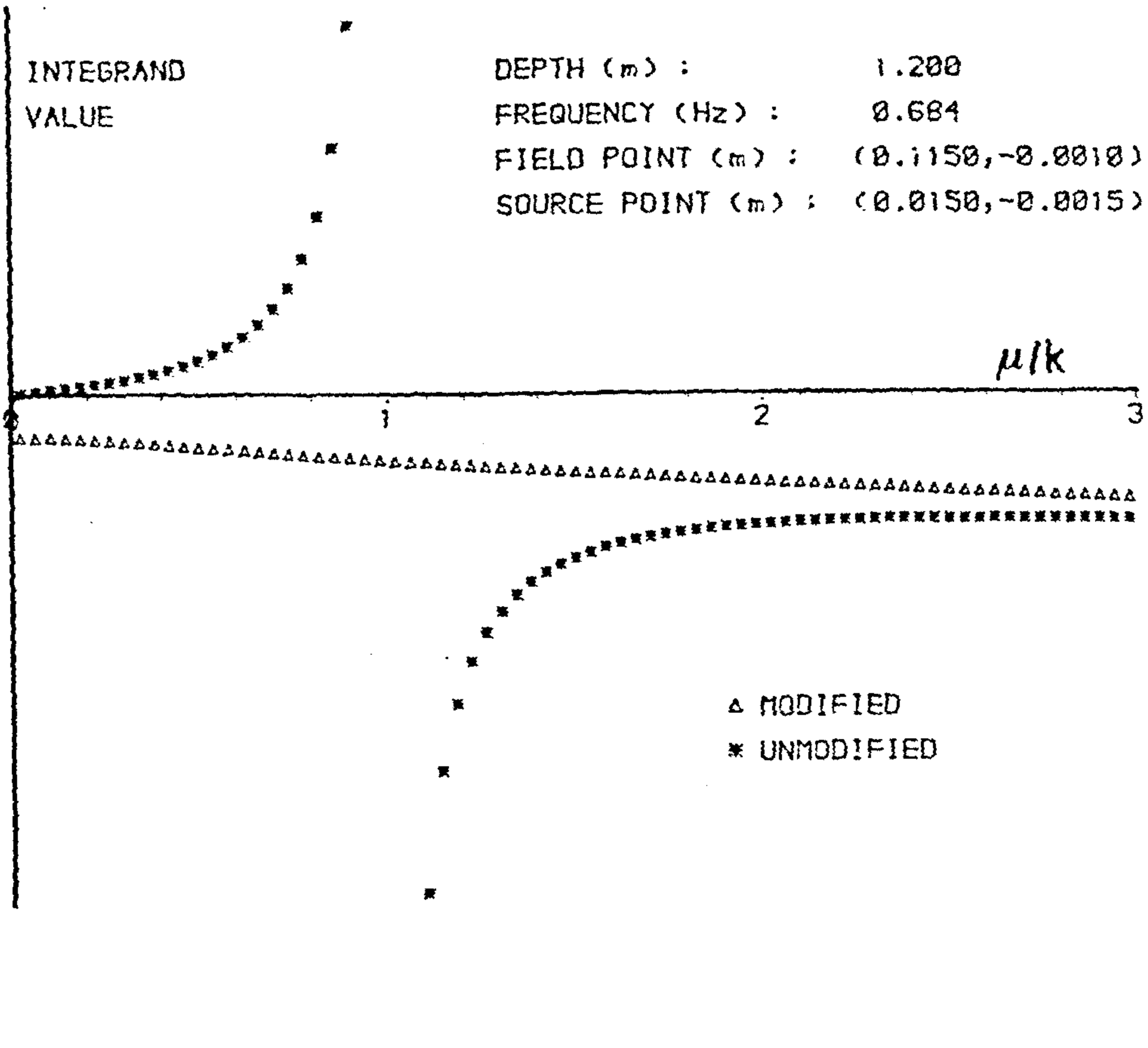

Fig.A2.2 2-DIMENSIONAL GREEN'S FUNCTION (X-GRADIENT)
TYPICAL BEHAVIOUR OF THE P.V.INTEGRAND

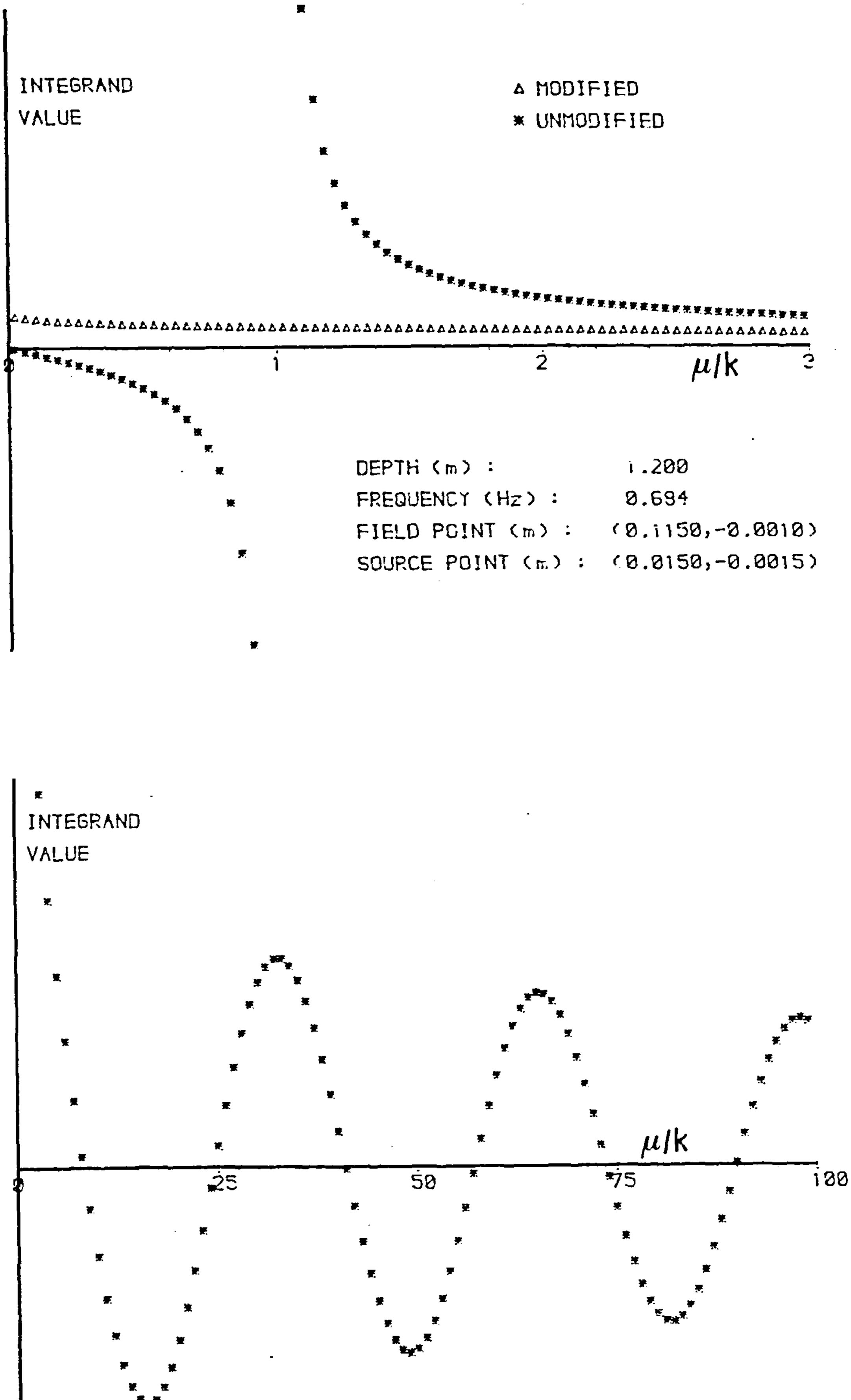

Fig.A2.3 2-DIMENSIONAL GREEN'S FUNCTION (Y-GRADIENT)
TYPICAL BEHAVIOUR OF THE P.V.INTEGRAND

APPENDIX A3. THE GREEN'S FUNCTION LIMIT AT ITS SOURCE.

Following the nomenclature of section (4.2.1), the Green's Function and its normal derivative may be expressed thus:

$$g_{ij} = \text{Log } R(\underline{x}_i, \underline{\xi}_j) + g^*_{ij} \qquad \text{(A3.1a)}$$

$$\frac{\partial g_{ij}}{\partial n} = \frac{\partial}{\partial n}\left\{\text{Log } R(\underline{x}_i, \underline{\xi}_j)\right\} + \frac{\partial g^*_{ij}}{\partial n} \qquad \text{(A3.1b)}$$

As the field point ($\underline{x}_i$) approaches the source point ($\underline{\xi}_j$), the logarithmic term in both of the above expressions outstrips the g* term and both functions have a "Log R" type of singularity. The normal expressions cannot, therefore, be used to evaluate the parameters.

The singularity is removed by distributing the source uniformly over the element length rather than concentrating it at the element centroid. Free surface effects are neglected.

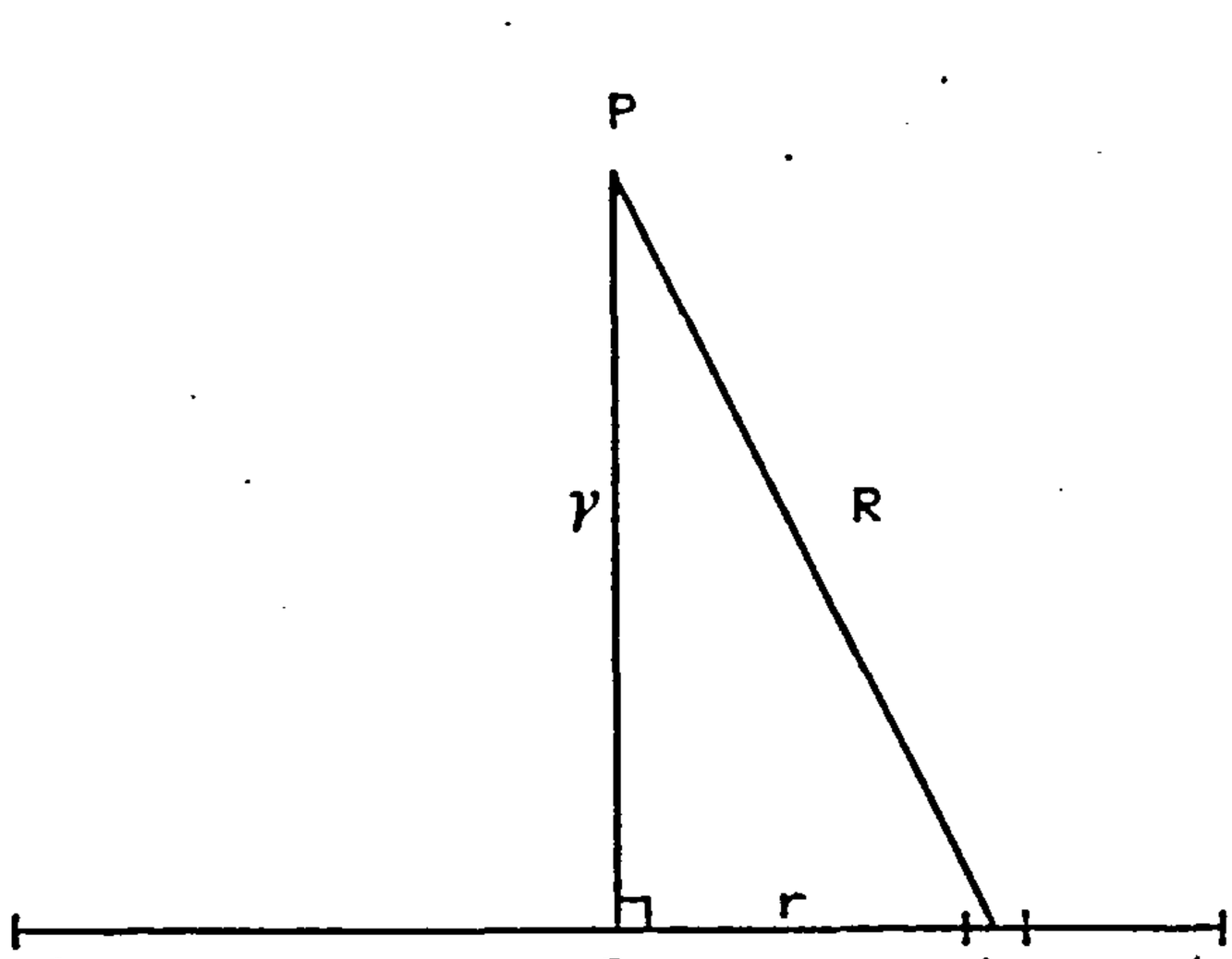

Fig.A3.1 THE GREEN'S FUNCTION LIMIT AT ITS SOURCE

Consider the potential Φ at P due to a unit source uniformly distributed over the element length:

$$\Phi = \frac{1}{l} \int_{-l/2}^{l/2} \text{Log } R \; dr \qquad \text{(A3.2)}$$

It is numerically convenient to re-arrange equation (A3.2) thus:

$$\Phi = \frac{2}{l} \int_{\epsilon}^{l/2} \text{Log } R \; dr \qquad \text{where } \epsilon \to 0 \qquad \text{(A3.3)}$$

Substituting $R^2 = (y^2+r^2)$ gives:

$$\Phi = \frac{2}{l} \int_{\epsilon}^{l/2} \text{Log}(r^2+y^2)^{\frac{1}{2}} \; dr$$

Integration by parts yields:

$$\Phi = \left\{ \frac{2r}{l} \text{Log}(r^2+y^2)^{\frac{1}{2}} - \frac{2r}{l} + \frac{2y}{l} \text{Tan}^{-1}\left[\frac{r}{y}\right] \right\}_{\epsilon}^{l/2} \qquad \text{(A3.4)}$$

In the limit as $y \to 0$:

$$\Phi = \text{Log } \frac{l}{2} - 1 - \frac{2\epsilon}{l} \text{Log } \epsilon + \frac{2\epsilon}{l}$$

In the limit as $\epsilon \to 0$:

$$\Phi = \text{Log } \frac{l}{2} - 1 \qquad \text{(A3.5)}$$

This may be regarded as the limiting value of g_{ij} when source and field points coincide.

From equation (A3.3):

$$\frac{\partial \phi}{\partial n} = \frac{\partial \phi}{\partial \gamma} = \frac{2}{l} \int_0^{l/2} \frac{\partial}{\partial \gamma}(\text{Log } R)\, dr \qquad \text{(A3.6)}$$

Substituting for R and integrating yields:

$$\frac{\partial \phi}{\partial n} = \frac{2}{l} \left\{ \text{Tan}^{-1} \left[\frac{l}{2\gamma} \right] \right\}$$

In the limit, as $\gamma \rightarrow 0$:

$$\frac{\partial \Phi}{\partial n} = \frac{\pi}{l} \qquad \text{(A3.7)}$$

This may be regarded as the limiting value of $\partial g_{ij}/\partial n$ when source and field point coincide.

APPENDIX A4. NUMERICAL DETAILS.

A4.1 Solution of the Modified Dispersion Equation.

The modified dispersion equation, as used in the evaluation of the Series Form of the Green's Function (see Appendix A2.4), can be written:

$$\mu_m \text{ Tan } \mu_m d + \nu = 0 \qquad \text{(A4.1)}$$

where: $\nu = \sigma^2/g$

μ_m = the m^{th} positive real root of the equation.

For purposes of clarity, the equation may be rearranged thus:

$$-\frac{\nu d}{\mu_m d} = \text{Tan } \mu_m d \qquad \text{(A4.2)}$$

The behaviour of both sides of the equation is shown in Fig A4.1. It can be clearly seen that the m^{th} positive root of the equation may be defined as:

$$(m - \tfrac{1}{2})\pi \leqslant \mu_m d \leqslant m\pi \qquad \text{(A4.3)}$$

The solution to equation (A4.1) may be obtained by utilising the Newton-Raphson iterative method:

$$(\mu_m)_{i+1} = (\mu_m)_i - \frac{f(\mu_m)_i}{f'(\mu_m)_i} \qquad \text{(A4.4)}$$

where: f' implies $\partial f/\partial \mu$

subscript i denotes the i^{th} iteration.

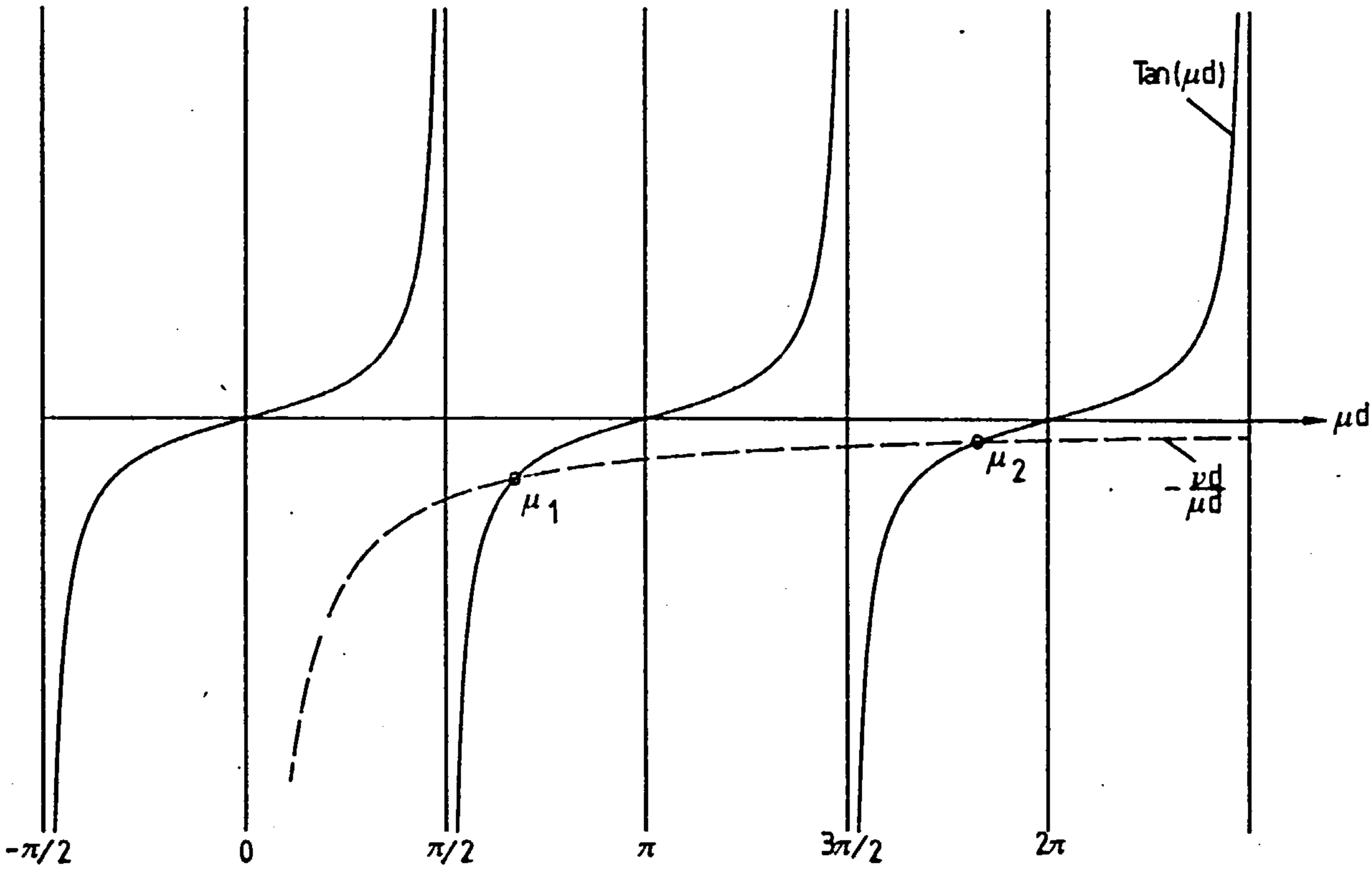

Fig. A4.1 SOLUTION OF MODIFIED DISPERSION EQUATION

Differentiation of equation (A4.1), followed by the appropriate substitution in equation (A4.4), leads to the following equation:

$$(\mu_m)_1 = (\mu_m)_o - \frac{(\mu_m)_o \text{ Tan } (\mu_m)_o d + \nu}{(\mu_m)_o d \text{ Sec}^2 (\mu_m)_o d + \text{Tan } (\mu_m)_o d} \qquad \text{(A4.5)}$$

where: $(\mu_m)_1$ is a reasonably accurate initial guess for μ_m.

$(\mu_m)_o$ is either $m\pi$ or $(m - \frac{1}{2})\pi$ according to equation (A4.3)

If $(\mu_m)_o d = m\pi$, substitution in equation (A4.5) gives:

$$(\mu_m)_1 = \frac{m\pi}{d} - \frac{\nu}{m\pi} \qquad \text{(A4.6)}$$

However, from Fig A4.1, it can be seen that:

$$m\pi - (\mu_m)_1 d \not> \pi/2$$

Thus, an initial guess $(\mu_m)_1$ defined by equation (A4.6) will only result in convergence within the range specified by equation (A4.3) if:

$$\nu d \not> \frac{m\pi^2}{2} \qquad \text{(A4.7)}$$

If νd does not comply with the conditions of equation (A4.7):

$$(\mu_m)_o = (m - \tfrac{1}{2})\frac{\pi}{d}$$

Since Tan $(m - \tfrac{1}{2})\pi = \pm \infty$, it can be seen that substitution of the above value of $(\mu_m)_o$ into equation (A4.5) will give an indeterminate initial guess resulting in non-convergence.

Since the initial guess specified by equation (A4.8) depends on a maximum value of νd, it may be postulated that, in this case:

$$(\mu_m)_1 d = (m - \tfrac{1}{2})\pi + \frac{1}{\nu d} \qquad \text{(A4.8)}$$

Using similar reasoning as above, it may be stated that an initial

guess defined by equation (A4.8) will only result in convergence within the specified range if:

$$\nu d \nless \frac{2}{\pi} \tag{A4.9}$$

A series of tests showed that rapid convergence occurred if:

$$(\mu_m)_1 = \frac{m\pi}{d} - \frac{\nu}{m\pi} \qquad \text{for } \frac{\nu d}{m} < 3.5 \tag{A4.10a}$$

$$(\mu_m)_1 = (m - \tfrac{1}{2})\frac{\pi}{d} + \frac{1}{\nu d^2} \qquad \text{for } \frac{\nu d}{m} \geqslant 3.5 \tag{A4.10b}$$

A4.2 Solution of a Complex Matrix Equation.

Consider the following matrix equation:

$$\underset{(n,n)}{[A]}\ \underset{(n,k)}{[X]} = \underset{(n,k)}{[B]} \tag{A4.11}$$

which must be solved for the unknown [X].

The elements of the matrices are the complex quantities:

$$A_{mj} = C_{mj} + iD_{mj} \qquad m = 1,n;\ j = 1,n; \tag{A4.12a}$$

$$X_{mj} = E_{mj} + iF_{mj} \qquad m = 1,n;\ j = 1,k; \tag{A4.12b}$$

$$B_{mj} = G_{mj} + iH_{mj} \qquad m = 1,n;\ j = 1,k; \tag{A4.12c}$$

Substitution of equations (A4.12) into equation (A4.11) gives:

$$\underset{(2n,2n)}{\begin{bmatrix}[C] & -[D]\\ [D] & [C]\end{bmatrix}} \underset{(2n,k)}{\begin{bmatrix}[E]\\ [F]\end{bmatrix}} = \underset{(2n,k)}{\begin{bmatrix}[G]\\ [H]\end{bmatrix}} \qquad \text{(A4.13)}$$

Possible methods of solution are as follows:

Method 1.

Equation (A4.13) may be solved directly for [E],[F] using the Gauss-Jordan elimination technique.

Array storage $(k = 4) = (2n)^2 + 2nk = 4n^2 + 8n$

CPU time $(k = 4) = \propto(2n)^3$

where: $\propto$ represents the time-based constant of proportionality for Gauss-Jordan solutions.

Method 2.

Expanding equation (A4.13) and using the notation C ≡ [C] etc. gives:

$$CE - DF = G \qquad \text{(A4.14a)}$$

$$DE + CF = H \qquad \text{(A4.14b)}$$

Premultiplying (A4.14a) by $C^{-1}DC^{-1}$, premultiplying (A4.14b) by C^{-1}

and adding the results gives:

$$(S^2+I)F = C^{-1}H + SC^{-1}G \qquad \text{(A4.15)}$$

where: $S = C^{-1}D$

I = the Unit Matrix.

Solution for the unknowns E and F may be obtained by the following procedure:

a) Evaluate C^{-1} from the solution of $CC^{-1} = I$

b) Evaluate $S = C^{-1}D$

c) Evaluate $J = C^{-1}H$

d) Evaluate $K = SC^{-1}G$

e) Evaluate F from the solution of $(S^2+I)F = (J-K)$

f) Evaluate E from back substitution $E = C^{-1}G + SF$

A little algebra shows that:

Array storage $(k = 4) = 3n^2$

CPU time $(k = 4) = \alpha(2n)^3 + \beta(3n^4 + 16n^3) + \gamma(8n)$

where: α, β, γ are the time-based constants of proportionality for Gauss-Jordan solutions, matrix multiplication and matrix addition/subtraction respectively.

Method 3.

Starting from equation (A4.15), solution for E and F may be obtained as follows:

a) Solve C(SG'H') = (DGH) to give:

$$S = C^{-1}D$$

$$G' = C^{-1}G$$

$$H' = C^{-1}H$$

b) Evaluate $SG' = SC^{-1}G$

c) Evaluate J = H' - SG'

d) Evaluate $L = S^2 + I$

e) Evaluate F from the solution of LF = J

f) Evaluate E from back substitution E = G' + SF

Array storage $(k = 4) = 3n^2 + 16n$

CPU Time $(k = 4) = \alpha(2n^3) + \beta(n^4+8n^3) + \gamma(8n)$

where: α, β, γ are as previously defined.

For $\beta = \gamma = 1$; n = 50; a comparison of the product (Array storage × Time) yields the following:

Method	$\alpha = 5$	$\alpha = 10$	$\alpha = 20$
1	1.00	1.00	1.00
2	3.18	1.68	0.93
3	1.36	0.78	0.49

It can clearly be seen that, providing $\alpha \geqslant 10$, Method 3 is the most efficient. An actual comparison between Methods 1 and 3 can be seen in table A4.1.

METHOD 1

NO.OF ELEMENTS	C.P.U TIME (SECS)	ARRAY STORAGE (kWORD)	STORAGE * TIME
19	1.82	1.60	2.91
25	3.98	2.70	10.74
31	7.38	4.09	30.18
37	12.42	5.77	71.69
43	19.20	7.74	148.61
49	28.09	10.00	280.82
55	39.41	12.54	494.22

METHOD 3

NO.OF ELEMENTS	C.P.U TIME (SECS)	ARRAY STORAGE (kWORD)	STORAGE * TIME
19	1.31	1.39	1.81
25	2.79	2.28	6.36
31	5.06	3.38	17.09
37	8.37	4.70	39.34
43	12.86	6.24	80.16
49	18.66	7.99	149.05
55	26.03	9.96	259.09

Table A4.1 Comparison of Methods of Solution of a Complex Matrix Equation.

A4.3 Numerical Integration of a Sinsuoidal Function using Simpson's Rule.

If a function f(x) is numerically integrated, using Simpson's Rule, in the range $x_o \leqslant x \leqslant x_n$, the error in the approximate integral can be shown to be:

$$E \approx \frac{-h^4}{180} \left\{ f^{(3)}(x_n) - f^{(3)}(x_o) \right\} \qquad \text{(A4.16)}$$

where: h is the interval length

$f^{(3)}$ implies $\partial^3 f / \partial x^3$

The interval length can be expressed as:

$$h = \frac{x_n - x_o}{N} \qquad \text{(A4.17)}$$

where: N is the number of intervals.

Substitution of equation (A4.17) into equation (A4.16) yields:

$$E \approx - \frac{(x_n - x_o)^4}{180N^4} \left\{ f^{(3)}(x_n) - f^{(3)}(x_o) \right\} \qquad \text{(A4.18)}$$

Consider the function f(x) = Sin kx:

Then: $f^{(3)}(x) = -k^3 \text{Cos } kx$

The error in numerical integration of the function in the range $0 \leqslant x \leqslant \alpha\pi/2$ is:

$$E_1 \approx \frac{-(\alpha\pi/2)^4}{180\ N_1^4}\left\{-k^3\ \mathrm{Cos}(\alpha\pi/2) + k^3\right\} \qquad \text{(A4.19)}$$

Similarly, the error in numerical integration in the range $\alpha\pi/2 \leqslant x \leqslant \pi/2$ is:

$$E_2 \approx \frac{[(\pi-\alpha\pi)/2]^4}{180\ N_2^4}\left\{-k^3\ \mathrm{Cos}(\alpha\pi/2)\right\} \qquad \text{(A4.20)}$$

The assumption is made that maximum efficiency of integration (i.e. a minimum number of subdivisions for a given error) is achieved when:

$$E_2 = E_1 \quad \text{and} \quad N_2 = N_1$$

Equating the two expressions yields:

$$\alpha = 0.667$$

It can thus be postulated that maximum efficiency of integration of a cyclic function is achieved when the cycle is sub-divided in the following ratios.

2 : 1 : 1 : 2 : 2 : 1 : 1 : 2

The total integral is the sum of the individual integrals over the subdivided intervals.

A4.4 Numerical Evaluation of the Incident Wave Potential.

Evaluations of the normal gradient of the incident wave velocity potential, at points (x_i,y_i) on the immersed surface of the body, are required for the formation of the matrices used in the discretised solution of the integral equations.

The incident wave velocity potential may be defined[86] in complex form thus:

$$\Phi_W(x,y;t) = \phi_W(x,y)e^{-i\sigma t} \qquad \text{(A4.21)}$$

where: $\phi_W(x,y) = \dfrac{-igH}{2\sigma} \dfrac{\text{Cosh } k(d+y)}{\text{Cosh } kd} e^{ikx}$

Expansion of e^{ikx} gives:

$$\text{Re}\left\{\phi_W(x,y)\right\} = \frac{gH}{2\sigma} \frac{\text{Cosh } k(d+y)}{\text{Cosh } kd} \text{Sin } kx \qquad \text{(A4.22a)}$$

$$\text{Im}\left\{\phi_W(x,y)\right\} = -\frac{gH}{2\sigma} \frac{\text{Cosh } k(d+y)}{\text{Cosh } kd} \text{Cos } kx \qquad \text{(A4.22b)}$$

The normal gradient is defined thus:

$$\frac{\partial\phi_W(x,y)}{\partial n} = \frac{\partial\Phi_W(x,y)}{\partial x}_{(n_x)} + \frac{\partial\phi_W(x,y)}{\partial y}_{(n_y)}$$

where: n_x,n_y are the direction cosines of the normal at (x,y) with respect to the positive x and y axes.

Differentiation of equation (A4.21) gives:

$$\mathrm{Re}\left\{\frac{\partial\phi}{\partial n}\right\} = F\left[n_x \mathrm{Cosh}\ k(d+y)\mathrm{Cos}\ kx + n_y \mathrm{Sinh}\ k(d+y)\mathrm{Sin}\ kx\right] \qquad \text{(A4.23a)}$$

$$\mathrm{Im}\left\{\frac{\partial\phi}{\partial n}\right\} = F\left[n_x \mathrm{Cosh}\ k(d+y)\mathrm{Sin}\ kx - n_y \mathrm{Sinh}\ k(d+y)\mathrm{Cos}\ kx\right] \qquad \text{(A4.23b)}$$

where: $F = \dfrac{gHk}{2\sigma\ \mathrm{Cosh}\ kd}$

$$\phi \equiv \phi_W(x,y)$$

A4.5 Numerical Evaluation of the Exciting Force components.

From equation (3.7.8):

$$F_i(e) = \mathrm{Re}\left\{F_{o_i}(e)\right\}e^{-i\sigma t} \qquad \text{(A4.24a)}$$

where: $$F_{o_i}(e) = \rho\left[\int_\Gamma \left\{\phi_W \frac{\partial\phi_i(f)}{\partial n} - \phi_i(f)\frac{\partial\phi_W}{\partial n}\right\}d\Gamma\right] \qquad \text{(A4.24b)}$$

But from equation (3.6.8):

$$\frac{\partial\phi_i(f)}{\partial n} = -i\sigma n_i \qquad \text{(A4.25)}$$

It must be noted that the potential and force terms are complex and may be defined:

$$\phi = \phi' + i\phi''$$

$$F = F' + iF''$$

where superscripts ' and " denote the real and imaginary parts respectively.

A little algebra, together with equating real and imaginary parts of equations (A4.24), gives:

$$\mathrm{Re}\left\{F_{o_i}\right\} = \rho\left[\int_{\Gamma}\left\{\sigma\phi''_W n_i - \phi'_i \frac{\partial\phi'_W}{\partial n} + \phi''_i \frac{\partial\phi''_W}{\partial n}\right\}d\Gamma\right] \qquad \text{(A4.26a)}$$

$$\mathrm{Im}\left\{F_{o_i}\right\} = -\rho\left[\int_{\Gamma}\left\{\sigma\phi'_W n_i + \phi''_i \frac{\partial\phi'_W}{\partial n} + \phi'_i \frac{\partial\phi''_W}{\partial n}\right\}d\Gamma\right] \qquad \text{(A4.26b)}$$

Note that, for the sake of clarity, the superscripts (e) and (f) have been omitted. It may be understood that:

$$F_{o_i} \equiv F_{o_i}{}^{(e)}$$

$$\phi_i \equiv \phi_i{}^{(f)}$$

Following the discretisation procedure described previously, equations (A4.26) may be expressed thus:

$$\mathrm{Re}\left\{F_{o_i}{}^{(e)}\right\} = \rho\sum_{j=1}^{N}\left\{\sigma\phi''_W(x_j,y_j)n_{ji} - \phi'_{ji}\frac{\partial\phi'_W(x_j,y_j)}{\partial n} + \phi''_{ji}\frac{\partial\phi''_W(x_j,y_j)}{\partial n}\right\}\Delta\Gamma_j \qquad \text{(A4.27a)}$$

$$\mathrm{Im}\left\{F_{o_i}{}^{(e)}\right\} = -\rho\sum_{j=1}^{N}\left\{\sigma\phi'_W(x_j,y_j)n_{ji} + \phi''_{ji}\frac{\partial\phi'_W(x_j,y_j)}{\partial n} + \phi'_{ji}\frac{\partial\phi''_W(x_j,y_j)}{\partial n}\right\}\Delta\Gamma_j \qquad \text{(A4.27b)}$$

Expanding equation (A4.24a) and taking the real part only gives:

$$F_i^{(e)} = Re\left\{F_{o_i}^{(e)}\right\} \text{Cos } \sigma t + Im\left\{F_{o_i}^{(e)}\right\} \text{Sin } \sigma t$$

$$= F_{A_i}^{(e)} \text{ Cos } (\sigma t+\delta) \qquad \text{(A4.28)}$$

where: $F_{A_i}^{(e)} = \left[Re^2\left\{F_{o_i}^{(e)}\right\} + Im^2\left\{F_{o_i}^{(e)}\right\}\right]^{1/2}$

$$\delta = \text{Tan}^{-1}\left[\frac{-Im\{F_{o_i}^{(e)}\}}{Re\{F_{o_i}^{(e)}\}}\right]$$

Note that $F_{Ai}^{(e)}$ represents the real amplitude of the exciting force in the i^{th} mode and δ represents its phase angle with respect to the incident wave.

A4.6 Numerical Evaluation of the Complex Amplitudes of Motion.

From equation (3.7.9):

$$F_{o_i}^{(e)} = \sum_{j=1}^{3}\left\{\left[-\sigma^2(m_{ij} + \mu_{ij}) - i\sigma\lambda_{ij} + c_{ij}\right]a_j\right\} \qquad \text{(A4.29)}$$

where: $F_{oi}^{(e)}$ is the complex exciting force amplitude.

m_{ij}, c_{ij} are coefficients defined in the equations of motion (3.5.4).

μ_{ij}, λ_{ij} are the added-mass and damping coefficients.

If the above parameters are known, equations (A4.29) can be solved for the complex amplitudes of motion, a_j.

Using the nomenclature of Appendix (A4.2), the equation may be expressed, in matrix terms, thus:

$$\underset{(3,3)}{[A]}\ \underset{(3,1)}{\{x\}} = \underset{(3,1)}{\{B\}} \qquad \text{(A4.30)}$$

where: $A_{ij} = C_{ij} + iD_{ij}$

$X_i = E_i + iF_i$

$B_i = G_i + iH_i$

Comparing equation (A4.30) with equation (A4.29), it may be stated that:

$$C_{ij} = -\sigma^2(m_{ij} + \mu_{ij}) + c_{ij} \qquad i = 1,2,3;\ j = 1,2,3 \qquad \text{(A4.31a)}$$

$$D_{ij} = -\sigma\lambda_{ij} \qquad i = 1,2,3;\ j = 1,2,3 \qquad \text{(A4.31b)}$$

$$E_i = \mathrm{Re}\{a_i\} \qquad i = 1,2,3 \qquad \text{(A4.31c)}$$

$$F_i = \mathrm{Im}\{a_i\} \qquad i = 1,2,3 \qquad \text{(A4.31d)}$$

$$G_i = \mathrm{Re}\{F_{oi}^{(e)}\} \qquad i = 1,2,3 \qquad \text{(A4.31e)}$$

$$H_i = \mathrm{Im}\{F_{oi}^{(e)}\} \qquad i = 1,2,3 \qquad \text{(A4.31f)}$$

From equations (3.5.4) the following substitutions may be made:

m_{11}, m_{22} = Mass of Floating Body.

m_{33} = Rotational Moment of Inertia of the Floating Body in the pitch mode.

$c_{22} = \rho_W\, g\, L_W$

$c_{33} = \rho_W\, g\, \forall\, H$

where: ρ_w = Mass density of water.

L_w = Waterline area per unit width of Body.

$\forall$ = Displaced volume per unit width of body.

H = Pitch Metacentric Height.

All other c_{ij}, m_{ij} are zero.

If the body is subject to any spring restraints to prevent drifting or to simulate mooring conditions, the spring constants may be added to the c_{ij} terms.

The real amplitudes of motion, together with their phase angles, may be evaluated in a similar fashion to the exciting force components described in appendix (A4.5).

A4.7 Numerical Evaluation of Reflection and Transmission Coefficients.

Consideration of equations (A6.15) in appendix A6 shows the following integral expressions require to be numerically evaluated.

$$I_1^{(s)} = -i\int_\Gamma f^{(s)}(a,b)\ g_o(0,b)\ e^{-ika}\ dr \qquad \text{(A4.32a)}$$

$$I_{ij}^{(f)} = -i\int_\Gamma f_j^{(f)}(a,b)\ g_o(0,b)\ e^{-ika}\ dr \qquad \text{(A4.32b)}$$

$$I_2^{(s)} = -i\int_\Gamma f^{(s)}(a,b)\ g_o(0,b)\ e^{ika}\ dr \qquad \text{(A4.32c)}$$

$$I_{2j}^{(f)} = -i\int_\Gamma f_j^{(f)}(a,b)\ g_o(0,b)\ e^{ika}\ dr \qquad \text{(A4.32d)}$$

where: (s) denotes the scattered component.

(f) denotes the forced or generated component.

Following the previously adopted discretisation procedure, and noting the complex expansions:

$$f = f_1 + if_2$$

$$e^{i\theta} = \text{Cos } \theta + i \text{ Sin } \theta$$

$$e^{-i\theta} = \text{Cos } \theta - i \text{ Sin } \theta$$

the following expression may be derived:

$$\text{Re}\left\{I_1^{(s)}\right\} = \sum_{m=1}^{N} \Delta\Gamma_m \, g_o(0, b_m) \left[f_2^{(s)}(\underline{\xi}_m) \text{ Cos } ka_m - f_1^{(s)}(\underline{\xi}_m) \text{ Sin } ka_m \right] \qquad \text{(A4.33)}$$

For brevity, only the real part of $I_1^{(s)}$ has been considered. All remaining real and imaginary parts have a similar format.

Substitution of the evaluated real and imaginary parts into equations (A6.19), (A6.20), and (A6.21) yields the Transmission Coefficient and phase angle.

The Reflection Coefficient may be similarly evaluated from consideration of equation (A6.23) *et seq.*

APPENDIX A5. BOUNDARY ELEMENT DISTRIBUTION.

In practice, the number of elements into which the source distribution boundary is subdivided is limited by available computer storage space. Apart from this physical limitation, the fact that the run-time for any particular solution is roughly proportional to the square of the number of elements emphasises the importance of restricting the number of elements to the minimum required for an acceptably accurate solution.

To ensure an adequate representation of the object boundary subject to the above limitations, Hogben, Osborne and Standing[42] have recommended the following guidelines, based on experience, for fixed three-dimensional objects.

1. Elements should be concentrated in areas where the body geometry (slope or curvature) changes rapidly with position.
2. Individual element dimensions should not exceed the local radius of curvature.
3. No element dimension should exceed 1/8 of the incident wavelength.
4. Element dimensions should change gradually between areas of high and low concentrations.
5. The dimensions of an element should not be more than 50% greater than those of neighbouring elements. If several small elements surround a larger one, the accuracy is that associated with the large element resulting in an inefficient distribution.

In the case of two-dimensional floating bodies, the author is unaware of the availability of similar guidelines. However, it may

be reasonably assumed that the principles remain the same.

In the case of an immersed surface which is substantially rectangular, the following formulation has ben adopted to comply with the above recommendations.

A5.1 Rectangular Immersed Surface with Square Edges.

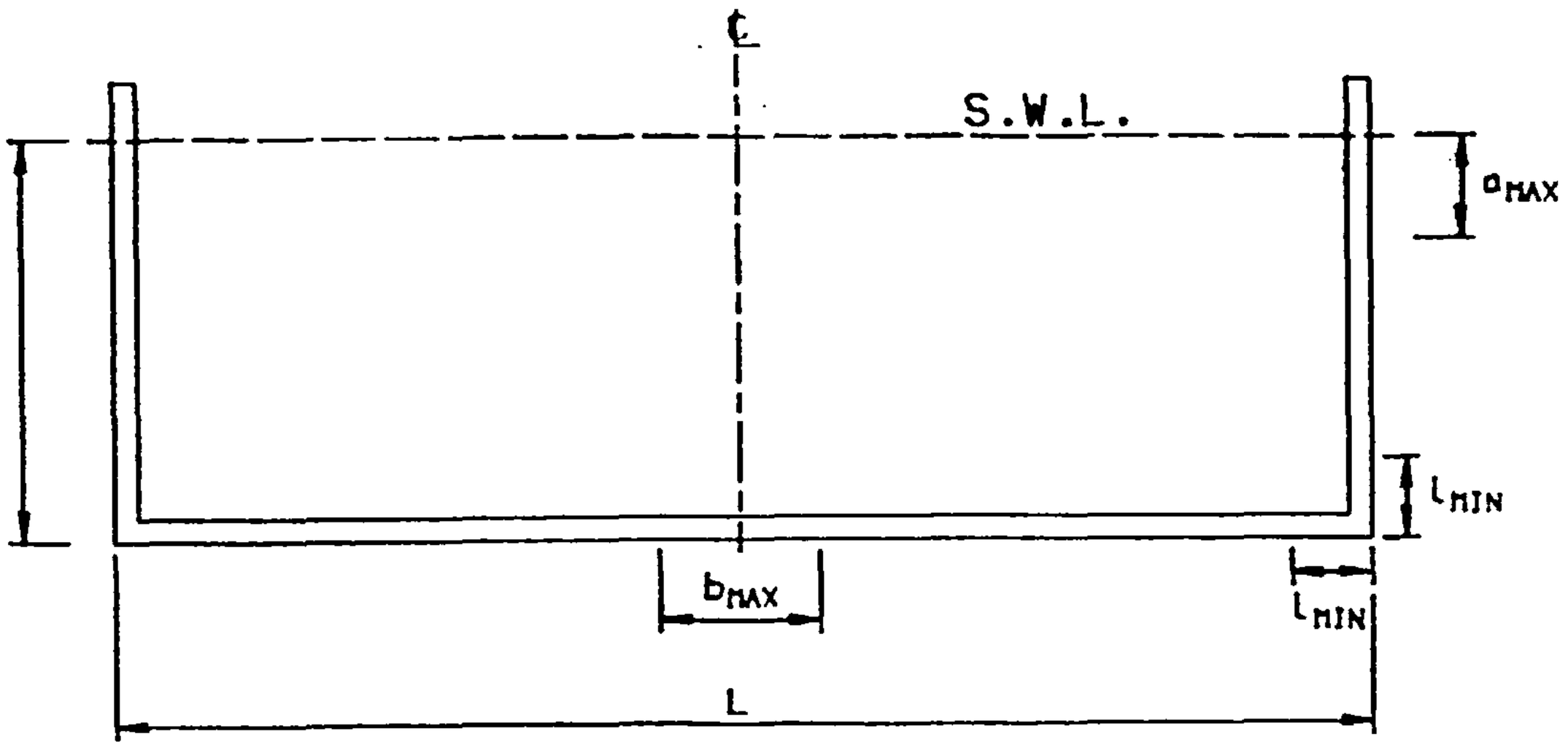

Fig. A5.1 ELEMENT DISTRIBUTION (SQUARE EDGES)

The element parameters may be defined thus:

Maximum element length on a vertical side = a_{max}

Maximum element length on the base = b_{max}

Number of elements on each vertical side = N_s

Number of elements on base = $2N_b + 1$

Minimum element size = l_{min}

These are illustrated in Fig. A5.1.

The element distribution on each side may be defined thus:

$$\gamma_1 = a_{max}$$

$$\gamma_i = a_{max}\ \alpha^{i-1} \qquad i = 1,2,\ldots,N_s;\quad \alpha \leqslant 1;$$

where: suffix i denotes the i^{th} element from the free surface.

α is the constant element length ratio pertaining to each vertical side.

The element distribution on the base may be defined thus:

$$\gamma_1 = b_{max}$$

$$\gamma_i = b_{max}\ \beta^{i-1} \qquad i = 1,2,\ldots,N_b;\quad \beta \leqslant 1$$

where: suffix i denotes the i^{th} element from the centroidal axis.

β is the constant element length ratio pertaining to the base.

A little algebra results in the following governing equations for the side elements:

$$N_s = \frac{\text{Log } F_1}{\text{Log } \alpha} \qquad \text{(A5.1)}$$

$$a_{max} = \frac{D(1-\alpha)}{1-\alpha^{N_s}} \qquad \text{(A5.2)}$$

$$\alpha = \left\{\frac{l_{min}}{\alpha_{max}}\right\}^{\frac{1}{N_s-1}} \qquad \text{(A5.3)}$$

where: $F_1 = \dfrac{\alpha l_{min}}{D(1-\alpha) + \alpha l_{min}}$

Similarly, the governing equations for the base elements are:

$$N_b = \frac{\text{Log } F_2}{\text{Log } \beta} \qquad \text{(A5.4)}$$

$$b_{max} = \frac{L(1-\beta)}{1 + \beta - 2\beta^{N_b+1}} \qquad \text{(A5.5)}$$

$$\beta = \left\{\frac{l_{min}}{b_{max}}\right\}^{\frac{1}{N_b}} \qquad \text{(A5.6)}$$

where: $F_2 = \dfrac{l_{min}(1+\beta)}{L(1-\beta) + 2\beta l_{min}}$

The procedure for evaluating the distribution is illustrated for the side elements. It can be taken that the procedure is exactly the same for the base elements.

1. A value for l_{min} is specified, generally as a proportion of the draught D.
2. A nominal value of $\propto$ is inserted in equation (A5.1) to give the real number N_s'.
3. The value of N_s is taken to be the nearest integer to N_s'
4. The values of N_s and $\propto$ are inserted into equation (A5.2) to give a value for a_{max}.
5. The value of a_{max} is inserted into equation (A5.3) to give an updated value of the element length ratio.
6. Steps 2 thru' 5 are repeated until successive values of the element length ratio compare within a specified tolerance.

In practice, the same nominal element length ratio is used for both side and base elements, resulting in a roughly symmetric increase in

side and base elements away from the submerged edge of the body. Depending on the aspect ratio of the immersed surface, the computed element length ratios generally differ by only a few percent either side of the input nominal value.

A5.2 Rectangular Immersed Surface with Radial Edges.

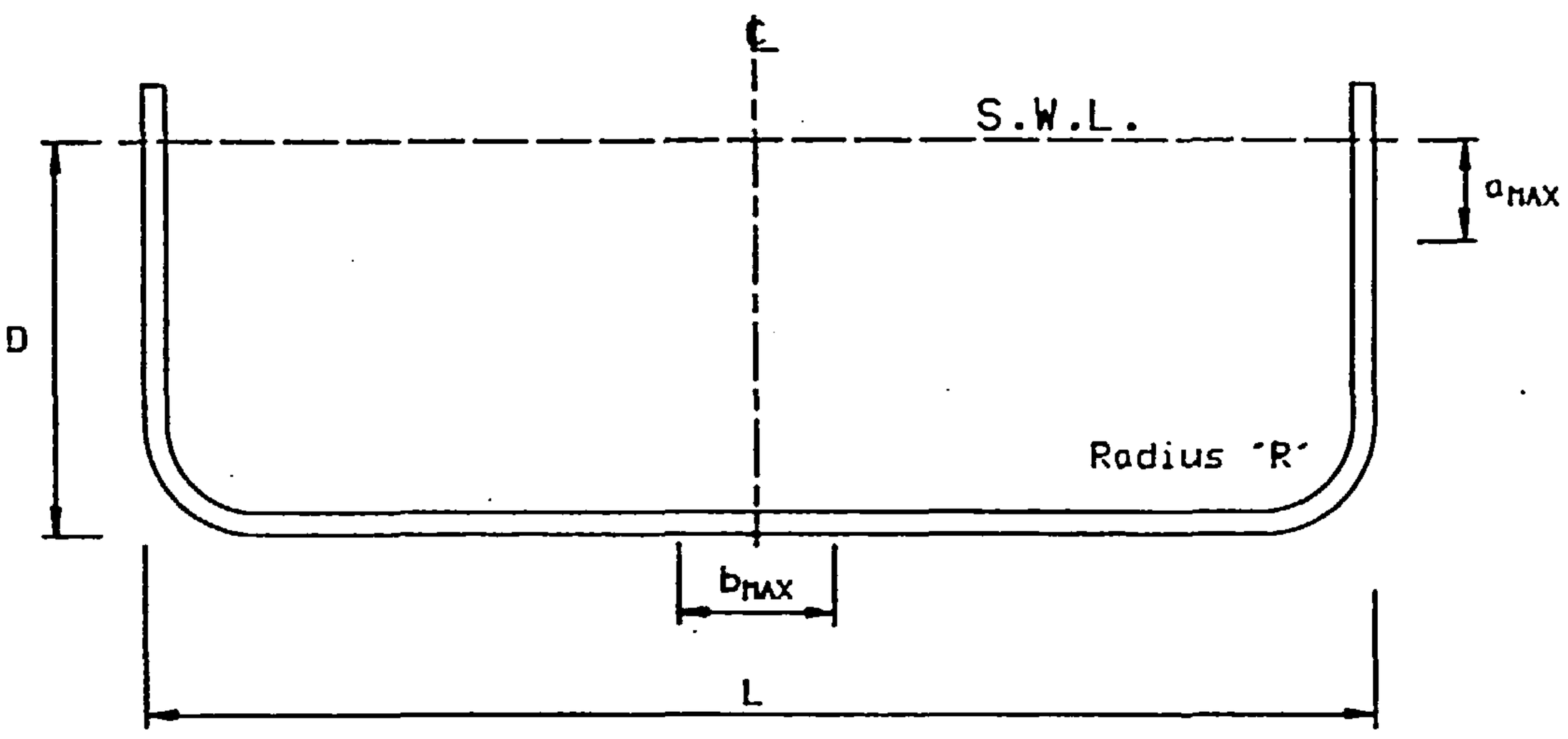

Fig.A5.2 ELEMENT DISTRIBUTION (RADIAL EDGES)

The element parameters may be defined thus:

Maximum element length on a vertical side = a_{max}

Maximum element length on the base = b_{max}

Number of elements on the straight portion of each side = N_s

Number of elements on the straight portion of the base = $2N_b + 1$

Number of constant length elements on each radial edge = N_c

These are illustrated in Fig A5.2

If it is assumed that the minimum element length occurs on the

radial edges, it may be stated that:

$$\text{Minimum element length, } l_{min} = \frac{\pi R}{2N_C}$$

The side and base element distributions are defined as for the square edged body.

By following the same procedure as in the case of the square edged body, the governing equations can be obtained:

$$N_S = \frac{\text{Log } F_1}{\text{Log } \alpha} \qquad \text{(A5.7)}$$

$$a_{max} = \frac{(D-R)(1-\alpha)}{1 - \alpha^{N_S}} \qquad \text{(A5.8)}$$

$$\alpha = \left\{\frac{\pi R}{2N_C a_{max}}\right\}^{\frac{1}{N_S}} \qquad \text{(A5.9)}$$

$$N_b = \frac{\text{Log } F_2}{\text{Log } \beta} \qquad \text{(A5.10)}$$

$$b_{max} = \frac{(L-2R)(1-\beta)}{1 + \beta - 2\beta^{N_b+1}} \qquad \text{(A5.11)}$$

$$\beta = \left\{\frac{\pi R}{2N_C b_{max}}\right\}^{\frac{1}{N_b+1}} \qquad \text{(A5.12)}$$

where: $F_1 = \dfrac{\pi R}{(D-R)(2N_C)(1-\alpha) + \pi R}$

$$F_2 = \frac{\pi R(1+\beta^{-1})}{(1-\beta)(L-2R)(2N_C) + 2\pi R}$$

The evaluation procedure is identical to that described for the square edged body with the exception that, in this case, the minimum element length is specified by the input parameter N_C.

APPENDIX A6. EVALUATION OF THE REFLECTION AND TRANSMISSION CHARACTERISTICS OF A FLOATING BODY.

From Section 3.3, the velocity potential describing the flow field in the presence of an incident wave train may be expressed in complex form as:

$$\Phi(x,y;t) = \mathrm{Re}\left\{\phi(x,y)e^{-i\sigma t}\right\} \qquad \text{(A6.1)}$$

where Re{ } denotes the real part, and the time parameter t is understood to be real throughout.

Application of the free-surface dynamic and kinematic boundary conditions, and appropriately linearising, gives the expression for the free-surface profile:

$$\eta(x;t) = -\frac{1}{g}\frac{\partial\Phi}{\partial t}(x,0;t)$$

Substitution from equation (A6.1) yields:

$$\eta(x;t) = \frac{\sigma}{g}\,\mathrm{Re}\left\{i\phi(x,0)e^{-i\sigma t}\right\} \qquad \text{(A6.2)}$$

For the sake of computational convenience, the free-surface profile may be non-dimensionalised thus:

$$\bar{\eta}(x;t) = \frac{\eta(x;t)}{H/2} \qquad \text{(A6.3)}$$

where: H represents the wave height.

Substitution in equation (A6.2) gives:

$$\bar{\eta}(x;t) = Re\left\{\bar{\phi}(x,0)e^{-i\sigma t}\right\} \qquad (A6.4)$$

where: the non-dimensionalised velocity potential $\bar{\phi}$ is defined by:

$$\bar{\phi}(x,0) = \frac{\phi}{A}(x,0) \qquad (A6.5a)$$

$$\text{where: } A = -\frac{igH}{2\sigma} \qquad (A6.5b)$$

From equation (3.3.2) it may be inferred that:

$$\bar{\phi} = \bar{\phi}_W + \bar{\phi}_S + \bar{\phi}_F \qquad (A6.6)$$

where: $\bar{\phi}$ is the total non-dimensional velocity potential.

$\bar{\Phi}_W$ is the non-dimensional velocity potential associated with the incident wave.

$\bar{\Phi}_S$ is the non-dimensional velocity potential associated with the scattered wave.

$\bar{\Phi}_F$ is the non-dimensional velocity potential associated with the generated wave.

The potential associated with the incident wave may be expressed, in complex form thus:

$$\Phi_W(x,y;t) = A\frac{\text{Cosh } k(d+y)}{\text{Cosh } kd}e^{i(kx-\sigma t)} = \phi_W(x,y)e^{-i\sigma t} \qquad (A6.7)$$

where A is defined by equation (A6.5b)

From equation (A6.5a) it can thus be seen that:

$$\bar{\Phi}_W(x,0) = e^{ikx} \qquad \text{(A6.8)}$$

Expression of the scattered and forced potentials in terms of the source distribution equation (4.2.4), bearing in mind the decomposition given by equation (3.4.10), and non-dimensionalising in accordance with equation (A6.5a), permits the non-dimensional scattered and generated wave potentials to be expressed in terms of the relevant source distribution and Green's Functions;

$$\bar{\Phi}_S = \frac{1}{A}\int_\Gamma f^{(s)}(a,b)\ g(x,y;a,b)\ d\Gamma \qquad \text{(A6.9)}$$

$$\bar{\Phi}_F = \frac{1}{A}\sum_{j=1}^{3} a_j \left\{\int_\Gamma f_j^{(f)}(a,b)\ g(x,y;a,b)\right\}\ d\Gamma \qquad \text{(A6.10)}$$

Substitution of these parameters into equation (A6.6) and thence into equation (A6.4) gives the generalised expression for the non-dimensional surface profile:

$$\bar{\eta}(x;t) = Re\left\{\left[e^{ikx} + \frac{1}{A}\int_\Gamma f^{(s)}(a,b)\ g(x,0;a,b)\ d\Gamma + \frac{1}{A}\sum_{j=1}^{3} a_j\left\{\int_\Gamma f_j^{(f)}(a,b)\ g(x,0;a,b)\ d\Gamma\right\}\right]e^{-i\sigma t}\right\} \qquad \text{(A6.11)}$$

Insertion of the appropriate numerical values into equation (A6.11) enables the surface profile at any point in the fluid domain to be evaluated. However, since localised wave effects in the immediate vicinity of the floating body are generally unimportant owing to

their rapid decay, the surface profile evaluation may be much simplified by the use of asymptotic values of the functions[72].

Consideration of equations (A2.2), (A2.4) and (A2.10) of Appendix A2 yields the following expressions:

$$g\ (x,y;a,b) = g_1(x,y;a,b) + ig_2(x,y;a,b) \qquad \text{(A6.12a)}$$

$$g_1(x,y;a,b) = g_o(y,b)\ \text{Sin}\ k|x-a| - f(\mu,\nu,d,y,b)e^{-\mu|x-a|} \qquad \text{(A6.12b)}$$

$$g_2(x,y;a,b) = -g_o(y,b)\ \text{Cos}\ k(x-a) \qquad \text{(A6.12c)}$$

where: g_o is defined by equation (A2.4) of Appendix A2.

From equation (A6.12b):

$$\lim_{|x|\to\infty} g_1(x,y;a,b) = g_o(y,b)\text{Sin}\ k|x-a|$$

Thus, in equation (A6.12a):

$$\lim_{|x|\to\infty} g_1(x,y;a,b) = g_o(y,b)\text{Sin}\ k|x-a| - ig_o(y,b)\text{Cos}\ k(x-a)$$

$$= -ig_o(y,b)\left\{\text{Cos}\ k(x-a) + i\text{Sin}\ k|x-a|\right\} \qquad \text{(A6.13)}$$

But for positive x: $\text{Sin}\ k|x-a| = \text{Sin}\ k(x-a)$

and for negative x: $\text{Sin}\ k|x-a| = -\text{Sin}\ k(x-a)$

Substitution in equation (A6.13), together with the expansions of $e^{\pm i\theta}$, gives the asymptotic values of the Green's Function:

$$g^+(x,y;a,b) = -ig_o(y,b)e^{ik(x-a)} \qquad \text{(A6.14a)}$$

$$g^-(x,y;a,b) = -ig_o(y,b)e^{-ik(x-a)} \qquad \text{(A6.14b)}$$

where the superscripts +/- denote the asymptotic values for positive and negative values of x.

Substitution of these expressions in equation (A6.11) yields the following expressions for the non-dimensional surface profile at large distances upstream (x negative) and downstream (x positive):

$$\bar{n}^{+}(x;t) = \mathrm{Re}\left\{e^{i(kx-\sigma t)}\left[1 + \frac{1}{A}I_1(s) + \frac{1}{A}\sum_{j=1}^{3} a_j I_{1j}(f)\right]\right\} \qquad \text{(A6.15a)}$$

$$\bar{n}^{-}(x;t) = \mathrm{Re}\left\{e^{i(kx-\sigma t)} + e^{-i(kx-\sigma t)}\left[\frac{1}{A}I_2(s) + \frac{1}{A}\sum_{j=1}^{3} a_j I_{2j}(f)\right]\right\} \qquad \text{(A6.15b)}$$

where:

$$I_1(s) = -i\int_{\Gamma} f^{(s)}(a,b)\; g_o(0,b)\; e^{-ika}\; dr$$

$$I_{1j}(f) = -i\int_{\Gamma} f_j^{(f)}(a,b)\; g_o(0,b)\; e^{-ika}\; dr$$

$$I_2(s) = -i\int_{\Gamma} f^{(s)}(a,b)\; g_o(0,b)\; e^{ika}\; dr$$

$$I_{2j}(f) = -i\int_{\Gamma} f_j^{(f)}(a,b)\; g_o(0,b)\; e^{ika}\; dr$$

The transmission coefficient, T, may be defined as the ratio of the surface profile at large distances downstream to that of the incident wave, with the incurrence of a phase shift β_T.

It must be noted that the transmission coefficient is a complex

quantity and that the value of T is taken to be the modulus:

$$T = |T' + iT''|$$

where: superscripts ' and " denote the real and imaginary parts respectively.

From equation (A6.4), the non-dimensional transmitted wave profile may be defined:

$$\bar{\eta}^{+}(x;t) = \mathrm{Re}\left\{T\bar{\phi}(x,0)\ e^{-i(\sigma t+\beta_T)}\right\} \qquad \text{(A6.16)}$$

Substitution from equation (A6.8) followed by re-arrangement gives:

$$\bar{\eta}^{+}(x;t) = \mathrm{Re}\left\{e^{i(kx-\sigma t)}Te^{-i\beta_T}\right\} \qquad \text{(A6.17)}$$

Comparison between equations (A6.17) and (A6.15a) shows that:

$$Te^{-i\beta_T} = 1 + \frac{1}{A}\left\{I_1(s) + \sum_{j=1}^{3} a_j I_{1j}(f)\right\} \qquad \text{(A6.18)}$$

Taking into account the complex quantities a_j and I_{1j}, the definition of A according to equation (A6.5b) and the decomposition of $e^{-i\beta_T}$, the real and imaginary parts of equation (A6.18) may be

compared to give the following expressions:

$$T \text{ Cos } \beta_T = 1 - \frac{2\sigma}{gH}\left[I_1''(s) + \sum_{j=1}^{3}\left\{a_j'' \; I_{1j}'(f) + a_j' \; I_{1j}''(f)\right\}\right] \qquad \text{(A6.19a)}$$

$$T \text{ Sin } \beta_T = - \frac{2\sigma}{gH}\left[I_1'(s) + \sum_{j=1}^{3}\left\{a_j' \; I_{1j}'(f) - a_j'' \; I_{1j}''(f)\right\}\right] \qquad \text{(A6.19b)}$$

where: superscripts ' and " denote the real and imaginary parts respectively.

The values of T and β_T may be evaluated from the expressions:

$$\beta_T = \text{Tan}^{-1}\left\{\frac{T \text{ Sin } \beta_T}{T \text{ Cos } \beta_T}\right\} \qquad \text{(A6.20a)}$$

$$T = \left\{(T \text{ Cos } \beta_T)^2 + (T \text{ Sin } \beta_T)^2\right\}^{\frac{1}{2}} \qquad \text{(A6.20b)}$$

It may be inferred from equation (A6.18) that:

$$T_S \; e^{-i\beta_{TS}} = 1 + \frac{1}{A} I_1(s) \qquad \text{(A6.21a)}$$

$$T_j \; e^{-i\beta_{Tj}} = \frac{1}{A} a_j \; I_{1j}(f) \qquad j = 1,2,3 \qquad \text{(A6.21b)}$$

where: T_S, β_{TS} are the transmission and phase shift components appropriate to the scattered mode.

T_j, β_{Tj} are the transmission and phase shift components resulting from body motion in the j^{th} mode.

As a consequence of the postulation made in Section 3.1, T_j may be regarded as the downstream generated wave ratio resulting from body

motion in the j^{th} mode. The individual components may be evaluated using the same procedure as for the overall components.

The reflection coefficient, R, may be defined as the ratio of the change in surface profile at large distances upstream to that of the incident wave with the incurrence of a phase shift β_R.

The employment of a similar procedure to that used in the formation of equation (A6.17) yields the following expression:

$$\bar{\eta}^{-}(x;t) = Re\left\{e^{i(kx-\sigma t)} + Re^{-i(kx+\sigma t)}\ e^{-i\beta R}\right\} \qquad (A6.22)$$

Comparison with equation (A6.15b) yields the expression:

$$Re^{-i\beta R} = \frac{1}{A}\ I_2(s) + \frac{1}{A}\sum_{j=1}^{3} a_j I_{2j}(f) \qquad (A6.23)$$

An identical procedure to that adopted previously results in expressions equivalent to (A6.19a) and (A6.19b) from which the overall and individual components may be evaluated.

From the application of Green's Theorem to the overall potential Φ and its complex conjugate, it may be shown[75] that:

$$TT^{*} + RR^{*} = 1$$

where: superscript * indicates the complex conjugate.

This may be interpreted as

$$|T|^2 + |R|^2 = 1$$

in which $|T|$ is the modulus of T as used above, and likewise for $|R|$.

In the case of an asymmetric body, the result provides a useful check on the solutions for the velocity potential components ϕ_S and ϕ_F obtained from the source distribution methods described in Chapter 4. It must be noted that, in the case of an axi-symmetric body with a symmetric element distribution, the nature of the formulations used dictates that this condition will be met regardless of the accuracy of the potential components, thereby suggesting the relationship to be of limited value.

Another relationship, derived by Newman[75] is:

$$|\beta_R - \beta_T| = \frac{\pi}{2} \quad \text{for symmetric fixed obstacles.}$$

but, like the previous relationship, this is of limited value in the case of symmetric element distributions.

APPENDIX A7. THE COMPUTER PROGRAM.

A7.1 Introduction.

Using the theoretical formulations and methods described in this dissertation, a computer program FLOATER has been compiled to predict the motions, forces and wave effects associated with the interaction between a substantially rectangular floating body and a train of regular waves.

It was decided at the outset to construct the program as a series of interlinked subroutines, rather than as a single entity, with each subroutine relating to a particular aspect of the numerical solution. In addition to providing a systematic and progressive checking facility, it was felt that such partitioning would render the program more amenable to possible modification for the purpose of extending its usage. In the case of any particular numerical procedure being required on more than one occasion, generalised subroutines were compiled to avoid unnecessary repetition.

Since the compilation of the computer program constitutes a major part of the study, it would appear illogical not to include a program listing within the dissertation for the purpose of providing a computational base for any further investigations within the field. However, it is the experience of this author that any advantage to be gained from direct transcription of a program listing, for the above mentioned purpose, is likely to be far outweighed by the considerable expenditure of time required to trace errors arising from possible inaccuracies in transcription which are not immediately obvious.

Consequently, program information is presented in the form of flow-charts where appropriate, together with details of each subroutine used in the program.

A7.2 Program Operation.

By means of an interactive initialisation program SETDATA, a data file is created containing parameters relating to a particular set of flume and body conditions. The parameters define the body geometry and inertia, the incident wave and the required computational accuracy. The latter parameter enables the computation of convergence criteria as described in section 4.7.4. The compilation of this 'user-friendly' initialisation program was intended to facilitate the creation of data files, in the format specified by the relevant input statements contained within the main program, without the necessity for prior examination of those statements.

The contents of a particular data file are read by FLOATER which then carries out the computational procedure as illustrated by the Flow-Chart in Fig.A7.1. As a consequence of the partitioned structure of FLOATER, output statements can be inserted at any stage of the computation procedure as desired by the user.

A7.3 Subroutines and Functions within the Program.

a) General

SIMPSN Numerical integration of a specified external function, between specified limits, using Simpson's Rule.

GJSOLN Solution of a matrix equation with multiple R.H.S. using the Gauss-Jordan elimination technique.

MATSOL Solution of a matrix equation with prior checking for zero determinant of the coefficient matrix (section 4.8).

b) Floating Body Parameters

RECTELS Computes immersed surface element distribution (centroids, lengths and direction cosines) for a substantially rectangular body according to the specified distribution parameters. (Appendix A5)

BORECT Computes inertia and flotation parameters (Moment of Inertia, Centroid, Centre of Buoyancy, Metacentric Height) for a substantially rectangular body.

c) Wave Parameters

DISPER Computes the incident wave number from the dispersion equation using the Newton-Raphson iterative technique.

d) Evaluation of the Green's Functions

GPV User-specified function defining the P.V. integrand of the integral form of the Green's Function. (Equation A2.7)

DGXPV As GPV but for the x-gradient.

DGYPV As GPV but for the y-gradient.

GPV User-specified function defining the modified form of GPV.

DGXPVM As GPVM but for the x-gradient. (Equation A2.9)

DGYPVM As GPVM but for the y-gradient.

GIMAG1 Computes the imaginary part of the Green's Function together with its x and y derivatives (Equation A2.4 and derivatives thereof).

GINT1 Numerical integration of the modified P.V.integrand of the Green's Function expressions in the range $0 \leqslant \mu \leqslant 2k$. The subroutine calls SIMPSN and performs the integration on any of the modified integrands as specified above. (Section 4.7.1a)

CYINT Cyclic numerical integration of the Green's Function expressions. The subroutine calls SIMPSN and performs the integration on any of the unmodified integrands as specified above. (Section 4.7.1b)

GINTEG Evaluation of the integral form of the real part of the Green's function or its x and y derivative as required (Appendix A2.3; Section 4.7.1). The subroutine calls GINT1, SIMPSN and CYINT. A flow-chart, showing the computational procedure, can be seen in Fig.A7.2.

MTANMD Evaluation of the mth positive root of the modified dispersion equation (Appendix A4.1) for use in the series formulation of the Green's Function expressions.

GSER1 Evaluation of the series formulation of the real part of the Green's Function together with its x and y derivatives. (Appendix A2.4; Section 4.7.2). A flow-chart of the computational procedure can be seen in Fig.A7.3.

GREENS Evaluates the real and imaginary part of the Green's Function, together with its x and y derivatives, for any pair of boundary elements. This subroutine calls the relevant subroutines, to enable computation using the integral or series formulation, depending on the physical separation of the element pair (Section 4.7.3). A flow-chart can be seen in Fig. A7.4

e) Evaluation of the Hydrodynamic Parameters.

SSD1 Forms the matrices required for the discretised solution of the Fredholm Integral Equations. (Sections 4.4/4.5/4.8). Solution of the resulting matrix equation, for the discretised source strength distribution function, is achieved by the methods described in Appendix A4.2.

MULAMB Evaluation of the discretised Velocity Potential (Section 4.6). Evaluation of the Added-Mass and Damping Coefficient matrices using the Velocity Potential components (Equations 3.6.7).

FIE Evaluation of the Exciting Force components (Appendix A4.5).

MOTION Evaluation of the components of Body Motion. (Appendix A4.6).

RTCOEF Evaluation of the Body Reflection and Transmission Characteristics (Appendix A6; Appendix A4.7)

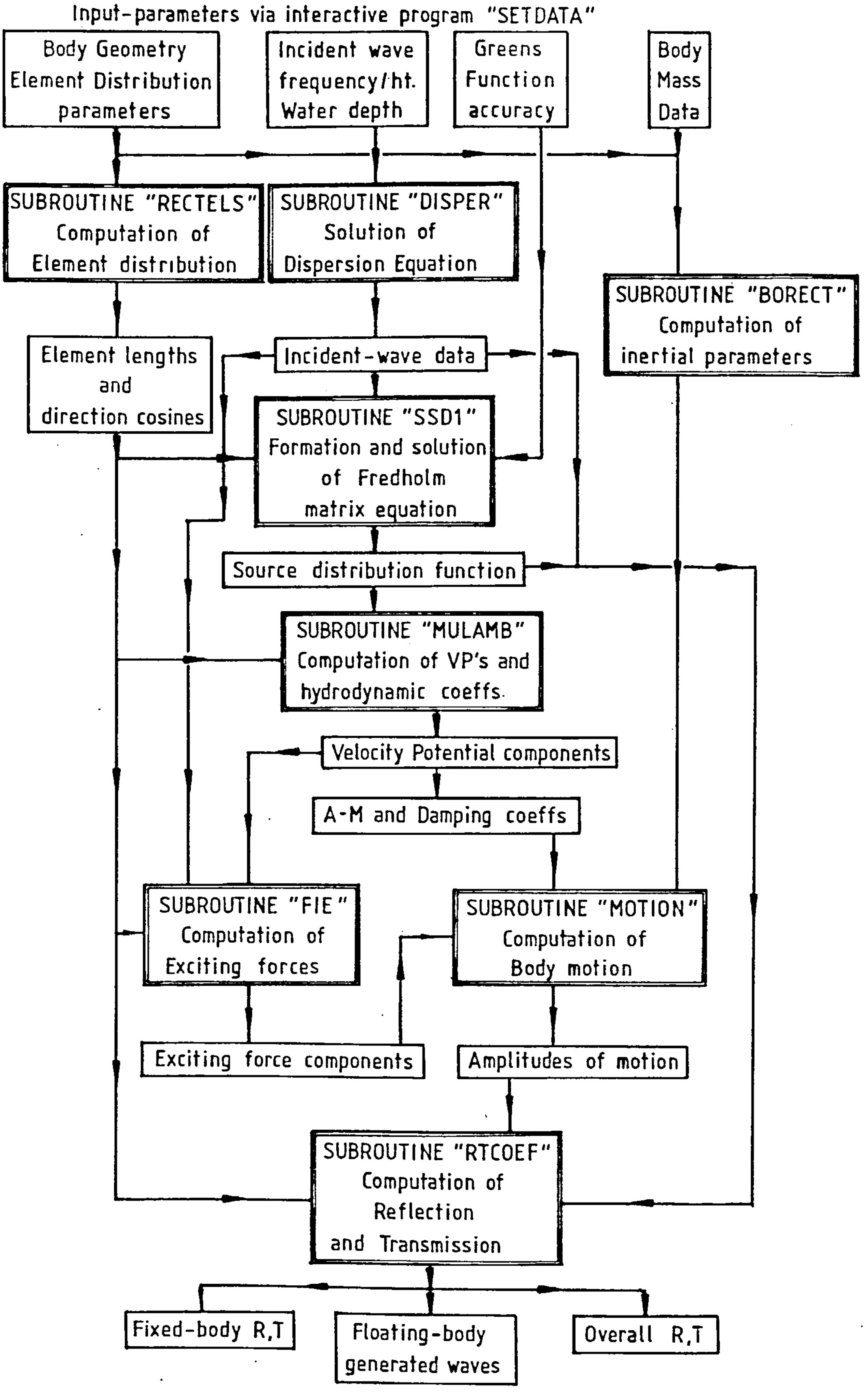

Fig. A7.1 FLOW-CHART FOR PROGRAM "FLOATER"

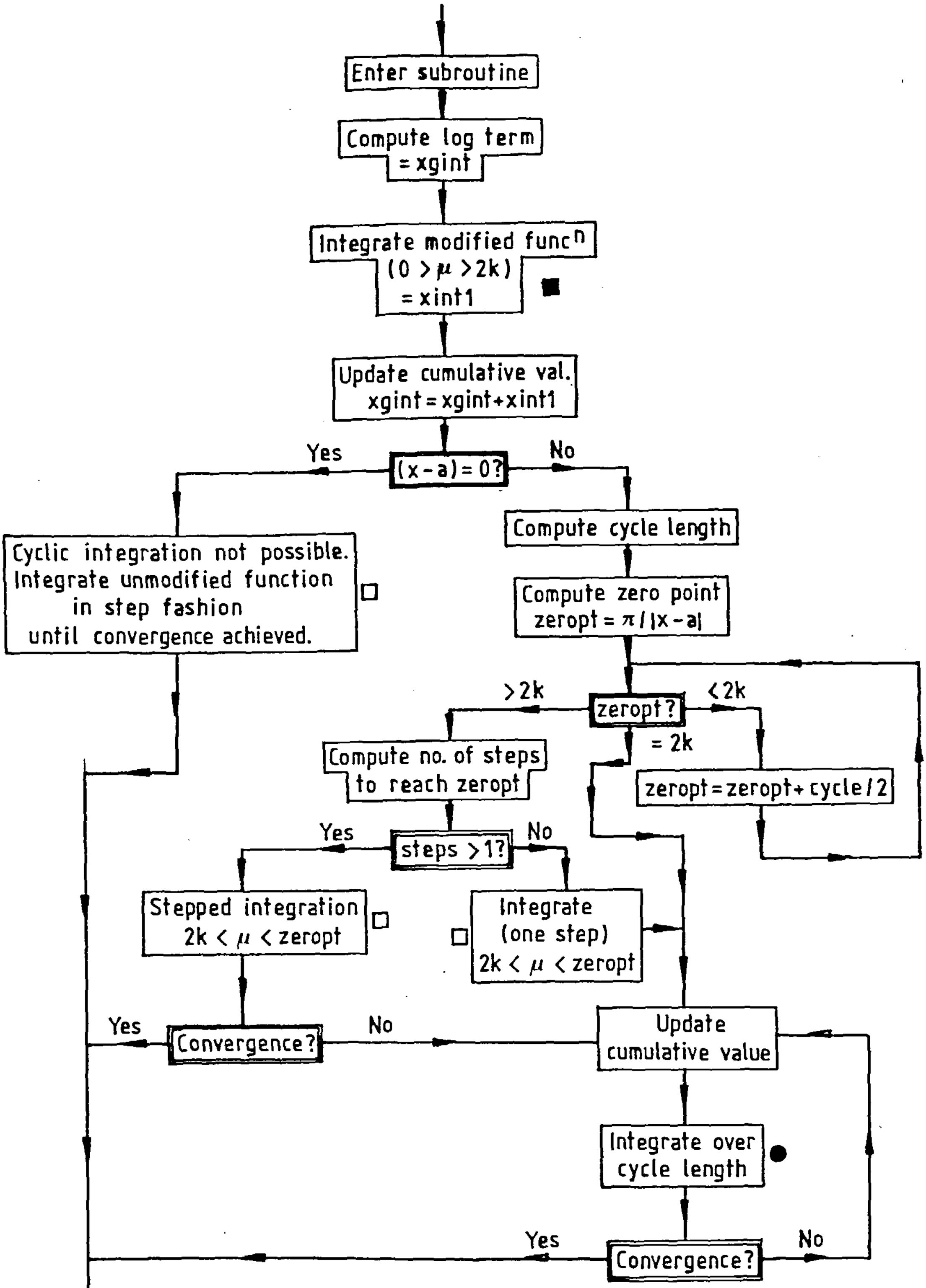

Fig. A7.2 GREEN'S FUNCTION INTEGRAL EVALUATION.
FLOW-CHART FOR SUBROUTINE "GINTEG"

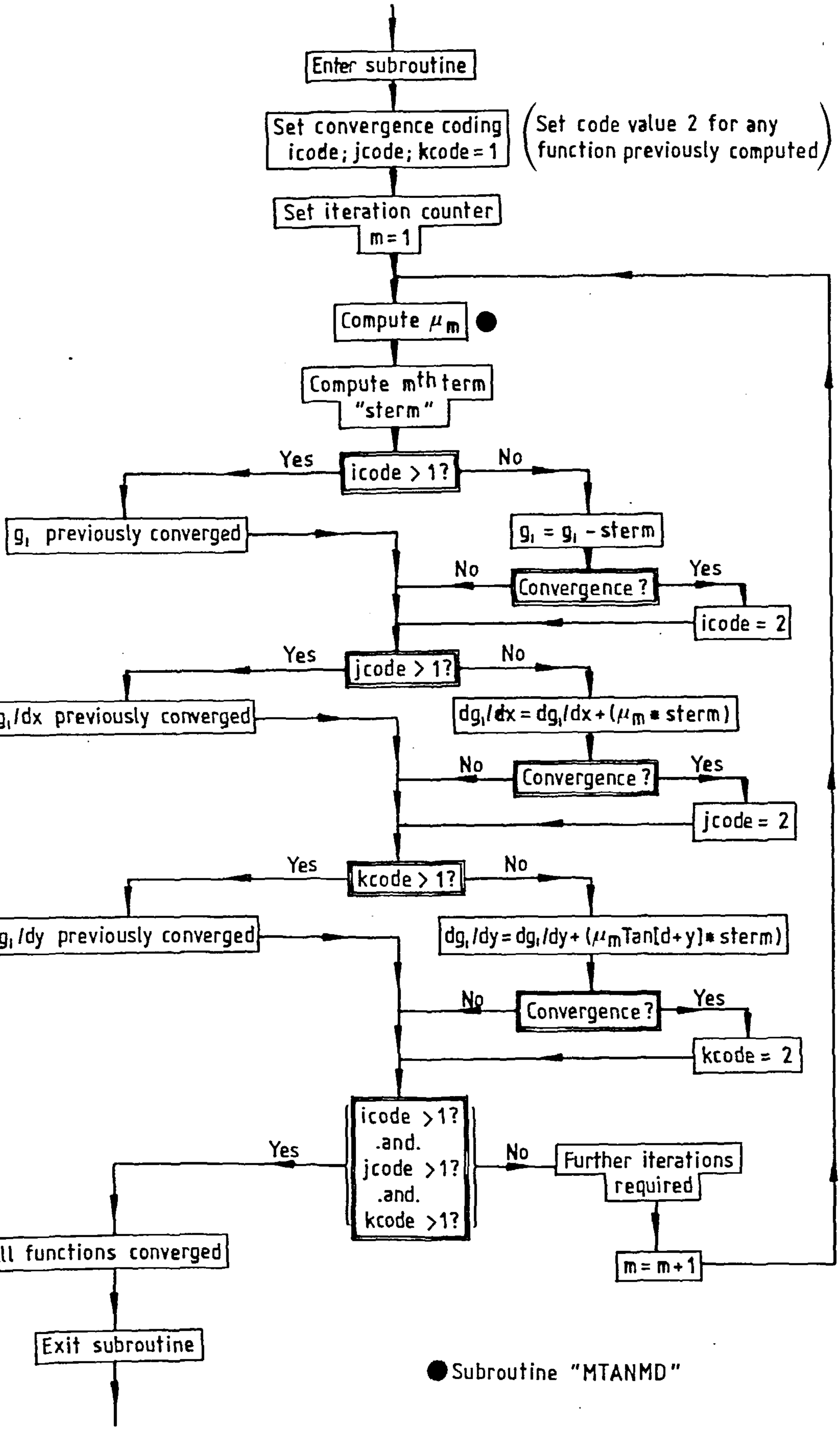

Fig.A7.3 GREEN'S FUNCTION SERIES EVALUATION.
FLOW-CHART FOR SUBROUTINE "GSER1"

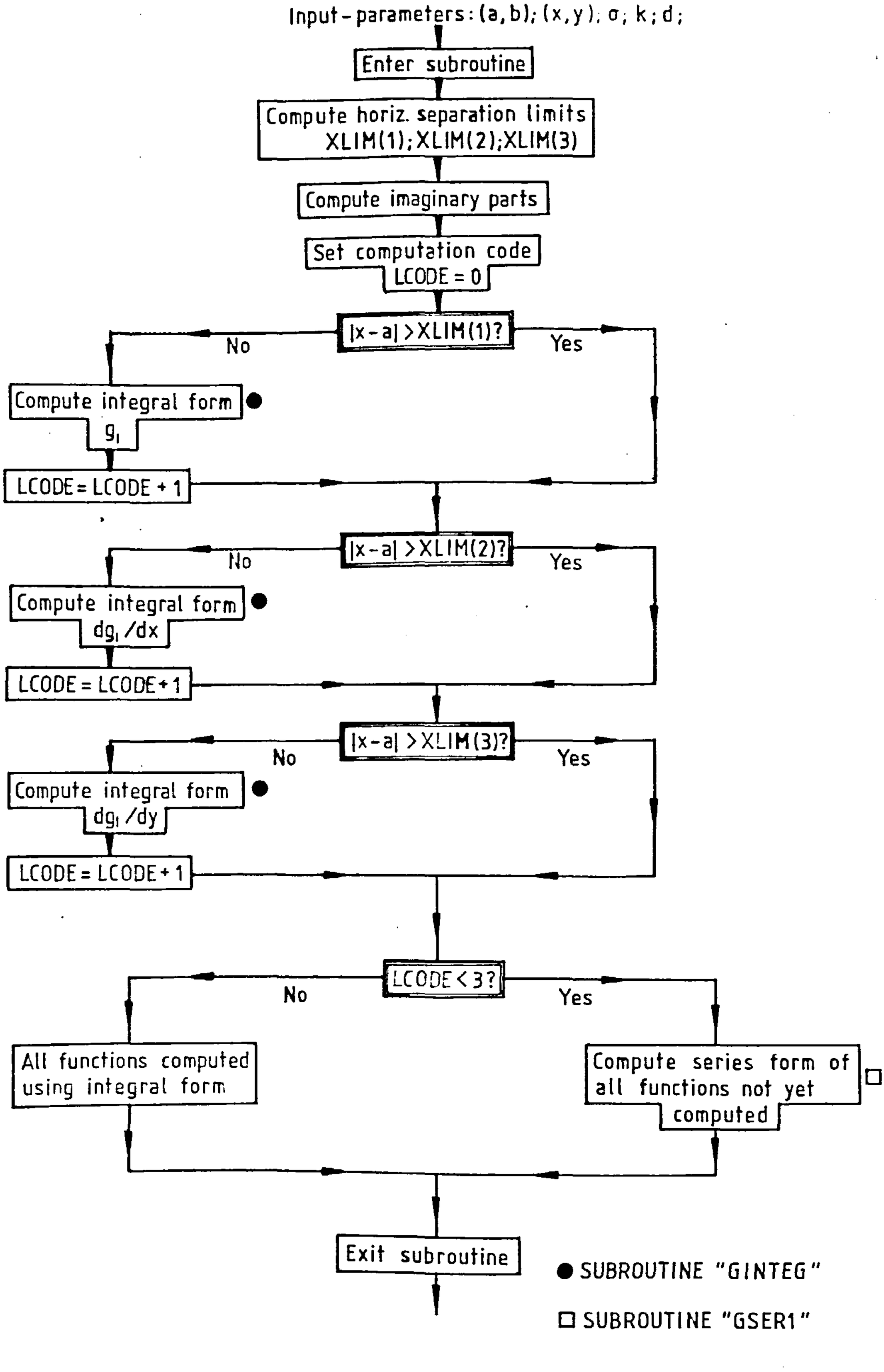

Fig.A7.4 GREEN'S FUNCTION EVALUATION
FLOW-CHART FOR SUBROUTINE "GREENS"

A7.4 Computer Operational Requirements.

In order to ascertain the viability of the boundary element computer program presented herein, details of the program storage requirements are presented, together with details of run-time performance in terms of CPU time. These details are presented in graphical form in Fig.A7.5.

The required computer storage space can be considered in two parts: the working space required for operation and storage of the fundamental parameters, and the storage space required for arrays dependent on the number of boundary elements. The basic operational space was found to be approximately 25 kWords whilst the element dependent array storage was equivalent to $6N^2 + 44N$ words.

$$\text{Thus: Total required working space} = \left\{25 + \frac{6N^2 + 44N}{1000}\right\} \text{ kWords}$$

Where: N = No. of boundary elements.

(It is understood that double precision variables occupy 2 words of storage space.)

A series of tests, carried out to determine the CPU time required for a complete solution, indicated that the required CPU time was proportional to the square of the number of elements. A feature of particular interest arising from the investigation of CPU time was the fact that, on average, 98% of the overall CPU time was consumed in constructing the matrix of Green's Functions required for the solution of the source strength distribution integral equation.

In terms of potential commercial usage of the boundary element program, the cost of each run is determined from the product of the required storage space and the overall CPU time consumed. This parameter is presented in Fig.A7.5.

It must be noted that the figures presented pertain to the operational requirements of a HONEYWELL 60/66 Main-Frame computer. Since CPU time varies considerably from computer to computer, it is suggested that the figures are used for comparative purposes only.

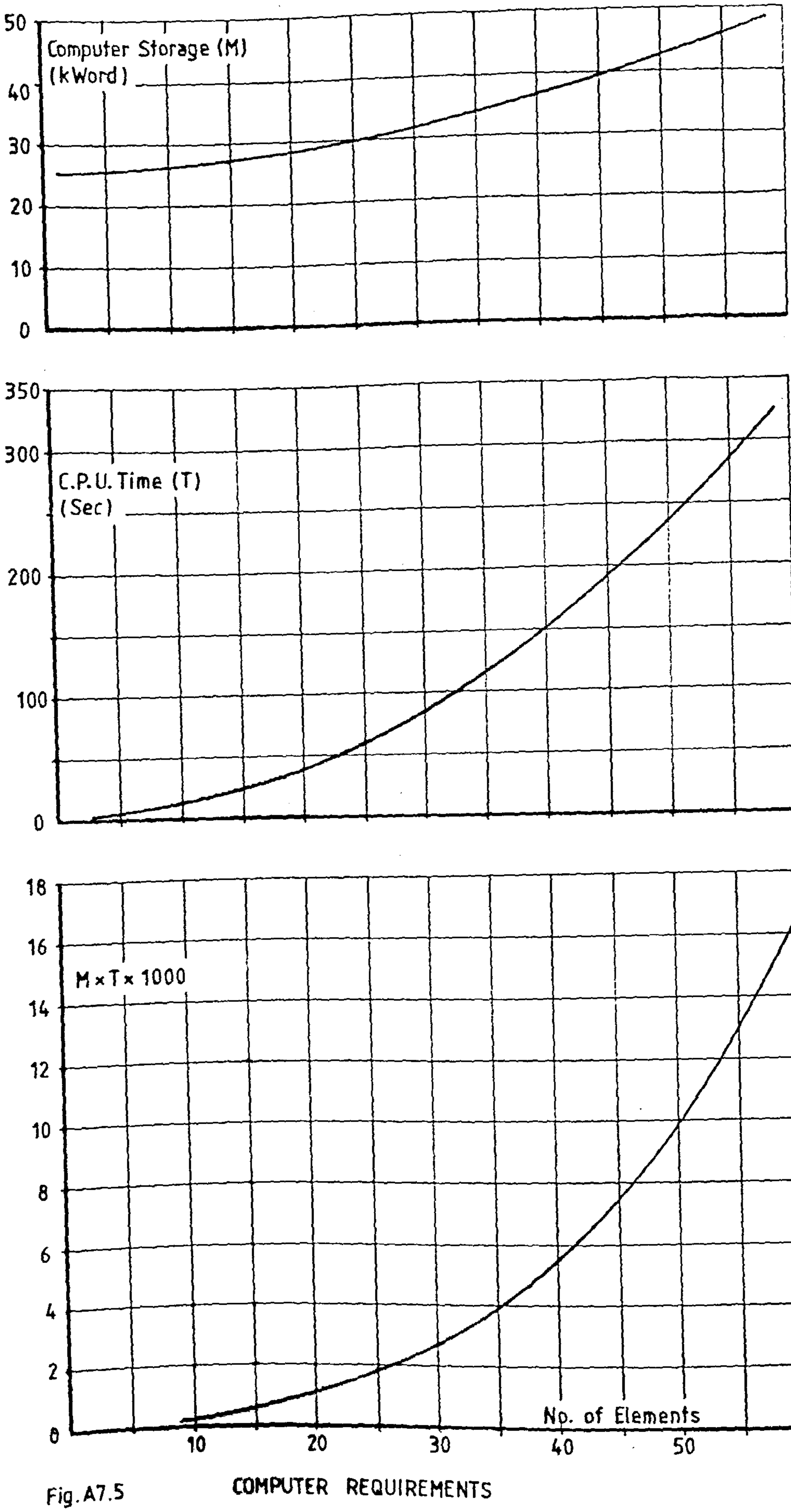

Fig. A7.5 COMPUTER REQUIREMENTS

APPENDIX A8. LIST OF REFERENCES.

1. ABRAMOVITZ, M. and STEGUN, I.A., (1964). 'Handbook of Mathematical Functions'. Nat. Bureau of Standards, Mathematics Ser.55, Washington D.C.

2. ADEE, B.H. and MARTIN, W., (1974). 'Analysis of Floating Breakwater Performance'. Proc. Floating Breakwater Conf., Univ. of Rhode Island, pp.21-40.

3. AU, M.C. and BREBBIA, C.A., (1982). 'Numerical Prediction of Wave Forces using the Boundary Element Method'. Applied Mathematical Modelling, Vol.6, pp.218-228.

4. BAI, K.J. and YEUNG, R., (1974). 'Numerical Solutions of Free Surface Problems'. Proc. 10th Symp. Naval Hydrodynamics, Camb., Mass., pp.609-647.

5. BANERJEE, P.K. and BUTTERFIELD, R., (1979). 'Developments in Boundary Element Methods'. Vol.1, Applied Science (Development Series), London.

6. BANERJEE, P.K. and SHAW, R.P., (1982). 'Developments in Boundary Element Methods'. Vol.2, Applied Science (Development Series), London.

7. BEARMAN, P.W. and GRAHAM, J.M.R., (1979). 'Hydrodynamic Forces on Cylindrical Bodies in Oscillatory Flow'. Proc. 2nd Int. Conf. on the Behaviour of Offshore Structures, BOSS'79, London, Vol.1, pp.309-322.

8. BETTS, C.V., BISHOP, R.E.D. and PRICE, W.G., (1977). 'The Symmetric Generalised Fluid Force applied to a Ship in a Seaway'. Trans RINA, Vol.119, Supplementary Papers, p.265.

9. BIRD, H.W.K. and SHEPHERD, R., (1982). 'Wave Interaction with Large Submerged Structures'. J. Wat. Ways. Harb. Div. ASCE, Vol.10, WW2, May, pp.146-162.

10. BLACK, J.L., MEI, C.C and BRAY, M.C.G., (1971). 'Radiation and Scattering of Water Waves by Rigid Bodies'. J. Fluid Mech., Vol.46, pp.151-164.

11. BLAGOVESCHENSKY, S.N., (1962). 'Theory of Ship Motions'. Dover Publ. Inc., New York.

12. COATES, L.E., (1983). 'Wave Forces on Vertical Cylinders - A Numerical and Experimental Investigation'. Ph.D. Thesis, The City University, London.

13. COUNT, B.M., (1975). 'Conformal Transformations of an Arbitrary Section to a Circular Section'. CEGB., Marchwood Eng. Lab., Elect. Res. Memo. No.531.

14. COUNT, B.M., (1976). 'The Sea-Keeping Problem'. *Ibid.*, Wave Power Res. Memo. No.21.

15. DEAN, R.G. and URSELL, F., (1959). 'Interaction of a Fixed, Semi-Immersed Circular Cylinder with a train of Surface Waves'. Tech. Rep. No.37, Hydrodynamics Lab., MIT., Camb., Mass.

16. DEAN, W.R., (1948). 'On the Reflection of Surface Waves by a Submerged Circular Cylinder'. Proc. Camb. Phil. Soc., Vol.44, pp.483-491.

17. De JONG, B., (1969). 'Computation of the Hydrodynamic Coefficients of Oscillating Cylinders'. Delft Univ. of Technology, Shipbuilding Lab., Rep. No.174A.

18. EATOCK-TAYLOR, R., (1982). 'Developments in Boundary Element Methods. Vol.2'. (Eds: BANERJEE, P.K. and SHAW, R.P.), Applied Science (Development Series), London.

19. FALTINSEN, O.M. and MICHELSEN, F.C., (1974). 'Motions of Large Structures in Waves at Zero Froude Numbers'. Proc. Int. Symp. on the Dynamics of Marine Vehicles and Structures in Waves, Univ. Coll. London, Paper No.11, pp.91-106.

20. FRANK, W., (1967). 'Oscillations of Cylinders in or below the Free Surface of Deep Fluids'. NSRDC Rep. No.2375, Washington D.C.

21. FROUDE, R.E., (1896). 'The Non-Uniform Rolling of Ships'. Trans. INA, Vol.37, p.293.

22. FROUDE, W., (1861). 'On the Rolling of Ships'. *Ibid.*, Vol.2, p.180.

23. GARRISON, C.J., (1974-5). 'Hydrodynamics of Large Objects at Sea'. J. of Hydronautics, Part 1, Vol.8, p.5; Part 2, Vol.9, p.58.

24. GARRISON, C.J., (1978). 'Hydrodynamic Loading of Large Offshore Structures - Three-Dimensional Source Distribution Methods'. Num. Methods in Offshore Structures, (Eds: ZIENKIEWICZ, O.C., LEWIS, R.W. and STAG, K.G.), Ch.3, pp.87-140, John Wiley, Chichester, England.

25. GARRISON, C.J. and CHOW, P.Y., (1972). 'Wave Forces on Submerged Bodies'. J.Wat. Ways. Harb. and Coastal Eng. Div. ASCE, Vol.98, No.WW3, pp.375-392.

26. GERRITSMA, J. and BEUKELMAN, W., (1964). 'The Distribution of the Hydrodynamic Forces on a Heaving and Pitching Ship Model in Still Water'. Int. Shipbuilding Progress, No.123, p.506.

27. GODA, Y., and SUZUKI, Y., (1976). 'Estimation of Incident and Reflected Waves in Random Wave Experiments'. Proc. 15th Coastal Eng. Conf., Honolulu, Vol.1, pp.828-845.

28. GRIM, O., (1953). 'Berechnung der durch Schwingungen eines Schiffkörpers erzeugten Hydrodynamische Kräfte'. Jahrbuch der STG, Vol.47, p.277. (Also available in English as BSRA translation No.1004).

29. GRIM, O., (1960). 'A method for more precise computation of Heaving and Pitching Motions both in Smooth Water and in Waves'. 3rd Symp. on Naval Hydrodyn., Scheveningen.

30. HANAOKA, T., (1959). 'On the Reverse Flow Theorem concerning Wave-Making Theory'. Proc. 19th Japan Nat. Cong. Applied Mech., p.223.

31. HASKIND, M.D., (1946). 'The Hydrodynamic Theory of Heaving and Pitching of a Ship.' Translated in SNAME Tech. and Res. Bull. No.1-12, (1953).

32. HASKIND, M.D., (1954). 'Approximate Methods of Determination of Hydrodynamic Characteristics of Ship Oscillations'. Izvestiya Akad. Naut. SSSR., Otd. Tech. Naut., No.11, p.66.

33. HASKIND, M.D., (1957). 'The Exciting Forces and Wetting of Ships in Waves'. Translated in DTMB Translation 307, (1962).

34. HASKIND, M.D. and RIMAN, I.S., (1946). 'A method of determining the Pitching and Heaving Characteristics of Ships'. Translated in DTMB Translation 253, (1955).

35. HAVELOCK, T.H., (1929) No title. Phil. Mag. Series 7, Vol.8, pp.569-576.

36. HAVELOCK, T.H., (1940). 'Waves Produced by the Rolling of a Ship'. Phil. Mag. Series 7, Vol.29, p.407.

37. HAVELOCK, T.H., (1942). 'The Damping of the Heaving and Pitching Motion of a Ship'. Phil. Mag. Series 7, Vol.33, p.666.

38. HAVELOCK, T.H., (1955). 'Waves due to a Floating Sphere making Periodic Heaving Oscillation'. Proc. Royal Soc. of London, Ser.A, Vol.231, p.1.

39. HEARN, G.E. and DONATI, E., (1981). 'Sea-keeping Theories - Applying Some Choice'. Trans. NECIES, Vol.97, pp.53-72.

40. HEARN, G.E., DONATI, E. and MAHENDRAN, I.K., (1982). 'Prediction, Measurement and Comparison of Fluid-Structure Interaction using Mathematical and Experimental Models'. Preprint of Report, Dept. of Naval Arch., Univ. of Newcastle upon Tyne.

41. HESS, J.L. and SMITH, A.M.O., (1967). 'Calculation of Potential Flow about Arbitrary Bodies'. Progress in Aeronautical Sciences, Vol.8, pp.1-138.

42. HOGBEN, N., OSBORNE, J. and STANDING, R.G., (1974). 'Wave Loading on Offshore Structures: Theory and Experiment'. Proc. Symp. Ocean Eng., Nat. Phys. Lab., London. RINA, pp.19-36.

43. HOGBEN, N. and STANDING, R.G., (1974). 'Wave Loads on Large Bodies'. Proc. Int. Symp. on the Dynamics of Marine Vehicles and Structures in Waves, Univ. Coll. London, Paper No.26, pp.258-277.

44. HWANG, J.H., (1969). 'Added-Mass of Two-Dimensional Cylinders with the Sections of Straight Frames Oscillating Vertically in a Free-Surface'. Int. Shipbuilding Progress, Vol.16, p.169.

45. IJIMA, T., CHOU, C.R. and YOSHIDA, A.A., (1976). 'A method of Analysis for Two-Dimensional Water Wave Problems'. Proc. 15th Coastal Eng. Conf., Honolulu, Vol.III, pp.2717-2736.

46. JASWON, M.A., (1964). 'Integral Equation Methods in Potential Theory I'. Proc. Royal Soc., Series A, Vol.275, pp.23-32.

47. JASWON, M.A. and SYMM, G.T., (1977). 'Integral Equation Methods in Potential Theory and Elastostatics'. Academic Press, London.

48. JOHN, F., (1949). 'On the Motion of Floating Bodies I'. Comm. Pure and Applied Math., Vol.2, p.13.

49. JOHN, F., (1950). 'On the Motion of Floating Bodies II'. *Ibid.*, Vol.3, p.45.

50. KATO, H., (1958). 'On the Frictional Resistance to the Roll of Ships'. J. of the Zosen Kiokai, Vol.102. (In Japanese).

51. KEIL, H., (1974). 'Die Hydrodynamischen Kräfte bei der Periodischen Bewegung Zweidimensionaler Körper an der Oberflache Flacher Gewasser'. Inst. fur Schiffbau, Hamburg, Rep.305.

52. KEUNING, J.A. and BEUKELMAN, W., (1979). 'Hydrodynamic Coefficients of Rectangular Barges in Shallow Water'. 2nd Int. Conf. on the Behaviour of Offshore Structures, BOSS'79, Imp. Coll. London.

53. KIM, C.H., (1969). 'Hydrodynamic Forces and Moments for Heaving, Swaying and Rolling Cylinders on Water of Finite Depth'. J. Ship Research, Vol.13, pp.137-154.

54. KIM, C.H. and CHOU, F., (1971). 'Hydrodynamic Characteristics of Barges'. Offshore Technology Conference, Houston.

55. KIM, W.D., (1965). 'On the Harmonic Oscillation of a Rigid Body on a Free Surface'. J. Fluid Mech., Vol.21, pp.427-451.

56. KOCHIN, N.E., (1939). 'The Two-Dimensional Problem of Steady Oscillations of Bodies under the Free Surface of a Heavy Incompressible Fluid'. Translated in SNAME Tech. and Res. Bull. No.1-9.

57. KOCHIN, N.E., (1940). 'The Theory of Waves Generated by Oscillations of a Body under the Free Surface of a Heavy Incompressible Fluid'. English Translation available as: SNAME Tech. and Res. Bull. No.1-10, (1952).

58. KORVIN-KROUKOVSKY, B.V. and JACOBS, W.D., (1957). 'Pitching and Heaving Motions of a Ship in Regular Waves'. Trans. SNAME, Vol.65, p.590.

59. KRYLOV, A.N., (1896). 'A New Theory of Pitching of Ships on Waves and of the Stresses Produced by this Motion'. Trans. INA, Vol.37, p.326.

60. KRYLOV, A.N., (1896). 'A General Theory of the Oscillations of a Ship on Waves'. Trans. INA, Vol.40, p.184.

61. LACEY, D.J., (1983). 'Wave-Obstacle Interaction for a Submerged Horizontal Cylinder'. Ph.D. Thesis, The City Univ., London.

62. LAMB, Sir HORACE, (1932). 'Hydrodynamics'. (6th Edn.), Dover Publications, New York.

63. LANDWEBER, L. and MACAGNO, M., (1957). 'Added-Mass of Two-Dimensional Forms oscillating in a Free Surface'. J. Ship Research, Vol.1, p.20.

64. LANDWEBER, L. and MACAGNO, M., (1959). 'Added-Mass of Three-Parameter Family of Two-Dimensional Forms oscillating in a Free Surface'. J. Ship. Research, Vol.2, p.36.

65. LEBRETON, J.C. and MARGNAC, M.A., (1966). 'Traitment sur Ordinateur de Quelques Problems concernant L'Action de la Houle sur Corps Flottants en Theorie Bidimensionelle'. Bulletin du Centre de Recherches et D'Essais de Chatou, No.18.

66. LEWIS, F.M., (1929). 'The Inertia of Water Surrounding a Vibrating Ship'. Trans. SNAME, Vol.37, p.1.

67. LOCKWOOD-TAYLOR, J., (1930). 'Some Hydrodynamical Inertia Coefficients'. Phil. Mag., Vol.9, Series 7, p.161.

68. MacCAMY, R.C. and FUCHS, R.A., (1954). 'Wave Forces on Piles - A Diffraction Theory'. U.S. Army Corps of Engineers, Beach Erosion Board. Technical Memo No.69.

69. MARTIN, P.A. and DIXON, A.G., (1983). 'The Scattering of Regular Surface Waves by a fixed, half-immersed Circular Cylinder'. Applied Ocean Research, Vol.5, No.1, pp.13-23.

70. MOGRIDGE, G.R. and JAMIESON, W.W., (1975). 'Wave Forces on a Circular Caisson - Theory and Experiment'. Can. J. Civil Eng., Vol.2, pp.540-548.

71. MONACELLA, V.J. (1976). 'The Disturbance due to a Slender Ship oscillating in Waves in a Fluid of Finite Depth'. J. Ship Research, Vol.10, No.4, pp.242-252.

72. NAFTZGER, R.A. and CHAKRABARTI, S.K., (1979). 'Scattering of Waves by two-dimensional Circular Obstacles in Finite Water Depths'. J. Ship Research, Vol.23, pp.32-42.

73. NEWMAN, J.N., (1962). 'The Exciting Forces on Fixed Bodies in Waves'. J. Ship Research, Vol.6, No.3, p.10.

74. NEWMAN, J.N., (1965). 'The Exciting Forces on a Moving Body in Waves'. J. Ship Research, Vol.9, p.190.

75. NEWMAN, J.N., (1977). 'Marine Hydrodynamics'. MIT Press, Camb., Mass.

76. OGILVIE, T.F. and TUCK, E.O., (1969). 'A Rational Strip Theory of Ship Motions Part I'. Univ. of Michigan, Coll. of Eng., Dept. of Naval Arch. and Mar. Eng., Report No.013.

77. OLIVEIRA, E.R.A., (1968). 'Plane Stress Analysis by General Integral Equation Method'. J. Eng. Mech. Div. ASCE, E.M.I., pp.79-101.

78. OSMENT, J., (1985). Doctoral Thesis, The City Univ., London.

79. PATEL, M.H., (1979). 'The Influence of Vortex Shedding on the Roll Motions of a Flat Bottomed Barge'. Presented at the Euromech 119 Colloquium on Vortex Shedding from Bluff Bodies in Oscillatory Flow, Imp. Coll. London, July 1979.

80. PATEL, M.H., (1979). Discussion of Paper by Keuning and Beukelman (Ref.52).

81. PETERS, A.S. and STOKER, J.J., (1957). 'The Motion of a Ship, as a Floating Rigid Body, in a Seaway'. Comm. Pure and Applied Math., Vol.10, p.399.

82. PORTER, W.R., (1960). 'Pressure Distributions, Added-Mass and Damping Coefficients for Cylinders Oscillating in a Free Surface'. Univ. of California, Inst. of Eng. Res., Series No.82, Issue No.16.

83. SALVASEN, N., (1969). 'On higher order theory for Submerged two-dimensional Bodies'. J. Fluid Mech., Vol.38, Part 2, pp.415-432.

84. SALVASEN, N., TUCK, E.O. and FALTINSEN, O., (1970). 'Ship Motions and Sea Loads'. Trans. SNAME, Vol.78, p.250.

85. SARPKAYA, T. and ISAACSON, M. de. St. Q., (1981). 'Wave Theories'. Ch.4, The Mechanics of Wave Forces on Offshore Structures. Van Nostrand Reinhold, New York.

86. SARPKAYA, T. and ISAACSON, M. de. St. Q., (1981). 'Wave Forces on Large Bodies". *Ibid.*, Ch.6.

87. SAYER, P. and URSELL, F., (1976). 'On the Virtual Mass at Long Wavelengths of a Half Immersed Cylinder heaving on Water of Finite Depth'. Eleventh Symp. on Naval Hydrodyn., Univ. Coll. London.

88. St. DENIS, M. and PIERSON, W.J., (1953). 'On the Motion of Ships in Confused Seas'. Trans. SNAME, Vol.61.

89. STEKLOW, W.A., (c. 1890). 'Integration der Differentialgleichungen der Mathematischen Physic'. (Compiled by Geronimus J.L.). Veb. Verlag Technik, Berlin.

90. SYMM, G.T. (1964). 'Integral Equation Methods in Potential Theory II'. Proc. Royal Soc., Series A, Vol.275, pp.33-46.

91. TANAKA, N. (1960). 'A Study on the Bilge Keels. Part 4. On the Eddy Making Resistance to the Rolling of a Ship Hull'. Japan Soc. of Naval Architects, Vol.109.

92. TASAI, F., (1959). 'On the Damping Force and Added-Mass of Ships Heaving and Pitching'. Rep. of Res. Inst. for Applied Mech., Kyushu Univ., Vol.7, No.26.

93. TASAI, F., (1961). 'Hydrodynamic Force and Moment Produced by Swaying and Rolling Oscillation of Cylinders on the Free Surface.' *Ibid.*, Vol.9, No.35.

94. TIMMAN, R. and NEWMAN, J.N., (1962). 'The Coupled Damping Coefficient of Symmetric Ships'. J. Ship Research, Vol.5, No.4.

95. URSELL, F., (1949). 'On the Heaving Motion of a Circular Cylinder on the Surface of a Fluid'. Quart. J. of Mech. and Applied Math., Vol.2, p.213.

96. URSELL, F., (1953). 'Short Surface Waves due to an Oscillating Immersed Body'. Proc. Royal Soc. of London, Series A, Vol.220, p.90.

97. URSELL, F., (1974). 'Note on the Virtual Mass Damping Coefficients in Water of Finite Depth'. Dept. of Math., Univ. of Manchester.

98. URSELL, F. (1976). 'On the Virtual Mass and Damping Coefficients in Water of Finite Depth'. J. Fluid Mech., Vol.76, Part 1, p.17.

99. URSELL, F., DEAN, R. and YU, Y.S., (1960) 'Forced Small Amplitude Water Waves; A Comparison between Theory and Experiment'. J. Fluid Mech., Vol.7, pp.33-52.

100. VAN OORTMERSSEN, G., (1979). Discussion of Paper by Keuning and Beukelman, Ref.52.

101.VUGTS, J.H. (1968). 'The Hydrodynamic Coefficients for Swaying, Heaving and Rolling Cylinders in a Free Surface'. Int. Shipbuilding Progress, Vol.15, pp.251-276.

102.VUGTS, J.H., (1968). 'Cylinder motions in Beam Seas'. Ned. Scheepstudiecent., TNO. Rep. No.1155.

103.WEHAUSEN, J.V., (1971). 'The Motion of Floating Bodies'. Ann. Rev. Fluid Mech., Vol.3, pp.237-268.

104.WEHAUSEN, J.V. and LAITONE, E.V., (1960). 'Surface Waves'. Handbuch der Physic (Ed. S. FLUGGE), Springer Verlag, Berlin, Vol.9, pp.446-778.

105.WENDEL, K., (1950). 'Hydrodynamische Massen und Hydrodynamische Massentragheitsmomente'. Jahrbuch det STG., Vol.44, p.207. (Also available as BSRA Translation No.288).

106.YAMAMOTO, T., (1980) 'Moored Floating Breakwater Response to Regular and Irregular Waves'. Applied Ocean Research, Vol.2, No.2, pp.114-122.

107.YAMAMOTO, T., YOSHIDA, A. and IJIMA, T., (1980). Dynamics of Elastically Moored Floating Objects'. *Ibid.*, pp.106-113.

108.YU, Y.S. and URSELL, F., (1961) 'Surface Waves generated by an Oscillating Circular Cylinder on Water of Finite Depth: Theory and Experiment'. J. Fluid Mech., Vol.11, pp.1529-551.

109.YUE, D.K.P., CHEN, H.S. and MEI, C.C., (1978). 'A Hybrid Element Method for Diffraction of Water Waves by Three-Dimensional Bodies'. Int. J. Num. Methods in Eng., Vol.12, No.2, pp.245-266.

APPENDIX A9. NOMENCLATURE

This appendix contains a list of the main symbols used in the text of this thesis. Any additional symbols which occur from time to time are defined as and when they occur.

a	Acceleration.
a_j	Complex amplitude of body motion in the j^{th} mode.
$\bar{a}_j$	Non-dimensional amplitude of body motion in the j^{th} mode.
a_I, a_R, a_T	Incident, reflected and transmitted components of wave amplitude.
$A_{ij} \rightarrow H_{ij}$	Matrix elements.
B	Body length in direction of wave travel.
C_m	m^{th} coefficient of the Green's Function series form.
d	Still water depth.
D	Body draught.
f	Source strength distribution function.
F	Force.
$F_i(e)$	Exciting force component in the i^{th} mode.
$\bar{F}_i(e)$	Non-dimensional exciting force component in the i^{th} mode.
g	Gravitational acceleration.
G, g_o, g_1, g_2	Green's Function components.
H	Wave height, Metacentric height.
I_3	Rotational Mass Moment of Inertia of the floating body in the pitch mode.
k	Wave Number. ($= 2\pi/L$)
l	Element length.

L	Incident wave length, Body length in direction of wave travel.
m	Mass, Source strength.
M	Moment.
n_x, n_y	Direction cosines with respect to the x and y coordinate axes.
n_j	Outward normal component scalar in the j^{th} direction.
$\underline{n}$	Outward normal vector with respect to the body surface.
p	Pressure.
r,R	Radial separation.
$\underline{r},\underline{R}$	Radius vector.
R.*R*	Reflection Coefficient.
t	Time Parameter.
T,*T*	Transmission Coefficient.
v,V	Velocity.
$\forall$	Displaced volume of floating body at equilibrium.
W	Waterline area of floating body at equilibrium.
$\underline{x} = (x,y)$	Cartesian coordinates of Field Point.
y_G	Cartesian coordinates of body centroid.
α_j	Body motion component in the j^{th} mode.
β	Phase angle.
Γ_j	Length of j^{th} boundary element.
$\Gamma(x,y)$	Immersed surface of the body.
δ_{ij}	Kronecker Delta.
Φ,Ψ	Velocity Potential.
ϕ	Spacial component of Velocity Potential.
$\bar{\Phi},\bar{\phi}$	Non-dimensional Velocity Potential.
λ_{ij}	Damping coefficient.

$\bar{\lambda}_{ij}$ Non-dimensional Damping Coefficient.

μ_{ij} Added-Mass Coefficient.

$\bar{\mu}_{ij}$ Non-dimensional Added-Mass Coefficient.

μ_m m^{th} positive real root of the modified dispersion equation.

ν Deep-water wave number. ($= \sigma^2/g$)

ρ Mass density.

σ Wave radial frequency.

$\underline{\xi} = (a,b)$ Cartesian Coordinates of Source Point.

η Free-surface displacement.

$\bar{\eta}$ Non-dimensional free-surface displacement.